

DISSERTATION ZUR ERLANGUNG DES DOKTORGRADES
DER FAKULTÄT FÜR CHEMIE UND PHARMAZIE
DER LUDWIG-MAXIMILIANS-UNIVERSITÄT MÜNCHEN

Investigations Concerning the Laser Ignition of Energetic Coordination Compounds

Manuel Benedikt Joas

aus

Wasserburg am Inn

2014

Erklärung

Diese Dissertation wurde im Sinne von § 7 der Promotionsordnung vom 28. November 2011 von Herrn Professor Dr. Thomas M. Klapötke betreut.

Eidesstattliche Versicherung

Diese Dissertation wurde eigenständig und ohne unerlaubte Hilfe erarbeitet.

München, den 12. September 2014

.....
(Manuel Benedikt Joas)

Dissertation eingereicht am: 16. September 2014

1. Gutachter: Professor Dr. Thomas M. Klapötke

2. Gutachter: Professor Dr. Konstantin Karaghiosoff

Mündliche Prüfung am: 30. Oktober 2014

Acknowledgements

First of all, I would like to thank Professor Dr. Thomas M. Klapötke for the opportunity to carry out my doctoral work about this very interesting topic within his research group. He was a great mentor, who supported me all the time, took care of my requests, and gave me the benefit of his extensive knowledge.

Furthermore, I am indebted to Professor Dr. Konstantin Karaghiosoff for being the second corrector of this thesis as well as numerous time consuming X-ray measurements and his enthusiasm for crystal structure analysis. He contributed a lot to the good atmosphere in our research group with his humor.

I also would like to express my thanks to Professor Dr. Dina Fattakhova-Rohlfing, Professor Dr. Wolfgang Beck, Professor Dr. Ingo-Peter Lorenz and Professor Dr. Hans-Christian Böttcher for being available as members of the examination board.

Next, I would like to thank Dr. Jörg Stierstorfer for all the help, his professional advice, the great interest he showed for this thesis, proofreading of many publications and the numerous serious discussions.

Dr. Burkhard Krumm is thanked for his advice in safety issues, the weekly football conversations and the shared antipathy for the "FC Hollywood".

Special thanks also go to Ms. Irene Scheckenbach for always being so friendly and for her engagement and help in handling the formality and bureaucracy of public institutions.

I am also deeply indebted to Mr. Stefan Huber, who spent a lot of time with me performing the laser ignition tests, measuring the sensitivities and talking about stuff concerning the everyday life.

Furthermore, I would like to thank:

- my students Norbert Szimhardt, Alexander Danner, Ivan Gospodinov and Lukas Brunner for their engagement, their enthusiasm and many good results;
- Thomas Reich, who became a great friend during the last three years;
- my lab colleague Dániel Izsák and of course the whole research group.

Finally and above all, I would like to thank my parents, my brother and my sisters, and especially my wonderful girlfriend, who have always been a very important part of my life and a great support. There are no words to describe how grateful I am.

Table of Contents

1. Introduction	1
1.1. History of Energetic Materials	1
1.2. Classification of Energetic Materials	2
1.3. Ignition and Initiation of Energetic Materials	5
1.4. Laser Ignition and Initiation	7
1.5. Motivation and Objective	13
1.6. References	14
2. Setup	17
2.1. Laser Ignition Setup	17
2.2. Measurement of Function Time t_f	19
2.3. References	20
3. Preparation and Crystal Structure of Diaqua(μ -5,5'-bistetrazolato- $\kappa^4 N^1, N^2, N^5, N^6$)copper(II)	21
3.1. Abstract	21
3.2. Introduction	21
3.3. Results and Discussion	22
3.4. Experimental Section	26
3.5. Conclusion	27
3.6. References	28
4. Transition Metal Complexes of 3-Amino-1-nitroguanidine as Laser Ignitable Primary Explosives: Structures and Properties	31
4.1. Abstract	31
4.2. Introduction	32
4.3. Results and Discussion	33
4.4. Conclusion	47
4.5. Experimental Section	48
4.6. References	54
5. Synthesis and Characterization of Various Photosensitive Copper(II) Complexes with 5-(1-Methylhydrazinyl)-1 <i>H</i> -tetrazole as Ligand and Perchlorate, Nitrate, Dinitramide, and Chloride as Anions	57
5.1. Abstract	57
5.2. Introduction	58

5.3.	Results and Discussion.....	59
5.4.	Conclusion	71
5.5.	Experimental Section	72
5.6.	References.....	74
6.	Photosensitive Metal(II) Perchlorates with 1,2-Bis[5-(1-methylhydrazinyl)tetrazol-1-yl]ethane as Ligand: Synthesis, Characterization and Laser Ignition.....	77
6.1.	Abstract.....	77
6.2.	Introduction.....	77
6.3.	Results and Discussion.....	79
6.4.	Conclusion	83
6.5.	Experimental Section	84
6.6.	References.....	87
7.	Polynuclear Chlorido Metal(II) Complexes with 1,2-Di(1 <i>H</i> -tetrazol-1-yl)ethane as Ligand Forming One- and Two-dimensional Structures	91
7.1.	Abstract.....	91
7.2.	Introduction.....	91
7.3.	Results and Discussion.....	92
7.4.	Conclusions.....	99
7.5.	Experimental Section	100
7.6.	References.....	103
8.	Investigations Concerning the Laser Ignition and Initiation of Various Metal(II) Complexes with 1,2-Di(1 <i>H</i> -tetrazol-1-yl)ethane as Ligand and a Large Set of Anions .	105
8.1.	Abstract.....	105
8.2.	Introduction.....	106
8.3.	Results and Discussion.....	107
8.4.	Conclusion	122
8.5.	Experimental Section	122
8.6.	References.....	124
9.	A Study on the Effect of the Metal Center, Ligand, and Anion on the Laser Ignitability of Energetic Coordination Compounds	129
9.1.	Abstract.....	129
9.2.	Introduction.....	129
9.3.	Results and Discussion.....	130
9.4.	Conclusion	141

9.5. Experimental Section	141
9.6. References	146
10. Laser Initiation of Tris(carbohydrazide)metal(II) Perchlorates and Bis(carbohydrazide)diperchloratocopper(II)	149
10.1. Abstract	149
10.2. Introduction	150
10.3. Results and Discussion	151
10.4. Experimental Section	156
10.5. Conclusion	157
10.6. References	157
11. Cocrystallization of Photosensitive Energetic Copper(II) Perchlorate Complexes with the Nitrogen-rich Ligand 1,2-Di(1 <i>H</i> -tetrazol-5-yl)ethane	161
11.1. Abstract	161
11.2. Introduction	162
11.3. Results and Discussion	163
11.4. Conclusion	171
11.5. Experimental Section	171
11.6. References	174
12. Summary	177
12.1. Summary and Conclusion	177
12.2. References	184
Appendix	185
A1. Supporting Information Chapter 4	185
A2. Supporting Information Chapter 5	189
A3. Supporting Information Chapter 8	198
A4. Supporting Information Chapter 10	212
A5. Supporting Information Chapter 11	214
A6. Experimental Data of Unpublished Compounds	220
A7. Unpublished Results of Laser Initiation Experiments	222
A8. Unpublished Results of Detonator Capability Testing	223
A9. List of Abbreviations	225
A10. List of Publications	227

1. Introduction

1.1. History of Energetic Materials

Energetic materials (EMs) not only found use in military applications but also in civil ones like airbags, explosives in mining, signal ammunition or fireworks, just to name a few. However, it was a long way from the incidental discovery of black powder (a mixture of 75 % potassium nitrate, 15 % charcoal and 10 % sulfur) by the Chinese 220 B.C. to the manifold practical applications of energetic materials nowadays. It have been the English monk Roger Bacon and the German one Berthold Schwarz who started to investigate black powder in Europe at the end of the 13th and beginning of the 14th century.^[1] At the same time, the military use of black powder as explosive and gun propellant began. The next step in the development of EMs was the synthesis of nitroglycerin (NG) by the Italian Ascanio Sobrero in the year 1846. This was the cornerstone for the industrial synthesis of nitroglycerin (Figure 1) in the 19th century by the Swedish Nobel family (Immanuel and Alfred) whose name is familiar to many people.^[2] Alfred Nobel, the son of Immanuel, made the highly explosive and sensitive nitroglycerine manageable for application by mixing it with kieselguhr yielding the so-called Dynamite explosive. It was also A. Nobel who replaced black powder with mercury(II) fulminate (MF) to initiate Dynamite reliably although MF (Figure 1) was already described by the two alchemists Cornelius Drebbel and Johann Kunckel von Löwenstern in the 17th century.^[3] MF became one of the most used primary explosives with an annual production e.g. in Germany of 100,000 kg in the beginning of the 20th century. Later, it was replaced by lead azide (LA), which was firstly synthesized by Theodor Curtius 1891 and patented by Lothar Wöhler 1907 for use as initiating substance.^[4]

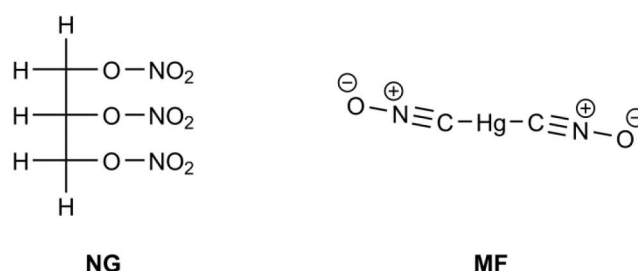


Figure 1. Molecular structures of NG and MF.

With the increasing demand for explosives, from the end of the 19th to the mid of the 20th century several more explosives (Figure 2) have been developed, e.g. nitroguanidine (NQ, 1877), trinitrotoluol (TNT, 1880), picric acid (PA, 1885–1888), triaminotrinitrobenzol (TATB, 1888), nitropenta (PETN, 1894), hexanitrostilbene (HNS, 1913), hexogen (RDX, 1920–1940), and octogen (HMX, 1943).^[1] Interestingly, some of them (like HNS, RDX,

PETN, or LA) are still in use and commercially produced on a large scale. Thus, RDX for example still represents the world's number one military secondary explosive.

During world war second, development of so-called polymer-bonded explosives (PBX) started to reduce the sensitivity and simplifying the manipulation by bounding an explosive powder into an inert matrix. One of the most prominent examples is SEMTEX (a mixture of PETN and RDX bonded with styrene-butadiene rubber), which was developed by the Czech Stanislav Brebera in the year 1966 and is still in use in modified forms.^[1,5]

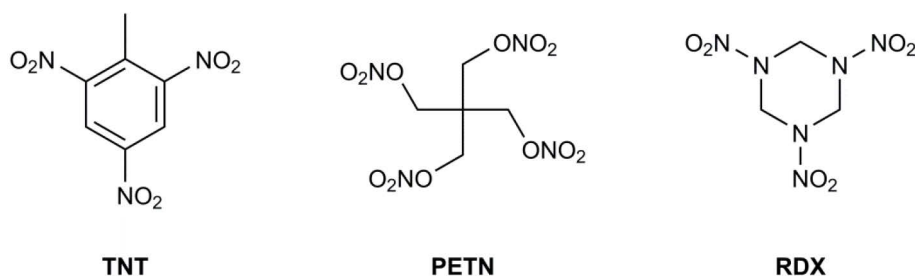


Figure 2. Molecular structures of TNT, PETN and RDX.

The recent development of new energetic materials not only deals with the safety and performance improvement of energetic materials, it also makes great efforts to replace toxic and environmental hazardous substances. Thus, the development of energetic materials is an ongoing process and chemists of the 21th century are confronted with these challenges.

1.2. Classification of Energetic Materials

Energetic materials are a widespread class of chemical compounds and compositions. According to the definition of the American Society for Testing and Materials,^[6] energetic materials are defined as chemical compounds or compositions that contain both fuel and oxidizer and readily react under release of energy and gas.

Further, energetic materials can be classified into four subclasses: (i) primary explosives, (ii) secondary explosives, (iii) pyrotechnics, and (iv) propellants. Subsequent, the classes are explained in detail.

Primary Explosives: Primary explosives, or also called primaries, are substances which, in contrast to secondary explosives, undergo a fast deflagration-to-detonation transition (deflagration: propagation velocity of reaction front < sonic velocity in combusting medium; detonation: propagation velocity of reaction front > sonic velocity in combusting medium) after initiation by a non-explosive simple initiating impulse (SII) and by nature, exhibit an increased sensitivity toward mechanical, thermal or electrical stimuli (e.g. impact, friction, heat, electrostatic discharge).^[1,7] Typical primary explosives exhibit values for the impact sensitivity lower than 4 J, friction sensitivity lower than 10 N, and detonation velocity lower than 5000 m s⁻¹.^[1] While secondary explosives are more powerful and less sensitive than

primaries, they cannot be initiated in such a facile way and therefore, primary explosives are required. The shockwave produced by the primary explosive is able to initiate the secondary explosive which might be a booster or the main charge. Depending on the application, the primary explosive does not necessarily have to generate a shockwave. In case of priming charges, the primary serves as sensitizer and allows the ignition of e.g. a propellant by flame without detonation. Hence, it is also necessary to further classify the term primary into: (i) real primary explosives which detonate and produce shockwaves, and (ii) priming compositions which are deflagrating substances that can contain a primary explosive for sensitization.^[7a] However, priming charges do not always consist of a primary explosive. Pyrotechnic mixtures can be simply initiated and producing a flame, too. Examples for real primary explosives (Figure 3) are lead azide (LA), lead styphnate (LS), diazodinitrophenol (DDNP) and triacetone triperoxide (TATP). Examples for currently used primary containing priming compositions are SINOXID ("sine oxid"; containing LS, tetrazene, barium nitrate, antimony trisulfide, lead oxide and calcium silicide) and SINTOX ("sine toxicum"; containing DDNP, zinc peroxide, titanium powder and tetrazene).^[8] Earlier, priming compositions on the basis of MF and potassium chlorate were used.^[7a]

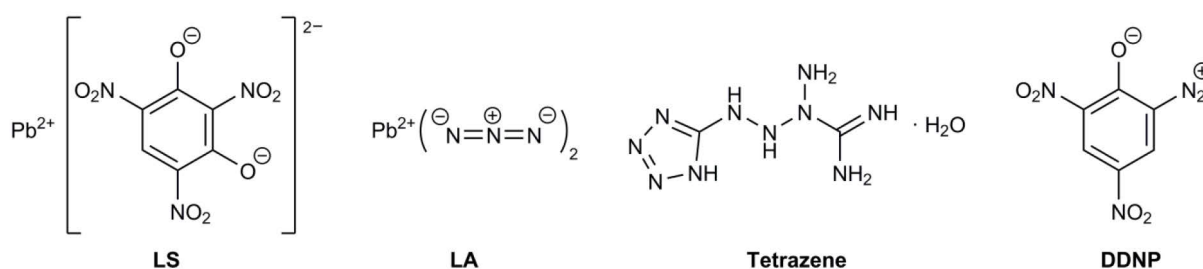


Figure 3. Molecular structures of LS, LA, tetrazene and DDNP.

Secondary Explosives: In contrast to primaries, secondary explosives are considerably less sensitive toward stimuli and commonly exhibit a better performance which means in detail a higher detonation velocity, heat of explosion, and detonation pressure. Typical secondary explosives exhibit values for the impact sensitivity higher than 4 J, friction sensitivity higher than 80 N, and detonation velocity in the range of 6500–9000 m s⁻¹.^[1,7b] But there are also exceptions like 2,4,6,8,10,12-hexanitrohexaazaisowurtzitane (CL-20), which exhibits a friction sensitivity of 48 N and a detonation velocity higher than 9000 m s⁻¹.

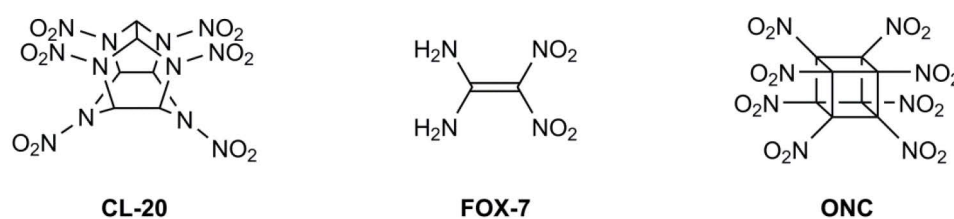


Figure 4. Molecular structures of the modern secondary explosives CL-20, FOX-7 and ONC.

Secondary explosives can be further divided into booster explosives and high explosives according to the NATO AOP-7 publication.^[7b] The difference is that booster explosives are more simply to initiate and generally transmit and augment the shockwave from the primary explosive to the main charge. The typical booster explosive in applications is PETN. The main charge consists of a high explosive like RDX or HMX and cannot simply be initiated. High explosives are intensively investigated and recent examples (Figure 4) are 1,1-diamino-2,2-dinitroethene (FOX-7) and octanitrocubane (ONC).^[9]

Pyrotechnics: In general, pyrotechnics are energetic materials which consist of an oxidizing and a reducing component. In contrast to explosives, the reducing and oxidizing units are not necessarily combined within one molecule. Instead, pyrotechnics are traditionally compositions and depending on the application, can produce heat (e.g. igniter, delay compositions), light (e.g. signal ammunition, flares, fireworks), smoke (e.g. military smoke screens) and sometimes sound (e.g. firecrackers).^[1] In respect to the initiation of explosives, pyrotechnic ignition compositions play an important role in e.g. electric match type and pyrotechnic fuse type blasting caps (Figure 5). The pyrotechnical mixture is ignited by a simple initiating impulse (burning fuse, electric current) and produces a flame output which is able to initiate the primary explosive. Typical oxidizers used for igniters are potassium perchlorate, potassium nitrate, or barium oxide and metals like titanium, magnesium, zirconium, or boron serve as fuel.^[1,8]

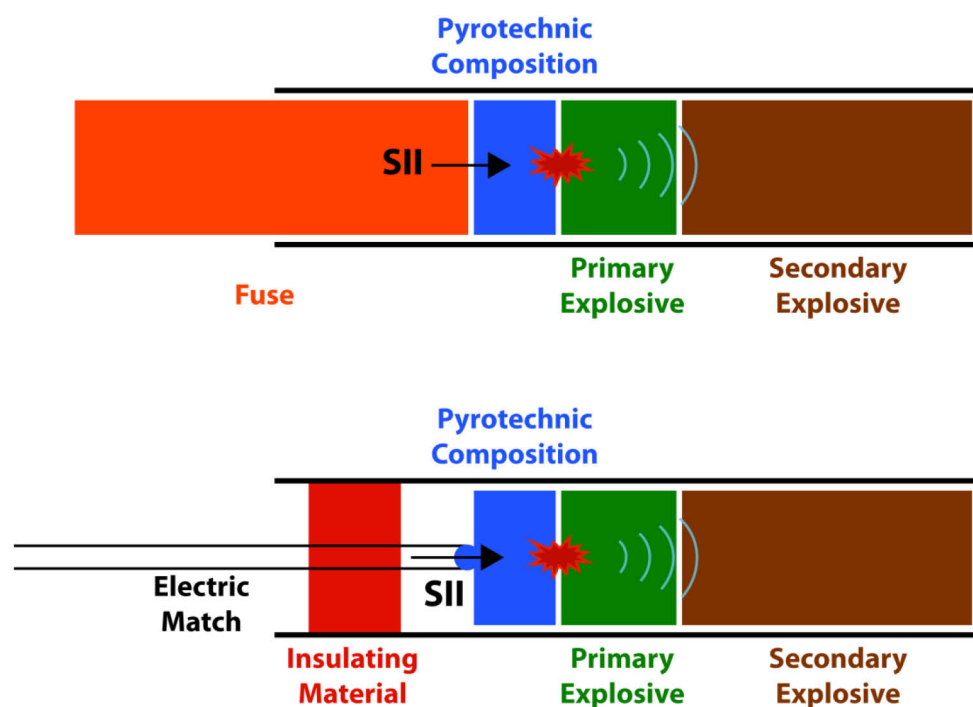


Figure 5. Schematic according literature of a fuse type (top) and electric match type (bottom) blasting caps using pyrotechnic composition as ignition charge.^[10]

Propellants: In contrast to explosives, propellants must not undergo a deflagration-to-detonation transition. Instead, propellants must exhibit a controlled combustion with reaction velocities in the range of a fast burning up to a deflagration (10^{-2} – 10^2 m s⁻¹).^[1] The important parameters for a propellant are the specific impulse and the combustion temperature. Propellants can be divided into gun propellants and rocket propellants. In the past, black powder was used as gun propellant but is replaced by single-based (nitrocellulose), double-based (nitrocellulose + nitroglycerine), and triple-based formulations (nitrocellulose + nitroglycerine + nitroguanidine) nowadays (Figure 6).^[1] Contrary, rocket propellants burn slower than gun propellants and can be further classified into solid and liquid propellants. A typical solid propellant consists of ammonium perchlorate (AP), aluminum (Al) and hydroxyl-terminated polybutadiene (HTPB) and is used e.g. in space shuttle solid rocket boosters.^[1] A typical liquid bipropellant (Figure 6) is nitrogen tetroxide (NTO) and monomethylhydrazine (MMH), which are hypergolic and react in combination. NTO and MMH are used in many orbital and deep space rockets.

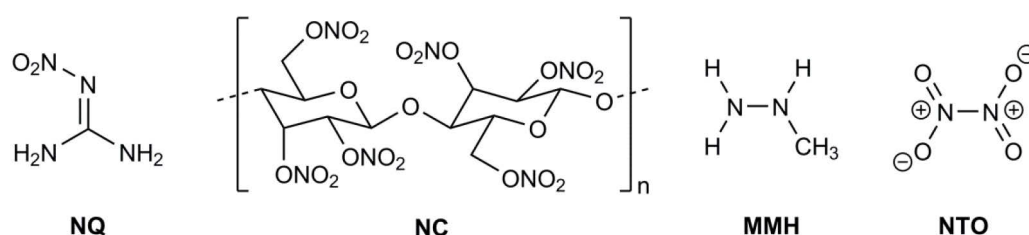


Figure 6. Molecular structures of NQ, NC, MMH and NTO.

1.3. Ignition and Initiation of Energetic Materials

As already mentioned briefly above, the ignition of energetic materials in general and the initiation of explosives in detail can occur in manifold ways.^[10] Depending on the output of the energetic material, the initiating system is called detonator (shockwave) or igniter (flame). The simplest method is the direct ignition by flame as it was already used in the past e.g. in form of the matchlock (15th to 17th century) to ignite black powder by a burning fuse. Flame as simple initiating impulse is still used to ignite energetic materials for example in fuse type blasting caps (see Figure 5 and 7, A).

Another method similar to flame as impulse is to ignite the explosive by heat (Figure 7, B + C). A bridgewire, which is heated by an electric current, is either in direct contact to the primary explosive (hot-wire initiator) or first to a pyrotechnical composition which then initiates the primary explosive by flame. This second type, called electric match, is the most common initiation method in blasting caps (Figure 5) worldwide. However, there is also a detonator type known which achieves detonation without a primary explosive. This type of detonator is called NPED (Non Primary Explosives Detonator)^[11] and uses the ability of

PETN to undergo a DDT after ignition by a pyrotechnic composition. NPEDs also represent a form of electric match type detonators but provide a higher degree of safety due to the absence of the sensitive primary explosive.

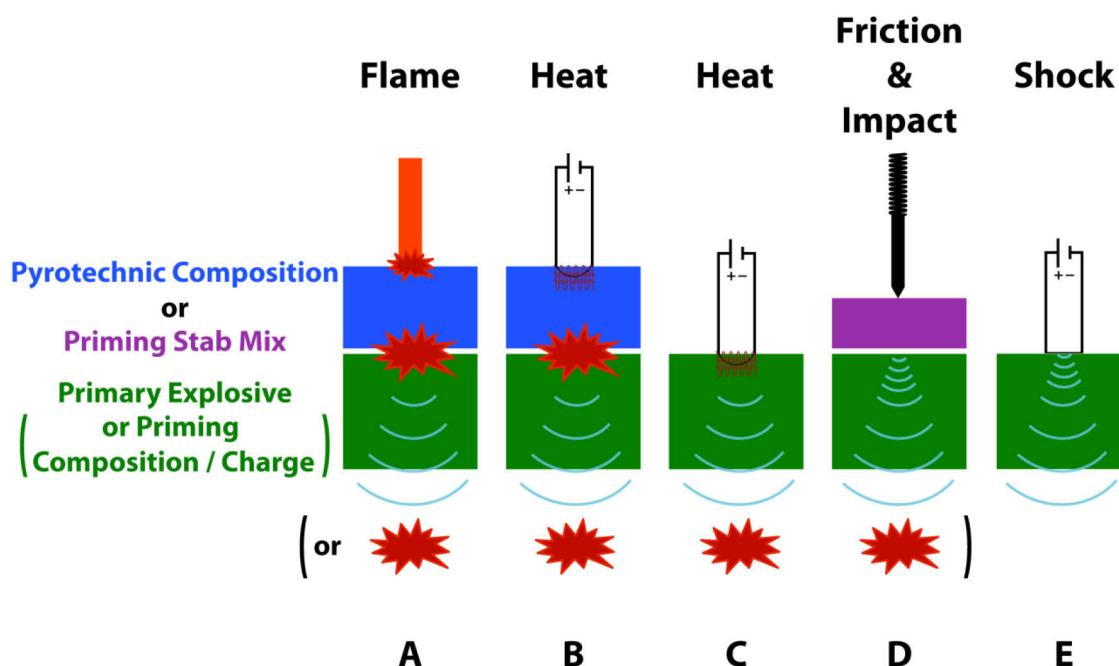


Figure 7. Schematic representation of common initiation and ignition methods for energetic materials. A) Fuse type. B) Electric match type. C) Hot-wire type. D) Percussion / Stab type. E) Exploding-bridgewire type.

In contrast, the initiation of bombs and grenades, or the ignition of gun propellants is generally achieved by an impact or friction impulse (Figure 7, D). Independent of the desired output signal, the primary explosive or priming charge must exhibit a high sensitivity toward friction to ensure initiation reliability. However, it hinders the handling of the explosive and increases the risk of unintended initiation. For detonators like the M55 stab detonator,^[10,12] lead azide based formulations are commonly used for the stab mix followed by lead azide as primary explosive. While for percussion caps, which only deflagrate, lead styphnate based (SINOXID, NOL-60) and also lead-free (SINTOX) formulations are applied.^[8,10] Oftentimes, tetrazene is added to increase the friction sensitivity in order to achieve a better ignitability.

Exploding-bridgewire (EBW) and exploding foil initiators (EFI) are relatively safe and very reliable electric type initiators (Figure 7, E). During their work for the Manhattan Project, Luis Alvarez and Lawrence Johnston invented EBWs because of the need for a precise and high reliable detonator system.^[13] The initiating impulse is a shockwave which is formed by the explosion of a thin bridgewire. The gold or platinum wire is heated very fast by the passing high current (such high currents are supplied by low-inductance, high voltage capacitors). While the metal vaporizes, the electrical resistance of the bridgewire rises rapidly and the current decreases. However, still much current passes through the metal vapor of high

density and so heating is continued up to the point where inertia is overcome. Explosive expansion of the metal vapor is the result. Further effects amplify the shock.^[10] This shockwave finally initiates the secondary explosive which, in practical use, is PETN due to technical reasons. The advantage of EBWs over classic type detonators (e.g. hot-wire, stab) is their precise and consistent function time (variations of $\leq 0.1 \mu\text{s}$).

However, all of the above mentioned initiating systems have some disadvantages. Stab detonators or percussion caps contain extremely friction and impact sensitive materials. Thus, there exist a high risk of unintended initiation and handling of these materials is problematic. And the electric type detonators are susceptible toward electrostatic discharge, electromagnetic interference and corrosion.^[14] In case of the safe EBWs and EFIs, stray currents would not initiate the detonator but might damage it.^[10] Further, a disadvantage of EBWs and EFIs is the bulky size of the required power sources.

1.4. Laser Ignition and Initiation

Due to the disadvantages of conventional initiators, a new ignition and initiation method was introduced at the end of the 1960s and beginning of the 1970s. The first published laser initiation experiments were done by the Russian research group of Brish *et al.* and by the Americans Menichelli and Yang.^[15] Brish *et al.* successfully initiated samples of PETN and LA by laser irradiation. As radiation source a neodymium glass laser ($\lambda = 1060 \text{ nm}$) operating in the Q-switched mode was used. LA was initiated by a laser pulse with an output power of up to 10 MW, a pulse length τ of 0.1 μs , and an energy of 0.5 J.^[15a] The pulse had a power density (also called irradiance or radiant flux density) at the surface of the explosive sample of up to 8 MW cm^{-2} . For initiation of PETN, the laser beam had to be focused to increase the power density at the surface. Further investigations with a neodymium glass and an additional ruby laser ($\lambda = 694 \text{ nm}$) were made by Brish *et al.* and four possible initiation mechanisms discussed:^[15b]

- (i) Light impact which could be excluded because the exerted light pressure was several orders of magnitude lower than the required pressures for shock explosion.
- (ii) Electrical breakdown could not fully be excluded but did not fit to all observations during the laser initiation experiments. E.g. no differences in the initiation of explosives were observed for dielectrics and metal powders.
- (iii) Photochemical initiation could be explained by a multiquantum photoelectric effect but the probability for initiation was low and a dependency between the laser wavelength (1064 or 694 nm) and the initiation threshold was not observed. Thus, photochemical initiation does not seem to be the appropriate mechanism for laser initiation.
- (iv) Thermal initiation hypothesis explains all experimental results. The laser radiation heats the explosive and leads to an increase of pressure inside the sample. The rapid

heating of the sample results in an explosive decomposition described as a conversion of light energy into shockwave energy.

While Brish *et al.* directly irradiated the explosive sample with the laser beam, Menichelli and Yang coated a glass window with a 1000 Å thick aluminum film and irradiation of this film generated shockwaves by vaporization of the metal similar to the functionality of EBWs.^[15c,15d] The generated shockwave is able to directly initiate secondary explosives. In the work of Menichelli and Yang,^[15c] a Q-switched ruby laser was successfully used ($E = 0.8$ to 4.0 J; $\tau = 25$ ns) to initiate PETN, RDX, and tetryl.

However, the practical use of these solid-state lasers (ruby and neodymium glass) was limited because of their large size. The advent of commercially available laser diodes (electrically pumped semiconductor laser) afforded new possibilities in the initiation and ignition of energetic materials,^[14a] although solid-state lasers were and are still used for investigations concerning the laser initiation of EMs. One of the first reports on diode laser ignition of explosives and pyrotechnics was published by Kunz and Salas in 1988. A GaAlAs diode laser with a power of 1 W, a wavelength of 830 nm, and a pulse duration of 2–10 ms was used to thermally ignite pentaammine(5-cyano-2H-tetrazolate)cobalt(III) perchlorate (CP, Figure 9) and a pyrotechnic mixture of titanium and potassium perchlorate (Ti/KClO₄).^[16] Contrary to the experiments of Brish *et al.* and Menichelli and Yang,^[15a-c] the laser beam was directly coupled to the explosive's surface by an optical fiber (core diameter of 100 μm) and not focused. CP and Ti/KClO₄ were tested upon laser irradiation in a pure and in a doped (carbon black, graphite and laser dye) form. Additionally, various particle sizes and compressed densities were investigated. In the work of Kunz and Salas, it was shown that the laser ignition threshold is strongly influenced by the absorptance of the energetic materials.^[16] Thus, CP exhibited a considerable lower absorptance at 830 nm than the Ti/KClO₄ mixture and therefore a higher energy was necessary for ignition (Ti/KClO₄: $E_{\text{crit.}} = 3$ mJ; CP: $E_{\text{crit.}} = 6$ –7 mJ). Doping CP with 0.8 % carbon black resulted in a similar absorptance ($\alpha \approx 0.8$) to Ti/KClO₄ and also the critical energy could be decreased to a Ti/KClO₄ similar value of 3 mJ. Additionally, absorptance measurements demonstrated that the particle size and pressed powder density influences the absorptance (α increases with a decrease of particle size and an increase of density) although the effect on the ignition threshold is low. One reason could be that an increasing density also increases the thermal conductivity and related to it the ignition threshold. Although the diode laser systems are relatively cheap, small in size and offer a significant higher safety over electric type ones, laser diodes provided a considerably lower output power than the solid-state lasers. Consequential, laser diode ignition exhibited long function times and was not suitable as replacement for fast-functioning electric type initiators like EBWs in the past.

Various further experiments with laser radiation as ignition and initiation source were conducted since the seventies. For example, the ignition of propellants,^[17] various pyrotechnic mixtures and metastable intermolecular composites (MICs),^[17b,18] the effects of the laser wavelength, gas pressure or dopants on the initiation thresholds,^[19] the development of laser initiated detonators,^[20] as well as a fundamental understanding of the initiation mechanism were investigated.^[14a,21] Remarkably is the development of a NPED which was successfully initiated by laser irradiation.^[20e] The presented NPED uses the principle of flying plate detonators and consists of a PETN/graphite/Al mixture as lasersensitive ignition charge. The ignition charge drives a thin metal plate (called flying plate) which initiates low density PETN ($\rho = 0.7 \text{ g cm}^{-3}$) by shock. This charge is followed by two further charges of higher density (PETN with a density of 1.0 g cm^{-3} and RDX with a density of 1.6 g cm^{-3}). A schematic of the setup is shown in Figure 8. Although no values are given for this detonator in the publication, it can be expected that the function times are in the range of milliseconds.

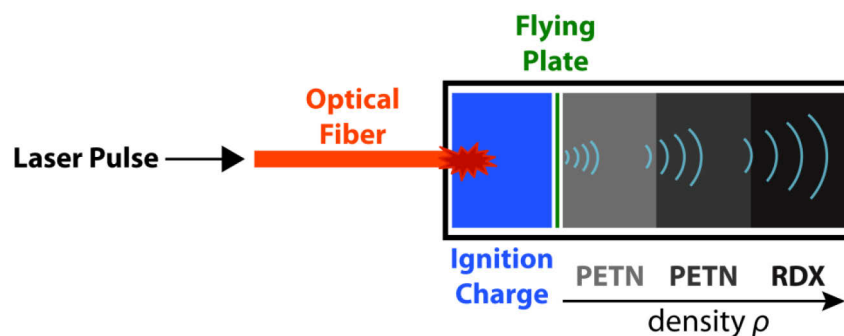


Figure 8. Schematic representation of the laser initiated NPED.

Other recent investigations deal with energetic coordination compounds (ECCs) which exhibit a high sensitivity toward laser irradiation. The investigations of ECCs on their behavior toward laser irradiation started with CP and its promising replacement tetraammine-*cis*-bis(5-nitro-2*H*-tetrazolato- N^2)cobalt(III) perchlorate (BNCP).^[16,22] BNCP (Figure 9 and Scheme 1) was already reported to exhibit initiating capabilities by Bates in 1986.^[23] Since that time BNCP was extensively investigated as initiating explosive suitable to undergo fast DDT after ignition by electric devices or laser irradiation. BNCP exhibits excellent energetic properties. E.g. a detonation velocity of 8.1 km s^{-1} was calculated for BNCP at a density of 1.97 g cm^{-3} .^[24] With the advent of more powerful diode lasers, the ignition delay times of BNCP could be decreased considerably and excellent values of 4–5 μs were possible.^[14a,20b,22a]

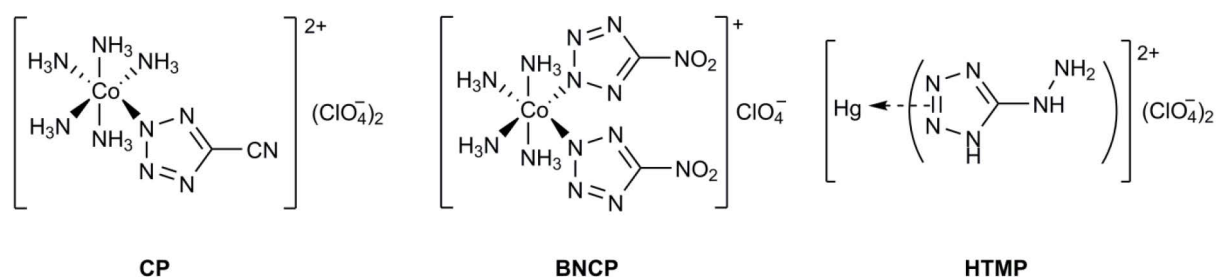
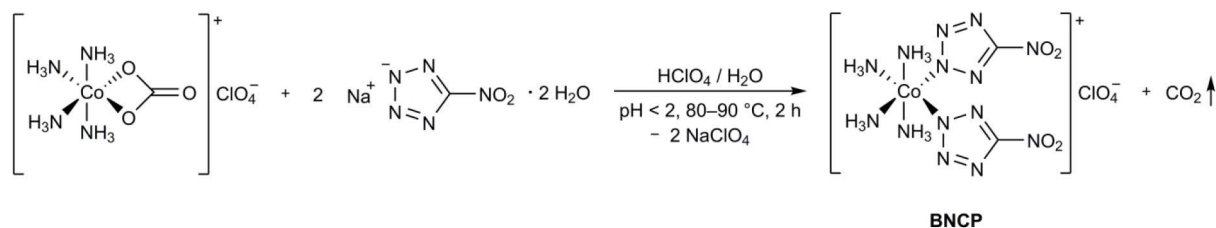


Figure 9. Molecular structures of the prominent laser ignitable explosives CP, BNCP, and HTMP.

At the beginning of the 21st century, Zhilin *et al.* investigated BNCP and some BNCP analogue tetraamminecobalt(III) perchlorate complexes with 1*H*-tetrazolate, 5-methyl-1*H*-tetrazolate, 5-amino-1*H*-tetrazolate, 5-nitriminotetrazolate, 1,5-diamino-1*H*-tetrazole, and 5-amino-1-methyl-1*H*-tetrazole as ligand upon laser irradiation ($\tau = 2$ ms, $E = 1.5$ J, $\lambda = 1064$ nm).^[24] Only the complexes with 5-nitro-2*H*-tetrazolate, 5-amino-1*H*-tetrazolate, and 1,5-diamino-1*H*-tetrazole as ligand detonated after initiation by laser irradiation while the others only combusted or even could not be ignited.^[24]



Scheme 1. Synthesis of BNCP according to literature.^[25]

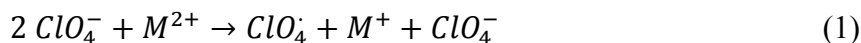
In order to obtain short ignition delay times, dopants are necessary to increase the absorbance of CP, BNCP, or its analogue cobalt(III) complexes in the near infrared.^[16,22a,24] Therefore, explosives with a higher self-absorbance have been investigated. One class of explosives which exhibit a high sensitivity toward laser irradiation is represented by metal complexes with various hydrazinoazoles as ligand.^[26] The advantage of this ligand type is the high positive enthalpy of formation for the azole combined with the low ionization potential of the hydrazine moiety. The following hydrazinoazoles have been investigated as ligands of mercury(II) perchlorate complexes: 3-hydrazino-5-aminopyrazole, 3-hydrazino-5-aminopyrazolone, 3-hydrazino-4-amino-1,2,4-triazole, 3-hydrazino-4-amino-5-methyl-1,2,4-triazole, 3-hydrazino-4-amino-5-mercapto-1,2,4-triazole and 5-hydrazino-1*H*-tetrazole.^[26] The 5-hydrazino-1*H*-tetrazolemercury(II) perchlorate (HTMP, Figure 9) coordination compound exhibited the highest sensitivity towards laser irradiation ($\tau = 30$ ns, $E = 1 \cdot 10^{-5}$ J) of the investigated azoles (e.g. 3-hydrazino-4-aminopyrazole: $\tau = 30$ ns, $E = 2.8 \cdot 10^{-4}$ J). Based on these results, four metal(II) perchlorate complexes ($M = \text{Co, Ni, Co, Cd}$) of the form $[\text{M}(\text{HATr})_2](\text{ClO}_4)_2$ with 3-hydrazino-4-amino-1,2,4-triazole (HATr) as ligand were synthesized and tested toward laser irradiation.^[27] All complexes were successfully initiated

and the critical initiation energies determined. A correlation between the initiation energy and the ionization potential was suggested to explain the order of the following values:^[27]

$$E: \text{Cu} (1.1 \cdot 10^{-5} \text{ J}) < \text{Cd} (5.03 \cdot 10^{-4} \text{ J}) < \text{Ni} (5.75 \cdot 10^{-4} \text{ J}) < \text{Co} (1.36 \cdot 10^{-3} \text{ J})$$

$$I_1+I_2: \text{Cu} (28.02 \text{ eV}) > \text{Cd} (25.90 \text{ eV}) > \text{Ni} (25.78 \text{ eV}) > \text{Co} (24.92 \text{ eV})$$

A mechanism (equation 1 and 2) for the initial stages in decomposition of the above mentioned compounds was claimed by Ilyushin *et al.*:^[27]



A highly active perchlorate radical is formed by a laser induced redox reaction between the metal cation and the anion. This radical subsequently oxidizes the organic ligand. The more noble metal cations (higher ionization potential) can easier be reduced. The suggested mechanism explains, in agreement with the experimental data, how the ionization potential of the central metal influences the initiation energy threshold and it fits to a thermal mechanism described by numerous researchers.^[14a,15b,21b,22a]

Concluding the results of the investigations carried out so far, the laser initiation seems to be a thermal mechanism although the mechanism itself and the influencing parameters are not completely understood up to the present.^[14a,15b,21b,22a] E.g. Ilyushin *et al.* described that it seems there is no dependence between optical properties and the laser initiation threshold for various cobalt(III) complexes, which is unexpected for a thermal process.^[26] A thermal initiation mechanism means that laser light is absorbed and converted into heat by e.g. internal conversion.^[28] At lower laser powers in the order of 10^{-1} – 10^1 W, the explosives undergo a DDT after being heated up to the auto-ignition temperature.^[22a] According to literature,^[22a] the explosive is shock initiated at higher power (approximately 10^2 W and more) and DDT no longer occurs. Hafenrichter *et al.* described four regimes for the laser initiation depending on the surface power density (irradiance):^[14a]

Region I: The power density is low and steady state temperature is reached before auto-ignition → no ignition occurs.

Region II: The power density is higher (kW cm^{-2}) and ignition occurs although a significant amount of energy is conducted away due to thermal conductivity of the materials → slow ignition delay times in the order of milliseconds.

Region III: At even higher power densities (MW cm^{-2}) the auto-ignition temperature is reached fast before large amounts of heat are conducted away → decreasing ignition delay times in the order of microseconds.

Region IV: At extremely high power densities (GW cm^{-2}), the explosive is shock initiated by laser ablation of the surface → ignition delay times in the order of nanoseconds.

While Region II can be compared with the hot-wire initiation of primary explosives or pyrotechnic compositions, the laser power densities in Region IV also make it possible to directly shock initiate secondary explosives by laser irradiation.^[29] The laser power densities of Region IV are achieved by solid-state lasers with laser powers of 100 W and more. In contrast, laser diodes (~1–10 W) only provide power densities which fall in the Regions II and III. However, more powerful laser diodes were developed gradually and therefore, laser diode initiators (LDI) become more and more attractive for applications due to the small sizes and low costs of the diodes.

All in all, laser initiation provides several advantages compared to the conventional initiation by electric devices.^[17b] However, it has to be separated between hot-wire, exploding-bridgewire and exploding foil initiators. A comparison of the electric type and typical laser type (e.g. Nd:YAG [$\text{Y}_{2.97}\text{Nd}_{0.03}\text{Al}_5\text{O}_{12}$] solid-state laser and GaAlAs or InGaAs diode laser)^[30] initiators is given in Table 1. Subsequent, the advantages and disadvantages are discussed according to literature.^[10,13b,14a,17b,22a]

Table 1. Comparison of electric and laser type detonators.

Parameter	Hot-wire ^[13b]	EBW ^[13b]	EFI ^[13b]	Nd:YAG laser ^[30]	Diode laser ^[31]
Current [A]	5	500	3000	10^1 – 10^2 ^[a]	10
Voltage [V]	20	500	1500	10^0 – 10^2 ^[a]	2
Power [W]	1	10^5	$3 \cdot 10^6$	$\geq 10^2$	1–10
Function time [s]	10^{-3}	10^{-6}	10^{-7}	10^{-7} – 10^{-6}	10^{-6} – 10^{-3}
Initiating charge	LA, LS, PETN	PETN	PETN, HNS	PETN, RDX, HMX, tetryl	BNCP, CP, pyrotechnic mixtures

[a] Current and voltage depends on the used laser pumping source (e.g. flash lamp, arc lamp, laser diode).

Hot-wire initiators are cheap in production and one of the most manufactured initiator. Hot-wires are operated with low current (~ 5 A) and voltage (~ 20 V) and therefore, only a small current source is necessary. On the other side, hot-wires are susceptible toward unintended initiation by electric impulses, e.g. electrostatic discharge, because of their low threshold and in addition, primary explosives (sensitive toward thermal and mechanical stimuli) are required for generation of a shockwave. Depending on the application, the slow and less consistent function times in the range of milliseconds can be neglected. EBWs and EFIs exhibit considerably faster function times with very minor standard deviations (down to 25 ns). Further, these two types of detonators do not consist of a primary explosive which highly increases the safety. But a main disadvantage of the EBWs and EFIs is the bulky size of their power sources and the required heavy cables making them inapplicable for many applications. Laser ignition and initiation therefore provides some advantages like the high isolation of the energetic material which cannot be achieved by electric type detonators. Unintended initiation by electric impulses is nearly not possible because the induced currents

are not able to produce a laser pulse exceeding the initiation energy threshold.^[22a] Further, a bridgewire which is susceptible to corrosion is missing, too, and therefore, considerably decreases the risk of failures in initiation. Further, the required currents for laser initiation are in the range of hot-wire detonators but the function times can achieve values of EBWs. In addition, the direct initiation of secondary explosives (e.g. RDX) by solid-state lasers offers new possibilities and increases the safety considerably.

Although solid state-lasers provide a considerable higher output power and therefore, can be used similar to the functionality of EBWs and EFIs, the configuration is relatively large compared to diode lasers. Standard diode lasers are only several millimeters in size and exhibit relative low costs making them suitable for applications.

Concluding these aspects and advantages, the laser initiation of explosives by laser diode radiation seems to be a very attractive and forward-looking initiation method. However due to the limited power of laser diodes, the explosives might be thermally ignited and undergo a DDT in contrast to the direct shock initiation by high-power solid-state laser radiation. The operating mode of laser diode initiators can be compared to that of electric hot-wires but with faster function times as demonstrated by literature.^[14a,22a]

1.5. Motivation and Objective

Although laser ignition and initiation was intensively investigated in the past, there is still a gap in knowledge. Consequently, the objective of this thesis was to systematically investigate the ignition and initiation of new and literature known explosives by diode laser irradiation. As it was shown in literature,^[16,22,26,32] energetic coordination compounds (ECCs), especially with azoles and hydrazine derivatives as ligands, represent potential photosensitive materials. With their advantage of allowing selective design, since the metal center, energetic ligand and oxidizing anion can be varied; the possibility for developing energetic materials with specific and targeted properties (e.g. high performance, short ignition delay times, high thermal and mechanical stability, environmental acceptability, high photosensitivity) is given.^[33] On the basis of similar complex structures, the influence of the metal center, ligand and anion on the laser initiation threshold should be investigated and trends formulated. This should also help to get new information about the relevant parameters for the laser initiation threshold and its dependency on optical properties. Further, the influence of light absorbing (e.g. carbon black or graphite) and scattering additives (e.g. magnesium oxide) on the initiation threshold was tested to verify the literature claimed thermal initiation mechanism.

For safety improvements of conventional laser-ignited DDT detonators, replacements, which are less sensitive toward mechanical stimuli, should be developed for the two standard explosives CP and BNCP. The replacements should achieve the requirements for a booster-explosive according to the NATO AOP-7 classification:^[7b]

- Impact sensitivity (IS): > 3 J.
- Friction sensitivity (FS): > 80 N.
- Thermal stability: $T_{\text{dec}} > 180$ °C.

Short function times (10^{-6} – 10^{-5} s) should be realized in combination with a maximum laser output power of 25 W at a maximum pulse length of 600 μs . Further, the explosive has to be capable to undergo DDT in a short time and generate a shockwave which is able to initiate a secondary explosive preferably RDX or HMX. In general, the potential replacement should be non-toxic and environmentally acceptable. Compounds which contain heavy metals or toxic moieties were only investigated due to academic interest.

Additionally, the investigated explosives should be tested on their potential use as environmentally acceptable replacements for lead containing primary explosives in conventional initiators e.g. percussion caps, blasting caps and stab detonators.

1.6. References

- [1] T. M. Klapötke, *Chemie der hochenergetischen Materialien*, 1. ed., Walter de Gruyter, Berlin, New York, **2009**.
- [2] http://www.nobelprize.org/alfred_nobel/biographical/articles/life-work/index.html (accessed July 21, **2014**).
- [3] W. Beck, J. Evers, M. Göbel, G. Oehlinger, T. M. Klapötke, *Z. Anorg. Allg. Chem.* **2007**, *633*, 1417–1422.
- [4] a) T. Curtius, *Ber. Dtsch. Chem. Ges.* **1891**, *24*, 3341–3349; b) L. Wöhler, *DE 196824*, March 2, **1907**.
- [5] <http://www.explosia.cz/en/?show=semtex> (accessed July 21, **2014**).
- [6] <http://www.astm.org/> (accessed July 21, **2014**).
- [7] a) R. Matyáš, J. Pachman, *Primary Explosives*, 1. ed., Springer, Heidelberg, New York, Dordrecht, London, **2013**; b) NATO Allied Ordnance Publication 7 - Edition 2, June, **2003**.
- [8] J. Köhler, R. Meyer, A. Homburg, *Explosivstoffe*, 10. ed., Wiley-VCH, Weinheim, New York, Chichester, Brisbane, Singapore, Toronto, **2008**.
- [9] T. M. Klapötke, A. J. Bellamy, S. Zeman, R. D. Chapman, R. P. Singh, H. Gao, J. M. Shreeve, *High Energy Density Materials*, Springer, Berlin, Heidelberg, **2007**.
- [10] P. W. Cooper, *Explosives Engineering*, Wiley-VCH, New York, Chichester, Weinheim, Brisbane, Singapore, Toronto, **1996**.
- [11] http://www.oricaminingservices.com/de/de/product/products_and_services/initiating_systems/page_initiating_systems/dynadet-c2-25ms/918 (accessed July 23, **2014**).

- [12] N. Mehta, K. Oyler, G. Cheng, A. Shah, J. Marin, K. Yee, *Z. Anorg. Allg. Chem.* **2014**, *640*, 1309–1313.
- [13] a) J. Coster-Mullen, *Atom Bombs: The Top Secret Inside Story of Little Boy and Fat Man*, J. Coster-Mullen, **2002**; b) R. Varosh, *Propellants, Explos., Pyrotech.* **1996**, *21*, 150–154.
- [14] a) E. S. Hafenrichter, B. W. Marshall, K. J. Fleming, *41st Aerospace Sciences Meeting and Exhibit*, Reno, USA, January 6–9, **2003**; b) J. E. Kennedy, *Spie 6287, Optical Technologies for Arming, Safing, Fuzing, and Firing II, 628708*, San Diego, USA, August 13, **2006**, 628708/1–628708/9.
- [15] a) A. A. Brish, I. A. Galeeva, B. N. Zaitsev, E. A. Sbimev, L. V. Tararinstev, *Fiz. Goreniya Vzryva* **1966**, *2*, 132; b) A. A. Brish, I. A. Galeeva, B. N. Zaitsev, E. A. Sbimev, L. V. Tararinstev, *Fiz. Goreniya Vzryva* **1969**, *5*, 475; c) L. C. Yang, V. J. Menichelli, *Appl. Phys. Lett.* **1971**, *19*, 473–475; d) L. C. Yang, J. Menichelli, *US 3812783*, May 28, **1974**.
- [16] S. C. Kunz, F. J. Salas, *13th International Pyrotechnics Seminar*, Grand Junction, USA, July 11–15, **1988**, 505–523.
- [17] a) T. Sofue, A. Iwama, *Propellants Explos.* **1979**, *4*, 98–106; b) L. deYong, T. Nguyen, J. Waschl, *Laser ignition of explosives, pyrotechnics and propellants*, Defence Science and Technology Organisation, . Canberra, Australia, **1995**; c) L. Strakovskiy, A. Cohen, R. Fifer, R. Beyer, B. Forch, *Laser Ignition of Propellants and Explosives*, ARL-TR-1699, Army Research Laboratory, Aberdeen Proving Groud, **1998**.
- [18] a) H. Östmark, N. Roman, *J. Appl. Phys.* **1993**, *73*, 1993–2003; b) R. Zhang, Y. Xue, J.-c. Jiang, X.-R. Lei, *33rd International Pyrotechnics Seminar*, Fort Collins, USA, July 16–21, **2006**, 787–792.
- [19] a) H. Östmark, R. Graens, *J. Energ. Mater.* **1990**, *8*, 308–322; b) H. Östmark, M. Carlson, K. Ekvall, *J. Energ. Mater.* **1994**, *12*, 63–83; c) G. Damamme, V. M. Lisitsyn, D. Malis, V. P. Tsipilev, *Condens. Matter* **2010**, 1–14; d) V. M. Lisitsyn, V. P. Tsipilev, G. Damamme, D. Malis, *Fiz. Goreniya Vzryva* **2011**, *47*, 106–116.
- [20] a) W. J. Kass, L. A. Andrews, C. M. Boney, W. W. Chow, J. W. Clements, J. A. Merson, F. J. Salas, R. J. Williams, *2nd NASA Aerospace Pyrotechnic Systems Workshop*, Albuquerque, USA, **1994**; b) E. S. Hafenrichter, B. Marshall, Jr., K. J. Fleming, *29th International Pyrotechnics Seminar*, Westminster, USA, July 14–19, **2002**, 787–793; c) A. Akinci, K. Thomas, A. Munger, L. Nunn, S. Clarke, M. Johnson, J. Kennedy, D. Montoya, *Proc. SPIE-Int. Soc. Opt. Eng.* **2005**, *5871*, 587109/1–587109/7; d) H. Moulard, E. Fousson, A. Ritter, J. Mory, *37th International Pyrotechnics Seminar*, Reims, France, May 17–19, **2011**, 348–356; e) J. G. Du, H. H. Ma, Z. W. Shen, *Propellants, Explos., Pyrotech.* **2013**, *38*, 502–504.
- [21] a) A. V. Chernai, *Fiz. Goreniya Vzryva* **1996**, *32*, 11–19; b) N. K. Bourne, *Proc. R. Soc. A* **2001**, *457*, 1401–1426; c) E. D. Aluker, A. G. Krechetov, A. Y. Mitrofanov, D. R. Nurmukhametov, M. M. Kuklja, *J. Phys. Chem. C* **2011**, *115*, 6893–6901; d) V. K. Golubev, **2012**, 591–598.

- [22] a) J. A. Merson, F. J. Salas, J. G. Harlan, *19th International Pyrotechnics Seminar*, Christchurch, New Zealand, Februar 21–25, **1994**, 191–206; b) J. W. Fronabarger, W. B. Sanborn, T. Massis, *22nd International Pyrotechnics Seminar*, Fort Collins, USA, July 15–19, **1996**, 645–652.
- [23] L. R. Bates, *Proc. Symp. Explos. Pyrotech.* **1986**, *13th*, III1–III10.
- [24] A. Y. Zhilin, M. A. Ilyushin, I. V. Tselinskii, A. S. Kozlov, I. S. Lisker, *Russ. J. Appl. Chem.* **2003**, *76*, 572–576.
- [25] A. Y. Zhilin, M. A. Ilyushin, I. V. Tselinskii, A. S. Brykov, *Russ. J. Appl. Chem.* **2001**, *74*, 99–102.
- [26] M. A. Ilyushin, I. V. Tselinsky, I. A. Ugryumov, A. Y. Zhilin, A. S. Kozlov, *6th New Trends in Research of Energetic Materials Seminar*, Pardubice, Czech Republic, April 22–24, **2003**, 146–152.
- [27] I. A. Ugryumov, M. A. Ilyushin, I. V. Tselinskii, A. S. Kozlov, *Russ. J. Appl. Chem.* **2003**, *76*, 439–441.
- [28] M. Hesse, H. Meier, B. Zeeh, *Spektroskopische Methoden der organischen Chemie*, 7. ed., Thieme, Stuttgart, New York, **2005**.
- [29] D. L. Paisley, *9th International Symposium on Detonation*, Portland, USA, **1989**, 1110–1117.
- [30] J. Eichler, H. J. Eichler, *Laser: Bauformen, Strahlführung, Anwendungen*, 7. ed., Springer, Heidelberg, Dordrecht, London, New York, **2010**.
- [31] http://www.lasercomponents.com/fileadmin/user_upload/home/Datasheets/real-light/915nm-980nm/g9xx-10wf-02bck-r.pdf (accessed July 30, **2014**).
- [32] M. Joas, Master Thesis, Ludwig-Maximilian University (Munich), **2011**.
- [33] V. P. Sinditskii, V. V. Seurshkin, *Defence Science Journal* **1996**, *46*, 371–383.

2. Setup

2.1. Laser Ignition Setup

The laser ignition experiments were performed with two different InGaAs laser diodes (Parameters see Table 1) of different output power. The laser diodes were operated in a single-pulsed mode and directly coupled to an optical fiber. The fiber had a core diameter of 105 μm , a cladding diameter of 125 μm and a buffer diameter of 250 μm . The optical fiber was connected via a ST type connector, with a 2.5 mm ceramic ferrule, either directly to the top of the sample and fixed with an optical two component adhesive (methylene-4,4'-diphenyldiglycidylether and polyoxypropylenediamine) as sealing (Figure 1, A), or to a sealing sapphire glass plate ($h = 0.2$ mm), which was placed between the ferrule and the sample pellet (Figure 1, B).

Table 1. Operating parameters of the laser diodes.

Parameter	LD1	LD2
Current I_{max} [A]	17	12
Voltage U [V]	~ 1.9	~ 5.5
Theor. output power P_{max} [W]	12	25
Exp. radiant power $\Phi_{\text{e,max}}$ [W]	12	20
Irradiance $E_{\text{e,max}}$ [kW cm^{-2}]	~ 139	~ 231
Theor. energy E_{max} [mJ]	1.2	15
Exp. energy E_{max} [mJ]	~ 1.2	$\sim 7.5^{\text{[a]}}$
Wavelength λ [nm]	940	940
Pulse length τ_{max} [s]	100	600

[a] The theoretical maximum energy E_{max} could not be achieved for the 25 W diode because of the limited capacity of the capacitor. The power of the capacitor decreased considerably with increasing pulse length.

The sample pellets were placed into an aluminum cap and the cap fixed with adhesive on aluminum witness plates ($L \times W \times H$: $50 \times 50 \times 5$ mm³), which had a small drill hole in the middle ($d = 2$ mm). An optical fiber could be placed into the hole for detection of the optical output signal (light flash). The sample pellets were prepared by two methods:

- (i) A small amount (~ 0.2 g) of the energetic material (< 100 μm) was carefully pestled with a defined amount of polytetrafluoroethylene or polyethylene as binder. Optional, a light absorbing or scattering additive was added.
- (ii) A larger amount (~ 1 g) of the energetic material was added to a boiling solution of polyethylene in *n*-hexane under vigorous stirring. Following, the suspension was cooled to room temperature under stirring and the solid filtered off. Optional, a light absorbing or scattering additive was added

Subsequent, the dry samples ($m = 155\text{--}200$ mg) were pressed to cylindrical pellets of 7.5 mm in diameter and an average height of 2.8–3.0 mm. A defined pellet density was obtained by varying the pressing power.

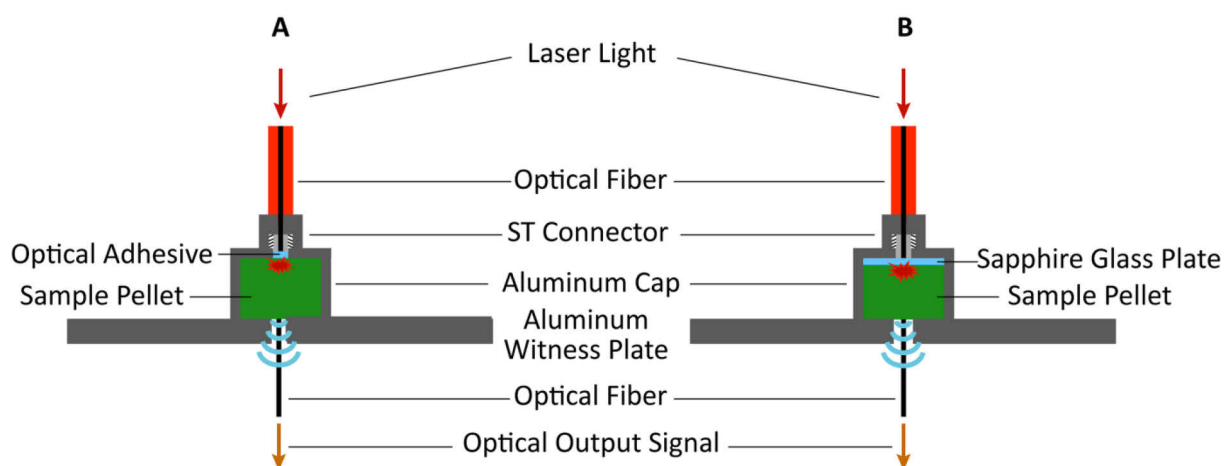


Figure 1 Schematic representation of the laser initiation setup. A) Optical adhesive as sealing. B) Sapphire glass plate as sealing.

Another setup for fast preliminary investigations is shown in Figure 2. The sample powder (without binder) was hand-tight pressed into a glass tube ($l = 20$ mm, $d = 3.0$ mm). The ceramic ferrule of the optical fiber was directly placed on top of the sample without any sealing. The ST connector of the fiber was fixed with adhesive to the glass tube.

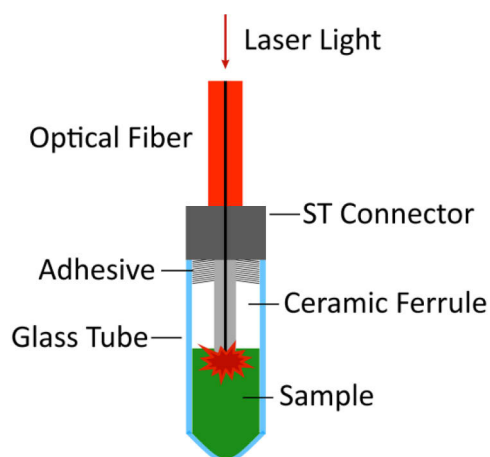


Figure 2. Schematic representation of the setup for preliminary laser investigations.

To reduce noise exposure and health hazards, all ignition and initiation tests were performed in a sand-filled wood box (Figure 3, A). Holes were drilled into the cover of the wood box and connected by an air hose to the exhaust air system (Figure 3, B).



Figure 3. Test environment for laser initiation experiments. A) Open wood box filled with sand. B) Closed wood box connected to the exhaust air system.

2.2. Measurement of Function Time t_f

The function time and its consistency are important parameters to describe the quality of initiators. According to Cooper,^[1] "the total function time of an electric initiator is defined as the time from the beginning of the input electrical signal until the 'breakout' time at the business end of the device". This definition can be transferred to laser initiators with the adaption that the total function time is the time from the beginning of the irradiation to the "breakout" at the end of the device. The function time t_f (eq. 1) can be separated into (i) the ignition delay time t_i , which is the time from beginning of the irradiation to the beginning of decomposition reaction of the energetic material, and (ii) the transit time t_t for the propagation of the reaction zone until "breakout" at the end of the device. The function time t_f was determined by the setup shown in Figure 4.

$$t_f = t_i + t_t \quad (1)$$

From the ignition delay time, information about the laser ignitability of explosives can be obtained but it is more complicated to be measured than the function time. However, for slow ignition delay times and for fast transit times t_t (fast DDT), t_i can be nearly equated to t_f .^[2]

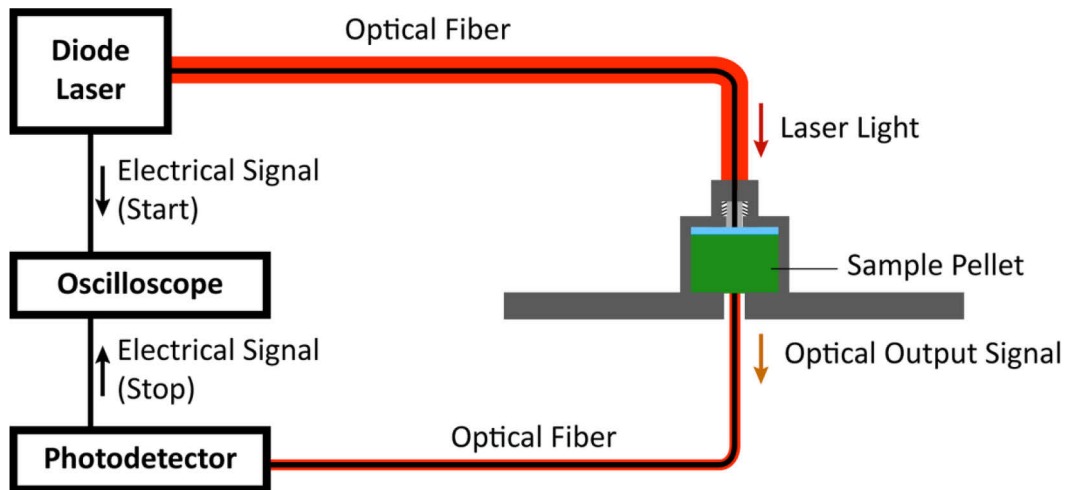


Figure 4. Schematic of the setup for determination of the function time t_f .

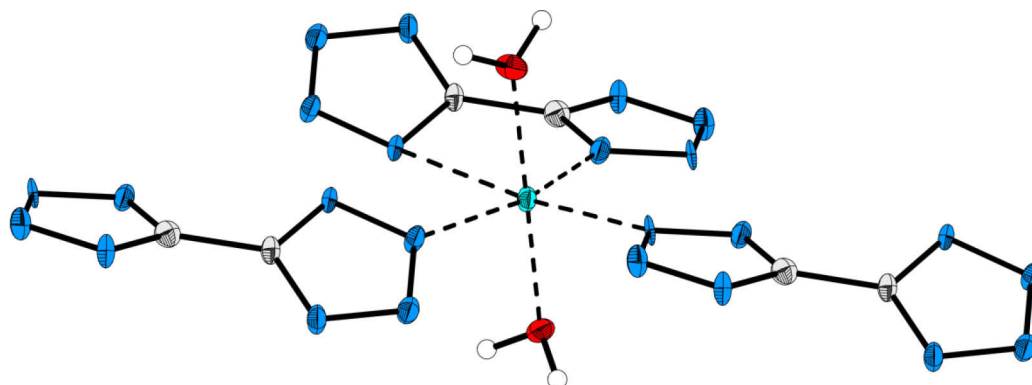
2.3. References

- [1] P. W. Cooper, *Explosives Engineering*, Wiley-VCH, New York, Chichester, Weinheim, Brisbane, Singapore, Toronto, **1996**.
- [2] E. S. Hafenrichter, B. W. Marshall, K. J. Fleming, *41st Aerospace Sciences Meeting and Exhibit*, Reno, USA, January 6–9, **2003**.

3. Preparation and Crystal Structure of Diaqua(μ -5,5'-bistetrazolato- $\kappa^4 N^1, N^2, N^5, N^6$)copper(II)

Reproduced with permission from M. Joas, T. M. Klapötke, J. Stierstorfer, *Crystals* **2012**, *2*, 958–966. Online: <http://www.mdpi.com/2073-4352/2/3/958>.

Copyright 2012 by the authors; licensee MDPI, Basel, Switzerland.



3.1. Abstract

The crystal structure of the coordination polymer diaqua(μ -5,5'-bistetrazolato- $\kappa^4 N^1, N^2, N^5, N^6$)copper(II) was determined by X-ray diffraction. The copper atoms are connected to chains over the bridging 5,5'-bistetrazolato ligand. The energetic properties of the compound were investigated, such as thermal behavior and sensitivities (shock, friction, electrical spark).

3.2. Introduction

The research of environmental friendly primary explosives as replacements for lead azide and lead styphnate is of great interest. Lead containing explosives cause environmental problems because of the heavy metal contamination of e.g., shooting ranges. As it was shown in the past, nitrogen-rich heterocycles like tetrazoles in combination with less toxic metal cations like copper(II), zinc(II) or iron (II/III) seem to be alternatives for lead azide. One heterocycle of interest is 5,5'-bistetrazole (5,5'-H₂BT).

Neutral 5,5'-bistetrazole (5,5'-H₂BT)^[1] and some of its salts (manganese, sodium) have been described in literature for a long time.^[2] However, the potential of this compound as an energetic material was first recognized by W. Friederich in 1956.^[3] Hiskey and Chavez further investigated the copper(II) and some nitrogen-rich salts (diammonium, hydrazinium, hydroxylammonium *etc.*) of 5,5'-bistetrazole as low-smoke pyrotechnics and reported the synthesis of 5,5'-H₂BT from sodium azide, sodium cyanide and manganese dioxide in

water.^[4,5] In addition, our research group pointed out the potential use of the barium and strontium salt in coloring pyrotechnical compositions and determined the crystal structures of all alkaline earth metal salts except radium (Be, Mg, Ca, Sr and Ba).^[6] However, the crystal structure of the diaqua(μ -5,5'-bistetrazolato- $\kappa^4 N^1, N^2, N^5, N^6$)copper(II) (**2**) was not determined until now. In this work, the structure of **2** was determined by low temperature single crystal X-ray diffraction and the purity approved by vibrational spectroscopy and elemental analysis. The sensitivities were tested according to BAM (*Bundesanstalt für Materialforschung und-prüfung*) methods.

3.3. Results and Discussion

Due to lower sensitivities, the monosodium 5,5'-bistetrazolate trihydrate (**1**) was synthesized instead of the neutral 5,5'-H₂BT. The preparation was carried out using slight modifications to the method described in literature.^[4] The intermediate manganese 5,5'-bistetrazolate was treated in a sodium carbonate solution with less hydrochloric acid to protonate only once. **1** was further reacted with a solution of copper(II) nitrate trihydrate in 2 M nitric acid, from which **2** precipitated after a few days as blue crystals.

Thermal ellipsoids in the structure depictions are drawn with 50% probability. Crystallographic data is given in Table 1.

2 crystallizes in the triclinic space group $P\bar{1}$ with two formula units in the unit cell and a calculated density of 2.335 g cm⁻³ which is very high even for a copper complex. The copper(II) central atom has an octahedral coordination sphere (Figure 1) which is Jahn-Teller distorted along the N2ⁱⁱ-N5 axis and not along the water-copper bonds which would have been expected. The Cu1-N5 bond (2.76 Å) is a very long and weak coordinative bond. However, this bond length is in agreement with the Cu-N bond of the similar bis(5-amino-1,2,4-triazol-3-yl)copper(II) complex.^[7] The Cu1-N2ⁱⁱ bond can be arranged as a normal coordinative bond but is with 2.27 Å still longer than the Cu1-O1, Cu1-O2, Cu1-N1 and Cu1-N6ⁱ bonds (all about 2.0 Å and similar to the Cu(II) complex in the literature).^[8] The bond angle between O1, Cu1 and the according N-atoms in the N2ⁱⁱ-N6ⁱ-N5-N1 plane is about 90°. The N2ⁱⁱ-N6ⁱ-N5-N1 torsion angle (-2.3°) is small, indicating a planar coordination of the nitrogen atoms to Cu1. The N-Cu-N angles (e.g., $\angle(N1-Cu1-N2^{ii}) = 100.1^\circ$ and $\angle(N1-Cu1-N5) = 72.2^\circ$) in the N2ⁱⁱ-N6ⁱ-N5-N1 plane deviate from 90° and indicate a distorted octahedral coordination sphere which is induced by the fixed geometry of the 5,5'-bistetrazolato ligand. The bond lengths of the ligand are in a typical range of 5,5'-bistetrazoles (about 1.30–1.35 Å for N–N bonds, 1.35 Å for C–N bond and 1.46 Å for the C–C bond). Supplementary, the N–N bond length of 1.30–1.35 Å is between N–N single (1.48 Å) and N=N double bonds (1.20 Å) which together with the nearly planar tetrazole rings ($\angle(N1-N2-N3-N4) = -0.7^\circ$) indicates an aromatic 6 π -system.^[9] However, the C-bridged tetrazole rings of the 5,5'-BT are twisted to

each other ($\angle(\text{N1-C1-C2-N5}) = 24.9^\circ$) due to sterical effects and the above mentioned weak bond between N5 and Cu1. Hydrogen bonds are formed between the water molecules and nitrogen atoms of neighbored 5,5'-BT ligands. All hydrogen bonds (Table 2) can be classified as moderate.^[10] The strongest hydrogen bond is between O2^v and N8 which is nearly linear ($\angle(\text{O2}^{\text{v}}-\text{H2B}\cdots\text{N8}) = 178^\circ$) and has a short O–H \cdots N contact of 1.85 Å. The weakest O–H \cdots N contact is between O1^{iv} and N4 with a H \cdots N distance of 2.06 Å and an O1^{iv}–H1B \cdots N4 angle of 135°.

Table 1. Crystallographic data for **2**.

X-ray parameter	2	X-ray parameter	2
Formula	C ₂ H ₄ CuN ₈ O ₂	μ / mm^{-1}	3.238
$M / \text{g mol}^{-1}$	235.68	θ range / °	4.76–26.24
Color	blue	Dataset ($h; k; l$)	–9:9; –9:9; –9:9
Habit	block	Reflections collected	3451
Crystal size / mm	0.19 × 0.18 × 0.07	Independent reflections	1342
Crystal system	triclinic	Observed reflections	1153
Space group	$P\bar{1}$	R_{int}	0.0713
$a / \text{Å}$	7.4137(13)	Data	1342
$b / \text{Å}$	7.4890(13)	Restraints	4
$c / \text{Å}$	7.5391(14)	Parameters	134
$\alpha / ^\circ$	118.928(19)	R_1 (obs.)	0.0448
$\beta / ^\circ$	109.295(17)	wR_2 (all data)	0.1158
$\gamma / ^\circ$	92.470(14)	S	1.090
$V / \text{Å}^3$	335.18(10)	Resd. dens. / e Å ^{–3}	–0.787 / 1.311
Z	2	Solution	SIR92
$\rho_{\text{calc.}} / \text{g cm}^{-3}$	2.335	Refinement	SHELXL-97
T / K	173(2)	Absorption correction	multi-scan
$F(000)$	234	CCDC	880415

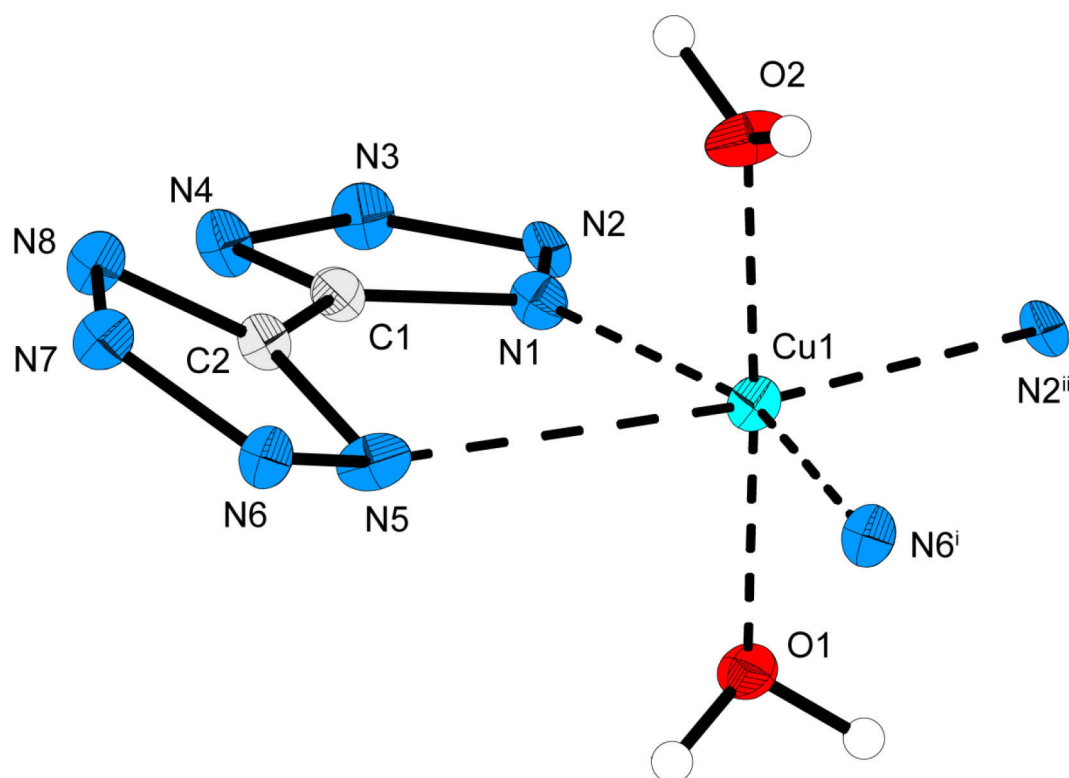


Figure 1. Coordination geometry of diaqua(μ -5,5'-bistetrazolato- $\kappa^4 N^1, N^2, N^5, N^6$)copper(II) (**2**). Symmetry codes: i: $1-x, -y, -z$; ii: $2-x, -y, 1-z$.

Table 2. Distances and angles of the hydrogen bonds of **2**.

D–H \cdots A	$d(\text{D–H}) / \text{\AA}$	$d(\text{H}\cdots\text{A}) / \text{\AA}$	$d(\text{D}\cdots\text{A}) / \text{\AA}$	$\angle(\text{D–H}\cdots\text{A}) / ^\circ$
O2 ⁱⁱⁱ –H2A \cdots N3	0.89(6)	1.99(5)	2.876(6)	170(7)
O1 ^{iv} –H1B \cdots N4	0.90(7)	2.06(6)	2.771(6)	135(8)
O2 ^v –H2B \cdots N8	0.89(5)	1.85(5)	2.746(8)	178(7)
O1 ^{vi} –H1A \cdots N7	0.90(5)	1.98(5)	2.812(6)	155(4)

Symmetry codes: iii: $x, y, 1+z$; iv: $1-x, -y, 1-z$; v: $1-x, -1-y, -z$; vi: $-1+x, -1+y, -1+z$.

The copper atoms are connected by the 5,5'-bistetrazolato ligand to chains between the a - and the c -axis (Figure 2). The chains are stacked parallel along the b - and the c -axis. One chain is hexagonal surrounded (Figure 3). The chains are stabilized among each other with hydrogen bonds between the N atoms of a 5,5'-bistetrazolato ligand and coordinated water molecules of a neighbored complex unit, shown in Figure 3.

The energetic properties of compound **2** were also investigated. An impact sensitivity of 30 J, a friction sensitivity of 80 N and an electrostatic discharge of 50 mJ were determined. **2** loses its coordinative bound water at about 160 °C. Decomposition starts at 238 °C in form of a detonation. The complex compound detonated on a hot-plate, while it was just deflagrating in flame with a green color.

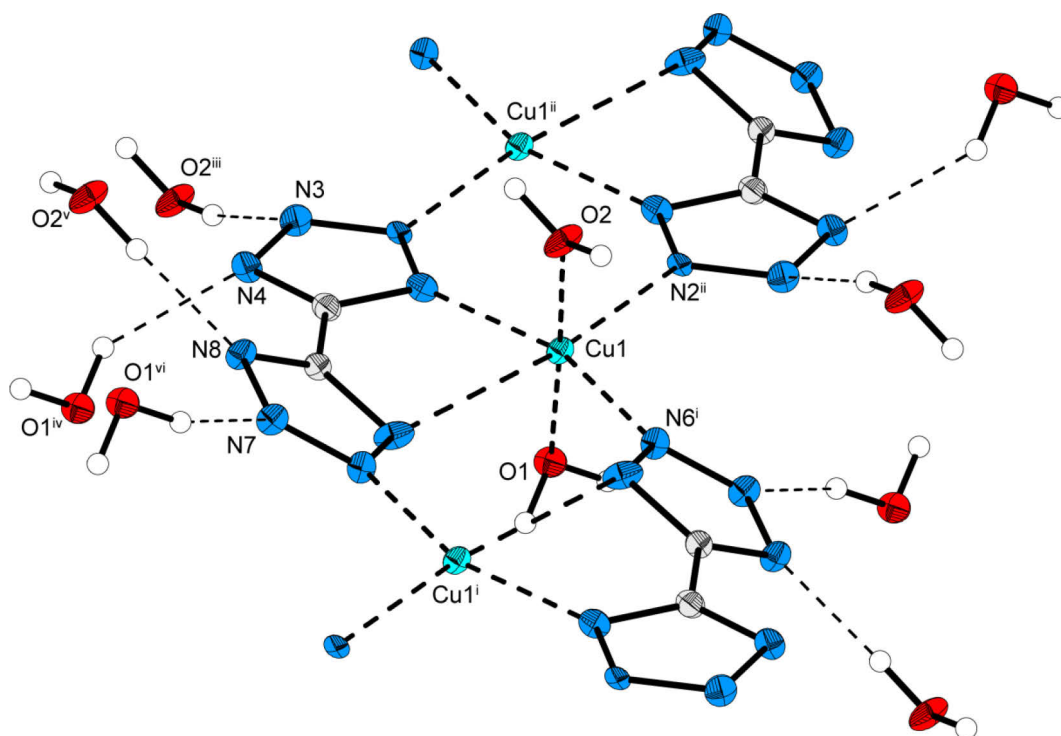


Figure 2. Hydrogen bonds of **2**. Symmetry codes: i: $1-x, -y, -z$; ii: $2-x, -y, 1-z$; iii: $x, y, 1+z$; iv: $1-x, -y, 1-z$; v: $1-x, -1-y, -z$; vi: $-1+x, -1+y, -1+z$.

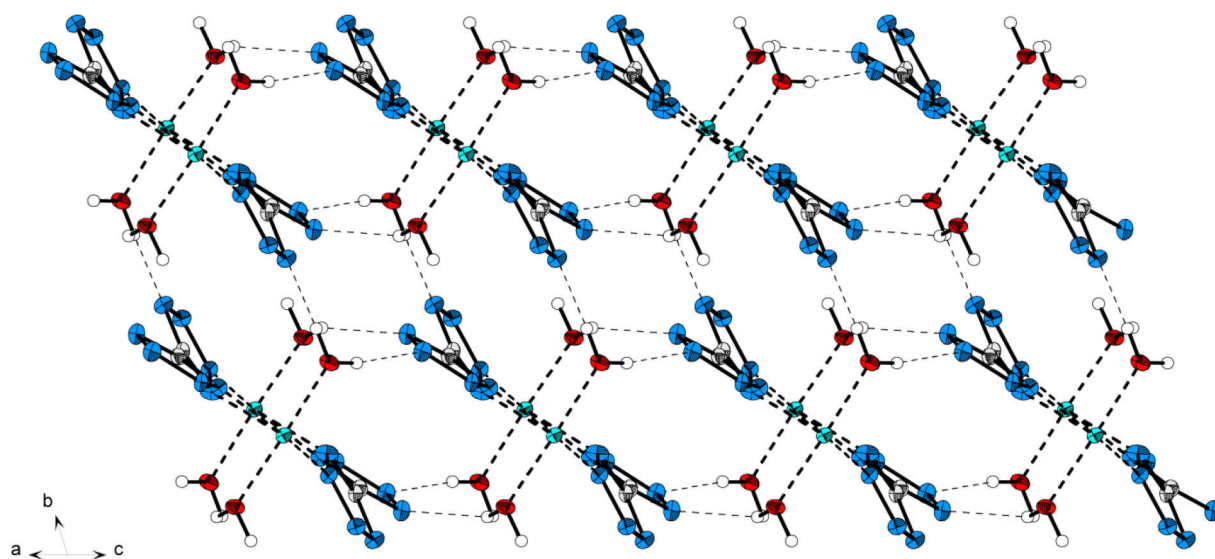


Figure 3. Packing scheme of **2**. The parallel stacked chains are stabilized by hydrogen bonds among each other.

3.4. Experimental Section

All chemicals were used as supplied (AppliChem, Sigma-Aldrich, VWR).

NMR spectra were recorded using the spectrometer JEOL Eclipse 400. The measurements were conducted in regular glass NMR tubes (\varnothing 5 mm) and at 25 °C. Tetramethylsilane (^1H , ^{13}C) was used as external standard. IR spectra were recorded using a PerkinElmer BX FT IR spectrometer on a Smiths DuraSamplIR II diamond ATR unit with pure samples.

The UV-VIS-NIR reflectance of solid samples was measured with a *Varian Cary 500* spectrometer in a wavelength range of 350–1300 nm.

The determinations of the carbon, hydrogen and nitrogen contents were carried out by combustion analysis using an Elementar Vario EL.

Decomposition temperatures were measured via differential thermal analysis (DTA) by using an *OZM Research DTA 552-Ex* instrument. The samples (~ 25 mg) were measured in open glass tubes (\varnothing 4 mm, length about 47 mm) at a heating rate of 5 °C in a range of 15–400 °C.

Crystal structures were determined by single crystal X-ray diffraction on an Oxford Diffraction Xcalibur 3 diffractometer with a Sapphire CCD detector, four circle kappa platform, Enhance molybdenum K_α radiation source ($\lambda = 71.073$ pm) and Oxford Cryosystems Cryostream cooling unit. Data collection and reduction were performed with the CRYCALISPRO software.^[11] The structures were solved with SIR92,^[12] refined with SHELXL-97^[13] and checked with PLATON,^[14] all integrated in the WinGX software suite.^[15] The finalized CIF files^[16] were checked with checkCIF.^[17] Intra- and intermolecular contacts were analyzed with Mercury.^[18] Illustrations of molecular structures were drawn with Diamond.^[19]

The sensitivities against impact (IS) and friction (FS) were determined according to BAM^[20] standards using a BAM drop hammer and a BAM friction apparatus.^[21–25] The compounds were classified in compliance with UN guidelines.^[26] The sensitivities against electrostatic discharge (ESD) were determined using an OZM Research ESD 2010 EN.

CAUTION! The compounds prepared herein are energetic compounds sensitive towards impact, friction and electric discharge. Therefore, proper protective measures (ear protection, Kevlar[®] gloves, face shield, body armor and earthed equipment) should be used.

Monosodium 5,5'-Bistetrazolate Trihydrate (1): Compound **1** was prepared similar to the literature procedure.^[4] To a solution of sodium cyanide (29.4 g, 600 mmol) and sodium azide (39.0 g, 600 mmol) in water (350 mL), manganese dioxide (33.0 g, 380 mmol) was added. A mixture of conc. sulfuric acid (58.8 g, 600 mmol), glacial acetic acid (47.7 g, 795 mmol) and copper(II) sulfate pentahydrate (1.20 g, 4.81 mmol) in water (150 mL) was added dropwise over the course of 2.5 h to the suspension under cooling in an ice bath to keep the temperature below 25 °C. After complete addition the reaction mixture was stirred at 80 °C for 3 h and

then cooled to room temperature over night. The brown solid was filtered off and suspended in water (350 mL). Sodium carbonate (45.0 g, 425 mmol) was dissolved in water (250 mL), poured to the suspension and stirred for 2 h at 90 °C. Afterwards the suspension was filtered hot and the slightly green filtrate acidified with conc. hydrochloric acid to pH 1. The precipitating white solid was filtered off and air dried. Concentration of the filtrate to half volume yielded more product. Total yield: 32.8 g (153 mmol, 51 %).

DTA (T_{onset} , 5 °C min⁻¹): 300 °C (dec.); IR (ATR, cm⁻¹): ν = 3531 (m), 3491 (m), 3480 (m), 3370 (vs), 3305 (s), 2981 (w), 2800 (w), 2739 (w), 2630 (m), 2451 (m), 2282 (w), 1897 (w), 1670 (m), 1619 (m), 1488 (w), 1444 (w), 1349 (s), 1293 (w), 1239 (w), 1206 (w), 1155 (w), 1105 (w), 1078 (w), 1052 (w), 1010 (m), 723 (w), 704 (w), 699 (w); ¹H NMR (*d*₆-DMSO, 400 MHz, ppm): δ = 4.97 (s, 1 H, CN₄H); ¹³C NMR (*d*₆-DMSO, 100 MHz, ppm): δ = 149.9 (s, CN₄); MS (FAB⁺): m/z = 23.0 (Na⁺); MS (FAB⁻): m/z = 137.0 (C₂HN₈⁻); EA (C₂H₇N₈NaO₃, 214.12 g mol⁻¹), calculated: C 11.22, H 3.30, N 52.33 %, found: C 11.77, H 3.18, N 52.16 %; Sensitivities (grain size: < 100 μm): IS: 40 J, FS: 288 N, ESD: 0.50 J.

Diaqua(μ-5,5'-bistetrazolato-κ⁴N¹,N²,N⁵,N⁶)copper(II) (2): Monosodium 5,5'-bistetrazolate trihydrate (**1**, 107 mg, 500 μmol) was dissolved in conc. nitric acid (7 mL) at 60 °C. A warm solution of copper(II) nitrate trihydrate (0.121 g, 500 μmol) in 2 M nitric acid (4 mL) was slowly added and the reaction mixture stirred for 10 min at 60 °C. The blue solution was reduced until a fine blue solid precipitated and then filled up with a large amount of water to dissolve the solid again. The solution was left at room temperature for crystallization. After a few days, **2** was obtained as blue crystals suitable for X-ray structure determination. The crystals were filtered off and washed with acetone. Yield: 110 mg (467 μmol, 93 %).

DTA (T_{onset} , 5 °C min⁻¹): 238 °C (dec.); IR (ATR, cm⁻¹): ν = 3177 (vs), 3016 (s), 2230 (w), 1623 (w), 1441 (w), 1360 (s), 1325 (m), 1235 (w), 1211 (m), 1184 (m), 1161 (w), 1129 (vw), 1113 (w), 1071 (m), 1024 (m), 780 (w), 735 (m), 675 (w), 662 (m); UV-VIS-NIR (nm): λ_{max} = 695, 1072; EA (C₂H₄CuN₈O₂, 235.65 g mol⁻¹), calculated: C 10.19, H 1.71, N 47.55 %, found: C 10.40, H 1.74, N 47.26 %; Sensitivities (grain size: < 100 μm): IS: 30 J, FS: 80 N, ESD: 0.05 J (dec.).

3.5. Conclusion

The coordination polymer diaqua(μ-5,5'-bistetrazolato-κ⁴N¹,N²,N⁵,N⁶)copper(II) (**2**) was prepared from copper(II) nitrate trihydrate and monosodium 5,5'-bistetrazolate trihydrate (**1**) in high yield and purity. The crystal structure could be determined and showed an interesting coordination polymer which forms parallel stacked chains. **2** is sensitive towards impact (IS: 30 J) and very sensitive towards friction (FS: 80 N). **2** only deflagrates in flame, whereas the hot-plate test showed detonation. The coordination polymer is nearly insoluble in water and

insoluble in acetone. Permanent dehydration of **2** is not possible because the coordinated crystal water participates in the strong H-bond network and complements the octahedral coordination sphere of the copper(II) centres.

3.6. References

- [1] Oliveri-Mandala, E.; Passalacqua, T. Bistetrazole and isomeric derivatives of tetrazole. *Gazz. Chim. Ital.* **1914**, *43*, 465–475.
- [2] Friederich, W. Process for the Production of Cyanotetrazole, Ditetrazole, Tetrazole Carbamide and Tetrazole and Their Salts. *US Patent 2,710,297*, 7 June 1955.
- [3] Friederich, W. Bitetrazole Compounds as Explosives and Primers. *DE Patent 945010*, 28 June 1956.
- [4] Chavez, D.E.; Hiskey, M.A.; Naud, D.L. High-nitrogen fuels for low-smoke pyrotechnics. *J. Pyrotech.* **1999**, *10*, 17–36.
- [5] Chavez, D.E.; Hiskey, M.A.; Naud, D.L. Low-Smoke Pyrotechnic Compositions. *US Patent 6,214,139*, 10 April 2001.
- [6] Fischer, N.; Klapötke, T.M.; Peters, K.; Rusan, M.; Stierstorfer, J. Alkaline earth metal salts of 5,5'-bistetrazole—from academical interest to practical application. *Z. Anorg. Allg. Chem.* **2011**, *637*, 1693–1701.
- [7] Biagini-Cingi, M.; Manotti-Lanfredi, A.M.; Ugozzoli, F.; Haasnoot, J.G. Synthesis and X-ray structure of the dinuclear μ -5,5'-diamino-3,3'-bis-1,2,4-triazolato(1-)-bis-(diethylenetriaminecopper(II)) triperchlorate, $[\{\text{Cu}(\text{dien})\}_2\text{Hdabt}](\text{ClO}_4)_3$. *Inorg. Chim. Acta* **1994**, *227*, 181–184.
- [8] Li, J.R.; Yu, Q.; Sanudo, E.C.; Tao, Y.; Song, W.C.; Bu, X.H. Three-dimensional homospin inorganic–organic ferrimagnet constructed from $(\text{VO}_3^-)_n$ chains linking $\{[5\text{-}(\text{Pyrimidin-2-yl})\text{tetrazolato}-(\text{Cu}^{\text{II}})_{1.5}]^{2+}\}_n$ layers. *Chem. Mater.* **2008**, *20*, 1218–1220.
- [9] Fischer, N.; Izsák, D.; Klapötke, T.M.; Rappenglück, S.; Stierstorfer, J. Nitrogen-rich 5,5'-bistetrazolates and their potential use in propellant systems: A comprehensive study. *Chem. Eur. J.* **2012**, *18*, 4051–4062.
- [10] Jeffrey, G.A. *An Introduction to Hydrogen Bonding*; Oxford University Press: New York, NY, USA, 1997.
- [11] *CrysAlisPro*, version 1.171.35.11; Oxford Diffraction Ltd.: Abingdon, UK, 2011.
- [12] Altomare, A.; Cascarano, G.L.; Giacovazzo, C.; Guagliardi, A. Completion and refinement of crystal structures with SIR92. *J. Appl. Cryst.* **1993**, *26*, 343–350.
- [13] Sheldrick, G.M. A short history of SHELX. *Acta Cryst.* **2008**, *A64*, 112–122.
- [14] Spek, L. *Platlon*; Utrecht University: Utrecht, Netherlands, 2011.

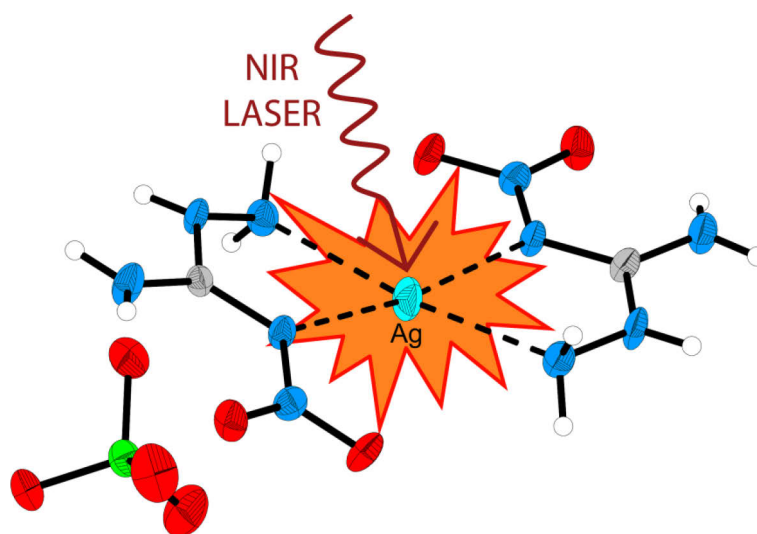
-
- [15] Farrugia, L.J. WinGX suite for small molecule single-crystal crystallography. *J. Appl. Cryst.* **1999**, *32*, 837–838.
- [16] Hall, S.R.; Allen, F.H.; Brown, I.D. The Crystallographic Information File (CIF): A new standard archive file for crystallography. *Acta Cryst.* **1991**, *A47*, 655–685.
- [17] CheckCIF/PLATON (Full Publication Check) Homepage. Available online: <http://journals.iucr.org/services/cif/checkcif.html> (accessed on 8 May 2012).
- [18] Macrae, C.F.; Edgington, P.R.; McCabe, P.; Pidcock, E.; Shields, G.P.; Taylor, R.; Towler, M.; van de Streek, J. Mercury: Visualization and analysis of crystal structures. *J. Appl. Crystallogr.* **2006**, *39*, 453–457.
- [19] Brandenburg, K. *Diamond 3.2 g*; Crystal Impact GbR: Bonn, Germany, 2011.
- [20] BAM Bundesanstalt für Materialforschung und -prüfung Homepage. Available online: <http://www.bam.de> (accessed on 8 May 2012)
- [21] NATO. *NATO Standardization Agreement (STANAG) on Explosive, Friction Sensitivity Tests*; Report No. 4489; ASSIST: Philadelphia, PA, USA, 17 September 1999.
- [22] WIWEB. *Standardarbeitsanweisung 4–5.1.02* (In German); Wehrwissenschaftliches Institut für Werk-, Explosiv- und Betriebsstoffe (WIWEB): Erding, Germany, 2002.
- [23] NATO. *NATO Standardization Agreement (STANAG) on Explosive, Friction Sensitivity Tests*; Report No. 4487; ASSIST: Philadelphia, PA, USA, 22 August 2002.
- [24] WIWEB. *Standardarbeitsanweisung 4–5.1.03* (In German); Wehrwissenschaftliches Institut für Werk-, Explosiv- und Betriebsstoffe (WIWEB): Erding, Germany, 2002.
- [25] Reichel & Partner GmbH Homepage. Available online: <http://www.reichel-partner.de/> (accessed on 8 May 2012).
- [26] United Nations Economic Commission for Europe (UNECE). *Recommendations on the Transport of Dangerous Goods, Manual of Tests and Criteria*, 4th ed.; UNECE: Geneva, Switzerland, 1999.

4. Transition Metal Complexes of 3-Amino-1-nitroguanidine as Laser Ignitable Primary Explosives: Structures and Properties

Reproduced with permission from N. Fischer, M. Joas, T. M. Klapötke, J. Stierstorfer, *Inorganic Chemistry* **2013**, 52, 13791–13802.

Online: <http://pubs.acs.org/articlesonrequest/AOR-QUc6Hvdigd2iDyM8bpVE>.

Copyright 2013 American Chemical Society.



4.1. Abstract

3-Amino-1-nitroguanidine (ANQ, **2**) was synthesized via hydrazinolysis of nitroguanidine. By dissolving **2** in solutions containing transition metal salts, several complexes $M^{2+}(\text{ANQ})_2\text{X}_2(\text{H}_2\text{O})_y$ with $M^{2+} = \text{Co}, \text{Ni}, \text{Cu}, \text{Zn}$ as well as $M(\text{ANQ})_2\text{X}(\text{H}_2\text{O})_y$ with $M = \text{Ag}$ could be isolated. In these cases, nitrate as well as perchlorate and chloride served as the respective anions X. Additionally, the ANQ complexes of Co, Ni, and Ag with dinitramide as the anion were synthesized from ANQ and silver dinitramide and by reacting the cobalt and nickel ANQ perchlorate complexes with ammonium dinitramide. The crystal structures of all described complexes were determined by low temperature single-crystal X-ray diffraction. Additionally, they were characterized using IR spectroscopy and elemental analysis. The decomposition temperatures were determined by differential scanning calorimetry and the sensitivities toward impact and friction were assessed using a BAM drophammer and a BAM friction tester (BAM = Bundesanstalt für Materialforschung und -prüfung). Additionally, the sensitivity toward electrostatic discharge was determined on a small-scale ESD device. The potential use of the nitrate, dinitramide and perchlorate containing species as primary explosives was investigated in a laser ignition test.

4.2. Introduction

In the continuous research toward new energetic materials, high-energy capacity transition metal complexes have become more and more popular.^[1-3] These materials mostly combine facile syntheses and good thermal stabilities with energetic properties similar to that of the prominent primary explosive lead azide, which should be replaced because of its high toxicity. For the synthesis of energetic complexes, especially nitrogen-rich heterocycles^[4] or guanidine-based ligands can be used.

The guanidine building block is one of the first structural moieties that has been known to the chemical and biological community and was discovered as early as 1866, when the first guanidine derivative was prepared by Hofmann.^[5] Since then, guanidine chemistry has evolved into an extremely wide ranging field of applications starting from bioorganic chemistry and biochemistry^[6] to inorganic chemistry, which most importantly can be traced back to a vast variability of derivatization of the guanidine moiety itself. Whereas a lot of correspondence can be found dealing with either aminated or nitrated guanidines such as aminoguanidine^[7] or nitroguanidine,^[8] only very few sources report on the synthesis^[9] and use of the mixed 3-amino-1-nitroguanidine (ANQ, **2**), which is the only today known guanidine derivative containing both, an amine and a nitro substituent. Nevertheless, it has found application as a useful intermediate for cyclization reactions yielding bis-nitraminotriazoles,^[10] for the synthesis of 5-nitriminotetrazole, which proceeds via a diazotization reaction and following cyclization of nitroguanyl azide,^[11] or as a cationic species in ionic energetic materials.^[12]

Because of the considerable amount of electron density at its amine and nitramine substituent, it expectedly shows fairly good characteristics as a ligand in transition metals complexes, which have not been described in the literature before. Furthermore, although amine substituted guanidine derivatives are subject to oxidative decomposition in air, ANQ is stable under ambient conditions.

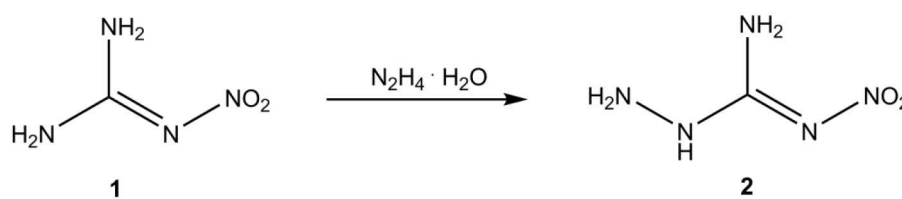
Ilyushin *et al.* report on the synthesis of a cobalt(III) complex bearing tetrazole as a ligand and perchlorate as the counterion and its use as nontoxic initiating explosive.^[13] Bearing this in mind, the choice of counterions was directed to anions such as the nitrate, dinitramide, or perchlorate anion, which frequently have been reported as counterions in ionic energetic materials.^[14,15] The first reported synthesis of a dinitramide compound was that of its ammonium salt.^[16] To overcome the problems, which nowadays are discussed regarding the safe handling of commonly used primary explosives such as lead azide, which aside from being toxic has a high impact and friction sensitivity, a new class of initiating charges, which are laser-ignitable primary explosives, are investigated.^[17] If insensitive toward impact and friction, these materials can easily be ignited by a short but highly energetic laser pulse with a

specific wavelength. This considerably reduces the probability of being accidentally ignited, which oftentimes happened while handling the commonly used impact and friction sensitive primary explosives. Here, the use of transition metal complexes has already been discussed, whereas the exact mechanism, by which transition metal containing complexes are ignited upon laser irradiation, is still under investigation.

As possible candidates for laser ignitable primary explosives, the ANQ complexes of Co^{2+} , Ni^{2+} , Cu^{2+} , Zn^{2+} , and Ag^+ with a choice of counterions (NO_3^- , $\text{N}(\text{NO}_2)_2^-$, ClO_4^- , Cl^-) were investigated including their synthesis and structure determination.

4.3. Results and Discussion

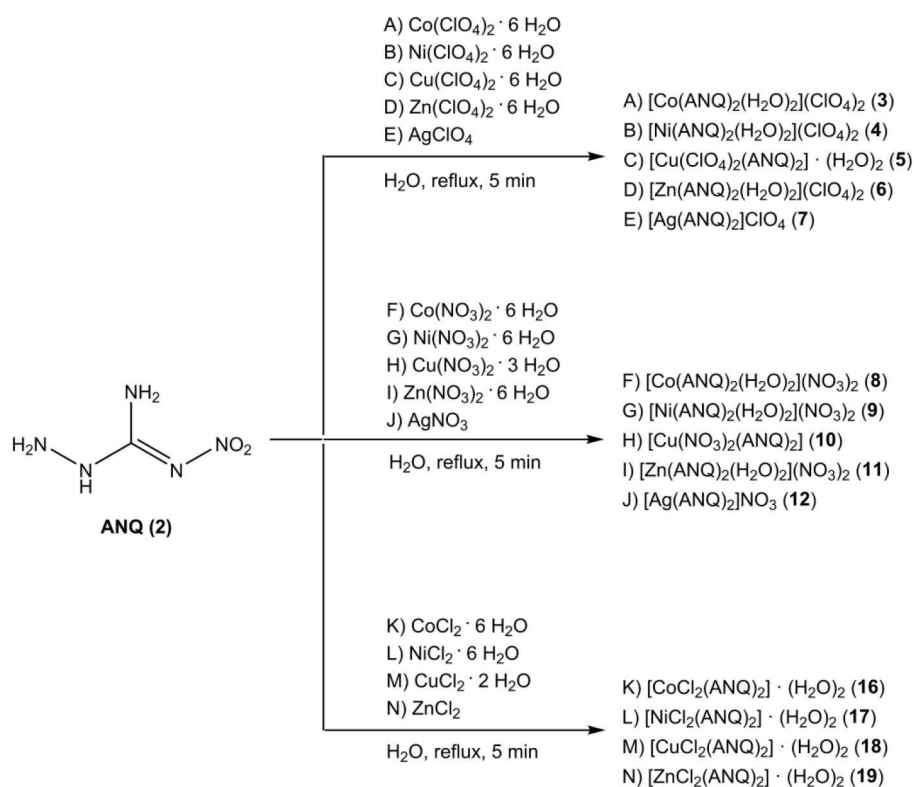
Synthesis: 3-Amino-1-nitroguanidine (ANQ, **2**) was synthesized in aqueous solution employing a hydrazinolysis reaction of commercially available nitroguanidine (**1**, see Scheme 1), whereas it is important to control the temperature accurately.^[18] The product itself shows fairly poor solubility in water and therefore can be recrystallized from hot water.



Scheme 1. Hydrazinolysis of nitroguanidine. Reaction conditions: stirring, 55 °C, 15 min.

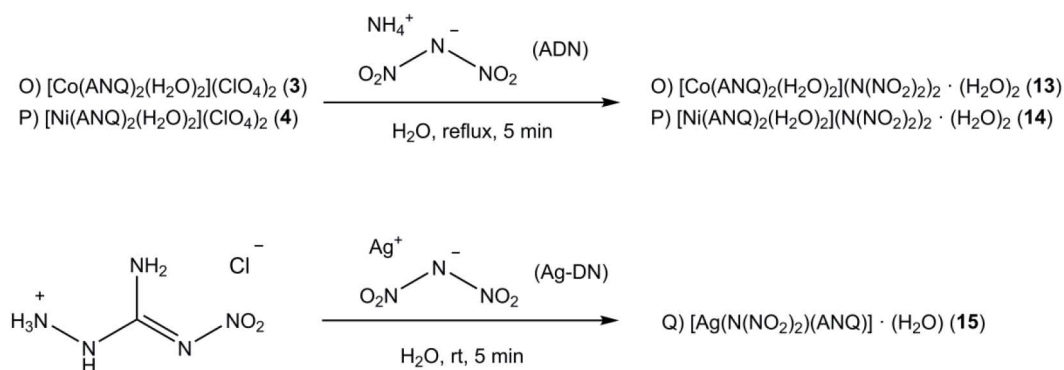
The formation of the perchlorate, nitrate, and chloride-based 3-amino-1-nitroguanidinium complexes **3–7**, **8–12**, and **16–19** proceeds after dissolving the respective Co^{2+} , Ni^{2+} , Cu^{2+} , Zn^{2+} , and Ag^+ perchlorates, nitrates, or chlorides, as indicated in Scheme 2, in a boiling solution of ANQ. The stoichiometry of the reaction of ANQ: metal salt was chosen to be 1:1 instead of 2:1 (which is the stoichiometry found in the crystalline products), because poorly water-soluble ANQ tends to precipitate from the mixture upon cooling down. In some cases, precipitated ANQ indeed had to be filtered off from the mixture, before crystals of the complex began to grow, which especially was observed for the zinc(II) complexes. The yields of the described reactions were determined only of the first isolated fraction of crystals and lie between < 10% and 49%, which presumably can be optimized by further evaporation of the mother liquors.

The ANQ complexes bearing a dinitramide counterion in the cases of the cobalt and nickel complexes **13** and **14** were synthesized from the respective metal perchlorate-containing solutions after addition of ammonium dinitramide in a stoichiometric ratio of metal perchlorate:ADN = 1:2 (see Scheme 3).



Scheme 2. Formation of perchlorate, nitrate, and chloride-based 3-amino-1-nitroguanidinium complexes **3–7**, **8–12**, and **16–19**.

The advantage of the perchlorate containing solutions as starting material over the nitrate or chloride containing solutions is the better solubility of the metal–ANQ perchlorates as compared to the nitrates or chlorides, so that they do not precipitate before the dinitramides were isolated from the mother liquors. Using potassium dinitramide instead is disadvantageous because of the simultaneous precipitation of both potassium perchlorate and the metal–ANQ dinitramides. The silver complex was formed after combining solutions of 3-amino-1-nitroguanidinium chloride^[19] and acetonitrile-stabilized silver dinitramide^[20] in a 1:1 stoichiometric ratio. After filtering off AgCl, the silver–ANQ dinitramide monohydrate crystallizes from the mother liquor in colorless needles.



Scheme 3. Formation of dinitramide-based 3-amino-1-nitroguanidinium complexes **13–15**

Single-crystal X-ray structure analysis: The low temperature determination of the crystal structures of **3–19** was performed on a Oxford Xcalibur3 diffractometer with a Spellman generator (voltage 50 kV, current 40 mA) and a KappaCCD detector. The data collection and reduction were carried out using the CrysAlisPro software.^[21] The structures were solved either with SIR-92^[22] or SHELXS-97,^[23] refined with SHELXL-97,^[24] and finally checked using the PLATON^[25] software integrated in the WinGX^[26] software suite. The absorptions were corrected by a Scale3 Abspack multiscan method.^[27] Selected data and parameter of the X-ray determinations are given in the Supporting Information in Tables S1–S3. Cif files have been deposited within the Cambridge Crystallographic Data Centre using the CCDC Nos. 900148 (**3**), 900144 (**4**), 900147 (**5**), 900149 (**6**), 900143 (**7**), 900142 (**8**), 900139 (**9**), 900141 (**10**), 900146 (**11**), 900140 (**12**), 900155 (**13**), 900154 (**14**), 900138 (**15**), 900152 (**16**), 900153 (**17**), 900151 (**18**) and 900156 (**19**).

The ANQ ligand shows a similar structure in all investigated complexes in this work. Recently we published the structure of neutral ANQ as well as some inorganic salts.^[12,19] The ligand is almost planar. The C–N bonds are significantly shorter than C–N single bonds, with lengths between 1.28 and 1.38 Å. Coordination to the metal centers take place by the outer hydrazine nitrogen atom N4 and nitrogen atom N1. The coordination angles N1–M–N4 approximately increase with the following order. Ag (ca. 68°) < Zn = Co < Ni < Cu (ca. 80°).

[Co(ANQ)₂(H₂O)₂](ClO₄)₂ (**3**) crystallizes in the monoclinic space group *P*2₁/*c* with two formula units in the unit cell. The molecular moiety is depicted in Figure 1. A similar coordination sphere has been described for diaqua-tetrakispicoline cobalt(II) diperchlorate.^[28]

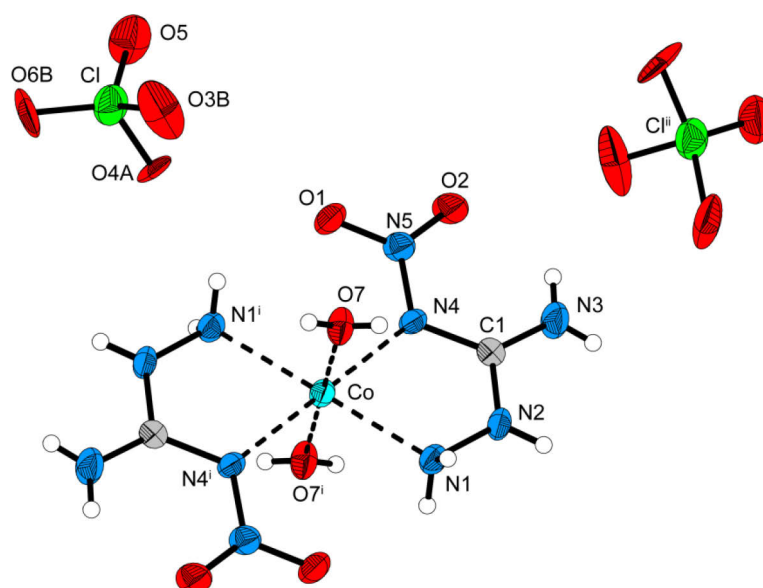


Figure 1. Molecular moiety of **3**. Thermal displacements of non-hydrogen atoms were set at 50 % probability. Hydrogen atoms are shown as spheres of arbitrary radius. Perchlorate anions are strongly disordered. Only selected split positions are depicted. Selected coordination distances [Å]: Co–O7 2.088(3), Co–N4 2.108(3), Co–N1 2.130(3); angles [°]: O7–Co–N4 89.24(11), O7–Co–N1 90.69(13), N4–Co–N1 75.76(11). Symmetry codes: i: 1–*x*, –*y*, –*z*; ii: 1–*x*, 0.5+*y*, 0.5–*z*.

The corresponding nickel complex $[\text{Ni}(\text{ANQ})_2(\text{H}_2\text{O})_2](\text{ClO}_4)_2$ (**4**) crystallizes in the orthorhombic space group $Pca2_1$ with four formula units in the unit cell. The molecular moiety is depicted in Figure 2. With the exception of the copper salt the densities of the perchlorates increase with rising atomic numbers (ρ [g cm^{-3}]: **3** (2.068) < **5** (2.128) < **4** (2.159) < **6** (2.193) < **7** (2.316)).

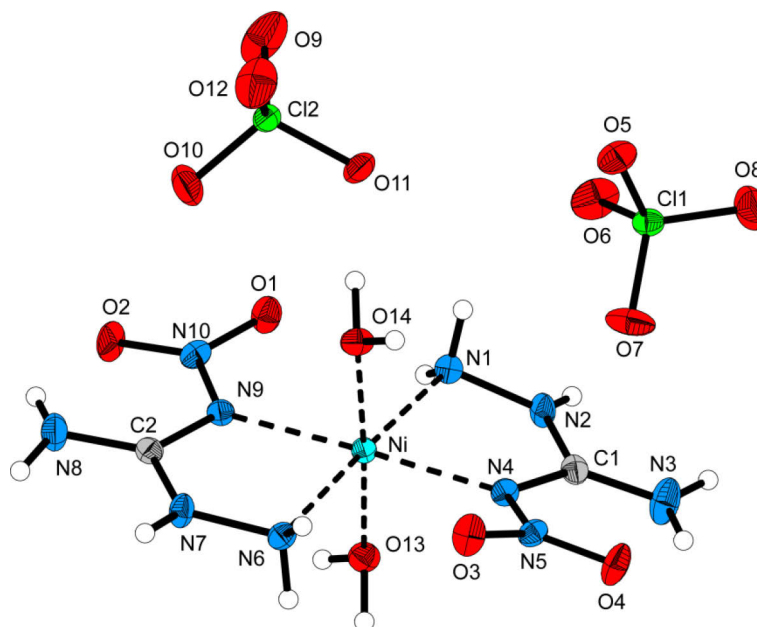


Figure 2. Molecular moiety of **4**. Thermal displacements of non-hydrogen atoms were set at 50 % probability. Hydrogen atoms are shown as spheres of arbitrary radius. Selected coordination distances [\AA]: Ni–N4 2.0692, Ni–O14 2.0764, Ni–N6 2.0821, Ni–N9 2.0877, Ni–N1 2.0891, Ni–O13 2.125; angles [$^\circ$]: N4–Ni–O14 94.8, N4–Ni–N6 101.9, O14–Ni–N6 86.6, O14–Ni–N9 87.0, N6–Ni–N9 77.5, N4–Ni–N1 76.7, O14–Ni–N1 95.0, N4–Ni–O13 88.4, N6–Ni–O13 93.9, N9–Ni–O13 89.8, N1–Ni–O13 84.5.

In agreement to all copper complexes investigated in this work, $[\text{Cu}(\text{ANQ})_2(\text{ClO}_4)_2](\text{H}_2\text{O})_2$ (**5**) also shows a Jahn-Teller^[29] distorted octahedral coordination sphere due to the d^9 electron configuration (see Figure 3). The elongation of the octahedron is due to longer Cu–OClO₃ coordination bonds in comparison to the Cu–N coordination bonds which is similar described for dimethylethylenediamine bisperchlorate.^[30] The water molecules do not participate in metal coordination. The triclinic unit cell ($P\bar{1}$) contains one molecular moiety.

The molecular structure of $[\text{Zn}(\text{ANQ})_2(\text{H}_2\text{O})_2](\text{ClO}_4)_2$ (**6**) is shown in Figure 4. The zinc(II) cations in **6**, which crystallizes in the monoclinic space group $P2_1/c$, have a centrosymmetric 6-fold coordination sphere.

The molecular moiety of $[\text{Ag}(\text{ANQ})_2]\text{ClO}_4$ (**7**), which crystallizes in the triclinic space group $P\bar{1}$, is depicted in Figure 5. The silver cations are coordinated by four nitrogen atoms in square planar arrangement.

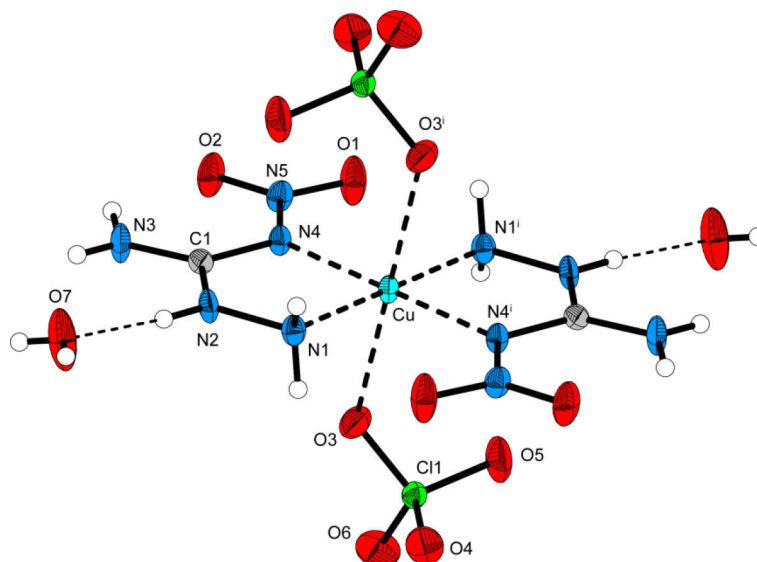


Figure 3. Molecular moiety of **5**. Thermal displacements of non-hydrogen atoms were set at 50 % probability. Hydrogen atoms are shown as spheres of arbitrary radius. Selected coordination distances [Å]: Cu–N1 1.982(2), Cu–N4 2.032(2), Cu–O3 2.4364(19), angles [°]: N1–Cu–N4 79.58(9), N1–Cu–O3 85.41(10), N4–Cu–O3 83.44(8). Symmetry codes: *i*: $-x, 1-y, -z$.

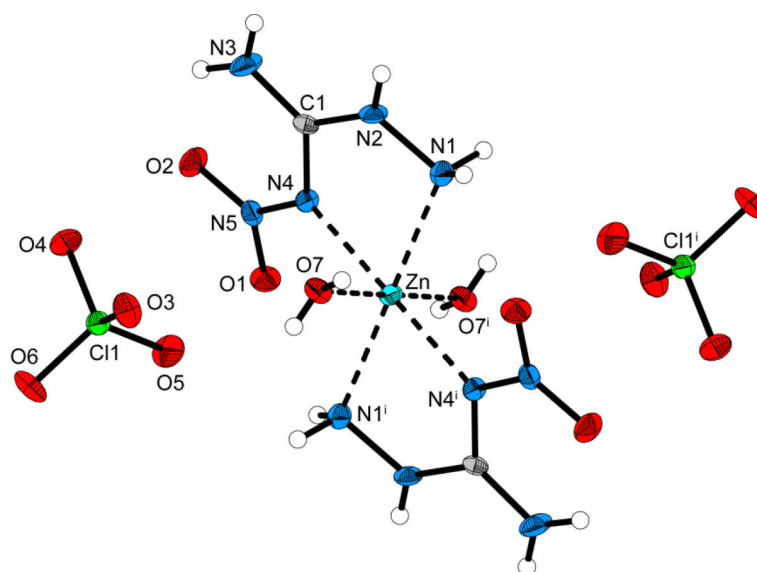


Figure 4. Molecular moiety of **6**. Thermal displacements of non-hydrogen atoms were set at 50 % probability. Hydrogen atoms are shown as spheres of arbitrary radius. Selected coordination distances [Å]: Zn–N4 2.106(2), Zn–N1 2.148(2), Zn–O7 2.164(2); angles [°]: N4–Zn–N1 74.70(8), N4–Zn–O7 88.51(8), N1–Zn–O7 84.43(10). Symmetry codes: *i*: $-x, 1-y, -z$.

One formula unit of $[\text{Co}(\text{ANQ})_2(\text{H}_2\text{O})_2](\text{NO}_3)_2$ (**8**) shown in Figure 6 is incorporated in the centrosymmetric triclinic unit cell. The nitrate anions do not participate in the coordination of the Co^{2+} centers.

Figure 7 is used exemplarily for the molecular structures of $[\text{Ni}(\text{ANQ})_2(\text{H}_2\text{O})_2](\text{NO}_3)_2$ (**9**) and $[\text{Zn}(\text{ANQ})_2(\text{H}_2\text{O})_2](\text{NO}_3)_2$ (**11**). The complexes are crystallizing isotypically in the triclinic space group $P\bar{1}$ showing almost the same unit cell dimensions (see Table S2 in the Supporting Information) and densities ($\rho[\text{g cm}^{-3}]$): **9** (2.011), **11** (1.992).

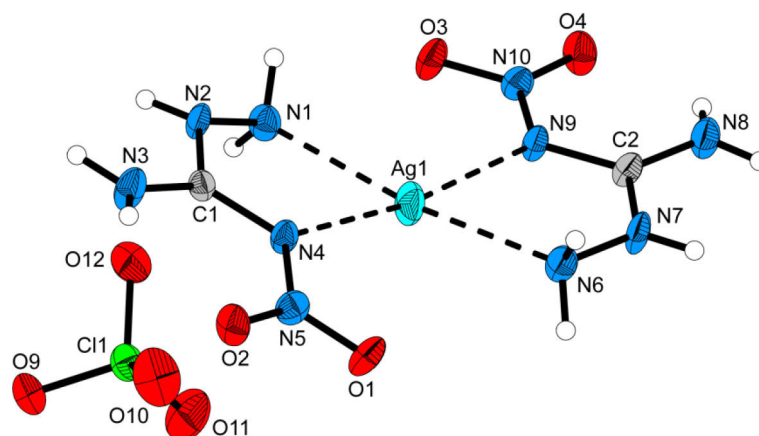


Figure 5. Molecular moiety of **7**. Thermal displacements of non-hydrogen atoms were set at 50 % probability. Hydrogen atoms are shown as spheres of arbitrary radius. Selected coordination distances [Å]: Ag1–N4 2.346(3), Ag1–N9 2.359(3), Ag1–N1 2.374(3), Ag1–N6 2.396(3); angles [°]: N4–Ag1–N9 175.12(8), N4–Ag1–N1 68.55(10), N9–Ag1–N1 116.31(10), N4–Ag1–N6 107.47(10), N9–Ag1–N6 67.88(10), N1–Ag1–N6 167.67(15).

The copper complex $[\text{Cu}(\text{ANQ})_2(\text{NO}_3)_2]$ (**10**) is shown in Figure 8. It crystallizes in the monoclinic space group $C2/c$ with a density of 2.171 g cm^{-3} . The Cu^{2+} cations reveal a distorted octahedral coordination sphere. This is indicated by the Cu–O bond lengths, which significantly differ from each other and the O5–Cu–O8 angle of $\sim 160^\circ$.

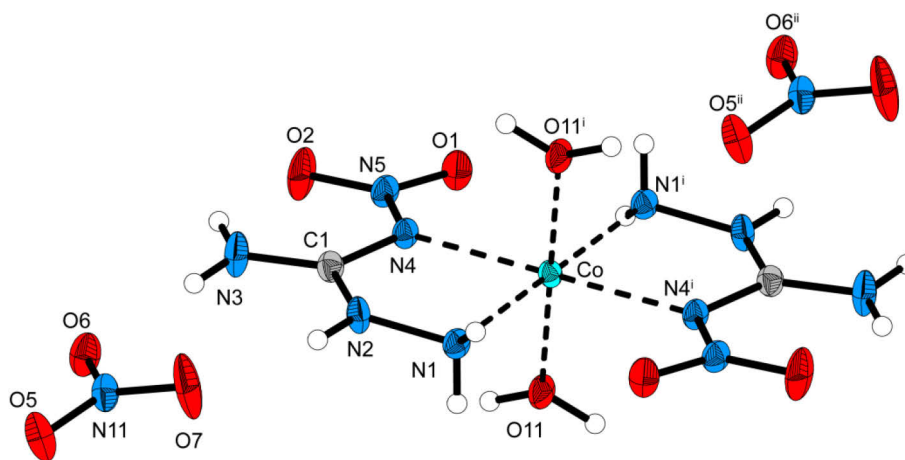


Figure 6. Molecular moiety of **8**. Thermal displacements of non-hydrogen atoms were set at 50 % probability. Hydrogen atoms are shown as spheres of arbitrary radius. Selected coordination distances [Å]: Co–O11 2.0623(11), Co–N1 2.1307(14), Co–N4 2.1543(13); angles [°]: O11–Co–N1 90.93(5), O11–Co–N4 88.74(5), N1–Co–N4 74.77(5). Symmetry codes: i: $1-x, 1-y, -z$; ii: $1-x, 1-y, -z$.

The density of complex $[\text{Ag}(\text{ANQ})_2\text{NO}_3]$ (**11**) is considerably smaller (2.235 g cm^{-3}) than that observed for silver(I) nitrate (4.35 g cm^{-3}).^[31] The silver cations in the structure of **11**, which crystallizes in the orthorhombic space group $Pbca$, are distorted tetrahedrally coordinated by only nitrogen atoms.

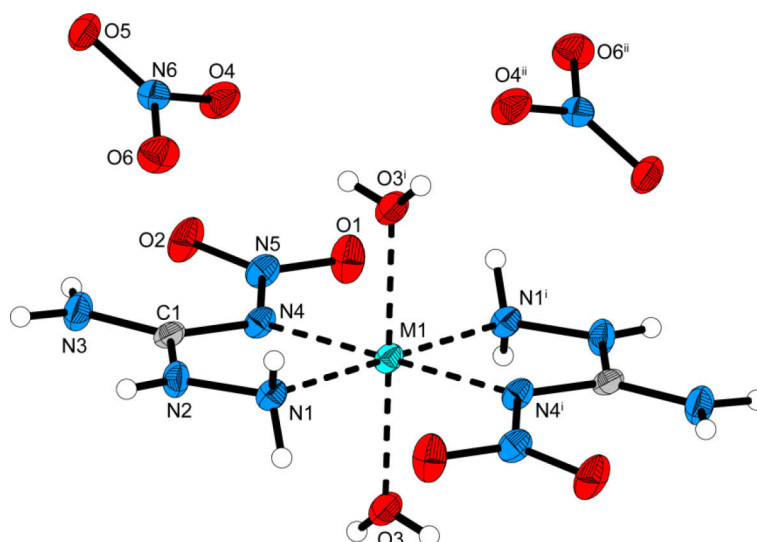


Figure 7. Molecular moiety of **9** (M1 = Ni) and **11** (M1 = Zn). Thermal displacements of non-hydrogen atoms were set at 50 % probability. Hydrogen atoms are shown as spheres of arbitrary radius. Selected coordination distances [Å]: **9**: Ni–N1 2.0587(19), Ni–O3 2.0805(18), Ni–N4 2.1023(19); **11**: Zn–N1 2.1144(17), Zn–O3 2.1315(15), Zn–N4 2.1650(15); angles [°] **9**: N1–Ni–O3 86.99(8), N1–Ni–N4 77.27(7), O3–Ni–N4 92.03(8); **11**: N1–Zn–O6 91.33(7), N1–Zn–N4 75.66(6), O6–Zn–N4 87.98(7). Symmetry codes: i: 2–*x*, 1–*y*, 1–*z*; ii: 1–*x*, 1–*y*, 1–*z*.

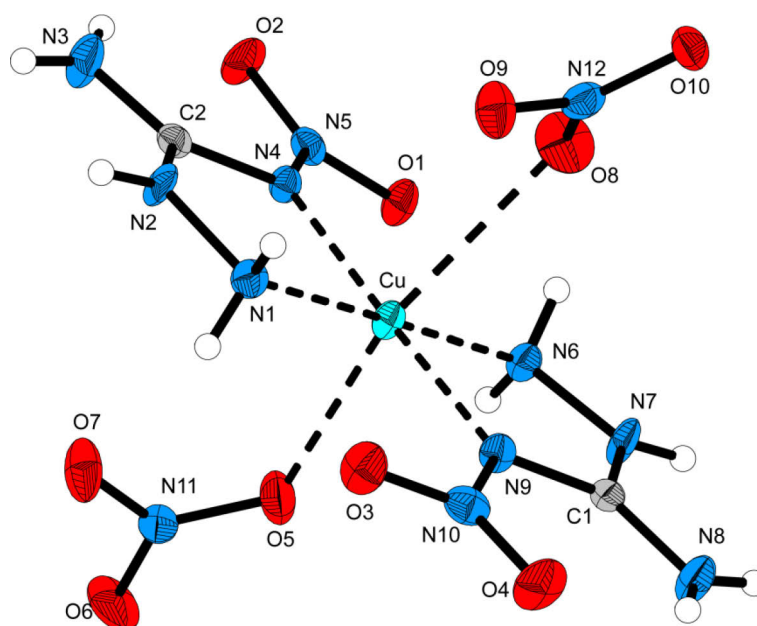


Figure 8. Molecular moiety of **10**. Thermal displacements of non-hydrogen atoms were set at 50 % probability. Hydrogen atoms are shown as spheres of arbitrary radius. Selected coordination distances [Å]: Cu–N6 1.982(2), Cu–N1 1.989(2), Cu–N4 2.0326(19), Cu–N9 2.0370(19), Cu–O5 2.3382(19); Cu–O8 2.586(2); angles [°]: N6–Cu–N1 178.8(1), N6–Cu–N4 99.67(8), N1–Cu–N4 79.69(8), N6–Cu–N9 79.02(9), N1–Cu–N9 101.65(9), N4–Cu–N9 178.13(8), N6–Cu–O5 84.27(9), N1–Cu–O5 94.70(9), N4–Cu–O5 94.28(7), N9–Cu–O5 86.93(8), O5–Cu–O8 160.18(7).

The dinitramide complexes **13** and **14** crystallize isotypically as tetrahydrates in the monoclinic crystal system within the space group $P2_1/c$. Two water molecules participate in the coordination sphere, while the others are connected to the dinitramide anions by formation

of hydrogen bonds (see Figure 10). The density of the cobalt complex **13** is slightly lower (1.964 g cm^{-3}) than that of nickel complex **14** (1.982 g cm^{-3}).

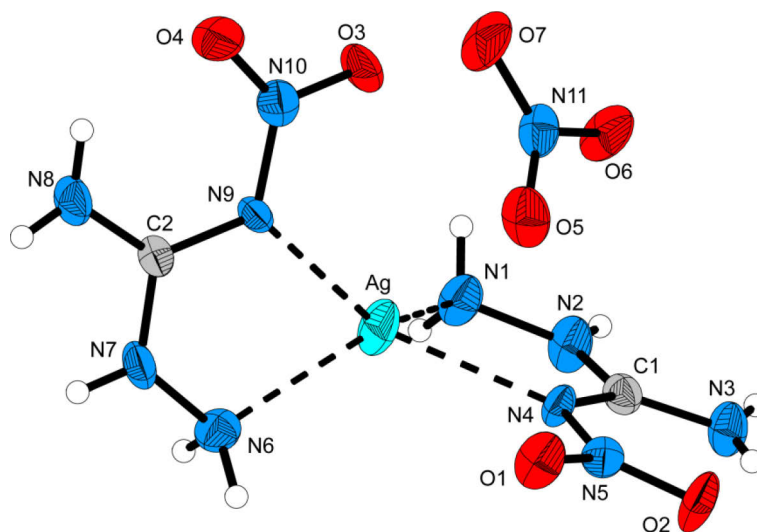


Figure 9. Molecular moiety of **12**. Thermal displacements of non-hydrogen atoms were set at 50 % probability. Hydrogen atoms are shown as spheres of arbitrary radius. Selected coordination distances [Å]: Ag–N6 2.344(4), Ag–N1 2.328(3), Ag–N9 2.301(3), Ag–N4 2.318(2); angles [°]: N9–Ag–N4 145.28(10), N9–Ag–N1 130.40(12), N4–Ag–N1 69.55(11), N9–Ag–N6 69.33(11), N4–Ag–N6 122.72(11), N1–Ag–N6 131.09(16).

The dinitramide anions are not planar and follow the twisted structure observed for, for example, lithium and potassium dinitramide.^[32]

The silver complex **15** could only be obtained crystalline (monoclinic, $P2_1/c$) as a monohydrate. The molecular motif is shown in Figure 11. The density of 2.456 g cm^{-3} is the highest observed in this work and is similar to that (2.488 g cm^{-3}) of silver dinitramide as its acetonitrile adduct.^[33]

Remarkably, the chlorido complexes $[M(\text{ANQ})\text{Cl}_2](\text{H}_2\text{O})_2$ (**16** ($M = \text{Co}^{2+}$), **17** ($M = \text{Ni}^{2+}$) and **19** ($M = \text{Zn}^{2+}$)) investigated in this work crystallize isotypically in the monoclinic space group $P2_1/n$. Also, **18** shows very similar unit-cell dimensions; however, for the space group $P2_1/c$. The molecular unit for **16**, **17**, and **19** is depicted in Figure 12. In contrast to the crystal water molecules the chlorido anions are enclosed in coordination. The densities of **16** (1.927 g cm^{-3}), **17** (1.950 g cm^{-3}), **18** (1.945 g cm^{-3}), and **19** (1.944 g cm^{-3}) are similar and in total the lowest observed in this work.

As already observed for the coordination sphere of the cations in **16**, **17**, and **19**, the copper cations in **18** possess an elongated octahedral coordination sphere due to the Jahn-Teller effect (see Figure 13). The copper chlorine coordination bonds are much longer ($\sim 2.71 \text{ Å}$) than the Cu–O bonds in the previously described complexes **5** and **10**. This is in agreement to the recently published structure of dichlorido-tetrakis-1,2,4-triazole copper(II), where the Cu–Cl bonds are even longer (2.83 Å).^[34]

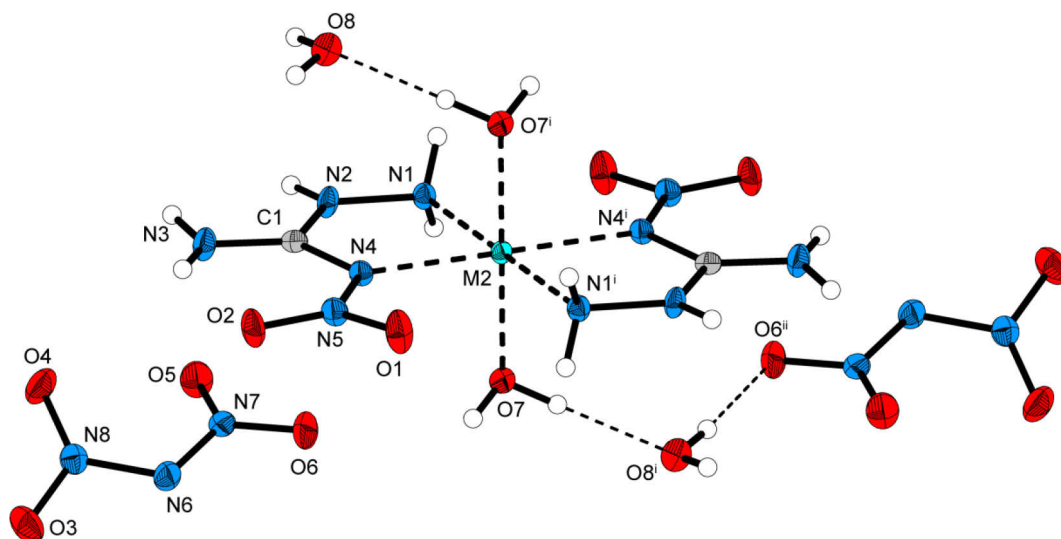


Figure 10. Molecular moiety of **13** ($M2 = Co$) and **14** ($M2 = Ni$). Thermal displacements of non-hydrogen atoms were set at 50 % probability. Hydrogen atoms are shown as spheres of arbitrary radius. Selected coordination distances [\AA]: **13**: Co–O7 2.0998(12), Co–N1 2.1128(14), Co–N4 2.1413(13); **14**: Ni–N1 2.0652(13), Ni–O7 2.0877(11), Ni–N4 2.1024(12); angles [$^\circ$]: **13**: O7–Co–N1 89.87(6), O7–Co–N4 90.67(5), N1–Co–N4 76.44(5); **14**: N1–Ni–O7 90.76(5), N1–Ni–N4 78.19(5), O7–Ni–N4 89.47(5). Symmetry codes: i: $1-x$, $1-y$, $1-z$.

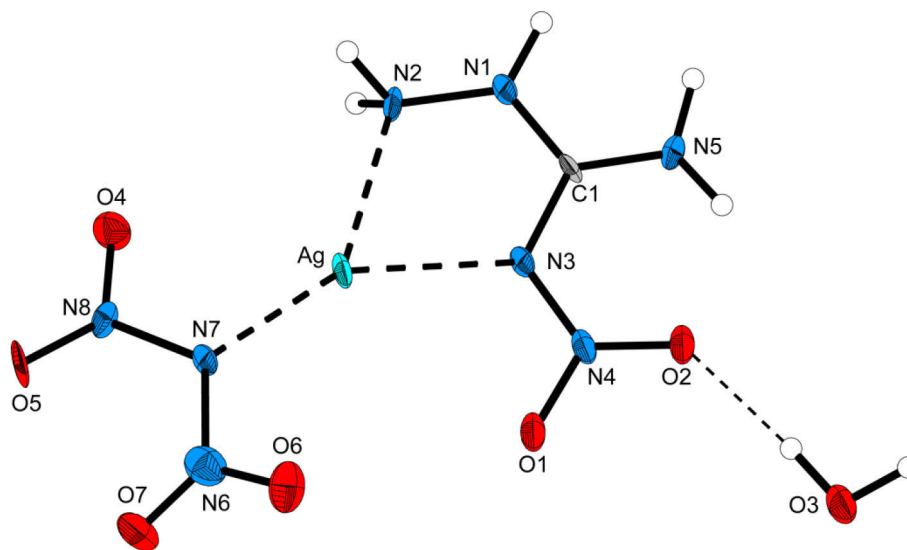


Figure 11. Molecular moiety of **15**. Thermal displacements of non-hydrogen atoms were set at 50 % probability. Hydrogen atoms are shown as spheres of arbitrary radius. Selected coordination distances [\AA]: Ag–N7 2.147(9), Ag–N3 2.260(9), Ag–N2 2.340(10); angles [$^\circ$]: N7–Ag–N3 147.4(4), N7–Ag–N2 142.3(3), N3–Ag–N2 70.1(3).

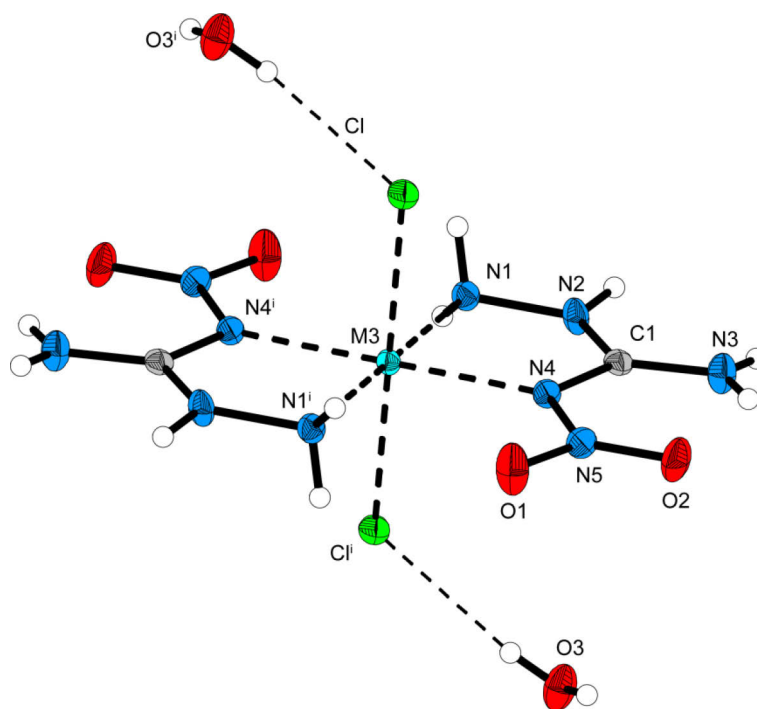


Figure 12. Molecular moiety of **16** ($M3 = \text{Co}$), **17** ($M3 = \text{Ni}$), and **19** ($M3 = \text{Zn}$). Thermal displacements of non-hydrogen atoms were set at 50 % probability. Hydrogen atoms are shown as spheres of arbitrary radius. Selected coordination distances (\AA): **16**: Co-N1 2.1212(14), Co-N4 2.1305(13), Co-Cl 2.4810(4); **17**: Ni-N1 2.0651(13), Ni-N4 2.0949(12), Ni-Cl 2.4600(4); **19**: Zn-N1 2.1071(15), Zn-N4 2.1439(14), Zn-Cl 2.5473(4); angles [$^\circ$]: **16**: N1-Co-N4 75.69(5), N1-Co-Cl 90.66(4), N4-Co-Cl 90.61(4); **17**: N1-Ni-N4 77.66(5), N1-Ni-Cl 89.71(4), N4-Ni-Cl 89.46(3); **19**: N1-Zn-N4 76.18(6), N1-Zn-Cl 89.24(5), N4-Zn-Cl 89.41(4). Symmetry codes: i: $1-x, -y, 1-z$.

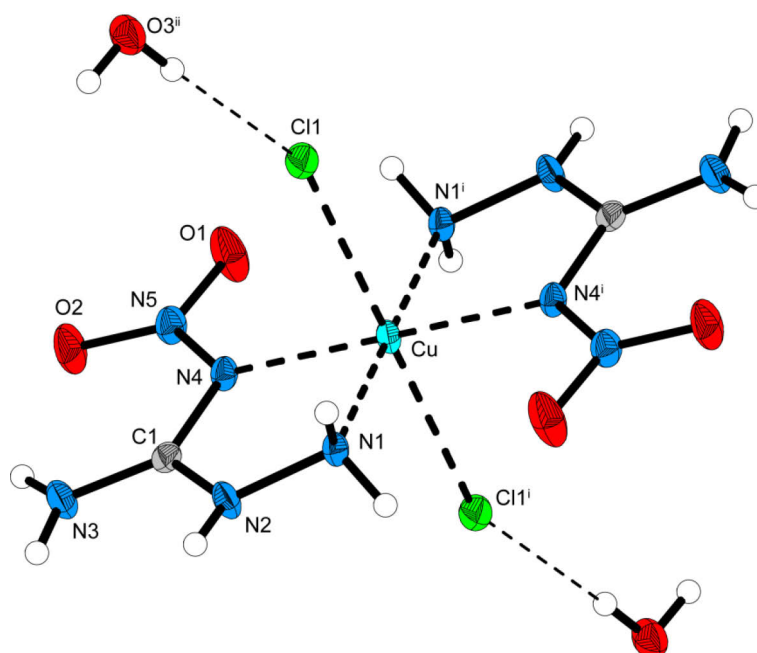


Figure 13. Molecular moiety of **18**. Thermal displacements of non-hydrogen atoms were set at 50 % probability. Hydrogen atoms are shown as spheres of arbitrary radius. Selected coordination distances [\AA]: Cu-N1 1.997(2), Cu-N4 2.053(2), Cu-Cl 2.7155(7); angles [$^\circ$]: N1-Cu-N4 79.14(8), N1-Cu-Cl 89.11(7), N4-Cu-Cl 89.90(6); Symmetry codes: i: $-x, -y, 2-z$; ii: $-x, -0.5+y, 0.5-z$.

IR spectroscopy: The assignments of absorptions were undertaken referring to values reported in literature.^[14,35] Strong absorptions are observed in all spectra in the region above 3000 cm^{-1} , indicating N–H and O–H valence vibrations. Here, the N–H valence vibration of the hydrazine moiety of the ligand is visible as a relatively sharp absorption band at $3430\text{--}3378\text{ cm}^{-1}$. This is in contrast to the absorptions of O–H valence vibrations at around $3300\text{--}3200\text{ cm}^{-1}$ of the crystal water containing complexes, which are broadened because of hydrogen bond formation. In comparison to the IR absorptions of neutral, uncomplexed ANQ, the N–H valence vibrations are observed at somewhat lower energies if complexed (3551 cm^{-1} in ANQ). Other important absorptions are the antisymmetric and the symmetric N–O valence vibration of the nitramine moiety both of which are present as strong absorptions in all spectra at $1687\text{--}1651\text{ cm}^{-1}$ (asym) and $1297\text{--}1275\text{ cm}^{-1}$ (sym). For both absorptions, again lower wave numbers are observed as compared to uncomplexed ANQ, which reveals values of 1692 and 1329 cm^{-1} for the absorptions of the aforementioned vibrations. A relatively strong absorption at $1245\text{--}1203\text{ cm}^{-1}$ can be assigned to the N–N valence vibration of the nitramine moiety, whereas a second absorption at slightly lower energy ($1139\text{--}1097\text{ cm}^{-1}$) can be attributed to the N–N valence vibration of the hydrazine moiety of the ligand. Furthermore, the characteristic absorptions of the nitrate and the perchlorate anion at $1385\text{--}1382$ and $1097\text{--}1083\text{ cm}^{-1}$ are observed in the respective IR spectra. The dinitramide anion can be detected by strong absorptions at $1539\text{--}1529\text{ cm}^{-1}$ (asymmetric in phase N–O valence vibration) and $1434\text{--}1431\text{ cm}^{-1}$ (asymmetric out of phase N–O valence vibration).

Sensitivities and Thermal Stability: The impact sensitivity tests were carried out according to STANAG 4489^[36] modified instruction^[37] using a BAM (Bundesanstalt für Materialforschung) drophammer.^[38] The friction sensitivity tests were carried out according to STANAG 4487^[39] modified instruction^[40] using the BAM friction tester. The classification of the tested compounds results from the “UN Recommendations on the Transport of Dangerous Goods”.^[41] Additionally, all compounds were tested upon the sensitivity toward electrical discharge using the Electric Spark Tester ESD 2010 EN.^[42] Because the described complexes are transition metal complexes with an energetic ligand together with energetic counterions such as nitrate, perchlorate, and dinitramide, we expect enhanced sensitivities toward outer stimuli. The perchlorates **3–7** are very sensitive toward impact, some of them (**5**, **7**) even bearing values of less than 1 J, which in the case of the silver complex is not least due to fact, that it crystallizes water free. Also the friction sensitivities are in a range between very sensitive (**3–6**) and extremely sensitive (**7**). The complexes bearing a nitrate counterion (**8–12**) at an average are less sensitive toward impact and friction than the perchlorate containing compounds, however they are still sensitive toward impact with two exceptions, the copper

(10) and the silver (12) complex, which crystallize water free, again are very sensitive toward impact, a trend that has already been observed for the perchlorate containing compounds 5 and 7. Almost the same argumentation can be applied to the friction sensitivities of the nitrates. Interestingly, the dinitramides 13–15, while still being comparatively sensitive, do not reach the high sensitivity levels of, for example, 7, 10, and 12 in terms of impact as well as friction sensitivity, presumably because of the inclusion of four (13, 14) and one (15) molecule of crystal water per formula unit, respectively. Holding no energetic anion, the four chloride complexes 16, 17, and 19 show moderate impact sensitivity and are less sensitive toward friction. Unfortunately, the yields of 18 allowed no determination of sensitivities.

Differential scanning calorimetry (DSC) measurements to determine the dehydration- and decomposition temperatures of 3–17 and 19 (about 1.5 mg of each energetic material) were performed in covered Al-containers containing a hole in the lid and a nitrogen flow of 20 mL min⁻¹ on a Linseis PT 10 DSC^[43] calibrated by standard pure indium and zinc at a heating rate of 5 °C min⁻¹. All decomposition temperatures are given as absolute onset temperatures, whereas dehydration temperatures are set at the minimum of the endothermic peak in the DSC curve.

Several interesting trends can be observed while comparing the decomposition temperatures of the complexes 3–17 and 19. The nickel complexes reveal the highest decomposition temperatures if compounds bearing the same anion are compared to each other (e.g., 4: 230 °C). For the perchlorates and nitrates, the zinc complexes follow the nickel complexes (e.g., 6: 198 °C) having the second highest decomposition temperatures again followed by the cobalt complexes (e.g., 3: 176 °C). The silver and especially the copper complexes decompose at relatively low temperatures oftentimes even below 100 °C (e.g., 5: 134 °C, 10: 77 °C). Comparing complexes with the same metal ion, the perchlorates have higher decomposition temperatures as the nitrates (e.g., 7: 148 °C, 12: 142 °C). Most of the chlorides show decomposition at even higher temperatures as the perchlorates except for the zinc complex (19: 172 °C). The dinitramides expectedly decompose at relatively low temperatures (13: 118 °C, 14: 142 °C), whereas the trend of higher decomposition temperatures of the nickel complexes is again confirmed. A detailed list of all decomposition and dehydration temperatures as well as the sensitivities toward impact, friction, and electrostatic discharge can be found in Table 1.

Most of the crystal water containing complexes can be dehydrated after heating (4, 6, 11, 13, 14–16, 19), indicated by an endothermic peak in the DSC curve, which is well-separated from the exothermic decomposition event. Some of the complexes decompose immediately after they start to lose their crystal water (3, 5, 9, 14), whereas for 8, no endothermic event before decomposition can be observed, although it crystallizes as a dihydrate.

Table 1. Sensitivities and thermal behaviour of **3–19**.

	IS (J)	FS (N)	ESD (J)	T_{dehydr} [°C]	T_{dec} [°C] #
3	3	10	0.03	170 ^[a]	176
4	3	10	0.04	162	230
5	<1	16	0.50	120 ^[a]	134
6	3	28	0.30	108, 154	198
7	<1	<5	0.01	– ^[b]	148
8	9	80	0.70	– ^[c]	139
9	4	120	0.08	160 ^[a]	186
10	<1	<5	0.50	– ^[b]	77
11	5	120	0.50	119	181
12	<1	<5	0.01	– ^[b]	142
13	5	80	0.70	85	118
14	3	80	0.60	138 ^[a]	142
15	2	7	0.10	71	108
16	10	360	0.70	144	186
17	10	360	0.70	150	250
19	10	360	0.70	104	172

[a] decomposition (exothermic) occurs immediately after dehydration (endothermic). [b] no crystal water contained. [c] no dehydration (endothermic event) observed before decomposition (exothermic event). # exothermic decomposition of the water free or dehydrated compounds.

UV–Vis–NIR Spectroscopy and Laser Ignition Tests: Further, the synthesized metal complexes **3–5**, **7–10**, as well as **13** and **14** were investigated upon their behavior toward single pulsed laser irradiation at a wavelength of 940 nm and a pulse length of 100 μs . The cobalt(II) complex **3**, copper(II) complex **5**, and also the silver(I) complex **7** could be initiated by a single pulse laser beam and led to detonation of samples, which previously to the experiment were pressed into pellets of approximately 8 mm diameter and 2 mm thickness. The nickel(II) complex **4** and all corresponding nitrate complexes **8–10** as well as even the complexes holding the highly energetic dinitramide anion **13–14** did not show any response to laser irradiation. The laser initiation mechanism (electronically, thermally, etc.) of transition metal complexes is still unknown. Related to that, the UV–Vis–NIR reflectance of the solid samples **3** ($[\text{Co}(\text{ANQ})_2(\text{H}_2\text{O})_2](\text{ClO}_4)_2$), **4** ($[\text{Ni}(\text{ANQ})_2(\text{H}_2\text{O})_2](\text{ClO}_4)_2$), **5** ($[\text{Cu}(\text{ANQ})_2(\text{ClO}_4)_2](\text{H}_2\text{O})_2$), and **7** ($[\text{Ag}(\text{ANQ})_2]\text{ClO}_4$) were measured on a Varian Cary 500 spectrometer in a wavelength range of 350–1300 nm. The measured diffuse reflectance R [%] was transformed after applying the Kubelka-Munk eq 1 to give the absorption function $F(R)$ (no unit).^[44]

$$\frac{K}{S} = \frac{(1-R_\infty)^2}{2R_\infty} \quad (1)$$

Where K is the absorption component, S the scattering component, and R_∞ the reflectance of an infinite thick sample.

The step in the absorption intensity $F(R)$ at 800 nm in Figure 14 is caused by a detector change. The spectra have only qualitative character. Due to technical limits no quantitative information about the absorption intensity can be obtained from the spectra. Commonly, R_∞ is technically approximated by a sample layer thick enough that the measuring instrument cannot detect differences in the thickness-dependent diffuse reflectance. However, not all samples could be coated on the object plate thick enough that there were no differences detectable anymore.

The information obtained from the UV–Vis–NIR spectra essentially is, that the four samples considerably differ in their absorption only at wavelengths in the visible and near UV region of the electromagnetic spectrum, what we would expect of four obviously differently colored samples. However in the NIR region, the samples 3–5 equally absorb radiation, especially at 940 nm, which is the wavelength of the laser beam used for laser initiation experiments. However, the silver complex shows no absorption at this wavelength.

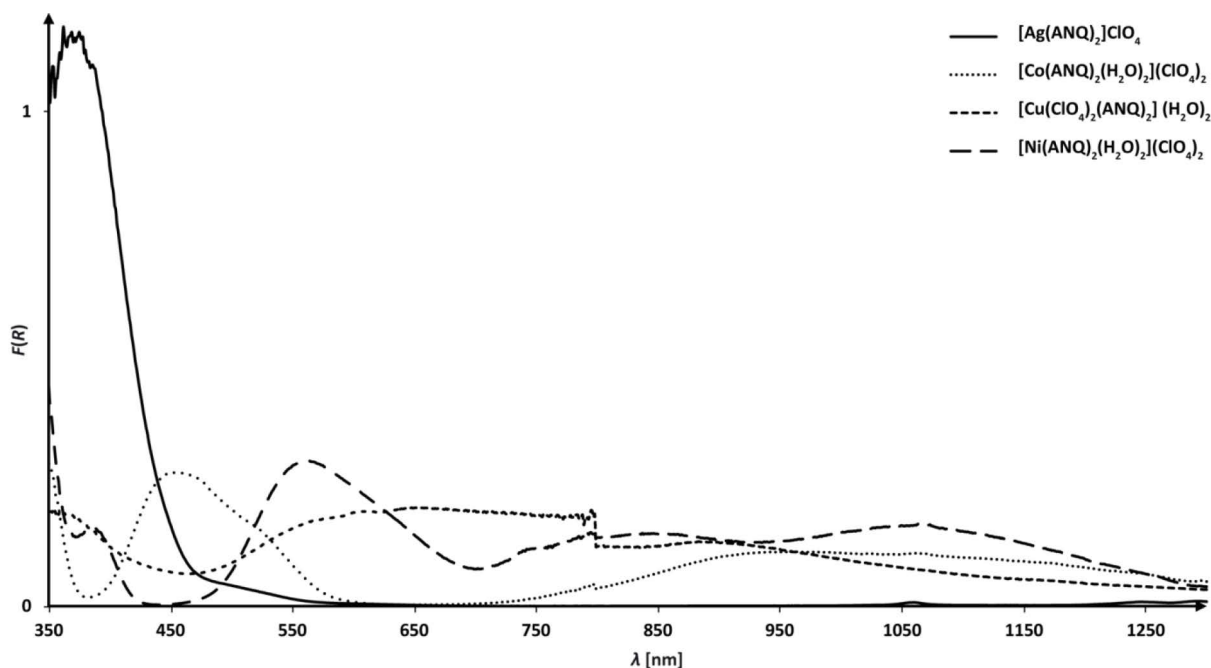


Figure 14. UV–Vis–NIR spectra of complexes 3–5 and 7. The absorption function $F(R)$ is obtained after applying the Kubelka–Munk equation.

Considering, that all metal perchlorates 3–5 except the silver(I) complex 7 were light absorbing at 940 nm together with the initiation results it seems that there is no relation between optical absorption properties and the photosensitivity toward pulsed laser irradiation, which is in agreement with the laser initiation experiments made by Ilyushin *et al.*^[13,45] The fact that only perchlorate compounds and no nitrates could be initiated fits to the literature

claimed initiation mechanism where an active perchlorate radical is formed by a one-electron transfer from the perchlorate anion to the metal cation induced by the laser beam.^[45]

Consequently, it seems, that the initiation of energetic materials by a short pulsed laser beam rather is an electronic process than a thermal one, especially when comparing the decomposition temperatures of the samples with their laser ignitability. For example, $[\text{Cu}(\text{ANQ})_2(\text{NO}_3)_2]$ (**10**) could not be initiated by the laser beam but shows the lowest thermal stability ($T_{\text{dec.}} = 77\text{ }^\circ\text{C}$) of the investigated compounds.

The role of the nature of the ligand in the laser initiation process is not yet fully understood and therefore under current investigation.

4.4. Conclusion

From the experimental study of energetic complexes based on 3-amino-1-nitroguanidine the following conclusions can be drawn:

- Combining boiling solutions of 3-amino-1-nitroguanidine (ANQ) and a transition metal ($M = \text{Co}, \text{Ni}, \text{Cu}, \text{Zn}, \text{Ag}$) perchlorate ($X = \text{ClO}_4$) or nitrate ($X = \text{NO}_3$) affords complexes $M^{2+}(\text{ANQ})_2(X^-)_2(\text{H}_2\text{O})_n$ ($n = 0, 2$) in the case of Co, Ni, Cu, and Zn or $M^+(\text{ANQ})_2(X^-)$ in the case of Ag, which readily crystallize from their aqueous mother liquors, but in minor yields. For Co, Ni, Cu, and Zn, the respective chlorides $M^{2+}(\text{ANQ})_2(X^-)_2(\text{H}_2\text{O})_2$ were also isolated following the same procedure.
- Complexes $M^{2+}(\text{ANQ})_2(X^-)_2(\text{H}_2\text{O})_4$ with $X = \text{N}(\text{NO}_2)_2$ were isolated in the case of $M = \text{Co}$ and Ni starting from the respective perchlorate containing complexes upon addition of ammonium dinitramide to the solutions. $\text{Ag}(\text{ANQ})(\text{N}(\text{NO}_2)_2)(\text{H}_2\text{O})$ crystallized after combining solutions of silver dinitramide and 3-amino-1-nitroguanidinium chloride (ANQ^+Cl^-).
- The complexes crystallize in the space groups $P\bar{1}$ (**5, 7–9, 11**), $P2_1/c$ (**3, 6, 13–15, 18**), $P2_1/n$ (**16, 17, 19**), $C2/c$ (**10**), $Pca2_1$ (**4**) and $Pbca$ (**12**) with densities between 1.927 (**16**) and 2.456 (**15**), whereas perchlorates, if hydrated, reveal higher densities than nitrates and chlorides. The highest densities are observed for the silver complexes.
- All perchlorate, nitrate, and chloride containing complexes crystallize as dihydrates, except for the silver complexes **7** and **12** and the copper complex **10**, which crystallize water free. The dinitramides crystallize as tetrahydrates (**13, 14**) and monohydrate (**15**), respectively. Most of the crystal water containing complexes can be dehydrated (**4, 6, 11, 13, 15–19**) without decomposition.
- Nickel complexes generally show the highest decomposition temperatures (**17**: 250 °C), whereas copper and silver complexes decompose at relatively low

temperatures (**10**: 77 °C). Also a trend of higher decomposition temperatures for chlorides and perchlorates as compared to nitrates and dinitramides is observed.

- All complexes bearing energetic counterions show enhanced sensitivities toward impact and friction, which especially applies to the solvate water free silver and copper complexes **7**, **10**, and **12** with values of < 1 J (IS) and < 5 N (FS).
- Selected perchlorate, nitrate and dinitramide containing complexes were tested upon their laser ignitability with a 100 μs laser pulse at 940 nm. Only the perchlorate containing complexes **3**, **5**, and **7** could successfully be initiated.
- UV–Vis–NIR spectra of the perchlorate containing complexes **3–5** and **7** were recorded and show, that there is no relationship between their absorption behavior at the designated wavelength of the laser beam (940 nm) and their initiation properties.

4.5. Experimental Section

Caution! The herein described metal complexes of ANQ are energetic materials with increased sensitivities towards shock and friction. Therefore, proper safety precautions (safety glass, face shield, earthed equipment and shoes, Kevlar gloves and ear plugs) have to be applied while synthesizing and handling the described compounds. All chemicals and solvents were employed as received (Sigma-Aldrich, Fluka, Acros). ¹H and ¹³C and ¹⁵N NMR spectra were recorded using a JEOL Eclipse 270, JEOL EX 400 or a JEOL Eclipse 400 instrument. The chemical shifts quoted in ppm in the text refer to typical standards such as tetramethylsilane (¹H, ¹³C) or nitromethane (¹⁵N). To determine the melting and decomposition temperatures of the described compounds a Linseis PT 10 DSC (heating rate 5 °C min⁻¹) was used. Infrared spectra were measured using a Perkin-Elmer Spectrum One FT-IR spectrometer as KBr pellets. Raman spectra were recorded on a Bruker MultiRAM Raman Sample Compartment D418 equipped with a Nd:YAG-Laser (1064 nm) and a LN-Ge diode as detector. Mass spectra of the described compounds were measured at a JEOL MStation JMS 700 using FAB technique. To measure elemental analyses, we employed a Netsch STA 429 simultaneous thermal analyzer.

3-Amino-1-nitroguanidine (2): Commercially available nitroguanidine (20 % H₂O, 25 g, 192 mmol) was dispersed in 250 mL of water and the mixture was heated to 55 °C. Hydrazine hydrate (10.5 mL, 216 mmol) was added dropwise over a period of 15 min and the temperature was kept at 55 °C for a further 15 min under constant stirring. After the mixture turned to a clear, orange solution, it was cooled to room temperature in an ice bath and the reaction was quenched with conc. hydrochloric acid (pH 7). 3-Amino-1-nitroguanidine starts to precipitate after the solution was cooled to 4 °C overnight. The product was separated by filtration and recrystallized from hot water. Yield: 10.3 g (86 mmol, 45 %). DSC

(5 °C min⁻¹): 184 °C (dec. 1), 200 °C (dec. 2); IR (KBr, cm⁻¹): $\tilde{\nu}$ = 3551 (s), 3411 (s), 3234 (s), 2025 (w), 1692 (m), 1637 (s), 1616 (vs), 1545 (m), 1502 (m), 1443 (m), 1384 (m), 1329 (m), 1134 (m), 1108 (m), 1088 (m), 1031 (m), 1005 (w), 963 (w), 870 (w), 772 (w), 745 (w), 696 (w), 622 (m), 571 (w), 482 (m). Raman (1064 nm, 200 mW, 25 °C, cm⁻¹): $\tilde{\nu}$ = 3319 (4), 3255 (13), 1659 (5), 1616 (4), 1580 (32), 1381 (13), 1287 (32), 1190 (5), 1111 (39), 1019 (5), 961 (100), 770 (27), 483 (30), 419 (33), 378 (10), 248 (13). ¹H NMR (DMSO-*d*₆, 25 °C, ppm) δ : 9.29 (s, 1 H, NH), 8.23 (s, 1 H, C-NH_AH_B), 7.52 (s, 1 H, C-NH_AH_B), 4.64 (s, 2 H, N-NH₂). ¹³C NMR (DMSO-*d*₆, 25 °C, ppm) δ : 161.5 (C(NNO₂)(N₂H₄)(NH₂)). ¹⁵N NMR (DMSO-*d*₆, 25 °C, ppm) δ : -13.3 (NO₂), -146.3 (NNO₂), -276.4 (NH/NH₂), -301.8 (NH/NH₂), -327.9 (NH/NH₂). MS (FAB⁻): *m/z* = 117.99 [M-H]⁻. EA (CH₅N₅O₂, 119.08) calcd: C 10.09, H 4.23, N 58.81 %; found: C 10.51, H 4.32, N 58.90 %. BAM drophammer: 20 J; friction tester: 144 N; ESD: 0.15 J (at grain size 100–500 μm).

Bis(3-amino-1-nitroguanidine)diaquacobalt(II) perchlorate (3): 3-Amino-1-nitroguanidine (0.50 g, 4.23 mmol) was dissolved in 20 mL of boiling water. Cobalt(II) perchlorate hexahydrate (1.548 g, 4.23 mmol) was added and the mixture was boiled until a clear solution resulted. The clear solution was filtered and slowly cooled to room temperature. After a few days, the product started to crystallize as red blocks. Yield: 35 % (788 mg, 1.48 mmol). The crystal density was 2.068 g cm⁻³. DSC (5 °C min⁻¹): 176 °C (dec.). IR (KBr, cm⁻¹): $\tilde{\nu}$ = 3548 (m), 3407 (s), 3321 (s), 3303 (s), 2964 (w), 2615 (w), 2231 (w), 2135 (w), 2059 (w), 1660 (s), 1579 (w), 1508 (m), 1480 (m), 1424 (m), 1385 (m), 1278 (s), 1211 (s), 1097 (vs), 938 (m), 820 (w), 808 (w), 779 (m), 717 (w), 671 (w), 663 (w), 627 (m), 599 (m), 520 (m). EA (C₂H₁₄Cl₂N₁₀O₁₄Co, 532.03) calcd: C 4.52, H 2.65, N 26.33 %; found: C 3.96, H 2.60, N 23.03 %. BAM drophammer: 3 J; friction tester: 10 N; ESD: 0.03 J (at grain size 500–1000 μm).

Bis(3-amino-1-nitroguanidine)diaquanickel(II) perchlorate (4): 3-Amino-1-nitroguanidine (0.50 g, 4.23 mmol) was dissolved in 20 mL of boiling water. Nickel(II) perchlorate hexahydrate (1.547 g, 4.23 mmol) was added and the mixture was boiled until a clear solution resulted. The clear solution was filtered and slowly cooled to room temperature. After a few days, the product started to crystallize as light purple blocks. Yield: 21 % (467 mg, 0.88 mmol). DSC (5 °C min⁻¹): 230 °C (dec.). IR (KBr, cm⁻¹): $\tilde{\nu}$ = 3527 (m), 3439 (s), 3401 (s), 3307 (s), 3247 (s), 2774 (w), 2626 (w), 2510 (w), 2219 (w), 2219 (w), 2054 (w), 2021 (w), 1657 (s), 1613 (s), 1569 (m), 1511 (s), 1492 (m), 1459 (m), 1412 (m), 1390 (m), 1283 (s), 1207 (s), 1108 (vs), 1083 (s), 938 (m), 814 (w), 776 (m), 716 (m), 672 (m), 625 (m), 600 (m), 515 (m). EA (C₂H₁₄Cl₂N₁₀O₁₄Ni, 531.79) calcd: C 4.52, H 2.65, N 26.34 %; found: C 4.72, H 2.50, N 25.98 %. BAM drophammer: 3 J; friction tester: 10 N; ESD: 0.04 J (at grain size 500–1000 μm).

Bis(3-amino-1-nitroguanidine)diperchloratocopper(II) dihydrate (5): 3-Amino-1-nitroguanidine (0.50 g, 4.23 mmol) is dissolved in 20 mL of boiling water. Copper(II) perchlorate hexahydrate (1.567 g, 4.23 mmol) is added and the mixture is boiled until a clear solution results. The clear solution is filtered and slowly cooled down to room temperature. After 1 h, the product starts to crystallize in blue blocks. Yield: 6.5 % (137 mg, 0.27 mmol). DSC (5 °C min⁻¹): 134 °C (dec.). IR (KBr, cm⁻¹): $\tilde{\nu}$ = 3500 (m), 3406 (s), 3285 (m), 3203 (m), 3076 (m), 1651 (s), 1610 (m), 1558 (w), 1511 (m), 1495 (s), 1432 (w), 1385 (m), 1322 (m), 1281 (s), 1212 (s), 1135 (s), 1108 (vs), 1083 (vs), 935 (m), 820 (w), 773 (w), 735 (w), 707 (w), 653 (w), 622 (m), 606 (m), 521 (m). EA (C₂H₁₄Cl₂N₁₀O₁₄Cu, 536.64) calcd: C 4.48, H 2.63, N 26.10 %; found: C 4.73, H 2.50, N 25.85 %. BAM drophammer: 1 J; friction tester: 16 N; ESD: 0.50 J (at grain size 100–500 μm).

Bis(3-amino-1-nitroguanidine)diaquazinc(II) perchlorate (6): 3-Amino-1-nitroguanidine (0.50 g, 4.23 mmol) is dissolved in 20 mL of boiling water. Zinc(II) perchlorate hexahydrate (1.575 g, 4.23 mmol) is added and the mixture is boiled until a clear solution results. The clear solution is filtered and slowly cooled to room temperature. Slow evaporation of the solvent affords **6** as colorless crystals. Yield: 21 % (441 mg, 0.82 mmol). DSC (5 °C min⁻¹): 198 °C (dec.). IR (KBr, cm⁻¹): $\tilde{\nu}$ = 3531 (m), 3487 (m), 3430 (s), 3338 (s), 3312 (s), 1655 (s), 1630 (m), 1576 (m), 1519 (m), 1495 (m), 1413 (m), 1384 (m), 1288 (s), 1217 (m), 1139 (s), 1090 (vs), 936 (m), 815 (w), 778 (m), 720 (w), 636 (m), 626 (m), 592 (w), 544 (w), 468 (w). EA (C₂H₁₄Cl₂N₁₀O₁₄Zn, 538.49) calcd: C 4.46, H 2.62, N 26.01 %; found: C 4.48, H 2.67, N 24.33 %. BAM drophammer: 3 J; friction tester: 28 N; ESD: 0.30 J (at grain size 100–500 μm).

Bis(3-amino-1-nitroguanidine)silver(I) perchlorate (7): 3-Amino-1-nitroguanidine (0.50 g, 4.23 mmol) is dissolved in 20 mL of boiling water. Silver(I) perchlorate (0.877 g, 4.23 mmol) is added and the mixture is boiled until a clear solution results. The clear solution is filtered and slowly cooled to room temperature. A fine gray precipitate, which forms upon standing of the solution after several hours, is removed by filtration, whereafter light yellow fascicular crystals began to grow. Slow evaporation of the solvent affords **7** in 22 % yield (407 mg, 0.91 mmol). DSC (5 °C min⁻¹): 148 °C (dec.). IR (KBr, cm⁻¹): $\tilde{\nu}$ = 3400 (s), 3305 (s), 3228 (s), 1656 (s), 1623 (s), 1583 (m), 1504 (m), 1460 (m), 1401 (m), 1291 (s), 1203 (m), 1095 (vs), 1023 (m), 1001 (m), 923 (m), 801 (w), 774 (w), 704 (w), 624 (m), 584 (m), 485 (w). EA (C₂H₁₀ClN₁₀O₈Ag, 445.48) calcd: C 5.39, H 2.26, N 31.44 %; found: C 5.68, H 2.94, N 31.31 %. BAM drophammer: < 1 J; friction tester: < 5 N; ESD: 0.01 J (at grain size 100–500 μm).

Bis(3-amino-1-nitroguanidine)diaquacobalt(II) nitrate (8): 3-Amino-1-nitroguanidine (0.50 g, 4.23 mmol) is dissolved in 20 mL of boiling water. Cobalt(II) perchlorate hexahydrate (1.231 g, 4.23 mmol) is added and the mixture is boiled until a clear solution

results. The clear solution is filtered and slowly cooled down to room temperature. **8** starts to crystallize in red blocklike crystals after 30 min. Yield: 47 % (910 mg, 1.99 mmol). DSC ($5\text{ }^{\circ}\text{C min}^{-1}$): $139\text{ }^{\circ}\text{C}$ (dec.). IR (KBr, cm^{-1}): $\tilde{\nu} = 3409$ (s), 3329 (m), 3273 (s), 3237 (m), 3196 (m), 1666 (s), 1638 (m), 1588 (m), 1524 (s), 1486 (s), 1384 (vs), 1340 (s), 1315 (m), 1275 (s), 1219 (s), 1111 (s), 1044 (m), 1028 (m), 937 (m), 825 (w), 814 (w), 780 (m), 694 (m), 647 (w), 616 (w), 597 (w), 523 (m). EA ($\text{C}_2\text{H}_{14}\text{N}_{12}\text{O}_{12}\text{Co}$, 457.14) calcd: C 5.25, H 3.09, N 36.77 %; found: C 5.59, H 2.94, N 36.51 %. BAM drophammer: 7 J; friction tester: 240 N; ESD: 0.50 J (at grain size 500–1000 μm).

Bis(3-amino-1-nitroguanidine)diaquanickel(II) nitrate (9): 3-Amino-1-nitroguanidine (0.50 g, 4.23 mmol) is dissolved in 20 mL of boiling water. Nickel(II) nitrate hexahydrate (1.230 g, 4.23 mmol) is added and the mixture is boiled until a clear solution results. The clear solution is filtered and slowly cooled to room temperature. After a few minutes, the product starts to crystallize as light purple plates. Yield: 49 % (950 mg, 2.08 mmol). DSC ($5\text{ }^{\circ}\text{C min}^{-1}$): $186\text{ }^{\circ}\text{C}$ (dec.); IR (KBr, cm^{-1}): $\tilde{\nu} = 3412$ (s), 3274 (s), 2637 (w), 2417 (w), 2296 (w), 2225 (w), 2142 (w), 2060 (w), 1972 (w), 1766 (m), 1662 (s), 1635 (s), 1522 (m), 1489 (s), 1385 (vs), 1278 (s), 1220 (s), 1111 (s), 1031 (m), 938 (m), 825 (w), 817 (w), 776 (m), 688 (m), 647 (w), 598 (w), 532 (m). EA ($\text{C}_2\text{H}_{14}\text{N}_{12}\text{O}_{12}\text{Ni}$, 456.90) calcd: C 5.26, H 3.09, N 36.79 %; found: C 5.57, H 2.94, N 36.07 %. BAM drophammer: 4 J; friction tester: 120 N; ESD: 0.08 J (at grain size 500–1000 μm).

Bis(3-amino-1-nitroguanidine)dinitratocopper(II) (10): 3-Amino-1-nitroguanidine (0.50 g, 4.23 mmol) is dissolved in 20 mL of boiling water. Copper(II) nitrate trihydrate (1.022 g, 4.23 mmol) is added and the mixture is boiled until a clear solution results. The clear solution is filtered and slowly cooled to room temperature. After 1 h, the product starts to crystallize as deep blue, blocklike crystals. Yield: 15 % (274 mg, 0.64 mmol). DSC ($5\text{ }^{\circ}\text{C min}^{-1}$): $77\text{ }^{\circ}\text{C}$ (dec.). IR (KBr, cm^{-1}): $\tilde{\nu} = 3439$ (m), 3412 (m), 3280 (m), 3126 (m), 1665 (s), 1629 (m), 1500 (m), 1382 (vs), 1281 (s), 1212 (s), 1141 (m), 1111 (m), 1045 (w), 943 (w), 820 (w), 773 (w), 724 (w), 705 (w), 653 (w), 603 (w), 565 (w), 480 (w). EA ($\text{C}_2\text{H}_{10}\text{N}_{12}\text{O}_{10}\text{Cu}$, 425.72) calcd: C 5.64, H 2.37, N 39.48 %; found: C 6.00, H 2.24, N 37.98 %. BAM drophammer: < 1 J; friction tester: < 5 N; ESD: 0.50 J (at grain size 100–500 μm).

Bis(3-amino-1-nitroguanidine)diaquazinc(II) nitrate (11): 3-Amino-1-nitroguanidine (0.50 g, 4.23 mmol) is dissolved in 20 mL of boiling water. Zinc(II) nitrate hexahydrate (1.258 g, 4.23 mmol) is added and the mixture is boiled until a clear solution results. The clear solution is filtered and slowly cooled to room temperature. Slow evaporation of the solvent affords **11** as colorless crystals. Yield: 25 % (492 mg, 1.06 mmol). DSC ($5\text{ }^{\circ}\text{C min}^{-1}$): $181\text{ }^{\circ}\text{C}$ (dec.). IR (KBr, cm^{-1}): $\tilde{\nu} = 3414$ (s), 3272 (s), 3240 (s), 3176 (s), 2763 (w), 2643 (w), 2426 (w), 2295 (w), 2223 (w), 2147 (w), 2064 (w), 1766 (w), 1663 (s), 1590 (m), 1526 (m), 1487 (s), 1384 (vs), 1280 (s), 1221 (s), 1114 (s), 1044 (m), 1030 (m), 935 (m), 827 (w), 813 (w),

780 (m), 745 (w), 696 (m), 638 (w), 584 (w), 527 (m). EA ($C_2H_{14}N_{12}O_{12}Zn$, 463.60) calcd: C 5.18, H 3.04, N 36.26 %; found: C 5.48, H 2.83, N 36.09 %. BAM drophammer: 5 J; friction tester: 120 N; ESD: 0.50 J (at grain size 100–500 μm).

Bis(3-amino-1-nitroguanidine)silver(I) nitrate (12): 3-Amino-1-nitroguanidine (0.50 g, 4.23 mmol) is dissolved in 20 mL of boiling water. Silver(I) nitrate (0.719 g, 4.23 mmol) is added and the mixture is boiled until a clear solution results. The clear solution is filtered and slowly cooled to room temperature. After 15 min, the product starts to crystallize as colorless blocks, which turn gray after several hours if not isolated and dried. Yield: 26 % (448 mg, 1.10 mmol). DSC ($5\text{ }^\circ\text{C min}^{-1}$): $142\text{ }^\circ\text{C}$ (dec.). IR (KBr, cm^{-1}): $\tilde{\nu} = 3432$ (s), 3401 (s), 3313 (s), 3219 (s), 3104 (m), 3010 (m), 2923 (m), 1665 (s), 1618 (s), 1580 (m), 1522 (m), 1473 (s), 1382 (s), 1355 (vs), 1292 (vs), 1245 (s), 1179 (s), 1108 (m), 1028 (m), 960 (m), 919 (m), 831 (w), 820 (w), 795 (w), 776 (w), 735 (w), 696 (m), 600 (m), 578 (m), 540 (m), 482 (w); EA ($C_2H_{10}N_{11}O_7Ag$, 408.04) calcd: C 5.89, H 2.47, N 37.76 %; found: C 6.25, H 2.28, N 37.30 %. BAM drophammer: 1 J; friction tester: < 5 N; ESD: 0.01 J (at grain size $< 100\text{ }\mu\text{m}$).

Bis(3-amino-1-nitroguanidine)diaquacobalt(II) dinitramide dihydrate (13): 3-Amino-1-nitroguanidine (0.50 g, 4.23 mmol) is dissolved in 15 mL of boiling water. Cobalt(II) perchlorate hexahydrate (1.55 g, 4.23 mmol) is added and the mixture is boiled until a clear solution results. Ammonium dinitramide (1.05 g, 8.46 mmol) is added to the solution and dissolved. The resulting solution is allowed to slowly cool to room temperature. The product crystallizes in flat orange prisms in 46 % yield (1.13 g, 1.94 mmol). DSC ($5\text{ }^\circ\text{C min}^{-1}$): $118\text{ }^\circ\text{C}$ (dec.); IR (KBr, cm^{-1}): $\tilde{\nu} = 3597$ (m), 3406 (s), 3302 (s), 3244 (s), 1658 (s), 1630 (m), 1612 (m), 1529 (s), 1512 (s), 1454 (s), 1434 (s), 1390 (m), 1344 (m), 1281 (s), 1204 (vs), 1178 (s), 1123 (m), 1099 (s), 1031 (s), 952 (m), 936 (m), 827 (w), 808 (w), 778 (w), 761 (w), 732 (m), 688 (w), 640 (w), 594 (w), 507 (m); EA ($C_2H_{18}N_{16}O_{16}Co$, 581.20) calcd: C 4.13, H 3.12, N 38.56 %; found: C 4.65, H 2.78, N 38.68 %. BAM drophammer: 5 J; friction tester: 80 N; ESD: 0.70 J (at grain size 100–500 μm).

Bis(3-amino-1-nitroguanidine)diaquanickel(II) dinitramide dihydrate (14): 3-Amino-1-nitroguanidine (0.50 g, 4.23 mmol) is dissolved in 15 mL of boiling water. Nickel(II) perchlorate hexahydrate (1.55 g, 4.23 mmol) is added and the mixture is boiled until a clear solution results. Ammonium dinitramide (1.05 g, 8.46 mmol) is added to the solution and dissolved. The resulting solution is allowed to slowly cool to room temperature. The product crystallizes in light purple plates in 36 % yield (0.888 g, 1.53 mmol). DSC ($5\text{ }^\circ\text{C min}^{-1}$): $142\text{ }^\circ\text{C}$ (dec.). IR (KBr, cm^{-1}): $\tilde{\nu} = 3405$ (s), 3302 (s), 3243 (s), 1658 (s), 1612 (m), 1539 (s), 1512 (s), 1454 (s), 1434 (s), 1388 (m), 1344 (m), 1283 (s), 1205 (vs), 1178 (s), 1122 (m), 1099 (s), 1022 (s), 952 (w), 936 (m), 827 (w), 808 (w), 778 (w), 761 (m), 749 (w), 732 (m), 688 (m), 640 (w), 593 (w), 509 (m); EA ($C_2H_{18}N_{16}O_{16}Ni$, 580.96): calcd C 4.13, H 3.12, N

38.58 %; found: C 4.57, H 2.99, N 38.09 %. BAM drophammer: 3 J; friction tester: 80 N; ESD: 0.60 J (at grain size 100–500 μm).

3-Amino-1-nitroguanidinedinitramidosilver(I) hydrate (15): Ten millimoles of silver dinitramide acetonitrile adduct was prepared according to the literature.^[20] 1-Amino-3-nitroguanidinium chloride^[19] (1.00 g, 6.4 mmol) was dissolved in 10 mL of boiling water. After the solution was cooled to about 60 °C, the silver dinitramide acetonitrile adduct, dissolved in 5 mL of acetonitrile, was added to the solution. After which the mixture was stirred under the exclusion of light at 35 °C for a further 2 h. The mixture was filtrated and **15** crystallizes from the clear filtrate in colorless needles. Yield: 0.61 g (2.50 mmol, 39 %). DSC (5 °C min⁻¹): 71 °C (dehydr.), 108 °C (dec.). IR (KBr, cm⁻¹): $\tilde{\nu}$ = 3398 (m), 3304 (m), 3218 (m), 1671 (m), 1622 (m), 1580 (m), 1539 (s), 1431 (s), 1344 (m), 1297 (s), 1205 (vs), 1176 (vs), 1108 (w), 1031 (s), 951 (w), 827 (w), 761 (w), 732 (w), 706 (w), 594 (w), 484 (w), 470 (w). ¹H NMR (DMSO-*d*₆, 25 °C, ppm) δ : 9.31 (s, 1 H, NH), 8.19 (s, 1 H, C–NH_AH_B), 7.69 (s, 1 H, C–NH_AH_B), 4.76 (s, 2 H, N–NH₂), 3.36 (s, 2 H, H₂O). ¹³C NMR (DMSO-*d*₆, 25 °C, ppm) δ : 160.9 (C(NNO₂)(N₂H₄)(NH₂)). ¹⁴N NMR (DMSO-*d*₆, 25 °C, ppm) δ : –11.0 (NO₂), –14.5 (NNO₂). *m/z* (FAB⁺): 120.1 [C(NNO₂)(N₂H₃)(NH₂)+H⁺], 107.0 [Ag⁺]; *m/z* (FAB⁻): 106.0 [N(NO₂)₂⁻]; EA (AgCH₇N₈O₇, 244.12) calcd: C 3.42, H 2.01, N 31.93 %; found: C 3.31, H 1.80, N 31.61 %; BAM drophammer: 2 J; friction tester: 7 N; ESD: 0.10 J.

Bis(3-amino-1-nitroguanidine)dichlorocobalt(II) dihydrate (16): 3-Amino-1-nitroguanidine (0.50 g, 4.23 mmol) is dissolved in 15 mL of boiling water. Cobalt(II) chloride hexahydrate (1.006 g, 4.23 mmol) is added and the mixture is boiled until a clear solution results. The solution is allowed to slowly cool to room temperature. The product starts to crystallize in red blocklike crystals in 32 % yield (0.555 g, 1.37 mmol). DSC (5 °C min⁻¹): 186 °C (dec.). IR (KBr, cm⁻¹): $\tilde{\nu}$ = 3457 (s), 3393 (vs), 3295 (s), 3245 (s), 3029 (m), 2963 (m), 1667 (s), 1626 (s), 1577 (m), 1521 (m), 1491 (s), 1430 (m), 1384 (m), 1277 (vs), 1217 (s), 1106 (s), 1015 (w), 931 (m), 777 (w), 748 (w), 705 (m), 594 (m). EA (C₂H₁₄Cl₂N₁₀O₆Co, 404.04) calcd: C 5.95, H 3.49, N 34.67 %; found: C 5.93, H 3.47, N 34.42 %. BAM drophammer: 10 J; friction tester: 360 N; ESD: 0.70 J (at grain size 100–500 μm).

Bis(3-amino-1-nitroguanidine)dichloronickel(II) Dihydrate (17): 3-Amino-1-nitroguanidine (0.50 g, 4.23 mmol) is dissolved in 15 mL of boiling water. Nickel(II) chloride hexahydrate (1.005 g, 4.23 mmol) is added and the mixture is boiled until a clear solution results. The solution is allowed to slowly cool to room temperature. The product starts to crystallize in light blue blocklike crystals in 42 % yield (0.722 g, 1.79 mmol). DSC (5 °C min⁻¹): 250 °C (dec.). IR (KBr, cm⁻¹): $\tilde{\nu}$ = 3378 (s), 3303 (s), 3245 (s), 2963 (m), 2923 (m), 2549 (m), 2457 (m), 1687 (vs), 1626 (m), 1519 (w), 1494 (m), 1432 (w), 1379 (m), 1277 (m), 1217 (m), 1196 (m), 1120 (m), 1094 (m), 1037 (m), 975 (m), 935 (m), 775 (w), 746 (w), 728 (w), 705 (w), 562 (m), 537 (m). EA (C₂H₁₄Cl₂N₁₀O₆Ni, 403.80) calcd: C 5.95, H 3.49, N

34.69 %; found: C 6.04, H 3.28, N 34.91 %. BAM drophammer: 10 J; friction tester: 360 N; ESD: 0.70 J (at grain size < 100 μm).

Bis(3-amino-1-nitroguanidine)dichlorocopper(II) Dihydrate (18): 3-Amino-1-nitroguanidine (0.50 g, 4.23 mmol) is dissolved in 15 mL of boiling water. Copper(II) chloride dihydrate (0.721 g, 4.23 mmol) is added and the mixture is boiled until a clear solution results. The solution is allowed to slowly cool to room temperature. Eventually precipitating 3-amino-1-nitroguanidine is filtered off. The product starts to crystallize in deep blue blocklike crystals in minor yield. Unfortunately, no analytical data except the crystal structure could be obtained, because ANQ started to precipitate immediately after the isolation of a single crystal of **18**.

Bis(3-amino-1-nitroguanidine)dichlorozinc(II) dihydrate (19): 3-Amino-1-nitroguanidine (0.50 g, 4.23 mmol) is dissolved in 15 mL of boiling water. Zinc(II) chloride (0.577 g, 4.23 mmol) is added and the mixture is boiled until a clear solution results. The solution is allowed to slowly cool to room temperature. 3-Amino-1-nitroguanidine precipitates as a colorless solid first, which is filtered off. The product starts to crystallize after several days in colorless blocks in minor yield. DSC (5 $^{\circ}\text{C min}^{-1}$): 172 $^{\circ}\text{C}$ (dec.). IR (KBr, cm^{-1}): $\tilde{\nu}$ = 3388 (s), 3244 (s), 3030 (m), 2961 (m), 1665 (s), 1628 (s), 1580 (m), 1521 (m), 1494 (s), 1432 (m), 1284 (vs), 1219 (s), 1111 (s), 1017 (w), 931 (m), 778 (m), 752 (w), 706 (m), 598 (m). EA ($\text{C}_2\text{H}_{14}\text{Cl}_2\text{N}_{10}\text{O}_6\text{Zn}$, 410.48) calcd: C 5.85, H 3.44, N 34.12 %; found: C 6.02, H 3.27, N 33.49 %. BAM drophammer: 10 J; friction tester: 360 N; ESD: 0.70 J (at grain size < 100 μm).

4.6. References

- [1] (a) Tao, G.-H.; Parrish, D. A.; Shreeve, J. M. *Inorg. Chem.* **2012**, *51*, 5305–5312. (b) Tao, G.-H.; Twamley, B.; Shreeve, J. M. *Inorg. Chem.* **2009**, *48*, 9918–9923.
- [2] Tappan, B. C.; Huynh, M. H.; Hiskey, M. A.; Chavez, D. E.; Luther, E. P.; Mang, J. T.; Son, S. *F. J. Am. Chem. Soc.* **2006**, *128*, 6589–6594.
- [3] Zhao, H.; Qu, Z. R.; Ye, H. Y.; Xiong, R. G. *Chem. Soc. Rev.* **2008**, *37*, 84–100.
- [4] Singh, R. P.; Verma, R. D.; Meshri, D. T.; Shreeve, J. M. *Angew. Chem., Int. Ed.* **2006**, *45*, 3584–3601.
- [5] Hofmann, A. W. *J. Chem. Soc. Trans.* **1866**, *19*, 249–255.
- [6] (a) Berlinck, R. G. S.; Burtoloso, A. C. B.; Trindade-Silva, A. E.; Romminger, S.; Morais, R. P.; Bandeira, K.; Mizuno, C. M. *Nat. Prod. Rep.* **2010**, *27* (12), 1871–1907. (b) Saczewski, F.; Balewski, L. *Expert Opin. Ther. Pat.* **2009**, *19* (10), 1417–1448.
- [7] Neumann, F. W.; Shriner, R. L. *Org. Synth.* **1946**, *26*, 7–8.
- [8] Davis, T. L. *Org. Synth.* **1927**, *7*, 68–69.

- [9] (a) Jousselein, L. *Compt. Rend.* **1879**, 88, 1086. (b) Pellizzari, G. *Gazz. chim. ital.* **1891**, 21, 405–409.
- [10] Metelkina, E. L.; Novakova, T. A.; Berdonosova, S. N.; Berdonosov, D. Yu. *Russ. J. Org. Chem.* **2005**, 41 (3), 440–443.
- [11] ÓConnor, T. E.; Fleming, G.; Reilly, J. *J. Soc. Chem. Ind. London* **1949**, 68, 309–310.
- [12] Fischer, N.; Klapötke, T. M.; Stierstorfer, J. *Z. Naturforsch. B* **2012**, 67 (6), 573–588.
- [13] Zhilin, A. Y.; Ilyushin, M. A.; Tselinskii, I. V.; Kozlov, A. S.; Lisker, I. S. *Russ. J. Appl. Chem.* **2003**, 76 (4), 572–576.
- [14] Christe, K. O.; Wilson, W. W.; Petrie, M. A.; Michels, H. H.; Bottaro, J. C.; Gilardi, R. *Inorg. Chem.* **1996**, 35 (17), 5068–5071.
- [15] Gao, Y.; Gao, H.; Piekarski, C.; Shreeve, J. M. *Eur. J. Inorg. Chem.* **2007**, 31, 4965–4972.
- [16] Bottaro, J. C.; Penwell, P. E.; Schmitt, R. J. *J. Am. Chem. Soc.* **1997**, 119, 9405–9410.
- [17] Hafenrichter, E. S.; Marshall, B., Jr.; Fleming, K. J. *Proc. Int. Pyrotech. Semin.* **2002**, 29th, 787–793.
- [18] Castillo-Meléndez, J. A.; Golding, B. T. *Synthesis* **2004**, 10, 1655–1663.
- [19] Fischer, N.; Klapötke, T. M.; Lux, K.; Martin, F. A.; Stierstorfer, J. *Crystals* **2012**, 2, 675–689.
- [20] Ang, H.-G.; Fraenk, W.; Karaghiosoff, K.; Klapötke, T. M.; Mayer, P.; Nöth, H.; Sprott, J.; Warchhold, M. *Z. Anorg. Allg. Chem.* **2002**, 628, 2894–2900.
- [21] CrysAlisPro, Version 171.33.41; Oxford Diffraction Ltd.: Abingdon, U.K., 2009.
- [22] Altomare, A.; Cascarano, G.; Giacovazzo, C.; Guagliardi, A. *J. Appl. Crystallogr.* **1993**, 26, 343.
- [23] Sheldrick, G. M. *SHELXS-97, Program for Crystal Structure Solution*; University of Göttingen: Göttingen, Germany, 1997.
- [24] Sheldrick, G. M. *SHELXL-97, Program for the Refinement of Crystal Structures*; University of Göttingen: Göttingen, Germany, 1997.
- [25] Spek, A. L. *PLATON, A Multipurpose Crystallographic Tool*; Utrecht University: Utrecht, The Netherlands, 1998.
- [26] Farrugia, L. J. *J. Appl. Crystallogr.* **1999**, 32, 837–838.
- [27] Empirical absorption correction using spherical harmonics, implemented in SCALE3 ABSPACK scaling algorithm: CrysAlisPro, Version 171.33.41; Oxford Diffraction Ltd.: Abingdon, U.K., 2009.
- [28] Hu, S.; Barton, R. J.; Johnson, K. E.; Robertson, B. E. *Acta Crystallogr.* **1981**, A37, 229–238.
- [29] Jahn, H. A.; Teller, E. *Proc. R. Soc. London, A* **1937**, 161, 220–235.
- [30] Akitsu, T.; Einaga, Y. *Acta Crystallogr., Sect. E* **2004**, 60, m234–m236.

- [31] Lindley, P. F.; Woodward, P. J. *Chem. Soc. A* **1966**, 123–126.
- [32] Gilardi, R.; Flippen-Anderson, J.; George, C.; Butcher, R. J. *J. Am. Chem. Soc.* **1997**, *119*, 9411–9416.
- [33] Ang, H.-G.; Fraenk, W.; Karaghiosoff, K.; Klapötke, T. M.; Mayer, P.; Nöth, H.; Sprott, J.; Warchhold, M. *Z. Anorg. Allg. Chem.* **2002**, *628*, 2894–2900.
- [34] Vidmar, M.; Kobal, T.; Kozlevcar, B.; Segedin, P.; Golobic, A. *Acta Crystallogr., Sect. E* **2012**, *68*, m375–376.
- [35] Hesse, M.; Meier, H.; Zeeh, B. in *Spektroskopische Methoden in der Organischen Chemie*, 8th ed.; Thieme: Stuttgart, Germany, 2012.
- [36] *NATO standardization agreement (STANAG) on explosives, impact sensitivity tests, no. 4489*, 1st ed.; NATO: Brussels, Belgium, Sept. 17, 1999.
- [37] *WIWEB-Standardarbeitsanweisung 4–5.1.02, Ermittlung der Explosionsgefährlichkeit, hier der Schlagempfindlichkeit mit dem Fallhammer*; Wehrwissenschaftliches Institut für Werk-, Explosiv- und Betriebsstoffe: Erding, Germany, Nov. 8, 2002.
- [38] <http://www.bam.de>.
- [39] *NATO standardization agreement (STANAG) on explosive, friction sensitivity tests, no. 4487*, 1st ed.; NATO: Brussels, Belgium, Aug. 22, 2002.
- [40] *WIWEB-Standardarbeitsanweisung 4–5.1.03, Ermittlung der Explosionsgefährlichkeit oder der Reibeempfindlichkeit mit dem Reibeapparat*; Wehrwissenschaftliches Institut für Werk-, Explosiv- und Betriebsstoffe: Erding, Germany, Nov. 8, 2002.
- [41] Impact: insensitive > 40 J, less sensitive g 35 J, sensitive g 4 J, very sensitive e 3 J. Friction: insensitive > 360 N, less sensitive) 360 N, sensitive < 360 N a.> 80 N, very sensitive e 80 N, extremely sensitive e10 N. According to the UN Recommendations on the Transport of Dangerous Goods, (+) indicates not safe for transport.
- [42] <http://www.ozm.cz>.
- [43] <http://www.linseis.com>.
- [44] Kubelka, P.; Munk, F. *Z. Tech. Phys.* **1931**, *1*, 593–601.
- [45] Ugryumov, I. A.; Ilyushin, M. A.; Tselinskii, I. V.; Kozlov, A. S. *Russ. J. Appl. Chem.* **2003**, *76* (3), 439–441.

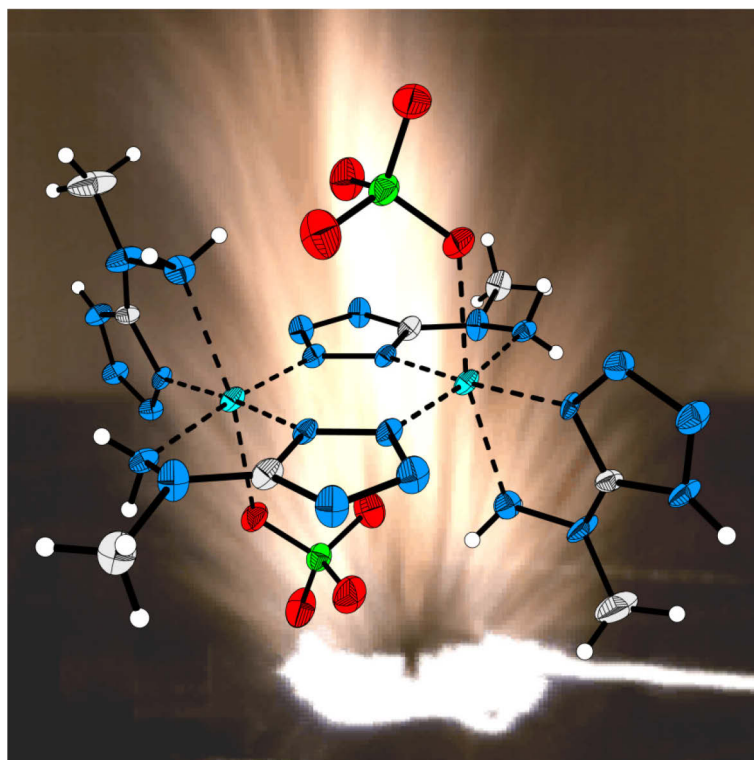
5. Synthesis and Characterization of Various Photosensitive Copper(II) Complexes with 5-(1-Methylhydrazinyl)-1*H*-tetrazole as Ligand and Perchlorate, Nitrate, Dinitramide, and Chloride as Anions

Reproduced with permission from M. Joas, T. M. Klapötke, J. Stierstorfer, N. Szimhardt,

Chemistry – A European Journal **2013**, *19*, 9995–10003.

Online: <http://dx.doi.org/10.1002/chem.201300688>.

Copyright 2013 WILEY-VCH Verlag GmbH & Co. KGaA, Weinheim.



5.1. Abstract

The preparation of 5-(1-methylhydrazinyl)-1*H*-tetrazole monohydrate (**1**·H₂O) and various copper(II) complexes with perchlorate (**2** and **3**), nitrate (**4**, **5**, and **6**), dinitramide (**7**), and chloride (**8**) is described. The coordination compounds (monomers, dimers, and polymers) were characterized through infrared spectroscopy and elemental analysis. Further, the structures of **2** and **4–8** were determined by single-crystal X-ray diffraction. Compound **1** can act as a bidentate ligand in its neutral form (HMHT) and as a μ_2 - or μ_3 -bridging ligand in its deprotonated form (MHT). The energetic properties of the synthesized complexes, such as

their sensitivities toward impact and friction, were determined, and laser ignition tests were performed. New information about the laser initiation process and the role of the anion in the initiation criterion was obtained. The perchlorate complexes **2** ($T_{\text{decomp}} = 217\text{ }^{\circ}\text{C}$) and **3** ($T_{\text{decomp}} = 206\text{ }^{\circ}\text{C}$) are potential primary explosives.

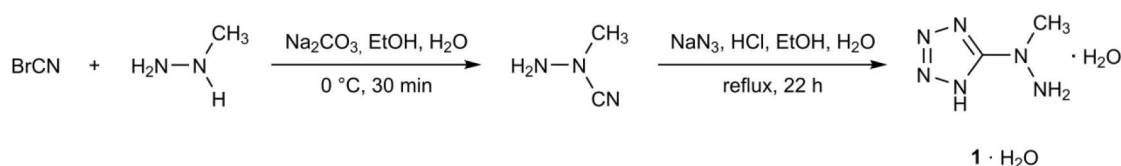
5.2. Introduction

The development of new energetic materials achieving several aspects such as environmental acceptability and high performance is of great interest.^[1] The greatest scientific importance is placed on alternatives to RDX (hexogen), perchlorate- free high-energy dense oxidizers, and lead-free primary explosives. However, in recent years, new applications for energetic materials have appeared. Interesting materials in this regard are photosensitive primers and detonator systems for civil as well as military applications. In particular, energetic transition metal complexes showed great sensitivity toward laser irradiation.^[2] The most prominent representatives are tetrammine-cis-bis(5-nitrotetrazolato- N^2)cobalt(III) perchlorate (BNCP)^[3] and 5-hydrazinotetrazolemercury(II) perchlorate (HTMP),^[4] but copper(II)^[2b] and nickel(II)^[5] complexes were also tested successfully on laser irradiation. The initiation of secondary explosives or pyrotechnics by high-power laser irradiation has already been investigated extensively for 40 years.^[6] In these examples, a thermal initiation process was discussed. Thermal laser initiation is a nonselective and relatively slow initiation process.^[7] The threshold energy for thermal excitation depends on the light absorption intensity of the compound at the wavelength of the initiating light. This means that light absorbing particles such as soot help by forming hot spots, which lead to the decomposition of the irradiated compound. In contrast, the other initiation mechanism discussed is selective, is photoelectronic in nature, and seems to be the mechanism that plays an important role in low-energy short-pulse laser irradiation.^[8] This initiation mechanism is much faster, and initiation only takes place if the wavelength of the laser beam corresponds to an electronic excitation that leads to the formation of active radicals.^[2c, 8]

Tetrazole and triazole derivatives with reactive groups such as nitro or hydrazine are interesting ligands for photosensitive coordination compounds.^[2a,c,9] In particular, 5-hydrazino-1*H*-tetrazole, which was already described by Thiele in the 19th century,^[10] seems to be an interesting ligand for transition metal complexes.^[4] However, the dissolved compound can be oxidized easily by air, which complicates the synthesis of metal complexes. A better ligand, which is less susceptible to oxidation, seems to be the 5-(1-methylhydrazinyl)-1*H*-tetrazole (**1**, HMHT). To the best of our knowledge, only the copper(II) and silver(I) salt of deprotonated **1** have so far been described in the literature.^[11] Consequently, the new copper(II) complexes of **1** with perchlorate, nitrate, dinitramide, and chloride as anions were synthesized, characterized, and tested upon laser irradiation.

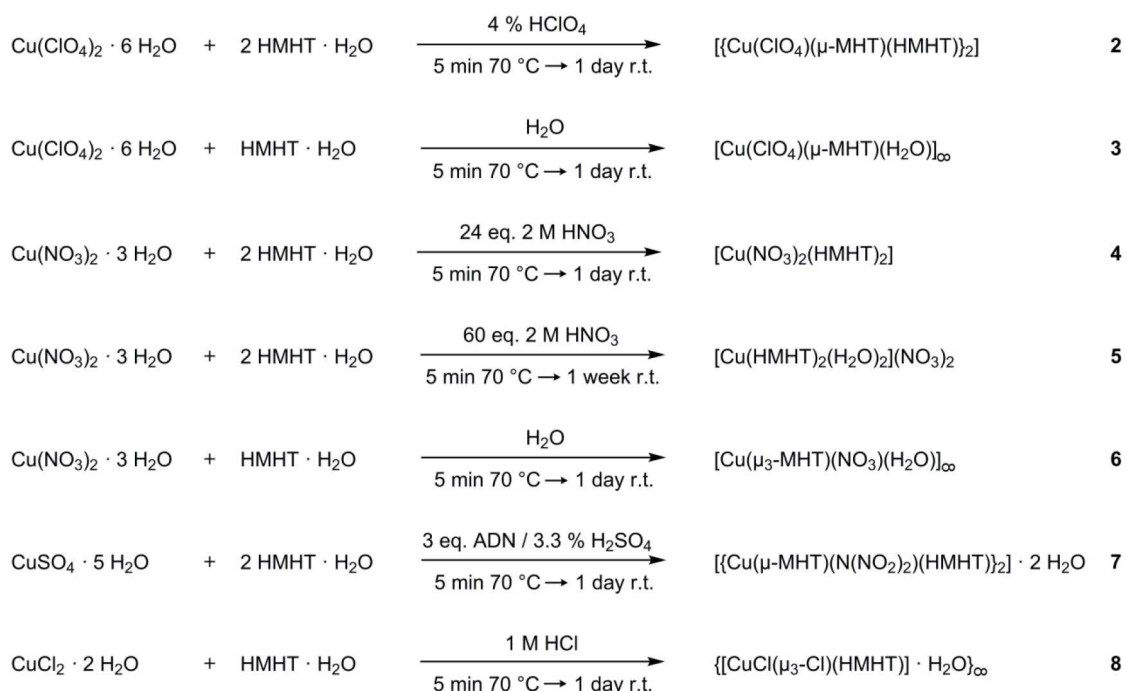
5.3. Results and Discussion

Synthesis: The nitrogen-rich ligand 5-(1-methylhydrazinyl)-1*H*-tetrazole (**1**, HMHT) can be synthesized through two routes. One involves the substitution reaction of monomethylhydrazine with cyanogen bromide to 1-methylhydrazinecarbonitrile and further cyclization with sodium azide to the monohydrate of **1**, in a yield of 40% (Scheme 1).^[12] The other route starts with the formation of the highly explosive cyanogen azide from cyanogen bromide and sodium azide in an acetonitrile/water mixture.^[11] The cyanogen azide is then further reacted with monomethylhydrazine to form the water-free compound **1** in a lower yield of 11%. However, the first route is much safer and avoids the handling of the extremely sensitive cyanogen azide.



Scheme 1. Synthesis of **1**·H₂O.

The copper(II) complexes were prepared by adding a solution of a copper(II) salt in the corresponding acid or water to a warm solution of **1**·H₂O in water (Scheme 2). Most of the products were obtained directly from the mother liquor as single crystals suitable for X-ray diffraction. Only compound **3** precipitated as a powder and single crystals could not be obtained by recrystallization. Compound **4** could also be obtained through the dehydration of **5** at 80 °C for 2 h.



Scheme 2. Synthesis of complexes **2–8**.

Crystal structures: The detailed data of the X-ray measurements and refinements are available in the Supporting Information (Table S1 and several other figures and tables).

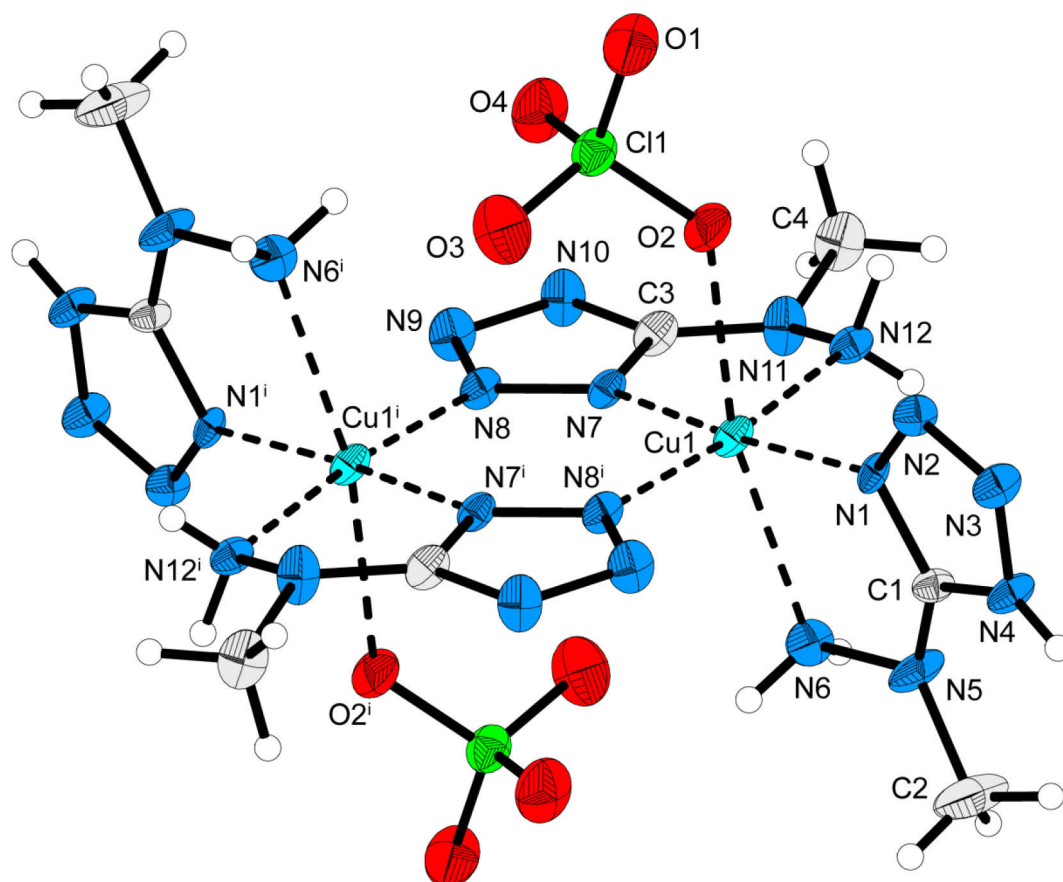


Figure 1. Molecular unit of **2**. Thermal ellipsoids of non-hydrogen atoms are drawn at the 50 % probability level. Selected bond lengths [Å]: Cu1–N1 1.973(3), Cu1–N7 1.956(4), Cu1–N6 2.385(4), Cu1–N12 2.076(4), Cu1–O2 2.485(3), Cu1–N8ⁱ 2.008(4), N1–C1 1.333(5), N1–N2 1.355(5), N2–N3 1.279(5), N3–N4 1.355(5), N4–C1 1.333(6), N5–C1 1.334(6), N5–C2 1.433(6), N5–N6 1.420(5), C11–O1 1.432(4); selected bond angles [°]: N1–Cu1–N6 74.9(1), N1–Cu1–N8ⁱ 91.7(1), N1–Cu1–N12 94.1(1), O2–Cu1–N6 162.3(1), N7–Cu1–N12 80.0(2), N1–C1–N4 107.4(4), N4–C1–N5 128.4(4), C1–N5–C2 123.9(4), C2–N5–N6 119.9(4), O3–C11–O2 109.0(2); selected torsion angles [°]: N1–Cu1–N12–N7 –179.1(1), N1–Cu1–N8ⁱ–N7 178.8(1), N1–Cu1–O2–N6 1.8(4), N1–Cu1–N6–C1 1.2(2), Cu1–N1–C1–N5 9.2(6), N1–C1–N4–N3 1.3(5), N4–C1–N5–C2 7.8(8). Symmetry code: *i*: 1–*x*, 1–*y*, 2–*z*.

The perchlorate complex **2** crystallizes as green plates in the monoclinic space group $P2_1/n$ with two formula units per unit cell and a calculated density of 1.873 g cm⁻³ at 173 K. The asymmetric unit consists of one half of the molecular unit. The copper(II) center is octahedrally coordinated and bridged over a 5-(1-methylhydrazinyl)tetrazolato ligand to a copper dimer (Figure 1). The coordination octahedron has a Jahn–Teller distortion along the O2–Cu1–N6 axis with typical values for a d⁹–Cu^{II} complex (Cu1–N6 = 2.385(4) and Cu1–O2 = 2.485(3) Å). The structure of the complex is not ideally octahedral owing to the O2–Cu1–N6 angle of 162.3(1)°. This deformation can be explained by the fixed structure of **1**. The bond lengths and angles of the deprotonated ligand 5-(1-methylhydrazinyl)tetrazolato (C3–N10 = 1.334(6) Å) and the neutral 5-(1-methylhydrazinyl)tetrazole (C1–

$N6 = 2.054(2)$ Å, and $N4-N6-N4^i-N6^i = -0.0(1)^\circ$) and two monodentate nitrate anions in axial positions ($Cu1-O1 = 2.491(2)$ Å and $O1-Cu-O1^i = 180.0(0)^\circ$) (Figure 2). The coordination sphere shows Jahn–Teller distortion along the $Cu1-O1$ axis. The structure of the neutral HMHT ligand in **4** is similar to that of complex **2**. The bond lengths and angles of the coordinated nitrate anion are in agreement with the literature values.^[14] The complex monomers are connected to each other over three nearly linear hydrogen bonds (Table 1) between the HMHT ligand and the nitrate anions of a neighboring complex unit (Figure 3).

Table 1. Distances and angles of selected hydrogen bonds in **4**.

$D-H\cdots A^{[a]}$	$D-H / \text{Å}$	$H\cdots A / \text{Å}$	$D\cdots A / \text{Å}$	$D-H\cdots A / ^\circ$
$N1-H1\cdots O1^{ii}$	0.81(4)	1.92(4)	2.699(3)	162(3)
$N6-H6A\cdots O3^{iii}$	0.83	2.28(2)	3.083(3)	164(2)
$N6-H6B\cdots O2^{iv}$	0.81	2.29(3)	3.083(3)	165(2)

[a] Symmetry codes: ii: $1+x, y, z$; iii: $-x, -0.5+y, 1.5-z$; iv: $x, 0.5-y, -0.5+z$.

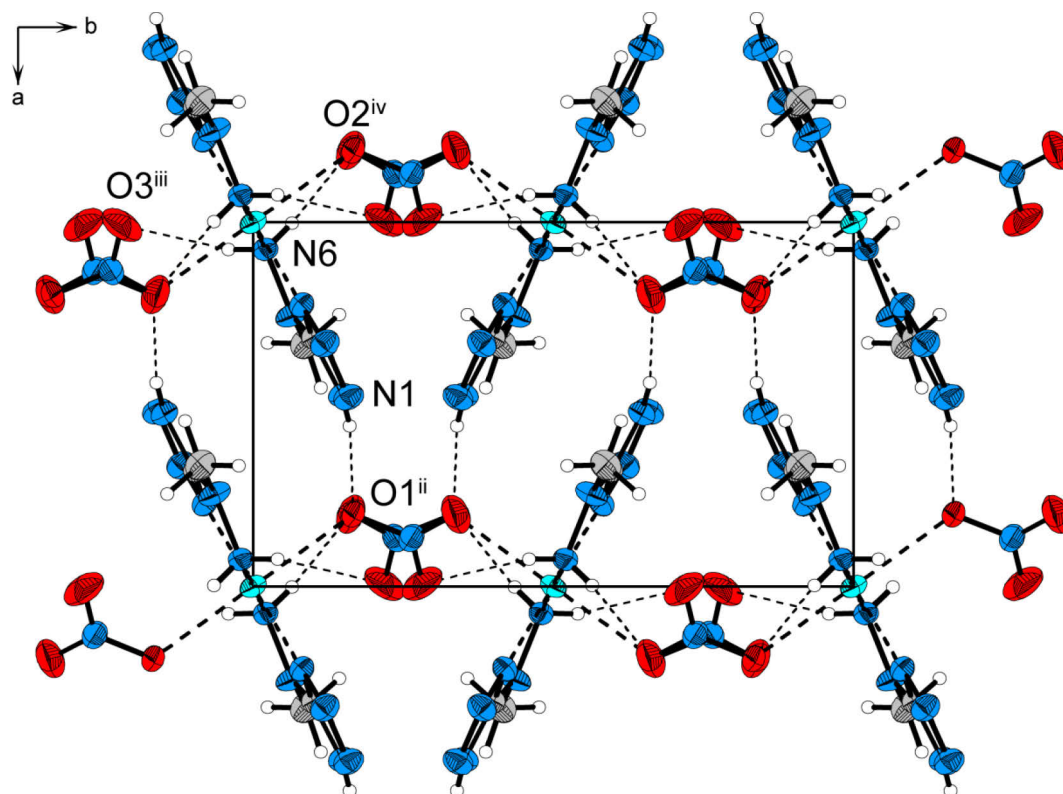


Figure 3. Packing of **4** and stabilization by hydrogen bonds (view along the c axis). Symmetry codes: ii: $1+x, y, z$; iii: $-x, -0.5+y, 1.5-z$; iv: $x, 0.5-y, -0.5+z$.

The diaqua complex **5** crystallizes as blue blocks in the triclinic space group $P\bar{1}$ with one formula unit per unit cell and a calculated density of 1.903 g cm^{-3} at 173 K. The copper(II) center has an octahedral coordination sphere with Jahn–Teller distortion along the copper–aqua bonds (Figure 4). The $Cu1-O1$ bond ($2.477(3)$ Å) of the aqua ligand is similar to the $Cu-O$ bond of the nitrate ligand in complex **4**. The nitrate anions do not coordinate to the copper center; however, the bond lengths and angles are similar to those of the coordinated

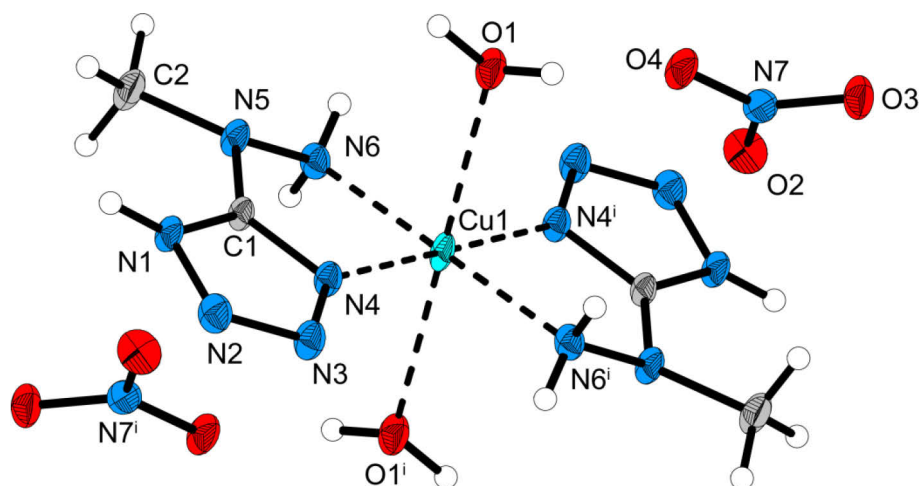


Figure 4. Molecular unit of **5**. Thermal ellipsoids of non-hydrogen atoms are drawn at the 50 % probability level. Selected bond lengths [Å]: Cu1–N4 1.984(3), Cu1–N6 2.040(3), Cu1–O1 2.477(3), N1–C1 1.333(4), N4–C1 1.323(4), N5–C1 1.349(4), N5–N6 1.432(4); selected bond angles [°]: O1–Cu1–N6 81.5(1), O1–Cu1–N4 92.3(1), N4–Cu1–N6 80.8(1), N5–N6–Cu1 109.5(2), N4–C1–N5 122.7(3); selected torsion angles [°]: N4–Cu1–O1–N6 –80.3(1), N6–Cu1–N4–C1 –10.5(2), C1–N4–N3–N2 0.0(3), Cu1–N4–C1–N5 –0.8(4). Symmetry code: *i*: $-x, 1-y, 1-z$.

nitrate of **4**. The complex units arranged in parallel fashion are connected through hydrogen bonds along the *a* axis to chains. The uncoordinated nitrate anions are stabilized by hydrogen bonds with the aqua ligand and the HMHT ligand (Figure 5). An overview of the distances and angles of selected hydrogen bonds in **5** is given in Table 2.

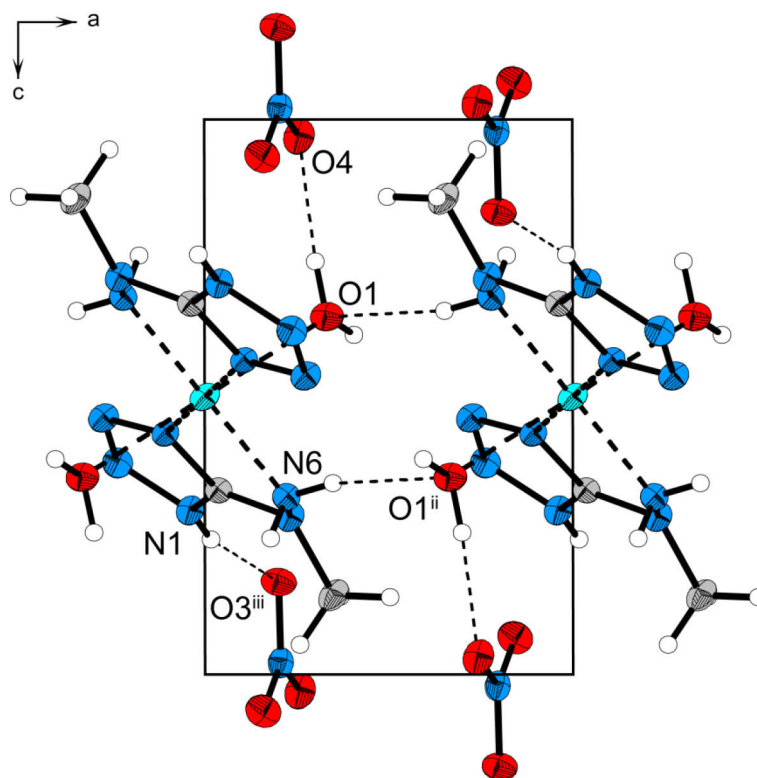


Figure 5. Unit cell of **5** and selected hydrogen bonds (view along the *b* axis). Symmetry codes: *ii*: $1-x, 1-y, 1-z$; *iii*: $x, -1+y, 1+z$.

Table 2. Distances and angles of selected hydrogen bonds in **5**.

D–H···A ^[a]	D–H / Å	H···A / Å	D···A / Å	D–H···A / °
N6–H6A···O1 ⁱⁱ	0.80(5)	2.28(5)	3.034(4)	159(4)
N1–H1···O3 ⁱⁱⁱ	0.83(3)	1.89(3)	2.703(4)	165(3)
O1–H1A···O4	0.89(3)	1.98(3)	2.864(4)	173(5)

[a] Symmetry codes: ii: $1-x, 1-y, 1-z$; iii: $x, -1+y, 1+z$.

Complex **6** crystallizes as dark green blocks in the monoclinic space group $P2_1/n$ with four formula units per unit cell and a calculated density of 2.125 g cm^{-3} at 173 K. The coordination sphere of the copper(II) center is octahedral, and the copper atoms are bridged over the 5-(1-methylhydrazinyl) tetrazolato ligand to linear chains along the a axis. Thus, a 1D coordination polymer is formed (Figure 6).

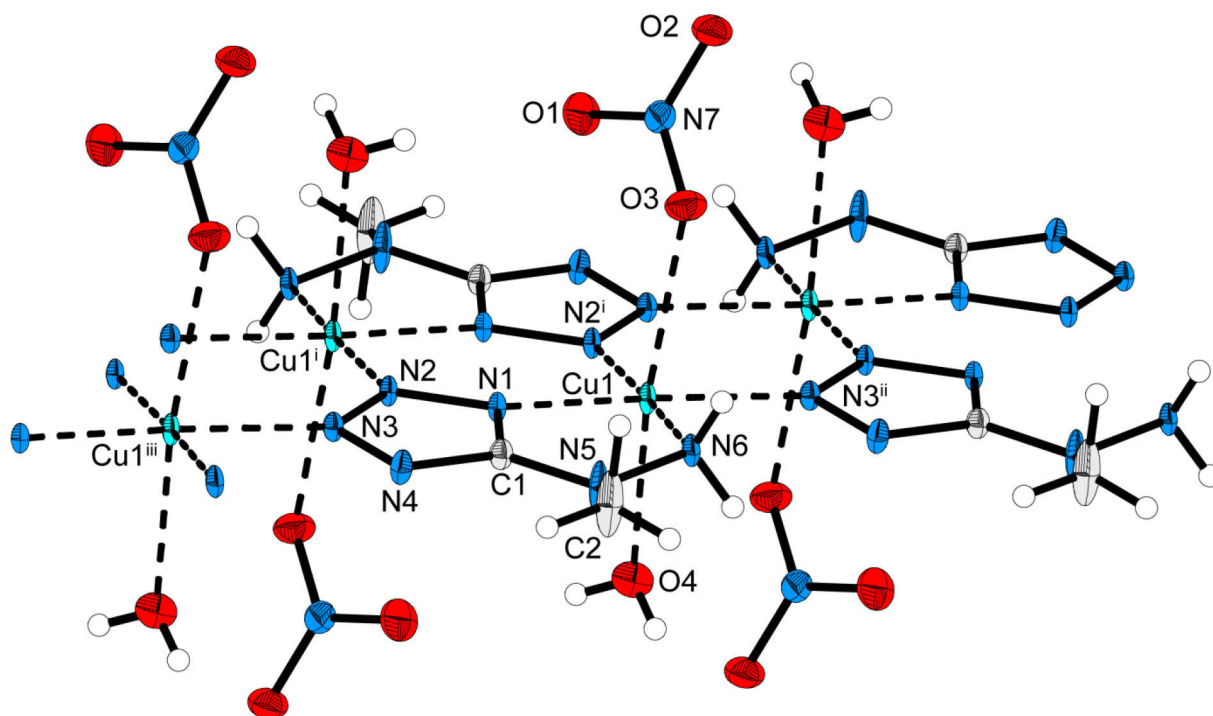


Figure 6. Polymeric structure of **6** along the a axis. Thermal ellipsoids of non-hydrogen atoms are drawn at the 50 % probability level. Selected bond lengths [Å]: Cu1–N1 2.017(2), Cu1–N6 2.033(2), Cu1–O3 2.505(2), Cu1–O4 2.327(2), Cu1–N2ⁱ 1.979(2), Cu1–N3ⁱⁱ 2.032(1), N1–N2 1.349(2), N2–N3 1.309(2), O3–N7 1.249(2); selected bond angles [°]: N1–Cu1–N6 80.4(1), N1–Cu1–O4 91.1(1), N6–Cu1–O5 91.5(1), C1–N1–N2 104.6(1), N1–C1–N5 121.5(2), O2–N7–O3 120.3(2); selected torsion angles [°]: N1–Cu1–N6–N2ⁱ $-21.1(7)$, Cu1–N1–C1–N5 2.4(2), Cu–N6–N5–C2 $-166.7(2)$, N1–N6–N3ⁱⁱ–N2ⁱ 0.3(1), O1–N7–O2–O3 179.9(3). Symmetry codes: i: $-x, -y, 1-z$; ii: $1+x, y, z$; iii: $-1+x, y, z$.

The copper(II) center is coordinated by one aqua ligand (Cu1–O4 = 2.327(2) Å) and one nitrate ligand (Cu1–O3 = 2.505(2) Å) in the Jahn–Teller-distorted axial positions. In the equatorial positions, four nitrogen atoms are coordinated in a nearly quadratic planar arrangement (Cu1–N1 = 2.017(2), Cu1–N6 = 2.033(2), Cu1–N2ⁱ = 1.979(2), Cu1–N3ⁱⁱ = 2.032(1) Å, N1–N6–N3ⁱⁱ–N2ⁱ = 0.3(1)°; symmetry codes: i: $-x, -y, 1-z$; ii: $1+x, y, z$) to the copper(II) center. The coordination octahedron is slightly distorted (N1–Cu1–

$N6 = 80.4(1)^\circ$) because of the fixed structure of the MHT ligand, which shows typical bond lengths and angles compared to the other complexes discussed. The MHT ligand in its deprotonated form acts as a chelating and μ_3 -bridging ligand at the same time. Hydrogen bonds between the aqua, nitrate, and MHT ligands stabilize the linear chains to each other in the *bc* plane (Table S2 and Figure S3 in the Supporting Information).

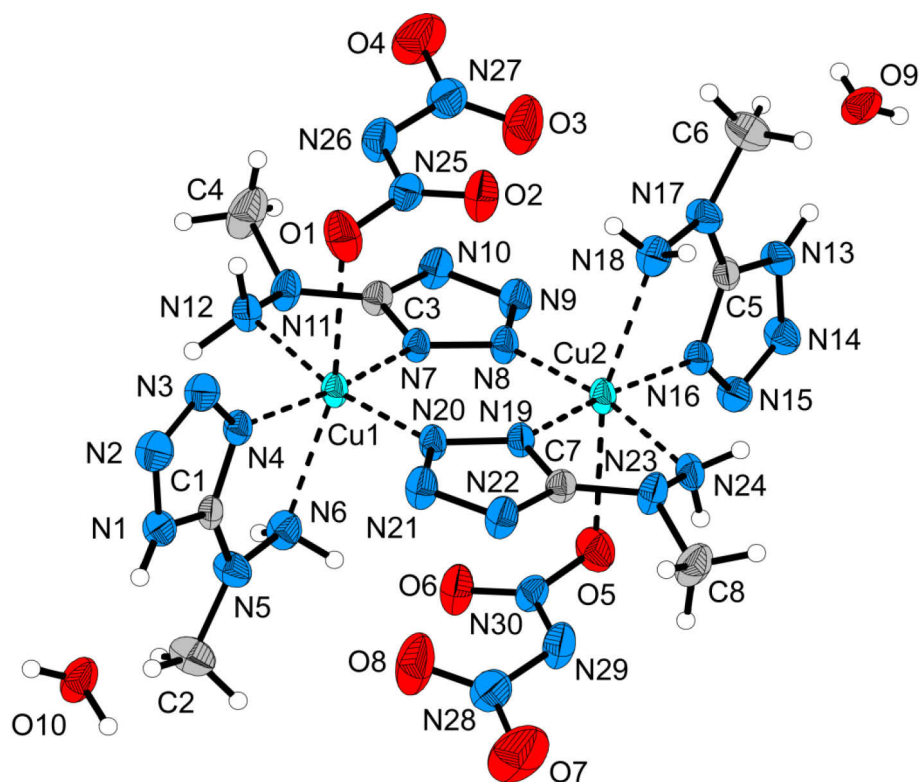


Figure 7. Asymmetric unit of copper(II) dimer **7**. Thermal ellipsoids of non-hydrogen atoms are drawn at the 50 % probability level. Selected bond lengths [Å]: Cu1–N4 1.990(3), Cu1–N6 2.385(3), Cu1–N7 1.963(3), Cu1–N12 2.076(3), Cu1–N20 2.010(3), Cu1–O1 2.702(4), N1–C1 1.331(4), N1–N2 1.364(4), N5–C1 1.338(5), N19–N20 1.359(4), O1–N25 1.256(4), N25–N26 1.360(6); selected bond angles [°]: N4–Cu1–N6 74.8(1), N7–Cu1–N4 172.0(1), N7–Cu1–N12 79.9(1), N4–Cu1–N12 92.2(1), N7–Cu1–N20 93.9(1), N4–Cu1–N20 94.1(1), N6–Cu1–O1 161.6(1), N5–N6–Cu1 106.1(2), C1–N5–N6 114.1(3), N6–N5–C2 120.2(3), C3–N7–Cu1 114.5(2), N11–N12–Cu1 110.5(2), C3–N11–C4 118.6(4), O1–Cu1–N4 87.2(1), O2–N25–O1 121.4(4), O1–N25–N26 112.2(3); selected torsion angles [°]: N4–Cu1–O1–N6 –12.6(3), N4–Cu1–O1–N12 –92.7(1), N4–N20–N7–N12 7.3(1), Cu1–N4–C1–N5 –11.8(5), Cu1–N6–N5–C1 13.5(4), Cu1–N6–N5–C2 –179.5(3), C1–N5–N6–C2 –167.1(5), C1–N1–N2–N3 –0.8(4), Cu1–N12–N11–C3 –20.5(4), Cu1–N12–N11–C4 –160.1(3), N7–C3–N11–C4 156.2(4), O1–N25–O2–N26 –177.2(6), O1–N25–N26–N27 –171.7(4), O2–N25–N27–O3 27.0(3).

The dinitramide **7** crystallizes as green plates in the orthorhombic space group $Pca2_1$ with four formula units per unit cell and a calculated density of 1.854 g cm^{-3} at 293 K. The asymmetric unit consists of a copper(II) complex dimer, which is similar to the structure of **2**, with two crystal water molecules (Figure 7). The asymmetric unit is equal to the formula unit. The copper(II) centers are coordinated octahedrally by HMHT ligands (Cu1–N4 = 1.990(3), Cu1–N6 = 2.385(3), Cu1–N7 = 1.963(3), Cu1–N12 = 2.076(3) Å) and dinitramide anions (Cu1–O1 = 2.702(4) Å). Two chelating μ_2 -bridging MHT ligands connect both copper(II)

centers (Cu1–N20 = 2.010(3), N20–N19 = 1.359(4), and Cu2–N19 = 1.969(3) Å) to a complex dimer. The octahedral coordination sphere is Jahn–Teller distorted along the O1–Cu1–N6 (and accordingly O5–Cu2–N18) axis. The bond length of Cu1–N6 (2.385(3) Å) is in the typical range for Jahn–Teller distortions,^[15] in contrast to the weak and long Cu1–O1 bond (2.702(4) Å). However, the Cu1–O1 distance is smaller than the sum of the Van der Waals (VdW) radii (2.9 Å)^[16] and according to the literature, should be described as a coordinative bond.^[17] Thus, the dinitramide can be regarded as a coordinating ligand. The N–Cu–N angles deviate from 90° owing to the fixed structure of the HMHT ligand (N4–Cu1–N6 = 74.8(1), N7–Cu1–N4 = 172.0(1)°). Further, the methyl group of the deprotonated MHT ligand is not in the plane of the copper(II) center and the tetrazole ring (Cu1–N12–N11–C4 = –160.1(3) and N7–C3–N11–C4 = 156.2(4)°), in contrast to the protonated HMHT ligand (Cu1–N6–N5–C2 = –179.5(3)°) or the perfect planar system of **8**. The nitro groups of the dinitramide anion are twisted with respect to each other with a torsion angle of O2–N25–N27–O3 = 27.0(3)°. The bond lengths (O1–N25 = 1.256(4), N25–N26 = 1.360(6) Å) and angles (O2–N25–O1 = 121.4(4), O1–N25–N26 = 112.2(3)°) of the dinitramide anion are in agreement with literature values.^[18] The crystal water forms a large set of hydrogen bonds (Figure S4 in the Supporting Information) to the dinitramide anion and the MHT ligand. The complex dimers are further interconnected through hydrogen bonds between the MHT and HMHT ligands to form a 3D network (Figure S4 in the Supporting Information).

The chloride complex **8** crystallizes as green rods in the orthorhombic space group *Pbcm* with four formula units per unit cell and a calculated density of 2.098 g cm^{–3} at 100 K. The formula unit, which is equal to the asymmetric unit, consists of one copper center, one 5-(1-methylhydrazinyl)-1*H*-tetrazole, and two chlorido ligands. The copper(II) center is octahedrally coordinated by one chelating HMHT ligand (Cu1–N4 = 1.966(3) and Cu1–N6 = 2.087(3) Å) in its protonated form and four chlorido ligands. One chlorido ligand is terminal (Cu1–Cl2 = 2.279(9) Å), and the other three μ_3 -chlorido anions (Cu1–Cl1 = 2.264(1) and Cu1–Cl1ⁱ = 3.049(1) Å; symmetry code: *i*: *x*, 0.5–*y*, 1–*z*) connect the copper centers to linear chains along the *c* axis (Figure 8). The axial Cu–Cl1ⁱ and Cu–Cl1ⁱⁱ (symmetry code: *ii*: *x*, 0.5–*y*, –*z*) bonds of 3.049(1) Å are in the range of values given in the literature for Cu–Cl coordination bonds.^[19] The perfect torsion angles are also remarkable. All atoms of the asymmetric unit (e.g., C1–N1–O1–C2 = 0.0 and N1–O1–H1A–H1B = 180.08°) are in one plane. The linear chains along the *c* axis are stabilized with respect to each other over a versatile hydrogen-bond network (Table S3 and Figure S5 in the Supporting Information).

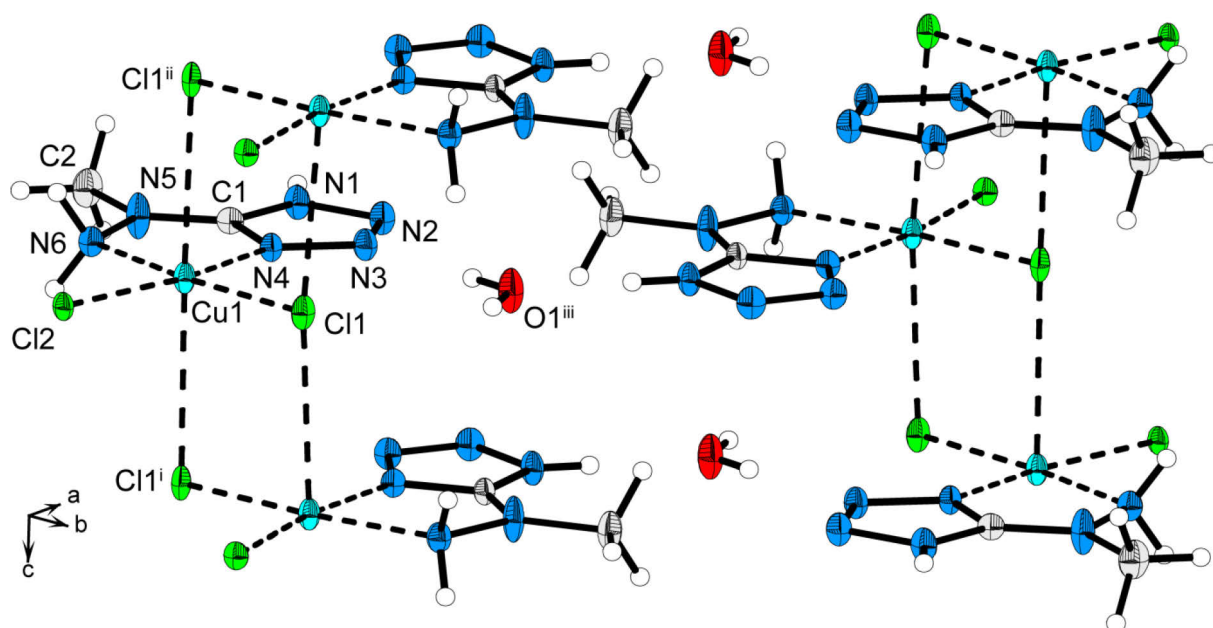


Figure 8. Polymeric structure of **8**. Thermal ellipsoids of non-hydrogen atoms are drawn at the 50 % probability level. Selected bond lengths [Å]: Cu1–N4 1.966(3), Cu1–N6 2.087(3), Cu1–Cl1 2.264(1), Cu1–Cl2 2.279(9), Cu1–Cl1ⁱ 3.049(1), C1–N1 1.334(5), N1–N2 1.375(5), C1–N5 1.325(5), N5–C2 1.445(5); selected bond angles [°]: N4–Cu1–N6 79.0(1), N4–Cu1–Cl1 92.1(1), N6–Cu1–Cl1 171.0(1), N4–Cu1–Cl2 169.5(1), N6–Cu1–Cl2 90.6(1), C1–N4–Cu1 114.8(3), N5–C1–N4 121.5(3), N1–C1–N4 107.9(3); selected torsion angles [°]: N4–Cu1–N6–N5 0.0, Cl2–Cu1–N6–N5 180.0, Cl1–Cl2–N6–N4 0.0, N5–C1–N4–N3 180.0, N4–Cu1–Cl1–Cl2 180.0. Symmetry codes: i: $x, 0.5-y, 1-z$; ii: $x, 0.5-y, -z$; iii: $1-x, 0.5+y, 0.5-z$.

Infrared spectroscopy: All the described compounds were investigated through IR spectroscopy. Raman spectroscopy was not performed because of the high photosensitivity of the compounds to laser light.

The neutral ligand **1**·H₂O shows a broad absorption band ($\nu_{s+as}(\text{H}_2\text{O})$) of the crystal water between 3700 and 3400 cm⁻¹. Further, very clear asymmetric and symmetric N–H stretching vibrations can be observed at 3311, 3208, and 3173 cm⁻¹. A broad absorption band at 2934 cm⁻¹ can be assigned to the C–H valence vibrations of the methyl group.^[20] In addition, the spectrum shows typical N–H deformation modes between 1650 and 1560 cm⁻¹ ($\delta(\text{N–H}) = 1661$ and 1594 cm⁻¹), C–N and N–N stretching modes in the range 1450 to 1000 cm⁻¹, and various tetrazole ring vibrations below 1000 cm⁻¹.^[21] The according vibrations of the HMHT ligand are shifted upon complexation to higher wavenumbers for the neutral form and to lower wavenumbers for the deprotonated MHT ligand (Figure 9). Complex **2** shows two types of infrared bands for the ligand: 1) blueshifted HMHT (e.g., $\delta(\text{N–H}) = 1672$ and 1603 cm⁻¹) and 2) redshifted MHT vibrations (e.g., $\delta(\text{N–H}) = 1640$ and 1561 cm⁻¹). According to the literature, the broad and very strong vibration at 1055 cm⁻¹ can be assigned to the perchlorate anion.^[21a,22] The corresponding perchlorate band of **3** can be found at 1071 cm⁻¹. The IR spectrum of **3** shows only the absorption bands of the deprotonated MHT ligand (e.g., $\nu(\text{N–H}) = 3267, 3188, \text{ and } 3133$ cm⁻¹ or $\delta(\text{N–H}) = 1637$ and 1574 cm⁻¹).

Relatively sharp H₂O stretching vibration signals at 3546 and 3484 cm⁻¹ indicate the coordination of the aqua ligand. On comparison of the tetrazole vibrations of **3** and **6**, a complex formula of [Cu(ClO₄)(MHT)(H₂O)]_∞ similar to the nitrate **6** can be suggested for the perchlorate **3** (Figure 9).

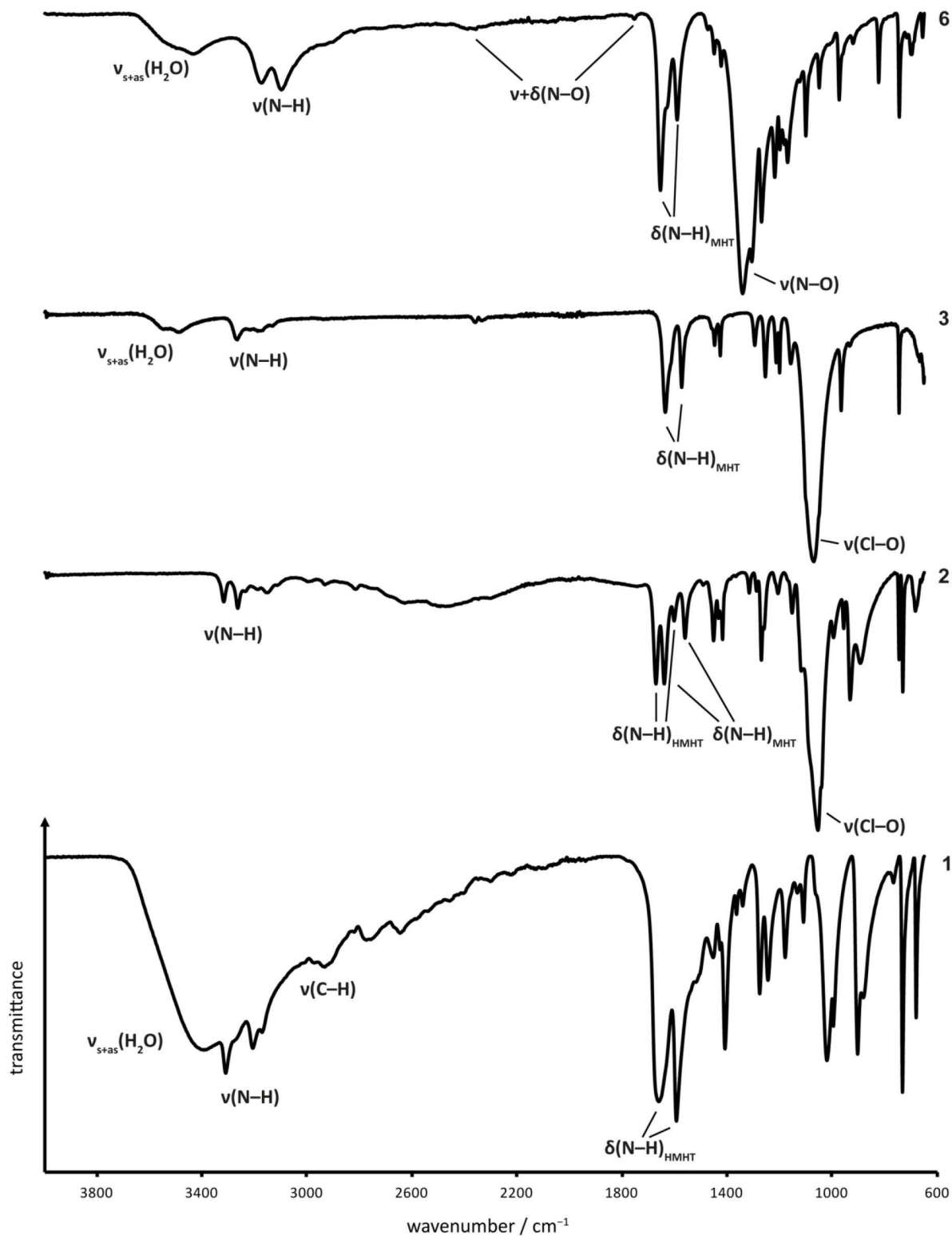


Figure 9. IR spectra of **1**, **2**, **3** and **6**.

The IR spectra of the nitrate complexes **4** and **5** show similar absorption bands for the HMHT ligand. The spectrum of **5** further shows two sharp absorption bands for the coordinated aqua ligand ($\nu_{s+as}(\text{H}_2\text{O}) = 3540$ and 3356 cm^{-1}). The absorption bands of the nitrate anion can be observed at 2482, 2452, 1758, and 1331 cm^{-1} for the monodentate nitrate of **4**, and at 2454, 2441, 1751, and 1353 cm^{-1} for the noncoordinating nitrate of **5**.^[23] These similar absorption bands for both nitrate complexes **4** and **5** show that there is only weak coordination of the nitrate to the copper(II) center in **4**. The monodentate nitrate of the coordination polymer **6** exhibits absorption bands at 2478, 1755, and 1342 cm^{-1} , similarly to complexes **4** and **5**. The vibrations of the deprotonated MHT ligand of **6** are shifted (e.g., 3175, 3099, 1655, 1591, and 1450 cm^{-1}) relative to those of **4** and **5** as a result of the different coordination situation (HMHT acts as a bidentate ligand in **4** and **5**; MHT is a μ_3 -bridging ligand with four coordination sites). As expected, the C–H stretching vibration of the methyl group at about 2950 cm^{-1} is not shifted compared to those of **4**, **5**, and **6**. The valence vibration of the aqua ligand appears as a broad band at 3437 cm^{-1} . The absorption signals of the MHT and HMHT ligands in complex **7** appear at nearly the same wavenumbers as for the similar perchlorate dimer complex **2**. However, the N–H valence vibrations are shifted to lower wavenumbers, for example, from 3318 and 3265 cm^{-1} in **2** to 3298 and 3226 cm^{-1} in **7**. This is the result of strong hydrogen bonds between the tetrazole ring and the crystal water ($\text{N1–H1}\cdots\text{O10} = 170(3)^\circ$, $\text{N1}\cdots\text{O10} = 2.703(6) \text{ \AA}$). The noncoordinating crystal water of **7** is indicated by a broad band at 3490 cm^{-1} . As a result of complexation, typical dinitramide vibrations of **7** ($\nu_{as}(\text{NO}_2) = 1512 \text{ cm}^{-1}$, $\nu_s(\text{NO}_2) = 1163 \text{ cm}^{-1}$, and $\nu_{as}(\text{N}_3) = 1011 \text{ cm}^{-1}$) are redshifted compared to those of noncoordinating dinitramide anions.^[18] The HMHT vibrations of complex **8** are similar to those discussed above.

Energetic properties and laser initiation: All the synthesized copper(II) complexes and the free ligand **1** were tested in terms of friction, impact, and electrostatic discharge. In addition, the temperature stability was measured. The compounds were classified according to the UN Recommendations on the Transport of Dangerous Goods.^[24]

The ligand **1**·H₂O is classified as insensitive toward impact (40 J), sensitive toward friction (324 N), and shows an electrostatic discharge sensitivity of 1.0 J. It is stable up to 188 °C and its crystal water is removed between 65 and 100 °C. An overview of the decomposition temperatures and mechanical sensitivities of the copper(II) complexes **2–8** is given in Table 3. Compounds **2** and **3** can both be classified as primary explosives with good temperature stabilities (**2**: $T_{\text{decomp}} = 217 \text{ °C}$; **3**: $T_{\text{decomp}} = 206 \text{ °C}$) and good performances. The explosive power of the aqua complex **3** even seems to be higher than that of the water-free dimer **2**. Ignition of confined samples with the same amount of **2** and **3** on an aluminum plate showed that **3** induced a deeper dent in the aluminum plate than **2** (Figure S7 in the Supporting

Information). The ignitability of the perchlorates **2** and **3** was further tested through a hot needle test (Figure 10). The aqua ligand of **3** is removed between 160 and 180 °C. The decomposition temperatures of the nitrate complexes **4**, **5**, and **6** are the same (163 °C). An endothermic signal between 80 and 100 °C can be observed in the DSC and DTA plots of the aqua complex **5** (indicating the loss of the aqua ligand), whereas the DTA plot of the coordination polymer **6** does not exhibit any endothermic signals before exothermic decomposition ($T_{\text{decomp}} = 163$ °C). This result indicates a stronger bonding between the aqua ligand and the copper(II) center in **6** ($\text{Cu1-O4} = 2.327(2)$ Å) than in **5** ($\text{Cu1-O1} = 2.477(3)$ Å), which is in agreement with the crystal structures. Further, the sensitivities toward impact, friction, and electrostatic discharge decrease from **4** to **5** to **6**, and can be classified as very sensitive to sensitive. Interestingly, the dinitramide compound **7** is less sensitive toward mechanical stimuli than the nitrates **4**, **5**, and **6**. However, **7** exhibits a low temperature stability ($T_{\text{decomp}} = 145$ °C). The chloride **8** is insensitive toward impact and sensitive toward friction. It shows a low performance when brought into a flame.

Table 3. Energetic properties and results of laser initiation of **2–8**.

parameter	2	3	4	5	6	7	8
formula	$\text{C}_8\text{H}_{22}\text{O}_8\text{Cl}_2\text{Cu}_2\text{N}_{24}$	$\text{C}_2\text{H}_7\text{O}_5\text{ClCuN}_6$	$\text{C}_4\text{H}_{12}\text{CuN}_{14}\text{O}_6$	$\text{C}_4\text{H}_{16}\text{CuN}_{14}\text{O}_8$	$\text{C}_2\text{H}_7\text{CuN}_7\text{O}_4$	$\text{C}_4\text{H}_{13}\text{CuN}_{15}\text{O}_5$	$\text{C}_2\text{H}_8\text{Cl}_2\text{CuN}_6\text{O}$
$T_{\text{dec. (onset)}} / \text{°C}^{[a]}$	217	206	163	163	163	145	185
IS / J ^[b]	1	1	2	2	3	10	40
FS / N ^[c]	5	5	32	96	108	120	252
ESD / J ^[d]	0.010	0.007	0.09	0.15	0.80	0.17	1.50
grain size / μm	< 100	< 100	< 100	< 100	< 100	< 100	< 100
flame color	blue	blue	green	green	green	green	blue-green
hot needle	det ^[f]	det ^[f]	defl ^[g]	dec ^[h]	defl ^[g]	defl ^[g]	decomp ^[h]
hot plate	det ^[f]	det ^[f]	defl ^[g]	defl ^[g]	defl ^[g]	defl ^[g]	decomp ^[h]
laser init ^[e]	det ^[f]	det ^[f]	det ^[f]	no reaction	det ^[f]	det ^[f]	not tested

[a] Decomposition temperatures determined by differential thermal analysis. [b] Impact sensitivity determined by BAM drophammer. [c] Friction sensitivity determined by BAM friction tester. [d] Electrostatic discharge determined by Electric Spark Tester ESD 2010 EN. [e] Laser initiation ($\lambda = 940$ nm, $\tau = 100$ μs). [f] Detonation. [g] Deflagration. [h] Decomposition.

Confined samples of the substance (≈ 200 mg **2–7** + 5% PTFE) were irradiated by a laser pulse with a wavelength of 940 nm and a pulse length of 100 μs . An overview of the results of laser initiation is given in Table 3. Complexes **2**, **3**, **4**, **6**, and **7** detonated after initiation by laser irradiation. This means that the perchlorate, nitrate, and dinitramide copper(II) complexes can be photosensitive, and it seems that the laser ignitability depends on the interaction between the energetic ligand and the metal center, and not on the anion. It appears plausible that the initiation process is not thermal when comparing the decomposition temperatures of the laser-ignitable complex **4** ($T_{\text{decomp}} = 163$ °C) and the non-ignitable **5** ($T_{\text{decomp}} = 163$ °C), because both compounds have the same thermal stability and show a similar optical absorption in the UV/Vis/NIR range (Figure S6 in the Supporting

Information). The optical absorption for **4** and **5** at 940 nm is nearly the same. All the investigated copper(II) complexes absorb at 940 nm. An appropriate electronic excitation from the ground state to an excited state at the wavelength of the laser seems to be the criterion for laser initiation. The anion is not important for this electronic excitation, but according to the literature, might play a role in the first steps of the explosive decomposition.^[2c] The anion serves as an oxidizing agent for the reducing hydrazine derivative **1**. All in all, comparing these investigated laser-ignitable copper(II) complexes with literature-known complexes such as bis(3-hydrazino-4-amino-1,2,4-triazole)metal(II) perchlorates (M = Co, Ni, Cu, Cd),^[2c,25] the laser initiation with single pulsed laser light ($\tau = 100 \mu\text{s}$) seems to be a laser-induced optical excitation.^[8b] The consequence of this electronic excitation is an exothermic decomposition reaction. Thus, it is not only the metal cation or the anion that is relevant for initiation, but rather, the energetic situation of the molecular orbitals of the irradiated compound. However, a thermal mechanism cannot be fully excluded.

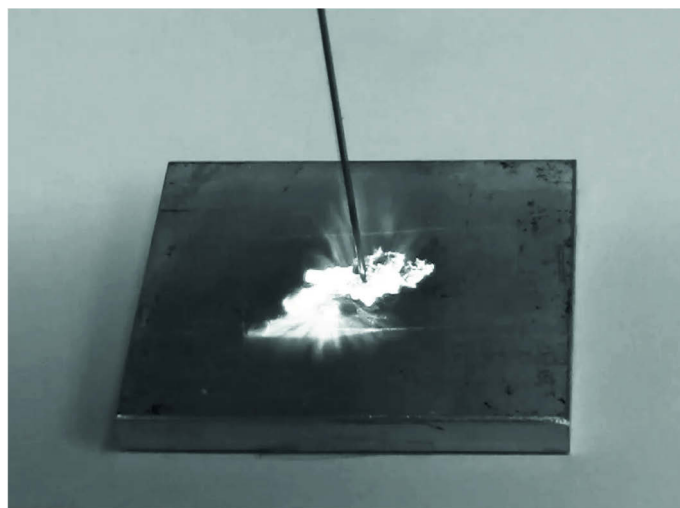


Figure 10. Hot needle test of **3** showing the moment of detonation.

5.4. Conclusion

The nitrogen-rich ligand 5-(1-methylhydrazinyl)-1*H*-tetrazole (**1**, HMHT) was prepared according to the literature procedure in a yield of 40%.^[12] It was further reacted with various copper(II) salts (perchlorate, nitrate, dinitramide, and chloride) to form the corresponding complexes: $[\{\text{Cu}(\text{ClO}_4)(\mu\text{-MHT})(\text{HMHT})\}_2]$ (**2**), $[\text{Cu}(\text{ClO}_4)(\mu\text{-MHT})(\text{H}_2\text{O})]_\infty$ (**3**), $[\text{Cu}(\text{NO}_3)_2(\text{HMHT})_2]$ (**4**), $[\text{Cu}(\text{HMHT})_2(\text{H}_2\text{O})_2](\text{NO}_3)_2$ (**5**), $[\text{Cu}(\mu_3\text{-MHT})(\text{NO}_3)(\text{H}_2\text{O})]_\infty$ (**6**), $[\{\text{Cu}(\mu\text{-MHT})(\text{N}(\text{NO}_2)_2)(\text{HMHT})\}_2] \cdot 2 \text{H}_2\text{O}$ (**7**), and $\{[\text{CuCl}(\mu_3\text{-Cl})(\text{HMHT})] \cdot \text{H}_2\text{O}\}_\infty$ (**8**). Compound **1** can serve as a neutral (bidentate) and anionic (μ_2 - and μ_3 -bridging) chelate ligand that differs in its coordination mode. Coordination monomers (**4** and **5**), dimers (**2** and **7**), and also polymers (**3**, **6**, and **8**) were obtained depending on the reaction conditions. X-ray

single-crystal structures of **2** and **4–8** were obtained. Further, all complexes were characterized via infrared spectroscopy, elemental analysis, and solid UV/Vis/NIR spectroscopy. The perchlorate compounds **2** (IS: 1 J, FS: 5 N, $T_{\text{decomp}} = 217\text{ }^{\circ}\text{C}$) and **3** (IS: 1 J, FS: 5 N, $T_{\text{decomp}} = 206\text{ }^{\circ}\text{C}$) are potential primary explosives with good thermal stabilities higher than $200\text{ }^{\circ}\text{C}$ and high explosive power. The nitrate complex **4** might serve in safe priming charges with a friction sensitivity of 32 N and an impact sensitivity of 2 J. The other copper(II) complexes (**5**, **6**, and **7**) could serve as green colorants in pyrotechnical mixtures, but further investigations are needed.

Laser initiation tests showed that complexes **2**, **3**, **4**, **6**, and **7** were successfully ignited by a short pulsed laser beam at 940 nm. For this work, it can be concluded that the anion is not of importance for the laser ignitability, and it seems that the laser initiation criterion of the investigated complexes depends on the interaction between the energetic ligand and the metal center. The compounds **2–4** might be of interest for laser-ignitable detonator systems.

5.5. Experimental Section

Caution! All of the copper(II) complexes and the free ligand **1** prepared herein are energetic materials that show sensitivities toward various stimuli. Proper protective measures (safety glasses, face shield, leather coat, earthed equipment, conductive floor and shoes, Kevlar gloves, and ear plugs) should be used when handling these compounds. Extra safety precautions should be taken when compounds **2** and **3** are handled. Both are extremely sensitive toward impact, friction, and electrostatic discharge. The handled scale of the compounds **2** and **3** should not be greater than 50 to 100 mg.

All chemicals were used as supplied by ABCR, Acros Organics, AppliChem, Sigma–Aldrich, and VWR. The syntheses of compounds **3–8** can be found in the Supporting Information.

The impact and friction sensitivity tests were performed according to standard methods by using a BAM (Bundesanstalt für Materialforschung) drop hammer and a BAM friction tester.^[26] The sensitivity toward electrostatic discharge was tested by using an OZM Research electric spark tester ESD 2010 EN.^[27] Decomposition temperatures were measured through differential thermal analysis (DTA) with an OZM Research DTA 552-Ex instrument or through differential scanning calorimetry (DSC) with a Linseis DSC-PT10.^[27a,28] The heating rate was $5\text{ }^{\circ}\text{C min}^{-1}$ in both cases, and it was measured in the range RT to $400\text{ }^{\circ}\text{C}$. The hot needle test was performed by fixing a small amount of the sample on an aluminum plate with tape, then touching it with the tip of a hot needle. Detonation of the compound indicated a primary explosive. The hot-plate test, in contrast, just shows the behavior of the unconfined sample toward heating on a hot plate, and does not necessarily allow conclusions to be drawn on its capability as a primary explosive.

Suitable single crystals of **2** and **4–8** were obtained directly from the mother liquor and mounted in Kel-F oil. The structures were determined with an Oxford Diffraction Xcalibur 3 diffractometer with a sapphire CCD detector, four-circle kappa platform, enhanced MoK α radiation source ($\lambda = 71.073$ pm), and Oxford Cryosystems Cryostream cooling unit. Data collection and reduction were performed with the CrysAlisPro software.^[29] The structures were solved with SIR92, SIR97, or SIR2004.^[30] The refinement was performed with SHELXL-97.^[31] The CIF files were checked at the checkCIF website.^[32] The non-hydrogen atoms were refined anisotropically and the hydrogen atoms isotropically if not calculated. The determination of the carbon, hydrogen, and nitrogen contents was carried out through combustion analysis with an Elementar Vario EL.^[33] Infrared spectra were recorded on a PerkinElmer BXII FTIR system with a Smith DuraSamplIR II diamond ATR unit.^[34] The UV/Vis/NIR reflectance of the solid samples was measured with a Varian Cary 500 spectrometer in the wavelength range 350–1300 nm.^[35] The reflectance R [%] was transformed by the Kubelka–Munk function to the absorption intensity $F(R)$.^[36]

5-(1-Methylhydrazinyl)-1H-tetrazole monohydrate (1): The nitrogen-rich ligand was synthesized according to the literature procedure.^[12] To a precooled solution of cyanogen bromide (10.6 g, 100 mmol), sodium carbonate (5.30 g, 50.0 mmol), ethanol (48 mL), and water (1 mL) was added drop wise under vigorous stirring a solution of monomethylhydrazine (4.60 g, 100 mmol) in ethanol (32 mL). After complete addition, the solution was allowed to warm up to RT and stirred until the CO₂ evolution ceased. The suspension was filtered and sodium azide was added to the filtrate. Over the course of one hour, a mixture of conc. hydrochloric acid (15 mL) and water (30 mL) was added dropwise. After the addition was completed, the reaction mixture was stirred for 22 h under reflux. The reaction mixture was cooled to RT, conc. hydrochloric acid was added until a pH of 1 was reached, and the solution was concentrated under reduced pressure until a white solid started to precipitate. The solid was filtered off, washed with ethanol, and recrystallized from a mixture of water/ethanol (1:1). The crystalline and colorless product was filtered off and dried in air. Yield: 5.27 g (39.9 mmol, 40 %); DTA (5 °C min⁻¹) onset: 188 °C (decomp); ¹H NMR (270 MHz, [D6]DMSO, 25 °C, TMS): $\delta = 3.13$ ppm (s, 3 H, -CH₃); ¹³C{¹H} NMR (68 MHz, [D6]DMSO, 25 °C, TMS): $\delta = 162.8$ (CN₄), 42.6 ppm (-CH₃); IR (ATR): $\tilde{\nu} = 3394$ (s), 3311 (s), 3208 (s), 3173 (s), 2934 (m), 2775 (m), 2647 (w), 1661 (vs), 1594 (vs), 1454 (m), 1409 (s), 1365 (w), 1342 (w), 1277 (m), 1245 (m), 1180 (m), 1134 (w), 1110 (w), 1021 (s), 996 (s), 904 (s), 882 (m), 767 (vw), 733 (s), 681 cm⁻¹ (s); elemental analysis calcd (%) for C₂H₈N₆O (132.11 g mol⁻¹): C 18.18, H 6.10, N 63.61; found: C 18.31, H 5.76, N 62.10; BAM impact: 40 J; BAM friction: 324 N; ESD: 1.00 J (at grain size 100–500 μ m)

Bis(μ -5-(1-methylhydrazinyl)tetrazolato-1 κ^2 N¹,N⁶-2 κ N²)bis(5-(1-methylhydrazinyl)-1H-tetrazole-1 κ^2 N⁴,N⁶)diperchloratodicopper(II) (2): A solution of copper(II) perchlorate hexahydrate (371 mg, 1.00 mmol) in 60 % perchloric acid (1.5 mL) was added to a warm solution (70 °C) of **1** (264 mg, 2.00 mmol) in water (20 mL). The blue solution was left to crystallize at RT. After one day, the product started to crystallize in the form of dark green plates, which were filtered off and dried in air. Yield: 545 mg (0.70 mmol, 70 %); DTA (5 °C min⁻¹) onset: 217 °C (decomp); IR (ATR): $\tilde{\nu}$ = 3318 (w), 3265 (w), 3237 (vw), 3188 (vw), 3152 (vw), 3116 (vw), 2997 (vw), 2933 (vw), 2817 (vw), 2629 (w), 2473 (w), 1672 (m), 1640 (m), 1603 (w), 1561 (w), 1492 (vw), 1453 (w), 1418 (w), 1317 (vw), 1289 (vw), 1270 (m), 1261 (w), 1207 (vw), 1153 (w), 1119 (m), 1112 (m), 1055 (vs), 1042 (s), 996 (w), 957 (w), 933 (m), 894 (m), 746 (m), 732 (m), 684 cm⁻¹ (w); elemental analysis calcd (%) for C₈H₂₂O₈Cl₂Cu₂N₂₄ (780.48 g mol⁻¹): C 12.31, H 2.84, N 43.07; found: C 12.76, H 2.83, N 42.63; BAM impact: 1 J; BAM friction: 5 N; ESD: 0.010 J (at grain size <100 μ m).

5.6. References

- [1] a) V. Thottampudi, F. Forohor, D. A. Parrish, J. M. Shreeve, *Angew. Chem.* **2012**, *124*, 10019–10023; *Angew. Chem. Int. Ed.* **2012**, *51*, 9881–9885; b) H. Gao, J. M. Shreeve, *Chem. Rev.* **2011**, *111*, 7377–7436; c) M. Rahm, S. V. Dvinskikh, I. Furo, T. Brinck, *Angew. Chem.* **2011**, *123*, 1177–1180; *Angew. Chem. Int. Ed.* **2011**, *50*, 1145–1148; d) R. Haiges, S. Schneider, T. Schroer, K. O. Christe, *Angew. Chem.* **2004**, *116*, 5027–5032; *Angew. Chem. Int. Ed.* **2004**, *43*, 4919–4924; e) D. E. Chavez, M. A. Hiskey, D. L. Naud, D. Parrish, *Angew. Chem.* **2008**, *120*, 8431–8433; *Angew. Chem. Int. Ed.* **2008**, *47*, 8307–8309; f) A. S. Kumar, V. D. Ghule, S. Subrahmanyam, A. K. Sahoo, *Chem. Eur. J.* **2013**, *19*, 509–518; g) E.-C. Koch, V. Weiser, E. Roth, *Angew. Chem.* **2012**, *124*, 10181–10184; *Angew. Chem. Int. Ed.* **2012**, *51*, 10038–10040; h) O. Bolton, L. R. Simke, P. F. Pagoria, A. J. Matzger, *Cryst. Growth Des.* **2012**, *12*, 4311–4314; i) T. M. Klapötke, C. Petermayer, D. G. Piercey, J. Stierstorfer, *J. Am. Chem. Soc.* **2012**, *134*, 20827–20836.
- [2] a) M. A. Ilyushin, I. V. Tselinsky, I. A. Ugryumov, A. Y. Zhilin, A. S. Kozlov, *6th New Trends in Research of Energetic Materials Seminar*, Pardubice, Czech Republic, April 22–24, **2003**; b) T. M. Klapötke, P. Mayer, K. Polborn, J. Stierstorfer, J. J. Weigand, *37th International Annual Conference of ICT*, Karlsruhe, Germany, June 27–30, **2006**; c) I.A. Ugryumov, M. A. Ilyushin, I. V. Tselinskii, A. S. Kozlov, *Russ. J. Appl. Chem.* **2003**, *76*, 439–441.
- [3] A. Y. Zhilin, M. A. Ilyushin, I. V. Tselinskii, A. S. Brykov, *Russ. J. Appl. Chem.* **2001**, *74*, 99–102.
- [4] Y.-h. Zhu, D.-l. Sheng, B. Yang, L.-k. Chen, F.-e. Ma, *Hanneng Cailiao* **2009**, *17*, 169–172.
- [5] S. G. Zhu, Y. C. Wu, W. Y. Zhang, J. Y. Mu, *Propellants Explos. Pyrotech.* **1997**, *22*, 317–320.

- [6] a) A. A. Brish, I. A. Galeeva, B. N. Zaitsev, E. A. Sbimev, L. V. Tararinstev, *Fiz. Goreniya Vzryva* **1969**, 5, 475; b) A. A. Brish, I. A. Galeeva, B. N. Zaitsev, E. A. Sbimev, L. V. Tararinstev, *Fiz. Goreniya Vzryva* **1966**, 2, 132; c) L. C. Yang, V. J. Menichelli, *Appl. Phys. Lett.* **1971**, 19, 473–475; d) H. Östmark, N. Roman, *J. Appl. Phys.* **1993**, 73, 1993–2003; e) M. Singh, R. Kumar, L. Kumar, V. S. Sethi, *33rd International Pyrotechnics Seminar*, Chandigarh, India, **2006**.
- [7] E. D. Aluker, A. G. Krechetov, A. Y. Mitrofanov, A. S. Zverev, M. M. Kuklja, *J. Phys. Chem. C* **2012**, 116, 24482–24486.
- [8] a) E. Aluker, N. Aluker, A. Krechetov, A. Mitrofanov, D. Nurmukhametov, A. Tupitzin, N. Poleeva, *14th New Trends in Research of Energetic Materials Seminar*, Pardubice, Czech Republic, April 13–15, **2011**; b) E. D. Aluker, A. G. Krechetov, A. Y. Mitrofanov, D. R. Nurmukhametov, M. M. Kuklja, *J. Phys. Chem. C* **2011**, 115, 6893–6901.
- [9] A. Y. Zhilin, M. A. Ilyushin, I. V. Tselinskii, A. S. Kozlov, I. S. Lisker, *Russ. J. Appl. Chem.* **2003**, 76, 572–576.
- [10] a) J. Thiele, J. T. Marais, *Liebigs Ann. Chem.* **1893**, 273, 144–160; b) J. Thiele, *Justus Liebigs Ann. Chem.* **1898**, 303, 57–75.
- [11] G.-H. Tao, D. A. Parrish, J. M. Shreeve, *Inorg. Chem.* **2012**, 51, 5305–5312.
- [12] J. J. Weigand, Dissertation, LMU (München), **2005**.
- [13] K. R. Maxcy, M. M. Turnbull, *Acta Crystallogr. Sect. C* **1999**, 55, 1986–1988.
- [14] Y. Komiyama, E. C. Lingafelter, *Acta Crystallogr.* **1964**, 17, 1145–1148.
- [15] M. Joas, T. M. Klapötke, J. Stierstorfer, *Crystals* **2012**, 2, 958–966.
- [16] A. F. Holleman, N. Wiberg, *Lehrbuch der Anorganischen Chemie*, 102nd ed., de Gruyter, Berlin, **2007**.
- [17] a) A. Ozarowski, R. Allmann, A. Pour-Ibrahim, R. Reinen, *Z. Anorg. Allg. Chem.* **1991**, 592, 187–201; b) A. Bieńko, K. Suracka, J. Mroziński, R. Kruszyński, D. C. Bieńko, *J. Mol. Struct.* **2012**, 1019, 135–142.
- [18] H.-G. Ang, W. Fraenk, K. Karaghiosoff, T. M. Klapötke, P. Mayer, H. Nöth, J. Sprott, M. Warchhold, *Z. Anorg. Allg. Chem.* **2002**, 628, 2894–2900.
- [19] P. C. Burns, F. C. Hawthorne, *Am. Mineral.* **1993**, 78, 187–189.
- [20] M. Hesse, H. Meier, B. Zeeh, *Spektroskopische Methoden der organischen Chemie*, 7th ed., Thieme, Stuttgart, **2005**.
- [21] a) T. M. Klapötke, C. M. Sabat, J. Stierstorfer, *Z. Anorg. Allg. Chem.* **2008**, 634, 1867–1874; b) T. M. Klapötke, P. Mayer, J. Stierstorfer, J. J. Weigand, *J. Mater. Chem.* **2008**, 18, 5248–5258; c) N. Fischer, D. Izsák, T. M. Klapötke, S. Rappenglück, J. Stierstorfer, *Chem. Eur. J.* **2012**, 18,

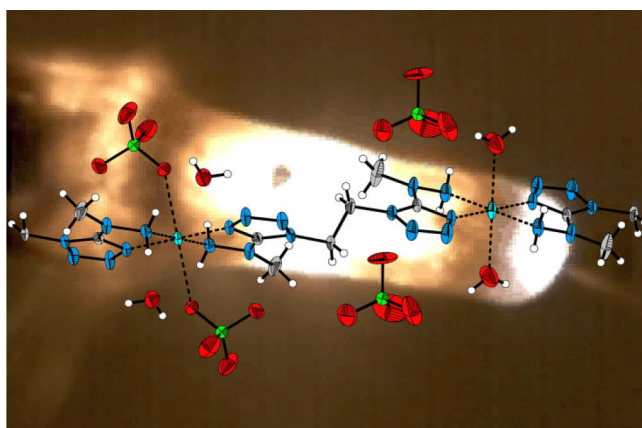
- 4051–4062; d) M. M. Degtyarik, P. N. Gaponik, V. N. Naumenko, A. I. Lesnikovich, M. V. Nikanovich, *Spectrochim. Acta Part A* **1987**, *43*, 349–353.
- [22] D. L. Lewis, E. D. Estes, D. J. Hodgson, *J. Cryst. Mol. Struct.* **1975**, *5*, 67–74.
- [23] a) A. B. P. Lever, E. Mantovani, B. S. Ramaswamy, *Can. J. Chem.* **1971**, *49*, 1957–1964; b) F. A. Miller, C. H. Wilkins, *Anal. Chem.* **1952**, *24*, 1253–1294.
- [24] Impact: insensitive > 40 J, less sensitive ≥ 35 J, sensitive ≥ 4 J, very sensitive ≤ 3 J; Friction: insensitive > 360 N, less sensitive = 360 N, sensitive < 360 N and > 80 N, very sensitive ≤ 80 N, extremely sensitive ≤ 10 N, According to: *Recommendations on the Transport of Dangerous Goods, Manual of Tests and Criteria*, 4th ed., United Nations, New York, **1999**.
- [25] E. S. Hafenrichter, B. Marshall, Jr., K. J. Fleming, *29th International Pyrotechnics Seminar*, Albuquerque, USA, **2002**.
- [26] a) NATO Standardization Agreement 4489, September 17, **1999**; b) NATO Standardization Agreement 4487, October 29, **2009**.
- [27] a) <http://www.ozm.cz> (accessed January 29, **2013**); b) NATO Standardization Agreement 4515, August 23, **2002**.
- [28] <http://www.linseis.com> (accessed January 29, **2013**).
- [29] a) CrysAlisPro 1.171.35.11, Oxford Diffraction Ltd., Abingdon, UK, **2011**; b) CrysAlisPro 1.171.36.21, Oxford Diffraction Ltd., Abingdon, UK, **2012**.
- [30] a) A. Altomare, G. Cascarano, C. Giacovazzo, A. Guagliardi, *J. Appl. Crystallogr.* **1993**, *26*, 343–350; b) A. Altomare, M. C. Burla, M. Camalli, G. L. Cascarano, C. Giacovazzo, A. Guagliardi, A. G. G. Moliterni, G. Polidori, R. Spagna, *J. Appl. Crystallogr.* **1999**, *32*, 115–119; c) M. C. Burla, R. Caliendo, M. Camalli, B. Carrozzini, G. L. Cascarano, L. De Caro, C. Giacovazzo, G. Polidori, R. Spagna, *J. Appl. Crystallogr.* **2005**, *38*, 381–388.
- [31] G. M. Sheldrick, *Acta Crystallogr. Sect. A* **2008**, *64*, 112–122.
- [32] a) S. R. Hall, F. H. Allen, I. D. Brown, *Acta Crystallogr. Sect. A* **1991**, *47*, 655–685; b) <http://journals.iucr.org/services/cif/checkcif.html> (accessed January 28, **2013**).
- [33] <http://www.elementar.de/>(accessed February 1, **2013**).
- [34] <http://www.perkinelmer.de/>(accessed February 1, **2013**).
- [35] <http://www.agilent.com/>(accessed April 15, **2013**).
- [36] P. Kubelka, F. Munk, *Z. Tech. Phys.* **1931**, *1*, 593–601.

6. Photosensitive Metal(II) Perchlorates with 1,2-Bis[5-(1-methylhydrazinyl)tetrazol-1-yl]ethane as Ligand: Synthesis, Characterization and Laser Ignition

Reproduced with permission from M. Joas, T. M. Klapötke, N. Szimhardt, *European Journal of Inorganic Chemistry* **2014**, 2014, 493–498.

Online: <http://dx.doi.org/10.1002/ejic.201301283>.

Copyright 2014 WILEY-VCH Verlag GmbH & Co. KGaA, Weinheim.



6.1. Abstract

The synthesis and characterization (including NMR spectroscopy, elemental analysis, X-ray diffraction, infrared spectroscopy and sensitivity measurements) of 1,2-bis[5-(1-methylhydrazinyl)tetrazol-1-yl]ethane (**1**) and its corresponding metal [Cu²⁺ (**2**), Co²⁺ (**3**), Ni²⁺ (**4**)] complexes is presented. The crystal structure of the copper(II) complex was determined and infrared spectra of all three coordination compounds were recorded. Furthermore, the behaviour of the metal(II) complexes towards single-pulsed laser irradiation was investigated and it was shown that all three perchlorate complexes detonated after initiation by monopulsed laser light. The initiation mechanism seems to be of thermal nature.

6.2. Introduction

The development of energetic materials has a long history.^[1] New research interests deal with environmental acceptability, high performance and mechanical and thermal stability.^[2] The investigation of insensitive munitions, for example, should help to prevent accidents like cook-off reactions caused by fuel fires. In particular, primary explosives are extremely sensitive towards mechanical stimuli. To prevent an undesired initiation it is necessary to develop safe detonator systems. One example is exploding-bridgewire (EBW) detonators.^[3] However, these detonators have the disadvantage that they are sensitive towards electric

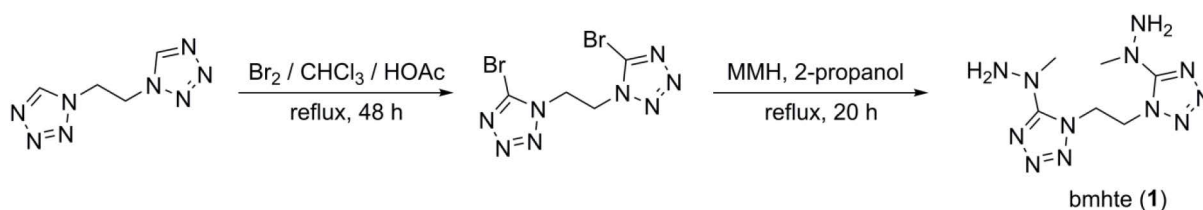
discharge;^[4] this led to the application of laser radiation as the ignition or initiation source. The first laser-ignition experiments of explosives like lead azide, pentaerythritol tetranitrate (PETN), cyclotrimethylenetrinitramine (RDX) or tetryl were performed 40 years ago by Brish *et al.* (Q-switched neodymium glass laser) as well as Menichelli and Yang (Q-switched ruby laser).^[5] Later, CO₂- and Nd:YAG laser systems of high power were used to ignite further secondary explosives, propellants and pyrotechnics.^[6] With the appearance of powerful and cheap laser diodes, single-pulsed laser irradiation became more and more interesting. In particular, the laser initiation of energetic metal complexes like tetraammine-*cis*-bis(5-nitrotetrazolato-*N*²)-cobalt(III) perchlorate (BNCP) and its analogues,^[7] 5-hydrazinotetrazolemercury(II) perchlorate or bis(3-hydrazino-4-amino-1,2,4-triazole)metal(II) perchlorates have been investigated with respect to their potential use as primary explosives.^[8] The most promising photosensitive primer has been BNCP, after the pentaammine(5-cyanotetrazolate)-cobalt(III) perchlorate (CP) became less attractive.^[9]

For the initiation of high explosives by laser irradiation, two mechanisms are discussed: (i) a nonselective thermal ignition and (ii) a selective and faster photoelectronic initiation.^[10] The thermal mechanism is explained by the “hot spot theory”.^[11] The ignitability of the irradiated compound depends on the absorption characteristics at the wavelength of the laser. Thus, light-absorbing particles such as soot help by forming hot spots. For the photoelectronic mechanism, an electronic excitation at the wavelength of the laser is discussed. In contrast to the thermal mechanism, light-absorbing particles have no influence on the ignitability. In this case, light-scattering particles such as nanosized magnesium oxide can decrease the initiation energy threshold.^[10c]

Independent of the initiation mechanism, it is necessary to develop energetic materials that exhibit a low energy threshold for laser initiation, a high performance, a fast deflagration-to-detonation transition (DDT) and good thermal and mechanical stabilities. As was shown by our research group, the copper complexes of the 5-(1-methylhydrazinyl)-1*H*-tetrazole ligand could nearly all be ignited by a single-pulsed diode laser and especially the perchlorate complexes showed good performance as primary explosives paired with a thermal stability higher than 200 °C.^[12] In this work, we attempt to increase the thermal and mechanical stabilities of the complexes by connecting two 5-(1-methylhydrazinyl)-1*H*-tetrazole units through an ethylene group to the 1,2-bis[5-(1-methylhydrazinyl)tetrazol-1-yl]ethane (bmhte) ligand, which is able to form coordination polymers. The bmhte ligand and its corresponding copper(II) nitrate complex has already been described in the literature and it had a thermal stability of 180 °C.^[13] To the best of our knowledge, the perchlorate complexes of (bmhte) with copper (**2**), cobalt (**3**) and nickel (**4**) as the central metal(II) ion have been undescribed up to now. The preparation, characterization and laser ignitability of the above-mentioned perchlorate complexes **2–4** is presented.

6.3. Results and Discussion

Synthesis: Ligand **1** was synthesized in several steps according to literature procedures.^[14] First, 1,2-di(1*H*-tetrazol-1-yl)ethane (DTE) was prepared by cyclization of ethylenediamine with triethyl orthoformate and sodium azide. In the second step, DTE was treated with bromine in chloroform and acetic acid. The final product **1** was obtained by substitution of the bromine group with monomethylhydrazine in 2-propanol (Scheme 1).



Scheme 1. Synthesis of **1** starting from 1,2-di(1*H*-tetrazol-1-yl)ethane.

The metal(II) complexes were obtained in high yields by treating the dissolved ligand **1** with the corresponding metal(II) (**2**: copper; **3**: cobalt; **4**: nickel) perchlorate hexahydrate in extensively diluted perchloric acid.

Crystal structure: Single crystals of compound **2** were obtained directly from the mother liquor by slow ethanol diffusion. The perchlorate complex **2** crystallizes as dark blue blocks in the triclinic space group $P\bar{1}$ with two formula units per unit cell and a calculated density of 1.861 g cm^{-3} at 173 K (Table 3). The asymmetric unit consists of one formula unit plus an additional copper centre (Figure 1). The two copper(II) centres exhibit different Jahn-Teller distorted octahedral coordination spheres. Cu1 is coordinated by two perchlorate moieties in the axial position [Cu1–O1 2.500(2) Å], whereas Cu2 is coordinated by two aqua ligands [Cu2–O9 2.423(4) Å]. Both copper atoms are connected to a one-dimensional chain (Figure 2) by the μ -bridging and chelating bmhte ligand [Cu1–N8 1.964(2) Å, Cu1–N12 2.018(3) Å, Cu2–N4 1.950(3) Å, Cu2–N11 2.047(3) Å].

The tetrazole rings of the bmhte ligand are aligned in an *anti* conformation [N1–C2–C3–N5 173.3(3)°] and are twisted with respect to each other [C1–N1–C2–C3 129.0(4)° and C2–C3–N5–C4 97.1(4)°]. The bond lengths [N1–C1 1.336(4) Å, N1–N2 1.387(4) Å, N2–N3 1.279(4) Å, N3–N4 1.358(4) Å and N4–C1 1.331(4) Å] and angles [C1–N1–N2 107.4(2)°, N3–N2–N1 107.5(3)° and N2–N3–N4 109.8(3)°] of the bmhte ligand are in the typical range of substituted tetrazoles and can be compared with the $[\text{Cu}(\text{NO}_3)_2(\text{bmhte})] \cdot 0.5 \text{ H}_2\text{O}$ complex.^[12,13,15] The perchlorato ligand exhibits typical bond lengths [Cl1–O2 1.425(3) Å] and angles [O2–Cl1–O1 110.27(17)°], however, the Cl1–O1 distance is with 1.445(2) Å slightly longer due to coordination of O1 to Cu1.^[12] The bond lengths [Cl2–O5 1.413(6) Å, Cl2–O7 1.555(9) Å and Cl2–O8 1.330(8) Å] and angles [O8–Cl2–O5 109.4(6)°, O8–Cl2–O7

116.2(8)° and O6-Cl2-O7 105.5(7)°] of the non-coordinating perchlorate partly differ from the standard values due to perchlorate disordering.

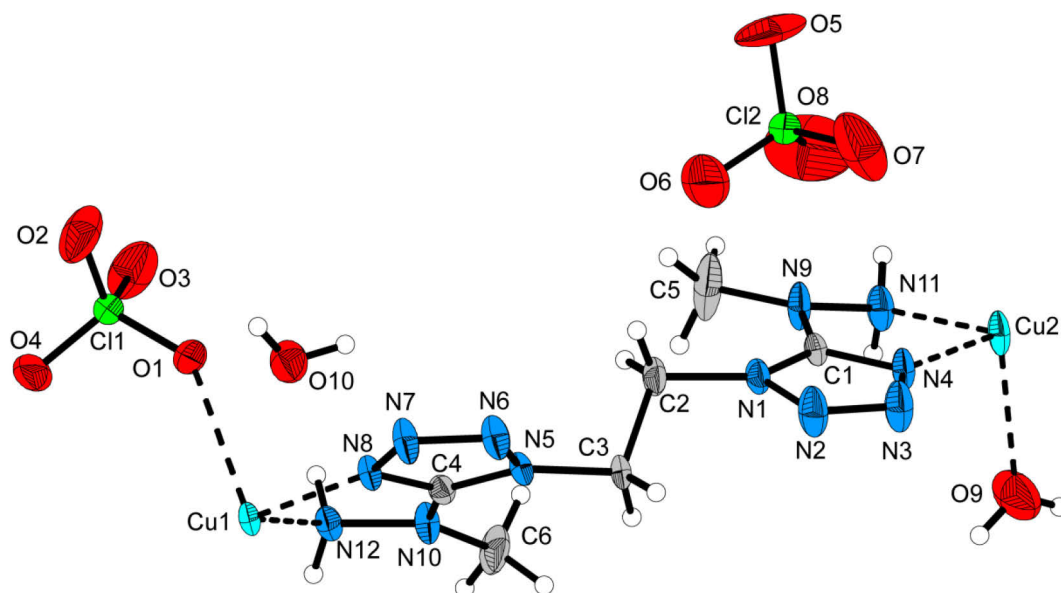


Figure 1. Asymmetric unit of **2**. Thermal ellipsoids of non-hydrogen atoms are drawn at the 50 % probability level except for Cl2 and Cl2A, which were refined isotropically owing to disorder. Only one position of the disordered perchlorate anion (Cl2/2A–O5/5A–O6/6A–O7/7A–O8/8A) is shown. Selected bond lengths [Å]: Cu1–O1 2.500(2), Cu1–N8 1.964(2), Cu1–N12 2.018(3), Cu2–O9 2.423(4), Cu2–N4 1.950(3), Cu2–N11 2.047(3), N1–C1 1.336(4), N1–N2 1.387(4), N1–C2 1.478(4), N2–N3 1.279(4), N3–N4 1.358(4), N4–C1 1.331(4), N9–C1 1.351(4), N9–N11 1.436(4), N9–C5 1.450(4), C2–C3 1.508(5), Cl1–O1 1.445(2), Cl1–O2 1.425(3), Cl1–O3 1.429(3), Cl1–O4 1.422(3); selected bond angles [°]: N8–Cu1–N12 79.78(11), O1–Cu1–N8 93.08(9), O1–Cu1–N12 93.73(11), N4–Cu2–N11 80.50(11), N4–Cu2–O9 90.83(12), N11–Cu2–O9 95.43(15), C1–N1–N2 107.4(2), C1–N1–C2 134.2(3), N3–N2–N1 107.5(3), N2–N3–N4 109.8(3), C1–N9–N11 111.6(3), C1–N9–C5 126.6(3), O2–Cl1–O1 110.27(17), O3–Cl1–O1 108.73(17), O4–Cl1–O1 111.41(15); selected torsion angles [°]: N12–Cu1–N8–C4 –15.1(2), N12–Cu1–N8–N7 177.9(4), N8–Cu1–N12–N10 19.3(2), N11–Cu2–N4–C1 –7.8(2), N11–Cu2–N4–N3 175.1(4), C1–N1–N2–N3 –1.0(4), N1–N2–N3–N4 0.1(4), N1–C2–C3–N5 173.3(3), N1–C1–N9–C5 –7.9(6), C2–N1–C1–N9 4.7(7), C1–N1–C2–C3 129.0(4), C2–C3–N5–C4 97.1(4).

The non-coordinating water molecules and perchlorate anions form strong hydrogen bonds to the complex unit (Table 1, Figure 3). The one-dimensional copper chains are further connected to each other by hydrogen bonds between the coordinating perchlorato ligand and the non-coordinating water molecule.

Table 1. Lengths and angles of selected hydrogen bonds in **2**.

D–H···A ^[a]	D–H [Å]	H···A [Å]	H···A [Å]	D–H···A [°]
O9–H9A···O8 ⁱⁱ	0.80(4)	2.07(4)	2.854(12)	167(4)
O9–H9B···O7 ⁱⁱⁱ	0.80(4)	2.23(4)	2.995(11)	161.(4)
O10–H10B···O3	0.74(4)	2.16(4)	2.857(5)	158(4)
N11–H11B···O7 ^{iv}	0.83(5)	2.29(5)	3.113(13)	172(4)
N12–H12A···O10 ^v	0.91(4)	1.92(4)	2.795(5)	159(3)
N12–H12B···O10	0.90(4)	2.11(4)	3.004(5)	179(4)

[a] Symmetry codes: ii: $-x, 1-y, 1-z$; iii: $-1+x, 1+y, z$; iv: $-1+x, y, z$; v: $-x, 2-y, -z$.

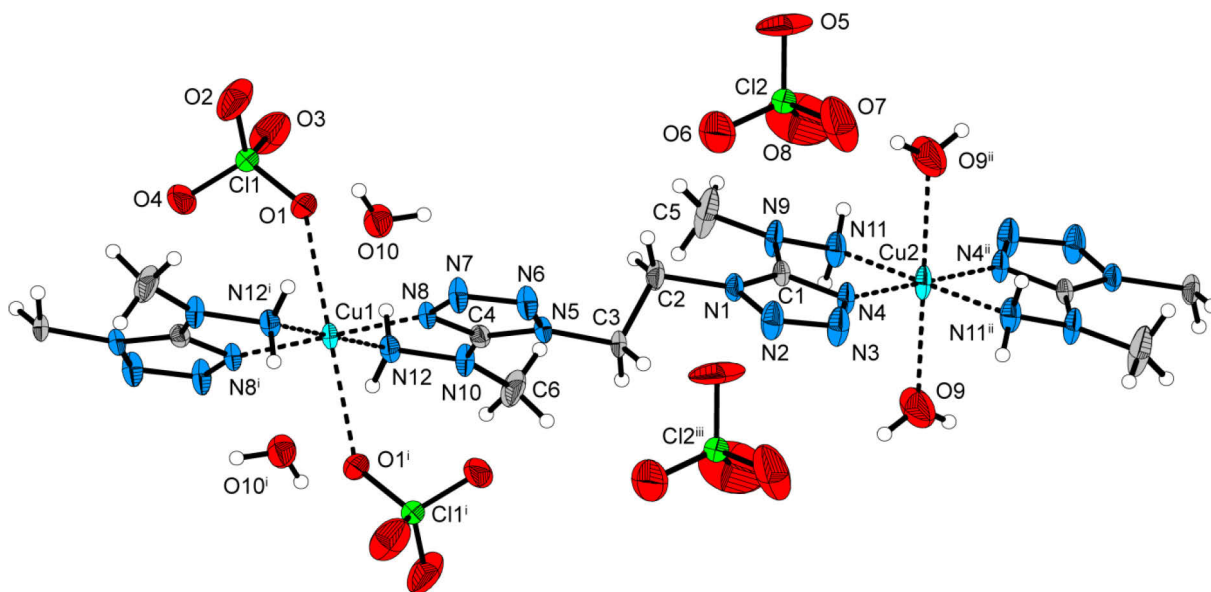


Figure 2. One-dimensional chain of **2**. Thermal ellipsoids of non-hydrogen atoms are drawn at the 50 % probability level except Cl2 and Cl2A, which were refined isotropically owing to disorder. Only one position of the disordered perchlorate anion (Cl2/2A–O5/5A–O6/6A–O7/7A–O8/8A) is shown. Symmetry codes: i: $1-x, 2-y, -z$; ii: $-x, 1-y, 1-z$; iii: $-1+x, 1+y, z$.

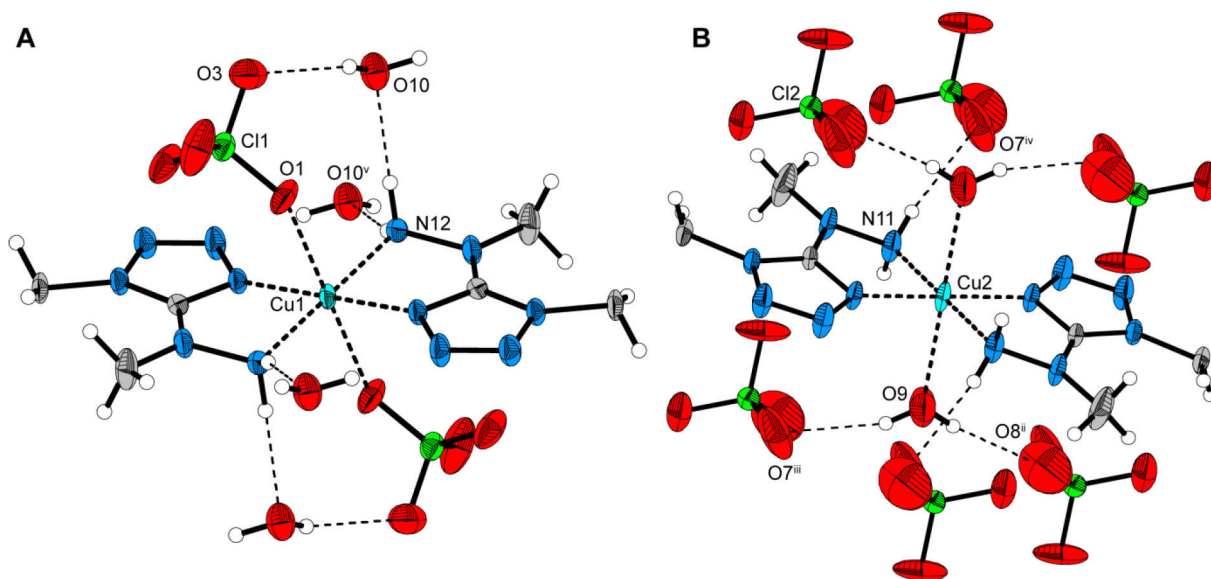


Figure 3. Selected hydrogen bonds in **2**. (A) The environment of Cu1. (B) The environment of Cu2. Thermal ellipsoids of non-hydrogen atoms are drawn at the 50% probability level except for Cl2 and Cl2A, which were refined isotropically owing to disorder. Only one position of the disordered perchlorate anion (Cl2/2A–O5/5A–O6/6A–O7/7A–O8/8A) is shown. Symmetry codes: ii: $-x, 1-y, 1-z$; iii: $-1+x, 1+y, z$; iv: $-1+x, y, z$; v: $-x, 2-y, -z$.

Infrared spectroscopy: All the described compounds were investigated by IR spectroscopy. Raman spectroscopy was not performed because of the high sensitivity of the compounds towards laser light.

The IR spectrum of the free ligand **1** shows relatively sharp absorption bands at 3286, 3187, 3180, 3007 and 2976 cm^{-1} , which can be assigned to the N–H and C–H stretching vibrations according to the literature.^[16] The C=N stretching vibration can be observed at

1651 cm^{-1} and the N–H deformation at 1561 cm^{-1} . Typical N=N, C–N and N–N stretching modes are in the range of 1445 to 1060 cm^{-1} and the fingerprint area below 1000 cm^{-1} .^[17] Owing to complexation, the N–H and C–H stretching vibrations of the bmhte ligand are shifted to lower [$\tilde{\nu}$ = 3265 (**2**); 3275, 3162 (**3**); 3260, 3162 cm^{-1} (**4**)] and also higher wavenumbers [$\tilde{\nu}$ = 3192, 3139 (**2**); 3046 (**3**); 3047 cm^{-1} (**4**)]. The C=N stretching and N–H deformation modes are all blueshifted [$\tilde{\nu}$ = 1657, 1584 (**2**); 1652, 1583 (**3**); 1654, 1581 cm^{-1} (**4**)]. For the copper(II) complex **2**, an additional vibration mode appeared at 1615 cm^{-1} . For the Cl–O stretching vibration of the perchlorate, one single band can be observed at 1073 cm^{-1} for **2**, whereas it is split into three signals for **3** ($\tilde{\nu}$ = 1102, 1084 and 1047 cm^{-1}) and **4** ($\tilde{\nu}$ = 1100, 1084 and 1048 cm^{-1}).^[18] As a result of the similar IR spectra and from the elemental analysis, related structures are suggested for $\{[\text{Co}(\mu\text{-bmhte})(\text{H}_2\text{O})_2](\text{ClO}_4)_2\}_n$ (**3**) and $\{[\text{Ni}(\mu\text{-bmhte})_{1.5}](\text{ClO}_4)_2 \cdot \text{H}_2\text{O}\}_n$ (**4**).

Energetic properties and laser ignition: All the synthesized metal(II) complexes **2–4** and the free ligand **1** were tested in terms of friction, impact and electrostatic discharge (ESD). In addition, the temperature stability was determined by means of differential thermal analysis. An overview of the energetic properties is given in Table 2. The compounds were classified according to the UN Recommendations on the Transport of Dangerous Goods.^[19]

Table 2. Energetic properties of the metal(II) complexes **2–4**.

	2	3	4
Formula	$\text{C}_6\text{H}_{18}\text{Cl}_2\text{CuN}_{12}\text{O}_{10}$	$\text{C}_6\text{H}_{18}\text{Cl}_2\text{CoN}_{12}\text{O}_{10}$	$\text{C}_9\text{H}_{23}\text{Cl}_2\text{N}_{18}\text{NiO}_9$
T_{decomp} [$^{\circ}\text{C}$] ^[a]	170	239	224
IS [J] ^[b]	1	1	5
FS [N] ^[c]	5	8	30
ESD [J] ^[d]	0.015	0.11	0.075
Grain size [μm]	100–500	< 100	< 100
Laser init.	detonation	detonation	detonation

[a] Decomposition onset temperature determined by differential thermal analysis with OZM Research DTA 552-Ex. [b] Impact sensitivity determined with BAM drop hammer. [c] Friction sensitivity determined with BAM friction tester. [d] Electrostatic discharge determined with Electric Spark Tester ESD 2010 EN.

Ligand **1** is classified as being sensitive towards impact (25 J) and friction (288 N). It further shows a low electrostatic discharge sensitivity of 0.75 J and is temperature-stable up to 265 $^{\circ}\text{C}$ (onset). The copper(II) and cobalt(II) perchlorate are both extremely sensitive towards friction (**2**: 5 N; **3**: 8 N) and very sensitive towards impact (**2** and **3**: 1 J). Complex **2** also shows a high sensitivity towards electrostatic discharge (**2**: 15 mJ), whereas **3** is less sensitive towards ESD (**3**: 0.11 J). Complex **2** heavily decomposes at 170 $^{\circ}\text{C}$ (onset) after dehydration between 130 and 155 $^{\circ}\text{C}$. The DTA plot of **3** shows a small endothermic signal between 120 and 130 $^{\circ}\text{C}$ that could indicate a dehydration process of coordinatively bonded water and

confirms the suggested structure. The onset point of exothermic decomposition is at 239 °C for **3**. Nickel(II) perchlorate **4** is less sensitive than **2** and **3**. It is classified as sensitive towards impact (5 J) and very sensitive towards friction (30 N). The sensitivity towards ESD is in a medium range (75 mJ) and the thermal stability is high with an exothermic decomposition onset of 224 °C. The non-coordinative water is removed between 50 and 100 °C as indicated by a broad endothermic signal in the DTA plot.

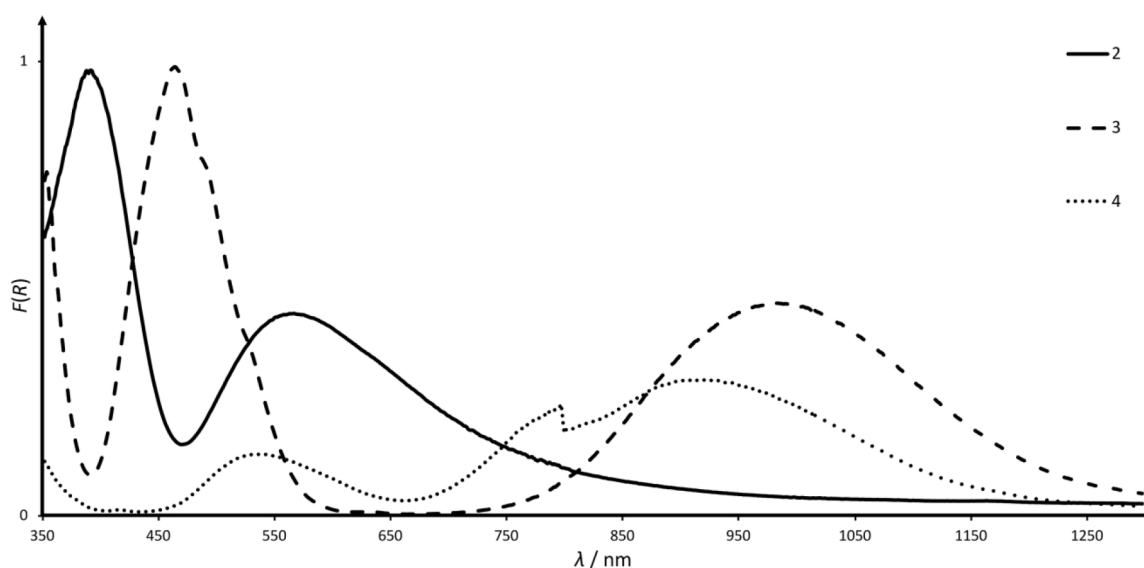


Figure 4. UV/Vis/NIR spectra of **2–4** in the range of 350 to 1300 nm. The step in the absorption intensity $F(R)$ at 800 nm is caused by a detector change. Owing to technical limitations, no quantitative information about the absorption intensity could be obtained from the spectra.

Laser ignition experiments with a diode laser were performed. Confined samples of **2–4** were directly irradiated with single-pulsed laser light in the near-infrared region ($\lambda = 940$ nm and $\tau = 100$ μ s). All three compounds exhibited a deflagration-to-detonation transition after ignition by laser irradiation. The ignition mechanism seems to be of thermal nature. No selectivity was observed as is expected for a photoelectronic process.^[10c] The UV/Vis/NIR spectra (Figure 4) show that all three complexes were absorbing at 940 nm. This also might be an indication for a thermal process because a strong light absorption at this wavelength implies a strong energy absorption and consequently a heating of the sample.

6.4. Conclusion

The syntheses of the literature-known ligand bmhte (**1**) and three new perchlorate complexes **2–4** are reported.^[13] The metal(II) complexes were further characterized by infrared and UV/Vis/NIR spectroscopy, elemental analysis, and for compound **2**, the crystal structure was also solved. The energetic properties of compounds **1–4** were determined and complexes **2–4** showed sensitivity towards laser light. Perchlorates **2–4** are potential photosensitive primary explosives.

6.5. Experimental Section

Caution! The prepared metal(II) complexes **2–4** and the free ligand **1** are energetic materials that are sensitive towards various stimuli. Proper protective measures (safety glasses, face shield, leather coat, earthed equipment, conductive floor and shoes, Kevlar gloves and ear plugs) should be used when handling these compounds. Extra safety precautions should be taken when compound **2** and **3** are handled. Both are extremely sensitive towards impact, friction and electrostatic discharge.

All chemicals were used as supplied by ABCR, Acros Organics, AppliChem, Grüssing, Sigma–Aldrich and VWR. The precursor 1,2-di(1*H*-tetrazol-1-yl)ethane and 1,2-bis(5-bromo-1*H*-tetrazol-1-yl)ethane were prepared by using literature procedures.^[14a] The impact (IS) and friction sensitivity (FS) tests were carried out according to standard methods by using a BAM (Bundesanstalt für Materialforschung und -prüfung) drop hammer and a BAM friction tester.^[20] The sensitivity towards electrostatic discharge was tested by using an OZM Research electric spark tester ESD 2010 EN.^[21] The grain size was determined by sieving. Decomposition temperatures were measured by differential thermal analysis (DTA) by using an OZM Research DTA 552-Ex instrument.^[21a] The heating rate was 5 °C min⁻¹ and it was measured in the range of room temp. to 400 °C.

Suitable single crystals of **2** were mounted in Kel-F oil. The structure was determined on an Oxford Diffraction Xcalibur 3 diffractometer with a Sapphire CCD detector, four circle kappa platform, Enhance molybdenum K_{α} radiation source ($\lambda = 71.073$ pm) and Oxford Cryosystems Cryostream cooling unit (Table 3). Data collection and reduction was performed with the CrysAlisPro software.^[22] The structure was solved with SIR2004.^[23] The refinement was performed with SHELXL-97.^[24] The CIF file was checked at the checkCIF website.^[25] The non-hydrogen atoms were refined anisotropically and the hydrogen atoms isotropically if not calculated. The determination of the carbon, hydrogen and nitrogen contents was carried out by combustion analysis using an Elementar Vario EL.^[26] IR spectra were recorded on a PerkinElmer BXII FTIR system with a Smith DuraSamplIR II diamond ATR unit.^[27] ¹H and ¹³C NMR spectra were recorded on a JEOL Eclipse 270 spectrometer.^[28] The UV/Vis/NIR reflectance of solid samples was measured with a Varian Cary 500 spectrometer in the wavelength range of 350–1300 nm.^[29] The reflectance R [%] was transformed by the Kubelka-Munk function to the absorption intensity $F(R)$.^[30]

Table 3. Crystal and structure refinement data for **2**.

	2
Formula	C ₆ H ₁₈ Cl ₂ CuN ₁₂ O ₁₀
M_r [g mol ⁻¹]	552.76
Color	dark blue
Habit	block
Crystal size [mm]	0.20 × 0.15 × 0.05
Crystal system	triclinic
Space group	$P\bar{1}$
a [Å]	7.1278(4)
b [Å]	7.4475(5)
c [Å]	20.5513(13)
α [°]	86.304(5)
β [°]	80.409(5)
γ [°]	66.461(6)
V [Å ³]	986.19(11)
Z	2
$\rho_{\text{calc.}}$ [g cm ⁻³]	1.861
T [K]	173
λ (Mo K α) [Å]	0.71073
$F(000)$	562
μ [mm ⁻¹]	1.46
θ range [°]	4.7–30.0
Dataset (h ; k ; l)	$-9 \leq h \leq 9$; $-9 \leq k \leq 9$; $-27 \leq l \leq 27$
Measured reflections	11539
Independent reflections	4677
Observed reflections	3406
R_{int}	0.041
Parameters	353
Restraints	2
R_1 (obs.)	0.045
wR_2 (all data)	0.116
S	1.07
resd. dens. [e Å ⁻³]	-0.46, 0.75
Solution	SIR2004
Refinement	SHELXL-97
Absorption correction	multi-scan

CCDC-954146 contains the supplementary crystallographic data for this paper. These data can be obtained free of charge from The Cambridge Crystallographic Data Centre via www.ccdc.cam.ac.uk/data_request/cif.

1,2-Bis[5-(1-methylhydrazinyl)tetrazol-1-yl]ethane (1): The compound was synthesized according to a literature procedure:^[13] a suspension of 1,2-bis(5-bromo-1*H*-tetrazol-1-yl)ethane (2.82 g, 8.71 mmol) and monomethylhydrazine (1.60 g, 34.8 mmol) in 2-propanol (30 mL) was heated for 20 h at reflux. The suspension was cooled to room temperature and the solvent was removed under reduced pressure. The residue was filtered, washed with water

and finally dried in air, yield: 1.99 g (7.83 mmol, 90 %); DTA (5 °C min⁻¹) onset: 221 °C (m.p.), 265 °C (decomp.). ¹H NMR (270 MHz, [D6]DMSO, 25 °C, TMS): δ = 4.92 (s, 4 H, -CH₂), 4.90 (s, 4 H, -NH₂), 3.15 (s, 6 H, -CH₃) ppm. ¹³C{¹H} NMR (68 MHz, [D6]DMSO, 25 °C, TMS): δ = 158.5 (-CN₄), 47.1 (-CH₂), 43.6 (-CH₃) ppm. IR (ATR): $\tilde{\nu}$ = 3286 (w), 3187 (w), 3180 (w), 3034 (vw), 3007 (vw), 2976 (w), 1651 (s), 1561 (m), 1445 (s), 1424 (m), 1405 (m), 1350 (w), 1332 (w), 1282 (w), 1268 (w), 1256 (w), 1224 (m), 1197 (w), 1162 (vw), 1120 (m), 1103 (m), 1092 (w), 1060 (s), 982 (m), 924 (m), 913 (s), 759 (w), 749 (m), 736 (m), 723 (vs), 699 (w), 688 (m) cm⁻¹. C₆H₁₄N₁₂ (254.26 g mol⁻¹): calcd. C 28.34, H 5.55, N 66.11 %; found C 27.94, H 5.33, N 63.98 %. BAM impact: 25 J; BAM friction: 288 N; ESD: 0.75 J (at grain size < 100 μm).

{[Cu(ClO₄)₂(μ-bmhte)]·2H₂O}{[Cu(μ-bmhte)(H₂O)₂](ClO₄)₂}]_n (2): Compound **1** (254 mg, 1.00 mmol) was dissolved in a mixture of water (15 mL) and perchloric acid (60 %, 1 mL) at 70 °C. A solution of copper(II) perchlorate hexahydrate (371 mg, 1.00 mmol) in water was added and the resulting solution turned dark blue. Ethanol was slowly diffused into the reaction mixture and after a few days, dark blue single crystals suitable for X-ray diffraction were obtained, yield 0.502 mg (0.91 mmol, 91 %). DTA (5 °C min⁻¹) onset: 170 °C (decomp.). IR (ATR): $\tilde{\nu}$ = 3581 (vw), 3524 (vw), 3265 (vw), 3192 (w), 3139 (vw), 3052 (w), 2950 (vw), 1657 (m), 1615 (w), 1584 (w), 1482 (w), 1461 (w), 1419 (w), 1396 (vw), 1374 (vw), 1324 (w), 1314 (w), 1255 (vw), 1230 (w), 1204 (vw), 1140 (w), 1073 (vs), 984 (w), 949 (m), 934 (w), 734 (m), 722 (m), 675 (w) cm⁻¹. UV/Vis/ NIR: λ_{max} = 392 nm. C₆H₁₈Cl₂CuN₁₂O₁₀ (552.73 g mol⁻¹): calcd. C 13.04, H 3.28, N 30.41 %; found C 14.14, H 3.37, N 29.54 %. ICP-AES calcd. (%): Cu 11.50; found Cu 12.65. BAM impact: 1 J; BAM friction: 5 N; ESD: 0.015 J (at grain size 100–500 μm).

{[Co(μ-bmhte)(H₂O)₂](ClO₄)₂}]_n (3): Compound **1** (254 mg, 1.00 mmol) was dissolved in a mixture of water (15 mL) and perchloric acid (60 %, 1 mL) at 70 °C. A solution of cobalt(II) perchlorate hexahydrate (366 mg, 1.00 mmol) in water was added. The product precipitated from the mother liquor as orange powder after a few days. The solid was removed by filtration and dried in air, yield 0.496 mg (0.90 mmol, 90 %). DTA (5 °C min⁻¹) onset: 239 °C (decomp.). IR (ATR): $\tilde{\nu}$ = 3615 (vw), 3367 (w), 3275 (m), 3162 (m), 3046 (m), 3002 (w), 2980 (w), 2948 (w), 2718 (vw), 2054 (vw), 1751 (vw), 1652 (s), 1583 (m), 1475 (m), 1439 (m), 1426 (w), 1418 (m), 1380 (m), 1332 (s), 1312 (s), 1237 (m), 1181 (w), 1148 (m), 1102 (vs), 1084 (vs), 1047 (vs), 1012 (m), 1000 (m), 959 (m), 952 (m), 921 (m), 825 (w), 729 (s), 695 (m), 681 (w) cm⁻¹. UV/Vis/NIR: λ_{max} = 464 nm. C₆H₁₈Cl₂CoN₁₂O₁₀ (548.12 g mol⁻¹): calcd. C 13.15, H 3.31, N 30.66 %; found C 13.58, H 3.29, N 30.21 %. ICP-AES calcd. (%): Co 13.30; found Co 14.03. BAM impact: 1 J; BAM friction: 8 N; ESD: 0.11 J (at grain size < 100 μm).

{[Ni(μ -bmhte)_{1.5}](ClO₄)₂·H₂O}_n (4): Compound **1** (254 mg, 1.00 mmol) was dissolved in a mixture of water (15 mL) and perchloric acid (60 %, 1 mL) at 70 °C. A solution of nickel(II) perchlorate hexahydrate (366 mg, 1.00 mmol) in water was added. The product precipitated from the mother liquor as violet powder after one week. The solid was removed by filtration, washed with water and dried in air, yield 0.380 mg (0.58 mmol, 87 %). DTA (5 °C min⁻¹) onset: 224 °C (decomp.). IR (ATR): $\tilde{\nu}$ = 3616 (vw), 3390 (w), 3260 (w), 3162 (m), 3047 (m), 3002 (w), 2950 (w), 2722 (vw), 1751 (vw), 1654 (s), 1581 (m), 1474 (m), 1439 (m), 1416 (m), 1314 (s), 1232 (m), 1180 (w), 1100 (vs), 1084 (vs), 1048 (s), 1011 (w), 1002 (w), 958 (w), 934 (w), 921 (m), 825 (w), 729 (m), 694 (m), 681 (w) cm⁻¹. UV/Vis/NIR: λ_{\max} = 913 nm. C₉H₂₃Cl₂N₁₈NiO₉ (656.99 g mol⁻¹): calcd. C 16.45, H 3.53, N 38.37 %; found C 16.75, H 3.83, N 38.48 %. ICP-AES calcd. (%): Ni 8.93; found Ni 8.20. BAM impact: 5 J; BAM friction: 30 N; ESD: 0.075 J (at grain size < 100 μ m).

6.6. References

- [1] T. M. Klapötke, *Chemie der hochenergetischen Materialien*, 1st ed., Walter de Gruyter, Berlin, New York, **2009**.
- [2] a) V. Thottempudi, F. Forohor, D. A. Parrish, J. M. Shreeve, *Angew. Chem.* **2012**, *124*, 10019; *Angew. Chem. Int. Ed.* **2012**, *51*, 9881–9885; b) H. Gao, J. M. Shreeve, *Chem. Rev.* **2011**, *111*, 7377–7436; c) M. Rahm, S. V. Dvinskikh, I. Furo, T. Brinck, *Angew. Chem.* **2011**, *123*, 1177; *Angew. Chem. Int. Ed.* **2011**, *50*, 1145–1148; d) R. Haiges, S. Schneider, T. Schroer, K. O. Christe, *Angew. Chem.* **2004**, *116*, 5027; *Angew. Chem. Int. Ed.* **2004**, *43*, 4919–4924; e) D. E. Chavez, D. Parrish, D. N. Preston, I. W. Mares, *Propellants Explos. Pyrotech.* **2012**, *37*, 647–652; f) T. M. Klapötke, B. Krumm, R. Moll, S. F. Rest, *Z. Anorg. Allg. Chem.* **2011**, *637*, 2103–2110.
- [3] R. Varosh, *Propellants Explos. Pyrotech.* **1996**, *21*, 150–154.
- [4] R. S. Lee, R. E. Lee, *16th International Pyrotechnics Seminar*, Jönköping, Sweden, June 24–28, **1991**, 384–398.
- [5] a) A. A. Brish, I. A. Galeeva, B. N. Zaitsev, E. A. Sbimev, L. V. Tararinstev, *Fiz. Goreniya Vzryva* **1966**, *2*, 132; b) A. A. Brish, I. A. Galeeva, B. N. Zaitsev, E. A. Sbimev, L. V. Tararinstev, *Fiz. Goreniya Vzryva* **1969**, *5*, 475; c) L. C. Yang, V. J. Menichelli, *Appl. Phys. Lett.* **1971**, *19*, 473–475.
- [6] a) T. Sofue, A. Iwama, *Propellants Explos.* **1979**, *4*, 98–106; b) H. Oestmark, N. Roman, *J. Appl. Phys.* **1993**, *73*, 1993–2003; c) L. deYong, T. Nguyen, J. Waschl, Defence Science and Technology Organisation, Canberra, Australia, **1995**, 1–74; d) M. Singh, R. Kumar, L. Kumar, V. S. Sethi, *33rd International Pyrotechnics Seminar*, Fort Collins, USA, July 16–21, **2006**, 1–12.

- [7] a) A. Y. Zhilin, M. A. Ilyushin, I. V. Tselinskii, A. S. Brykov, *Russ. J. Appl. Chem.* **2001**, *74*, 99–102; b) E. S. Hafenrichter, B. Marshall Jr, K. J. Fleming, *29th International Pyrotechnics Seminar*, Westminster, USA, July 14–19, **2002**, 787–793; c) A. Y. Zhilin, M. A. Ilyushin, I. V. Tselinskii, A. S. Kozlov, I. S. Lisker, *Russ. J. Appl. Chem.* **2003**, *76*, 572–576.
- [8] a) Y.-h. Zhu, D.-l. Sheng, B. Yang, L.-k. Chen, F.-e. Ma, *Hanneng Cailiao* **2009**, *17*, 169–172; b) I. A. Ugryumov, M. A. Ilyushin, I. V. Tselinskii, A. S. Kozlov, *Russ. J. Appl. Chem.* **2003**, *76*, 439–441.
- [9] J. W. Fronabarger, W. B. Sanborn, T. Massis, *22nd International Pyrotechnics Seminar*, Fort Collins, USA, July 15–19, **1996**, 645–652.
- [10] a) N. K. Bourne, *Proc. R. Soc. London Ser. A* **2001**, *457*, 1401–1426; b) E. D. Aluker, A. G. Krechetov, A. Y. Mitrofanov, A. S. Zverev, M. M. Kuklja, *J. Phys. Chem. C* **2012**, *116*, 24482–24486; c) E. D. Aluker, A. G. Krechetov, A. Y. Mitrofanov, D. R. Nurmukhametov, M. M. Kuklja, *J. Phys. Chem. C* **2011**, *115*, 6893–6901.
- [11] S. Zeman, *Struct. Bonding (Berlin)* **2007**, *125*, 195–271.
- [12] M. Joas, T. M. Klapötke, J. Stierstorfer, N. Szimhardt, *Chem. Eur. J.* **2013**, *19*, 9995–10003.
- [13] L. S. Kovacevic, T. M. Klapötke, S. M. Sproll, *Z. Anorg. Allg. Chem.* **2010**, *636*, 1079–1084.
- [14] a) T. M. Klapötke, S. M. Sproll, *Eur. J. Org. Chem.* **2009**, 4284–4289; b) T. M. Klapötke, S. M. Sproll, *J. Polym. Sci., Part A* **2010**, *48*, 122–127.
- [15] M. Joas, T. M. Klapötke, J. Stierstorfer, *Crystals* **2012**, *2*, 958–966.
- [16] M. Hesse, H. Meier, B. Zeeh, *Spektroskopische Methoden der organischen Chemie*, 7th ed., Thieme, Stuttgart, Germany, New York, **2005**.
- [17] a) T. M. Klapötke, C. M. Sabate, J. Stierstorfer, *Z. Anorg. Allg. Chem.* **2008**, *634*, 1867–1874; b) T. M. Klapötke, P. Mayer, J. Stierstorfer, J. J. Weigand, *J. Mater. Chem.* **2008**, *18*, 5248–5258; c) N. Fischer, D. Izsak, T. M. Klapötke, S. Rappenglueck, J. Stierstorfer, *Chem. Eur. J.* **2012**, *18*, 4051–4062; d) M. M. Degtyarik, P. N. Gaponik, V. N. Naumenko, A. I. Lesnikovich, M. V. Nikanovich, *Spectrochim. Acta Part A* **1987**, *43A*, 349–353.
- [18] D. L. Lewis, E. D. Estes, D. J. Hodgson, *J. Cryst. Mol. Struct.* **1975**, *5*, 67–74.
- [19] Impact: insensitive > 40 J, less sensitive \geq 35 J, sensitive \geq 4 J, very sensitive \geq 3 J; Friction: insensitive > 360 N, less sensitive = 360 N, sensitive < 360 N and > 80 N, very sensitive \leq 80 N, extremely sensitive \leq 10 N. According to *Recommendations on the Transport of Dangerous Goods, Manual of Tests and Criteria*, 4th edition, United Nations, New York, Geneva, **1999**.
- [20] a) NATO Standardization Agreement 4489, September 17, **1999**; b) NATO Standardization Agreement 4487, October 29, **2009**.
- [21] a) <http://www.ozm.cz> (accessed January 29, 2013); b) NATO Standardization Agreement 4515, August 23, **2002**.

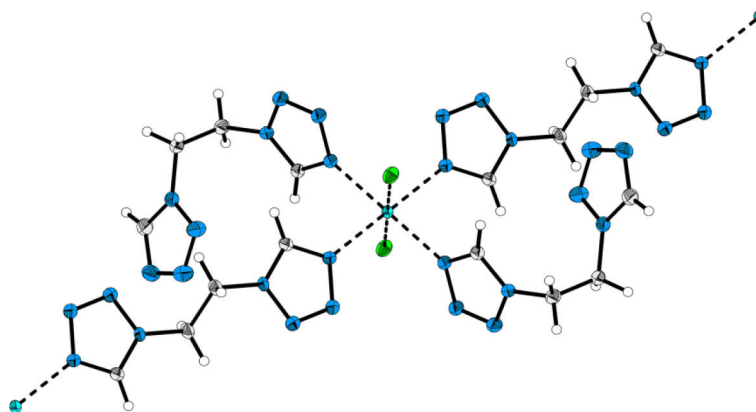
-
- [22] *CrysAlisPro*, v. 1.171.36.24, Oxford Diffraction Ltd., Abingdon, UK, **2012**.
- [23] M. C. Burla, R. Caliendo, M. Camalli, B. Carrozzini, G. L. Cascarano, L. De Caro, C. Giacovazzo, G. Polidori, R. Spagna, *J. Appl. Crystallogr.* **2005**, *38*, 381–388.
- [24] G. M. Sheldrick, *Acta Crystallogr., Sect. A* **2008**, *64*, 112–122.
- [25] a) S. R. Hall, F. H. Allen, I. D. Brown, *Acta Crystallogr., Sect. A* **1991**, *47*, 655–685; b) <http://journals.iucr.org/services/cif/checkcif.html> (accessed January 28, 2013).
- [26] <http://www.elementar.de/> (accessed February 1, 2013).
- [27] <http://www.perkinelmer.de/> (accessed February 1, 2013).
- [28] <http://www.jeol.co.jp/en/> (accessed July 24, 2013).
- [29] <http://www.agilent.com/> (accessed April 15, 2013).
- [30] P. Kubelka, F. Munk, *Z. Tech. Phys.* **1931**, *1*, 593–601.

7. Polynuclear Chlorido Metal(II) Complexes with 1,2-Di(1*H*-tetrazol-1-yl)ethane as Ligand Forming One- and Two-dimensional Structures

Reproduced with permission from M. Joas, T. M. Klapötke, *Zeitschrift für anorganische und allgemeine Chemie* **2014**, 640, 1886–1891.

Online: <http://dx.doi.org/10.1002/zaac.201400192>.

Copyright 2014 Wiley-VCH Verlag GmbH & Co. KGaA, Weinheim.



7.1. Abstract

The preparation and characterization of three metal(II) chlorido complexes with 1,2-di(1*H*-tetrazol-1-yl)ethane (dte) (**1**) as ligand is presented. The complexes have the following formula: $[\text{CoCl}_2(\mu\text{-dte})(\text{dte})_2]_n$ (**2**), $[\text{CuCl}_2(\mu\text{-dte})_2]_n$ (**3**), and $[\text{Cd}(\mu\text{-Cl})_2(\mu\text{-dte})]_n$ (**4**). Single crystal X-ray diffraction of all three metal complexes was performed and the structures are discussed. All three central metal atoms are connected to polynuclear structures by the μ -bridging ligand. Cobalt and copper are connected to one-dimensional chains. The central cadmium(II) atoms are additionally connected by the chloride anions to a two-dimensional network. Further, the cobalt(II) complex represents a special case with two terminal dte ligands.

7.2. Introduction

Coordination chemistry is an important field in inorganic chemistry. Coordination compounds are investigated in many different disciplines like e.g. homogeneous catalysis,^[1] bioinorganic chemistry,^[2] supramolecular chemistry,^[3] molecular magnetism,^[4] or energetic materials.^[5] Especially metal-organic frameworks (MOFs) gained public interest in the last years. A MOF is a *n*-dimensional network, which is formed between central metal atoms and bridging organic ligands. It further exhibits voids which e.g. can serve as gas storage, for gas

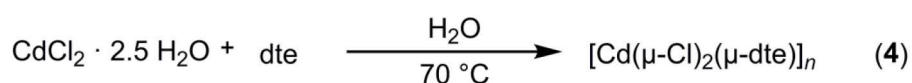
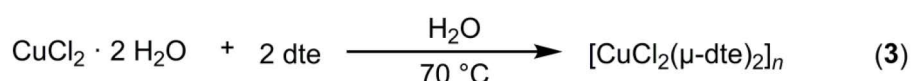
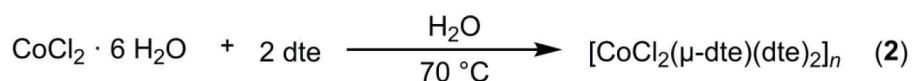
purification, and for catalysis.^[6] But MOFs are also newly interesting for energetic materials.^[5] Thus, the design and the structural characterization of polynuclear coordination compounds concerns researchers in the whole world.

One class of ligands, which are suitable for coordination polymers, are alkyl-bridged azoles. The crystal structures and properties of various metal(II) complexes with perchlorate as counterion and μ -bridging tetrazoles like 1,2-di(1*H*-tetrazol-1-yl)ethane (dte), 1,2-di(1*H*-tetrazol-1-yl)propane (dtp) and 1,2-di(1*H*-tetrazol-1-yl)butane (dtb) or anionic 1,2,4-triazoles like 1,2-di(1,2,4-triazol-4-yl)ethane have been presented by Koningsbruggen *et al.*^[7] Further, coordination compounds of dte with tetrafluoroborate, azide, and thiocyanate were investigated by different research groups.^[8] The research interest in these publications was focused on magnetic measurements and spin crossover effects. In addition, it was shown by X-ray measurements that anions like perchlorate or tetrafluoroborate did not coordinate to the central metal atom, whereas e.g. azide participated in coordination and acted as a linker between the metal atoms. Other small and well coordinating anions are halogenides. Copper(II) complexes with dtb and chloride as well as bromide as anions have been prepared by Linert *et al.*^[8g] The crystal structures were presented and three-dimensional structures of the form $[\text{Cu}(\mu\text{-}X)_2(\mu\text{-dtb})]_n$ ($X = \text{Cl}^-$ or Br^-) were obtained.

To the best of our knowledge, chlorido coordination compounds with dte as ligand are not literature known yet. Consequently, the first metal(II) complexes ($M = \text{Co}^{2+}$, Cu^{2+} , Cd^{2+}) with dte as ligand and chloride as counterion were synthesized and characterized by infrared spectroscopy, elemental analysis, and X-ray diffraction. The dte and chlorido ligands exhibited different coordination modes, thus one- and two-dimensional networks are formed.

7.3. Results and Discussion

Synthesis: The ligand 1,2-di(1*H*-tetrazol-1-yl)ethane (**1**) was synthesized according to the literature procedure of Kamiya and Saito in a yield of 66%.^[9] Aqueous solutions of **1** were further combined with aqueous solutions of the metal(II) chloride (CoCl_2 , CuCl_2 , and CdCl_2) to give the according coordination compounds (Scheme 1).



Scheme 1. Synthesis of metal(II) complexes **2–4** starting from dte and the corresponding metal(II) chlorides.

Crystal structures: X-ray suitable single crystals of **2–4** were obtained directly from the mother liquor. The X-ray data is given in Table 3.

The bond lengths and angles of the tetrazole rings of the compounds **2–4** are in the typical range of the free ligand and other 1-substituted tetrazoles.^[8a,10] The ligand is not discussed in detail. Two orientations are observed for the dte ligand: an *anti* conformation with N-C-C-N torsion angles around 180° and a *gauche* conformation with angles between 30° and 90°.

The cobalt(II) complex **2** crystallizes in the triclinic space group $P\bar{1}$ with one formula unit per unit cell and a calculated density of 1.777 g cm⁻³ at 173 K. The central cobalt(II) atom is surrounded by four tetrazole rings [$d(\text{Co1-N4}) = 2.1969(19)$ Å and $d(\text{Co1-N12}) = 2.1458(18)$ Å] and two chlorido ligands [$d(\text{Co1-Cl1}) = 2.4164(6)$ Å]. The coordination sphere is octahedral (Figure 1) with bond angles near 90° [$\text{N12-Co1-N4} = 92.95(7)^\circ$ and $\text{N12-Co1-Cl1} = 91.42(5)^\circ$] as expected for a d⁷ complex. The four surrounding tetrazole ligands differ in their coordination mode in an unusual type: two ligands are *anti*-oriented ($\text{N9-C6-C6}^{\text{ii}}\text{-N9}^{\text{ii}} = -180.0(2)^\circ$; symmetry code: ii: $-1-x, -y, 2-z$) and connect in a κ^2 -mode the central cobalt atoms via N12 and N12' to an one-dimensional chain, while the other two dte units are in a *gauche* conformation [$\text{N5-C3-C2-N1} = -80.0(3)^\circ$] and coordinate only with one site (κN^4) in a terminal mode. This is very unusual compared to other dte complexes, which exhibit in the most cases only μ -bridging dte units.^[7c,8a] Only less compounds with monodentate terminal dte ligands like the $[\text{Co}(\text{SCN})_2(\mu\text{-dte})(\text{dte})_2]_n$ are known.^[8e] The pseudohalogenide complex with thiocyanate exhibits a similar octahedral structure like the chlorido complex with two monodentate terminal dte units [$\text{N1-C2-C3-N5} = -64.6(3)^\circ$], one μ -bridging dte unit [$\text{N9-C6-C6}^{\text{i}}\text{-N9}^{\text{i}} = 180.0(2)^\circ$; symmetry code: i: $2-x, -y, -z$] and two terminal counterions (SCN- κN). However, the thiocyanate complex crystallizes in the monoclinic space group $P2_1/n$. Bond lengths and angles of both complexes are compared in Table 1.

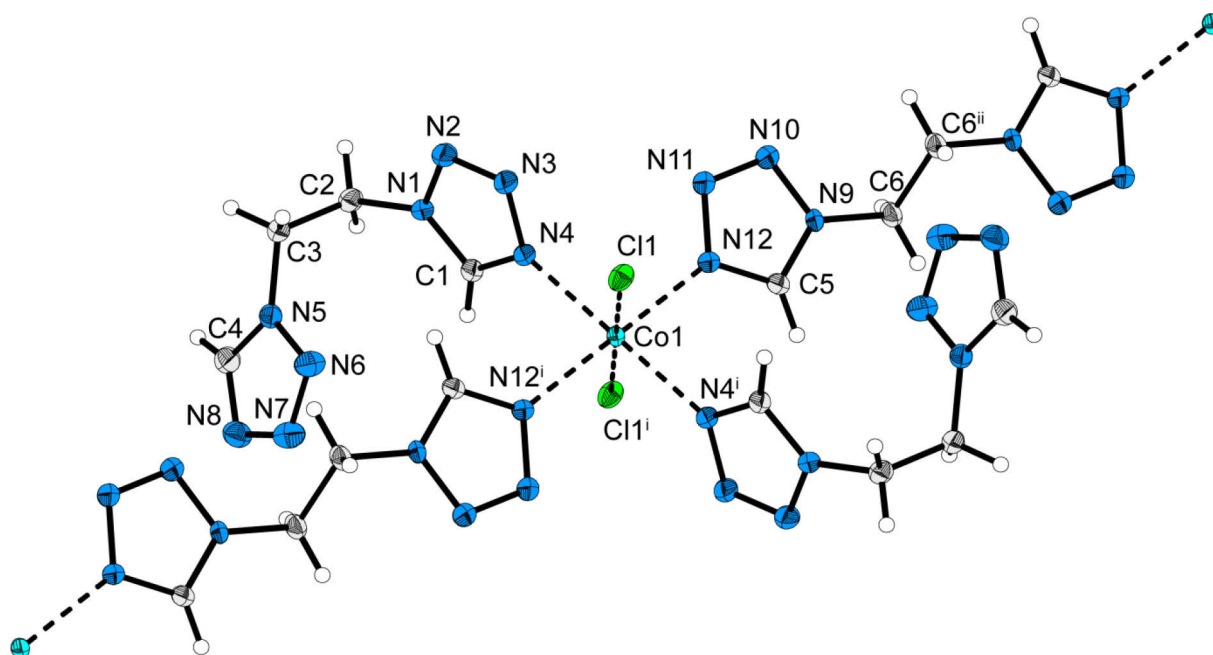


Figure 1. Coordination sphere of $[\text{CoCl}_2(\mu\text{-dte})(\text{dte})_2]_n$ (**2**). Thermal ellipsoids of non-hydrogen atoms are drawn at the 50 % probability level. Selected bond lengths [Å]: Co1–N4 2.1969(19), Co1–N12 2.1458(18), Co1–Cl1 2.4164(6), C1–N1 1.336(3), C1–N4 1.321(3), N1–C2 1.467(3), C2–C3 1.523(3), C3–N5 1.472(3), C4–N5 1.338(3), C4–N8 1.313(3), C5–N12 1.325(3), C5–N9 1.331(3), N9–C6 1.467(3). Selected bond angles [°]: N12–Co1–N4 92.95(7), N12–Co1–Cl1 91.42(5), N4–Co1–Cl1 92.70(5), N11–N12–Co1 125.45(14), N3–N4–Co1 128.90(14), N12–C5–N9 108.2(2), N4–C1–N1 108.6(2), C1–N1–C2 130.5(2), C5–N9–C6 128.8(2). Selected torsion angles [°]: Cl1–Co1–N12–N11 –68.62(17), Cl1–Co1–N4–N3 22.34(18), C1–N1–N2–N3 0.1(2), N1–N2–N3–N4 –0.1(2), N11–N10–N9–C5 0.1(2), N9–N10–N11–N12 0.1(3), N5–C3–C2–N1 –80.0(3), N9–C6–C6ⁱⁱ–N9ⁱⁱ –180.0(2). Symmetry codes: i: $-x, -y, 1-z$; ii: $-1-x, -y, 2-z$.

Table 1. Selected bond lengths [Å] and angles [°] of $[\text{CoCl}_2(\mu\text{-dte})(\text{dte})_2]_n$ and literature known $[\text{Co}(\text{SCN})_2(\mu\text{-dte})(\text{dte})_2]_n$.^[8e]

	X = Cl ⁻ [a]	X = SCN ⁻ [8c][a]
Co1–N4	2.1969(19)	2.165(2)
Co1–N12	2.1458(18)	2.195(2)
Co1–X1	2.4164(6)	2.060(2)
C1–N4	1.321(3)	1.304(3)
C4–N8	1.313(3)	1.299(4)
C5–N12	1.325(3)	1.309(3)
N12–Co1–N4	92.95(7)	87.43(7)
N12–Co1–X1	91.42(5)	92.12(7)
N4–Co1–X1	92.70(5)	89.29(7)

[a] X-ray diffraction measurement temperature was 173 K for $[\text{CoCl}_2(\mu\text{-dte})(\text{dte})_2]_n$. [b] X-ray diffraction measurement temperature was 293 K for $[\text{Co}(\text{SCN})_2(\mu\text{-dte})(\text{dte})_2]_n$.

It is noticeable for the thiocyanate complex that the Co–N bond of the *anti*-oriented dte is longer than the *gauche*-oriented in difference to the chloride complex **2**. The N–Co–N and N–Co–X angles are also deviating from each other which might be caused by the different anions.

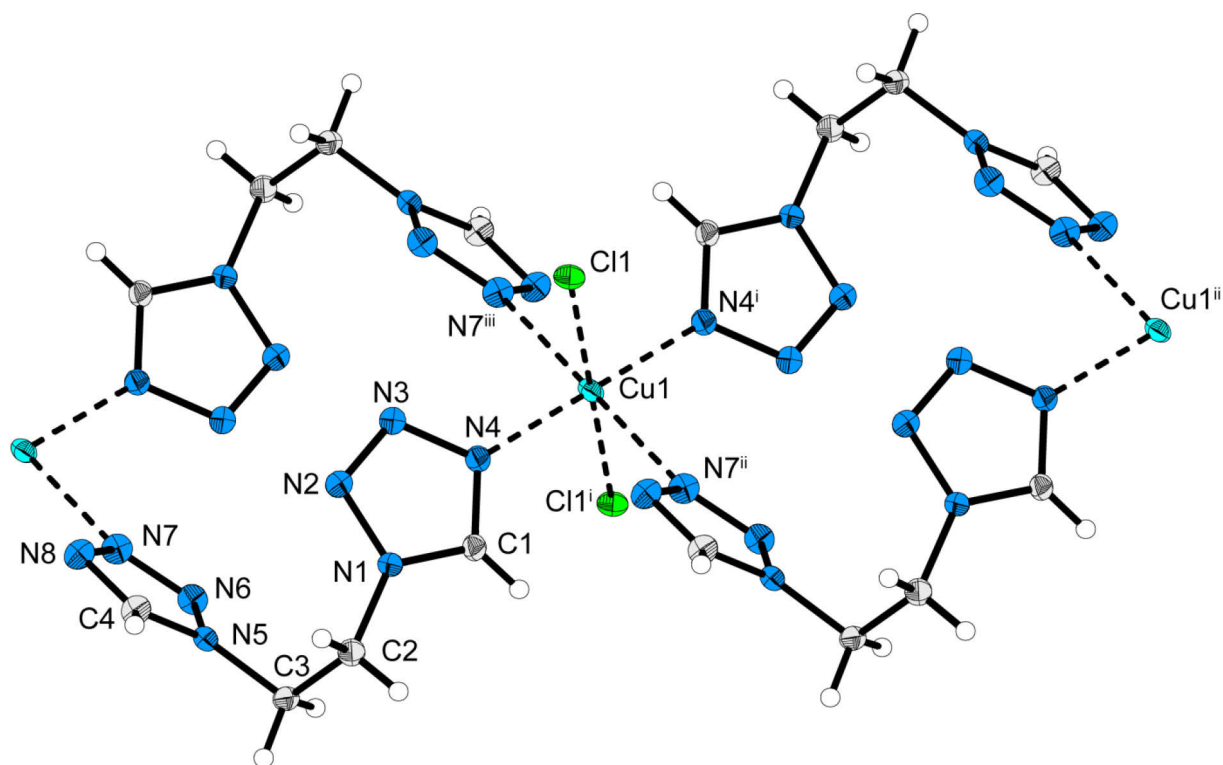


Figure 2. Coordination sphere of $[\text{CuCl}_2(\mu\text{-dte})_2]_n$ (**3**). Thermal ellipsoids of non-hydrogen atoms are drawn at the 50 % probability level. Selected bond lengths [Å]: Cu1–N4 2.0069(16), Cu1–N7ⁱⁱ 2.5771(18), Cu1–Cl1 2.2998(5), C1–N1 1.330(3), C1–N4 1.316(3), N1–C2 1.464(3), C2–C3 1.521(3), C3–N5 1.462(3), C4–N5 1.337(2), C4–N8 1.313(3). Selected bond angles [°]: N4–Cu1–Cl1 89.97(5), N4–Cu1–N7ⁱⁱ 85.640(57), Cl1–Cu1–N7ⁱⁱ 89.505(42), N3–N4–Cu1 126.66(12), Cu1–N7ⁱⁱ–N8ⁱⁱ 115.96(12), C1–N1–N2 108.35(17), C1–N1–C2 129.47(18), N1–C2–C3 111.66(17), C4–N5–C3 129.84(17), C4–N5–N6 108.05(16). Selected torsion angles [°]: Cl1–Cu1–N4–N3 46.24(16), Cu1–N4–C1–N1 173.60(13), N4–C1–N1–N2 0.7(2), C1–N1–N2–C2 178.09(25), N1–C2–C3–N5 –61.90(21), C4–N5–N6–C3 178.17(25), N7–N8–C4–N5 –0.3(2). Symmetry codes: i: 1–x, –y, 1–z; ii: 1+x, y, z; iii: –x, –y, 1–z.

The copper(II) complex **3** crystallizes in the monoclinic space group $P2_1/n$ with two formula units per unit cell and a calculated density of 1.832 g cm^{-3} at 173 K. The complex exhibits a Jahn-Teller distorted octahedral coordination sphere (Figure 2). The axial Cu1–N7 bond is strongly elongated [$d(\text{Cu1–N7}^{\text{ii}}) = 2.5771(18) \text{ Å}$; symmetry code: ii: 1+x, y, z] in comparison to the equatorial bonds [$d(\text{Cu1–N4}) = 2.0069(16) \text{ Å}$ and $d(\text{Cu1–Cl1}) = 2.2998(5) \text{ Å}$]. However, the axial Cu–N bond is still in the range of literature known Cu–N bonds of Jahn-Teller distorted complexes.^[11] The bond angles are near 90° with N4–Cu1–Cl1 = $89.97(5)^\circ$ and Cl1–Cu1–N7ⁱⁱ = $89.505(42)^\circ$. The N4–Cu1–N7ⁱⁱ angle is however deviating from 90° with $85.640(57)^\circ$, which might be a result of the unusual coordination of the second tetrazole ring to the central copper atom over the nitrogen atom N7 and not as expected via N8. Contrary to the literature known $[\text{Cu}(\mu\text{-Cl})_2(\mu\text{-dtb})]_n$ complex,^[8g] the chlorido ligands of **3** are terminal and not μ -bridging. Further, the literature complex exhibits an *anti*-oriented dtb which coordinates over the N4,N4' position. In complex **3**, the μ -dte ligand shows a *gauche* conformation [$\text{N1–C2–C3–N5} = -61.90(21)^\circ$]. Thus, one-dimensional chains are formed and not a three-dimensional network.

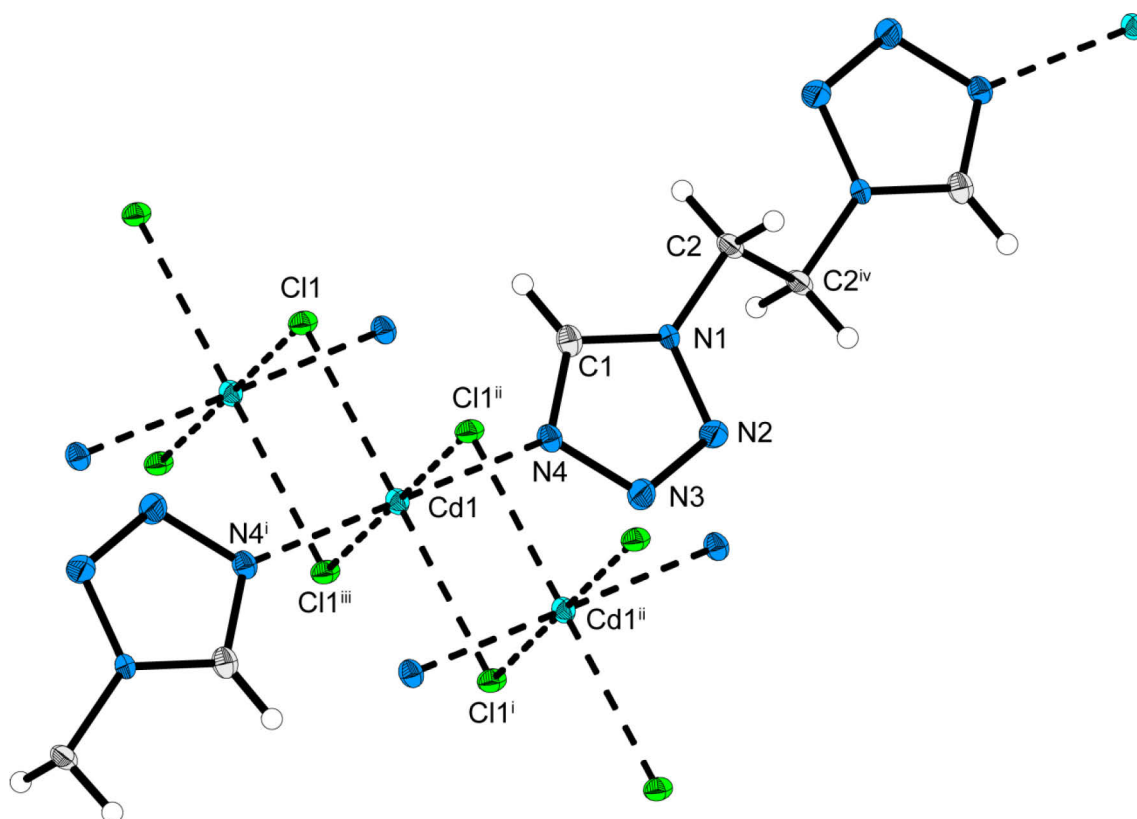


Figure 3. Coordination sphere of $[\text{Cd}(\mu\text{-Cl})_2(\mu\text{-dte})]_n$ (**4**). Thermal ellipsoids of non-hydrogen atoms are drawn at the 50 % probability level. Selected bond lengths [Å]: Cd1–N4 2.328(3), Cd1–Cl1 2.6545(10), Cd1–Cl1ⁱⁱ 2.6734(11), C1–N1 1.329(6), C1–N4 1.323(6), N1–C2 1.466(5). Selected bond angles [°]: N4–Cd1–Cl1 87.33(9), Cl1–Cd1–Cl1ⁱⁱ 96.684(35), N3–N4–Cd1 125.4(3), C1–N1–N2 108.4(4), C1–N4–N3 106.4(3), C1–N1–C2 129.4(4). Selected torsion angles [°]: Cl1–Cd1–N4–N3 –173.3(3), Cd1–N4–C1–N1 175.0(3), N4–C1–N1–N2 –0.9(5), C1–N1–N2–N3 0.7(5), C1–N1–N2–C2 –175.730(584), N1–C1–C2^{iv}–N1^{iv} 180.000(351). Symmetry codes: i: $-x, -y, -z$; ii: $-1+x, y, z$; iii: $1-x, -y, -z$; iv: $-x, 1-y, 1-z$.

The cadmium(II) complex **4** crystallizes in the triclinic space group $P\bar{1}$ with one formula unit per unit cell and a calculated density of 2.406 g cm^{-3} at 173 K. The central cadmium atom is surrounded by two tetrazole rings of the $\mu\text{-dte}$ ligand and four $\mu\text{-chlorido}$ ligands. Complex **4** exhibits an octahedral coordination sphere (Figure 3). The Cd–N [$d(\text{Cd1-N4}) = 2.328(3) \text{ \AA}$] and Cd–Cl [$d(\text{Cd1-Cl1}) = 2.6545(10) \text{ \AA}$ and $d(\text{Cd1-Cl1}^{\text{ii}}) = 2.6734(11) \text{ \AA}$; symmetry code: ii: $-1+x, y, z$] bonds are in a typical range for octahedral cadmium(II) complexes with chlorido and tetrazole-derivates as ligands.^[12] Two $\mu\text{-chlorido}$ ligands connect two central cadmium(II) atoms to a one-dimensional chain. This chain is further connected between the central cadmium atom via the N4,N4' positions of the *anti*-oriented $\mu\text{-dte}$ ligand [$\text{N1-C1-C2}^{\text{iv}}\text{-N1}^{\text{iv}} = 180.000(351)^\circ$] to a two-dimensional network. The structure can be compared with the literature known pseudohalogenide complex $[\text{Cd}(\mu\text{-SCN})_2(\mu\text{-dte})]_n$, which crystallizes in the monoclinic space group $P2_1/n$ (Table 2).^[8g]

Table 2. Selected bond lengths [\AA] and angles [$^\circ$] of $[\text{Cd}(\mu\text{-Cl}_2(\mu\text{-dte}))_n]$ and literature known $[\text{Cd}(\mu\text{-SCN})_2(\mu\text{-dte})]_n$.^[8g]

	$X = \text{Cl}^-$	$X = \text{SCN}^-$ ^{[8g][b]}
Cd1–N4	2.328(3)	2.4078(12)
Cd1–Cl1	2.6545(10)	–
Cd1–Cl1 ⁱⁱ	2.6734(11)	–
Cd1–N5	–	2.2706(11)
Cd1–S1 ⁱ	–	2.7048(3)
C1–N4	1.323(6)	1.3211(16)
N1–C2	1.466(5)	1.4651(16)
N4–Cd1–Cl1	87.33(9)	–
N4–Cd1–N5	–	89.36(4)
Cl1–Cd1–Cl1 ⁱⁱ	96.684(35)	–
N5–Cd1–S1 ⁱ	–	89.43(3)

[a] X-ray diffraction measurement temperature was 173 K for $[\text{Cd}(\mu\text{-Cl}_2(\mu\text{-dte}))_n]$. [b] X-ray diffraction measurement temperature was 100 K for $[\text{Cd}(\mu\text{-SCN})_2(\mu\text{-dte})]_n$; symmetry codes: i: $x, -1+y, z$; ii: $-1+x, y, z$.

Due to the different anion sizes, the distance between two connected cadmium atoms is with a value of 3.9806(5) \AA shorter for the chlorido complex **4** than for the thiocyanate compound which exhibits a value of 5.5553(3) \AA .

Infrared spectroscopy: IR spectra were recorded for the ligand **1** and all three metal complexes **2–4** and are shown in Figure 4.

Characteristic IR vibrations can be assigned for the free ligand **1** according to literature:^[13] a medium C–H valence vibration of the tetrazole ring at 3119 cm^{-1} , the very weak asymmetric and symmetric C–H valence vibration of the alkyl CH_2 group at 3025 and 2977 cm^{-1} , a $\text{N}=\text{N} + \text{C}_{\text{alkyl}}\text{-N}$ valence vibration at 1480 cm^{-1} , the asymmetric and symmetric deformation vibration of the CH_2 group at 1443 and 1428 cm^{-1} , $\text{C}_{\text{alkyl}}\text{-N}$ valence vibration at 1324 cm^{-1} , ring deformation vibration at 1253 cm^{-1} , a very strong C=N and N–N valence vibration at 1169 cm^{-1} and the C–C valence vibration at 1092 cm^{-1} . Further valence $\nu(\text{N-N})$ and deformation $\delta+\gamma(\text{ring}) + \gamma(\text{CH})$ vibrations are observed below 1050 cm^{-1} .

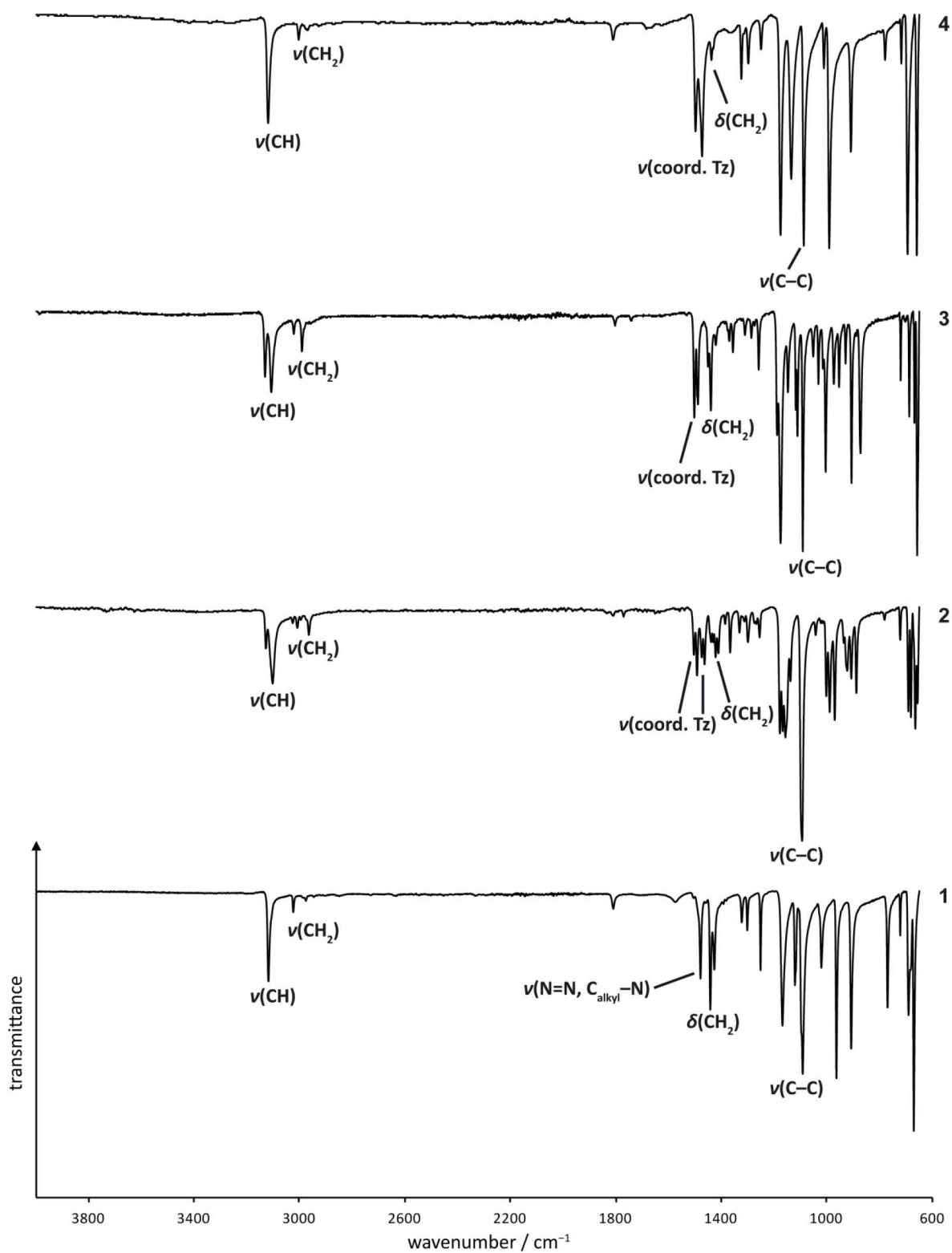


Figure 4. IR spectra of compounds 1–4.

The spectrum of the coordination compound **4**, which only exhibits an *anti*-oriented μ -dte ligand is similar to that of the free and also *anti*-oriented dte. The valence C–H vibration of the tetrazole is nearly identical [$\nu(\text{CH}) = 3121 \text{ cm}^{-1}$]. However, many vibrations are slightly shifted due to coordination e.g. $\delta(\text{CH}_2) = 1443 \text{ and } 1428 \text{ cm}^{-1} \rightarrow 1439 \text{ and } 1432 \text{ cm}^{-1}$, or $\nu(\text{C}=\text{N}, \text{N}-\text{N}) = 1169 \text{ cm}^{-1} \rightarrow 1176 \text{ cm}^{-1}$. Instead of the valence vibration $\nu(\text{N}=\text{N} + \text{C}_{\text{alkyl}}-\text{N})$ of the free ligand at 1480 cm^{-1} , two combined bond stretching vibrations characteristic for coordinated tetrazoles are observed at $1499 \text{ and } 1474 \text{ cm}^{-1}$.^[8a]

The spectrum of complex **3** shows some more vibration bands than the spectrum of **1** and **4** due to a lower symmetry of the *gauche*-oriented dte ligand. The symmetry is reduced by the different coordination sites of the tetrazole rings ($\kappa^2\text{N}^4, \text{N}^7$). Two instead of one absorption bands can be observed for valence vibration $\nu(\text{C}-\text{H})$ at $3132 \text{ and } 3109 \text{ cm}^{-1}$ or for $\nu(\text{C}=\text{N}, \text{N}-\text{N})$ at $1176 \text{ and } 1190 \text{ cm}^{-1}$.

The infrared spectrum of complex **2** is even more complicated owing to two different types of dte ligands. Two ligands are terminal and in a *gauche* conformation and the other one is μ -bridging and *anti*. This is represented in the infrared spectrum by nearly a double number of absorption bands compared to **1** and **4**. Exemplary, the following vibrations are listed: (i) $\nu(\text{C}-\text{H})$ at $3129 \text{ and } 3104 \text{ cm}^{-1}$; (ii) $\nu(\text{CH}_2)$ at $3027, 3010, 2996, \text{ and } 2966 \text{ cm}^{-1}$; (iii) $\nu(\text{coordinated tetrazole})$ $1505, 1493, 1476, \text{ and } 1465 \text{ cm}^{-1}$; (iv): $\delta(\text{CH}_2)$ at $1440, 1432, 1423, \text{ and } 1412$; (v) $\nu(\text{C}=\text{N}, \text{N}-\text{N})$ at $1179, 1168, \text{ and } 1158 \text{ cm}^{-1}$.

However, the C–C valence vibration of the CH_2-CH_2 group is for all complexes **2–4** only slightly affected by the different coordination modes of the tetrazoles [$\nu(\text{C}-\text{C})$ at 1095 cm^{-1} for **2**, at 1092 cm^{-1} for **3** and at 1088 cm^{-1} for **4**].

Finally it can be said, that the infrared spectroscopy data fits to the X-ray structures.

7.4. Conclusions

The nitrogen-rich heterocycle 1,2-di(1*H*-tetrazol-1-yl)ethane (**1**) was synthesized according to standard procedures in a high purity and a good yield of 66 %.^[9] Owing to the fact that no chlorido complexes with **1** as ligand were known, three polynuclear metal(II) chlorido complexes with dte as ligand, $[\text{CoCl}_2(\mu\text{-dte})(\text{dte})_2]_n$ (**2**), $[\text{CuCl}_2(\mu\text{-dte})_2]_n$ (**3**), and $[\text{Cd}(\mu\text{-Cl})_2(\mu\text{-dte})]_n$ (**4**), were prepared and characterized via infrared spectroscopy, elemental analysis, and single-crystal X-ray diffraction. Both ligands (dte and Cl^-) were able to coordinate in a terminal or a μ -bridging mode. Thus, one-dimensional chains were obtained for **2** and **3**, whereas **4** formed a two-dimensional network. The crystal structures of the chlorides **2** and **4** were further compared with the corresponding literature known thiocyanates.^[8e,8g] The halogenides and pseudohalogenides showed similar structures as it was expected.

7.5. Experimental Section

Caution! The ligand 1,2-di(1*H*-tetrazol-1-yl)ethane and all of the metal(II) complexes prepared herein are energetic materials, which are partly sensitive towards various stimuli. Although no problems were encountered during preparation and characterization of these compounds, proper protective measures (safety glasses, face shield, leather coat, earthed equipment, conductive floor and shoes, Kevlar gloves, and ear plugs) should be used when handling these compounds.

General Methods: All chemicals were used as supplied by ABCR, Acros Organics, AppliChem, Fluka, Sigma-Aldrich, and VWR. The impact and friction sensitivity tests were performed according to standard methods by using a BAM (Bundesanstalt für Materialforschung und -prüfung) drop hammer and a BAM friction tester.^[14] The sensitivity toward electrostatic discharge was tested by using an OZM Research electric spark tester ESD 2010 EN.^[15] Decomposition temperatures were measured by differential thermal analysis (DTA) with an OZM Research DTA 552-Ex instrument at a heating rate of 5 °C min⁻¹ and in a range of room temperature to 400 °C.^[15,16] The crystal structures were determined with an Oxford Diffraction Xcalibur 3 diffractometer with a Sapphire CCD detector, four circle kappa platform, Enhance molybdenum K_α radiation source ($\lambda = 71.073$ pm) and Oxford Cryosystems Cryostream cooling unit.^[17] Data collection and reduction were performed with the CrysAlisPro software.^[18] The structures were solved with SIR97.^[19] The refinement was performed with SHELXL-97.^[20] The CIF-files were checked at the checkCIF website.^[21] The non-hydrogen atoms were refined anisotropically and the hydrogen atoms isotropically if not calculated. Crystallographic data and structure refinement results are summarized in Table 3. The determination of the carbon, hydrogen, and nitrogen contents was carried out by combustion analysis with an Elementar Vario EL.^[22] Infrared (IR) spectra were recorded with a Perkin-Elmer BXII FT-IR system with a Smith DuraSamplIR II diamond ATR unit.^[23] ¹H and ¹³C NMR spectra were recorded with a JEOL Eclipse 270 spectrometer.^[24]

Table 3. X-ray data of complexes 2–4.

	2	3	4
Formula	C ₁₂ H ₁₈ Cl ₂ CoN ₂₄	C ₈ H ₁₂ Cl ₂ CuN ₁₆	C ₄ H ₆ CdCl ₂ N ₈
$M_r / \text{g mol}^{-1}$	628.33	466.78	349.47
Color	purple	blue	colorless
Habit	block	plate	plate
Crystal size / mm	0.11 × 0.08 × 0.06	0.2 × 0.2 × 0.1	0.17 × 0.10 × 0.05
Crystal system	triclinic	monoclinic	triclinic
Space group	$P\bar{1}$	$P2_1/n$	$P\bar{1}$
$a / \text{Å}$	6.8815(4)	8.3838(3)	3.9806(5)
$b / \text{Å}$	9.3593(7)	6.6051	6.5577(8)
$c / \text{Å}$	9.5343(6)	15.2829(5)	9.5195(11)
$\alpha / ^\circ$	101.107	90	79.127(10)
$\beta / ^\circ$	94.051	90.847(3)	84.383(10)
$\gamma / ^\circ$	101.228	90	82.272(10)
$V / \text{Å}^3$	587.29(7)	846.21(5)	241.14(5)
Z	1	2	1
$\rho_{\text{calc.}} / \text{g cm}^{-3}$	1.777	1.832	2.406
T / K	173	173	173
$\lambda (\text{Mo K}\alpha) / \text{Å}$	0.71073	0.71073	0.71073
$F(000)$	319	470	168
μ / mm^{-1}	1.02	1.64	2.80
θ range / °	4.2–27.0	4.1–26.0	4.2–25.2
Dataset ($h; k; l$)	$-8 \leq h \leq 6$ $-10 \leq k \leq 11$ $-12 \leq l \leq 11$	$-10 \leq h \leq 10$ $-7 \leq k \leq 8$ $-18 \leq l \leq 16$	$-4 \leq h \leq 4$ $-7 \leq k \leq 7$ $-11 \leq l \leq 11$
Measured reflections	3299	4219	2302
Independent reflections	2527	1650	875
Observed reflections	2146	1487	811
R_{int}	0.021	0.026	0.048
Parameters	214	148	82
Restraints	0	0	0
R_1 (obs.)	0.035	0.025	0.030
wR_2 (all data)	0.086	0.062	0.061
S	1.05	1.11	0.99
Resd. dens. / e Å ⁻³	–0.39; 0.37	–0.31; 0.29	–0.64; 1.36
Solution	SIR97	SIR97	SIR97
Refinement	SHELXL-97	SHELXL-97	SHELXL-97
Absorption correction	multi-scan	multi-scan	multi-scan
CCDC	891893	891891	898347

1,2-Di(1*H*-tetrazol-1-yl)ethane (1): The ligand **1** was synthesized according to the common method by Kamiya and Saito in a 500 mmol batch.^[9] Yield: 54.7 g (329 mmol, 66 %). DTA (5 °C min⁻¹) onset: 133 °C (melting), 194 °C (decomp.). ¹H NMR (270 MHz, [D6]DMSO, 25 °C, TMS): δ = 9.33 (s, 2 H, N₄CH), 5.04 ppm (s, 4 H, CH₂). ¹³C{¹H} NMR (68 MHz, [D6]DMSO, 25 °C, TMS): δ = 144.3 (N₄CH), 46.9 ppm (CH₂). IR (ATR): $\tilde{\nu}$ = 3119 (m), 3025 (vw), 2977 (vw), 1811 (vw), 1576 (vw), 1506 (vw), 1480 (m), 1460 (vw), 1443 (m), 1428 (m), 1393 (vw), 1383 (vw), 1324 (w), 1303 (w), 1252 (m), 1169 (m), 1122 (m), 1092 (s), 1022 (m), 964 (s), 908 (s), 770 (m), 722 (w), 691 (m), 683 (m), 671 (vs) cm⁻¹. C₄H₆N₈ (166.14 g mol⁻¹): calcd. C 28.92, H 3.64, N 67.44 %; found: C 28.80, H 3.49, N 66.41 %. BAM impact: 40 J; BAM friction 360 N; ESD: 0.75 J (at grain size 100–500 μ m).

Catena-poly[dichlorido(μ -1,2-di(1*H*-tetrazol-1-yl)ethane- κ^2 N⁴,N^{4'})bis(1,2-di(1*H*-tetrazol-1-yl)ethane- κ N⁴)cobalt(II)] (2): To a 70 °C warm solution of **1** (332 mg, 2.00 mmol) in water (20 mL) was added an aqueous solution of cobalt(II) chloride hexahydrate (239 mg, 1.00 mmol). The clear and red colored solution was left for crystallization at room temperature. After one week, X-ray suitable single crystals were obtained in form of purple blocks. The crystals were filtered off and air dried. Yield: 254 mg (0.40 mmol, 60 %). DTA (5 °C min⁻¹) onset: 182 °C (melting), 200 °C (dec.). IR (ATR): $\tilde{\nu}$ = 3129 (w), 3104 (m), 3027 (vw), 3010 (vw), 2996 (vw), 2966 (w), 1811 (vw), 1772 (vw), 1505 (w), 1493 (w), 1476 (w), 1465 (w), 1440 (w), 1432 (w), 1423 (w), 1412 (w), 1386 (vw), 1368 (w), 1332 (w), 1314 (vw), 1300 (w), 1276 (vw), 1268 (vw), 1256 (w), 1179 (m), 1168 (m), 1158 (m), 1139 (m), 1095 (vs), 1043 (w), 1023 (vw), 1015 (vw), 1003 (m), 990 (m), 971 (m), 936 (w), 924 (w), 908 (m), 889 (m), 722 (w), 691 (m), 682 (m), 665 (m), 657 (m) cm⁻¹. C₁₂H₁₆Cl₂CoN₂₄ (628.27 g mol⁻¹): calcd. C 22.94, H 2.89, N 53.51 %; found: C 22.97, H 2.74, N 52.94 %. BAM impact: 6 J; BAM friction: 360 N; ESD: 1.50 J (at grain size 100–500 μ m).

Catena-poly[dichloridodi(μ -1,2-di(1*H*-tetrazol-1-yl)ethane- κ^2 N⁴,N⁷)copper(II)] (3): To a 70 °C warm solution of **1** (332 mg, 2.00 mmol) in water (20 mL) was added an aqueous solution of copper(II) chloride dihydrate (170 mg, 1.00 mmol). The clear and blue colored solution was left for crystallization at room temperature. After one week, X-ray suitable single crystals were obtained. The blue plates were filtered off and dried in air. Yield: 360 mg (0.77 mmol, 77 %). DTA (5 °C min⁻¹) onset: 151 °C (melting), 195 °C (dec.). IR (ATR): $\tilde{\nu}$ = 3132 (w), 3109 (m), 3023 (vw), 2992 (w), 1804 (vw), 1743 (vw), 1504 (m), 1490 (m), 1451 (w), 1441 (m), 1422 (w), 1371 (w), 1357 (w), 1311 (vw), 1287 (w), 1275 (vw), 1259 (w), 1190 (m), 1176 (vs), 1148 (m), 1119 (m), 1112 (m), 1092 (vs), 1052 (w), 1033 (w), 1015 (w), 1005 (s), 974 (w), 954 (m), 907 (s), 890 (w), 873 (m), 721 (w), 703 (vw), 688 (m), 668 (m), 658 (vs) cm⁻¹. C₈H₁₂Cl₂CuN₁₆ (466.74 g mol⁻¹): calcd. C 20.59, H 2.59, N 48.02 %; found: C 20.59, H 2.50, N 47.33 %. BAM impact: 10 J; BAM friction: 324 N; ESD: 1.00 J (at grain size 500–1000 μ m).

Phyllo-poly[di(μ -chlorido)(μ -1,2-di(1*H*-tetrazol-1-yl)ethane- κ^2N^4,N^4)cadmium(II)] (4):

To a 70 °C warm solution of **1** (166 mg, 1.00 mmol) in water (20 mL) was added an aqueous solution of cadmium(II) chloride hemi-pentahydrate (228 mg, 1.00 mmol). The clear and colorless solution was left for crystallization at room temperature. After one week, X-ray suitable single crystals were obtained. The colorless prisms were filtered off and air dried. Yield: 310 mg (0.89 mmol, 89 %). DTA (5 °C min⁻¹) onset: 184 °C (dec.). IR (ATR): $\tilde{\nu}$ = 3121 (m), 3004 (w), 2972 (vw), 1812 (w), 1499 (m), 1474 (m), 1439 (w), 1432 (w), 1325 (w), 1299 (w), 1250 (w), 1176 (vs), 1136 (s), 1088 (vs), 1012 (w), 992 (vs), 910 (m), 780 (w), 718 (w), 694 (vs), 660 (vs) cm⁻¹. C₄H₆Cl₂CdN₈ (349.46 g mol⁻¹): calcd. C 13.75, H 1.73, N 32.06 %; found: C 13.84, H 1.71, N 31.73 %. BAM impact: 40 J; BAM friction: 360 N; ESD: 1.00 J (at grain size 500–1000 μ m).

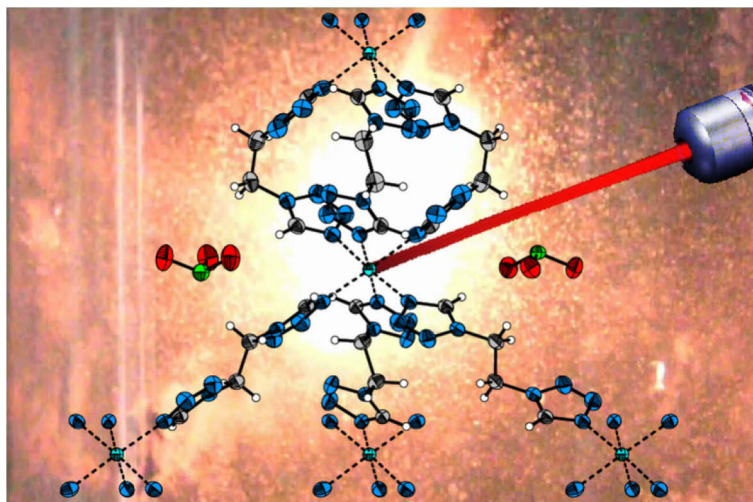
7.6. References

- [1] D. Steinborn, *Grundlagen der metallorganischen Komplexkatalyse*, 2nd ed., Vieweg+Teubner, Wiesbaden, **2010**.
- [2] S. J. Lippard, J. M. Berg, *Principles of Bioinorganic Chemistry*, 1st ed., University Science Books, Mill Valley, **1994**.
- [3] J.-M. Lehn, *Supramolecular Chemistry*, 1st ed., Wiley-VCH, Weinheim, **1995**.
- [4] O. Kahn, *Molecular Magnetism*, 1st ed., Wiley-VCH, Weinheim, New York, **1993**.
- [5] Q. Zhang, J. M. Shreeve, *Angew. Chem. Int. Ed.* **2014**, *53*, 2540–2542.
- [6] D. Farruseng, *Metal-Organic Frameworks: Applications from Catalysis to Gas Storage*, 1st ed., Wiley-VCH, Weinheim, **2011**.
- [7] a) K. P. J. van, Y. Garcia, O. Kahn, L. Fournes, H. Kooijman, A. L. Spek, J. G. Haasnoot, J. Moscovici, K. Provost, A. Michalowicz, F. Renz, P. Guetlich, *Inorg. Chem.* **2000**, *39*, 1891–1900; b) Y. Carcia, P. J. van Koningsbruggen, H. Kooijman, A. L. Spek, J. G. Haasnoot, O. Kahn, *Eur. J. Inorg. Chem.* **2000**, 307–314; c) P. J. van Koningsbruggen, Y. Garcia, G. Bravic, D. Chasseau, O. Kahn, *Inorg. Chim. Acta* **2001**, *326*, 101–105; d) P. J. van Koningsbruggen, Y. Garcia, H. Kooijman, A. L. Spek, J. G. Haasnoot, O. Kahn, J. Linares, E. Coddjovi, F. Varret, *J. Chem. Soc. Dalton Trans.* **2001**, 466–471.
- [8] a) J. Schweifer, P. Weinberger, K. Mereiter, M. Boca, C. Reichl, G. Wiesinger, G. Hilscher, P. J. van Koningsbruggen, H. Kooijman, M. Grunert, W. Linert, *Inorg. Chim. Acta* **2002**, *339*, 297–306; b) R.-Y. Li, X.-Y. Wang, T. Liu, H.-B. Xu, F. Zhao, Z.-M. Wang, S. Gao, *Inorg. Chem.* **2008**, *47*, 8134–8142; c) R.-Y. Li, B.-W. Wang, X.-Y. Wang, X.-T. Wang, Z.-M. Wang, S. Gao, *Inorg. Chem.* **2009**, *48*, 7174–7180; d) P.-P. Liu, A.-L. Cheng, N. Liu, W.-W. Sun, E.-Q. Gao, *Chem. Mater.* **2007**, *19*, 2724–2726; e) P.-P. Liu, A.-L. Cheng, Q. Yue, N. Liu, W.-W. Sun, E.-Q. Gao, *Cryst. Growth Des.* **2008**, *8*, 1668–1674; f) P.-P. Liu, Y.-Q. Wang, C.-Y. Tian, H.-Q.

- Peng, E.-Q. Gao, *J. Mol. Struct.* **2009**, *920*, 459–465; g) J.-H. Yu, K. Mereiter, N. Hassan, C. Feldgitscher, W. Linert, *Cryst. Growth Des.* **2008**, *8*, 1535–1540.
- [9] T. Kamiya, Y. Saito, *DE 2147023*, March 29, **1973**.
- [10] K. Karaghiosoff, T. M. Klapötke, C. M. Sabate, *Chem. Eur. J.* **2009**, *15*, 1164–1176.
- [11] a) J.-B. Tommasino, G. Chastanet, B. Le Guennic, V. Robert, G. Pilet, *New J. Chem.* **2012**, *36*, 2228–2235; b) O. Reckeweg, A. Schulz, F. J. DiSalvo, *Z. Naturforsch.* **2013**, *68b*, 296–300.
- [12] Y.-L. Yao, L. Xue, Y.-X. Che, J.-M. Zheng, *Cryst. Growth Des.* **2009**, *9*, 606–610.
- [13] a) C. M. Grunert, P. Weinberger, J. Schweifer, C. Hampel, A. F. Stassen, K. Mereiter, W. Linert, *J. Mol. Struct.* **2004**, *687-708*, 41–52; b) M. Hesse, H. Meier, B. Zeeh, *Spektroskopische Methoden der organischen Chemie*, 7th ed., Thieme, Stuttgart, New York, **2005**.
- [14] a) NATO Standardization Agreement 4489, September 17, **1999**; b) NATO Standardization Agreement 4487, October 29, **2009**.
- [15] <http://www.ozm.cz> (accessed March 13, **2014**).
- [16] NATO Standardization Agreement 4515, August 23, **2002**.
- [17] <http://www.agilent.com/> (accessed March 13, **2014**).
- [18] *CrysAlisPro 1.171.35.11*, Oxford Diffraction Ltd., Abingdon, UK, **2011**.
- [19] A. Altomare, M. C. Burla, M. Camalli, G. L. Cascarano, C. Giacovazzo, A. Guagliardi, A. G. G. Moliterni, G. Polidori, R. Spagna, *J. Appl. Crystallogr.* **1999**, *32*, 115–119.
- [20] G. M. Sheldrick, *Acta Crystallogr., Sect. A* **2008**, *64*, 112–122.
- [21] <http://journals.iucr.org/services/cif/checkcif.html> (accessed March 24, **2014**).
- [22] <http://www.elementar.de/> (accessed March 13, **2014**).
- [23] <http://www.perkinelmer.de/> (accessed March 13, **2014**).
- [24] <http://www.jeol.co.jp/en/> (accessed April 2, **2014**).

8. Investigations Concerning the Laser Ignition and Initiation of Various Metal(II) Complexes with 1,2-Di(1*H*-tetrazol-1-yl)ethane as Ligand and a Large Set of Anions

Unpublished work.



8.1. Abstract

The preparation of metal(II) complexes with 1,2-di(1*H*-tetrazol-1-yl)ethane (dte, **1**) as ligand and their behavior toward laser irradiation is presented. Iron (**2**), cobalt (**3**), nickel (**4**), copper (**5**), zinc (**6**), and cadmium (**7**) perchlorate as well as cobalt (**8**), nickel (**9**), copper (**10**), zinc (**11**), and cadmium (**12**) nitrate complexes were synthesized and characterized by IR spectroscopy, UV/Vis/NIR spectroscopy, and elemental analysis. Furthermore, copper(II) coordination compounds with chloride (**13**), chlorate (**14**), nitrite (**15**), dinitramide (**16**), nitrocyanamide (**17** and **18**), nitroformate (**19**), cyanodinitromethanide (**20**), and azide (**21**) as anions were synthesized and characterized. In addition, the crystal structures of **10–12**, **14–17** and **19–20** were determined by single crystal X-ray diffraction. In all cases, compound **1** acts as a μ -bridging ligand. All copper(II) complexes exhibit an octahedral coordination sphere which is in all cases Jahn-Teller distorted except for **10** and **14**. Further, the energetic properties and especially the laser ignitability of the metal(II) complexes were investigated. All metal(II) perchlorate complexes **2–7** and metal(II) nitrate complexes **8–12** had the same stoichiometry. They only differed in their metal(II) center. Thus, a good comparability of the laser ignitability is provided. Additional, **1** as ligand enabled the formation of copper(II) complexes with rather unusual anions like chlorate or nitrite. Thus, a large set of comparable compounds could be investigated. Further, the metal(II) complexes with perchlorate, chlorate, and azide as anions are potential primary explosives with good thermal stabilities.

8.2. Introduction

The development and investigation of energetic materials is of long history and a static performance improvement of explosives, pyrotechnics, and fuels is one of various motivations. Safety and environmental acceptability are other motive forces. Thus, research groups in the whole world pursue these goals and presented many different new and environmental friendly molecules.^[1] Especially in the field of secondary explosives, great efforts are made to develop new energetic materials as replacements for hexogen (RDX), which is produced and applied in large scale. However, it is also very important to find new lead-free primary explosives even though the amount of primary explosive in most applications is commonly low.^[2] For example, many percussion caps still contain lead styphnate (LS), which led to environmental contamination and health hazards due to its heavy metal content.^[3] The solution are green primary explosives which might be found in materials like the potassium salt of 4,6-dinitro-7-hydroxybenzofuroxan (KDNP) as a replacement for lead styphnate (LS) and copper(I) 5-nitrotetrazolate (DBX-1) as a replacement for lead azide (LA).^[4] Another materials class which is suitable for lead-free primary explosives are energetic transition metal complexes with prominent compounds like pentaammine(5-cyano-1*H*-tetrazolate)cobalt(III) perchlorate (CP), tetraammine-*cis*-bis(5-nitro-2*H*-tetrazolato)cobalt(III) perchlorate (BNCP) and various triscarbohydrazidemetal(II) perchlorates ($[M(\text{chz})_3](\text{ClO}_4)_2$ and $M = \text{Co}^{2+}, \text{Ni}^{2+}$ and Zn^{2+}).^[5]

Especially metal-organic frameworks (MOFs) represent a new concept in the development of energetic materials.^[6] However, a part of the presented energetic coordination compounds like trishydrazinecobalt(II) perchlorate (CHP) and trishydrazinenickel(II) perchlorate (NHP) are too sensitive for a commercial use even though they have an energetic performance of secondary explosives. In contrast, trishydrazinenickel(II) nitrate is less sensitive and was already investigated as possible replacement for lead azide.^[7]

But it is not only the improvement of energetic materials which is of interest for researchers in the whole world; there is also a demand for safer initiation methods. Away from classic primary explosives, which are sensitive toward e.g. impact or friction, exploding bridgewire (EBW) and foil initiators (EFI) have been established as non-primary detonators.^[8] However, due to technical reasons electrical type detonators exhibit some disadvantages also in safety.^[9] Thus, alternatives are demanded and laser initiation represents a safer initiation method.

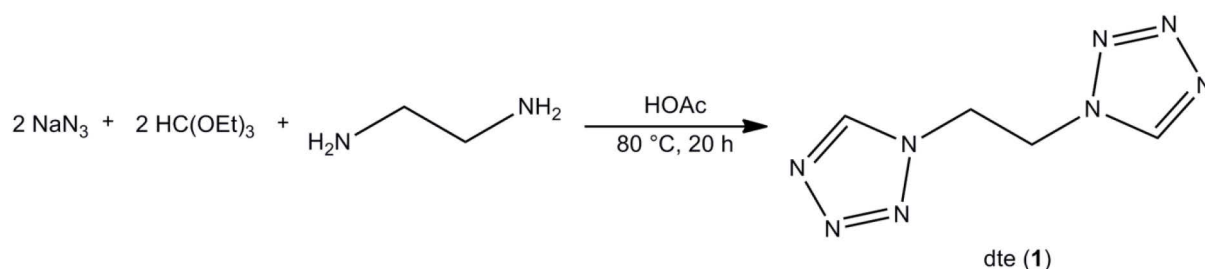
In the late 1960s and early 1970s, the first laser initiation experiments were made by Brish *et al.* as well as Menichelli and Yang.^[10] Common explosives like lead azide (LA), pentaerythritol tetranitrate (PETN), or cyclotrimethylentrinitramine (RDX) were irradiated by Q-Switched neodymium glass and ruby lasers of high power (about 0.5 J and 10 MW).

However, initiation of explosives by neodymium or ruby lasers was of less practical use due to their large size. Firstly the introduction of laser diodes in the 1980s lead to practical applications of laser initiation systems.^[9] At this time, the laser diodes had the disadvantage of low output power implicating slow ignition delay times in the millisecond range. However, for the replacement of fast functioning detonators like the above mentioned EBWs and EFIs, the ignition delay time has to be in the microsecond range.^[9] The use of more powerful laser diodes is one approach to achieve the required ignition times. Another approach is to develop compounds which have a low initiation energy threshold and one class of energetic materials with this property are transition metal complexes with nitrogen-rich ligands and oxidizing anions. Examples are 5-hydrazino-1*H*-tetrazolemercury(II) perchlorate (HMTP) or the bis(3-hydrazino-4-amino-1,2,4-triazole)metal(II) perchlorates (metal = cobalt, nickel, copper, and cadmium) with initiation energies lower than 1 mJ.^[11]

On the basis of the above mentioned coordination compounds and according to the rules for designing energetic coordination compounds,^[12] our research group investigated various metal complexes with ligands like 5-(1-methylhydrazinyl)-1*H*-tetrazole (HMHT), 1,2-bis[5-(1-methylhydrazinyl)-1*H*-tetrazol-1-yl]ethane (BMHTE) and 3-amino-1-nitroguanidine (ANQ) as laser ignitable compounds.^[13] Another good ligand for photosensitive complexes might be 1,2-di(1*H*-tetrazol-1-yl)ethane (dte, **1**). The structures of a few metal(II) complexes (metal = iron, cobalt, nickel, and copper) with dte as ligand and perchlorate and azide as anions were already described in literature as polynuclear coordination compounds.^[14] But to the best of our knowledge, these complexes were not investigated on their energetic properties nor presented as potential primary explosives. In this work, the synthesis, characterization, and laser initiation of literature known and unknown metal(II) complexes with dte as a μ_2 -bridging ligand and a large set of anions, even unusual ones like chlorate or nitrite, is presented. Further, the influence of the metal center and the anion on the laser ignitability was investigated bearing in mind that the initiation mechanism is presumably of thermal nature and the ignition criterion depends on some more parameters like the particle size or the pressed density.

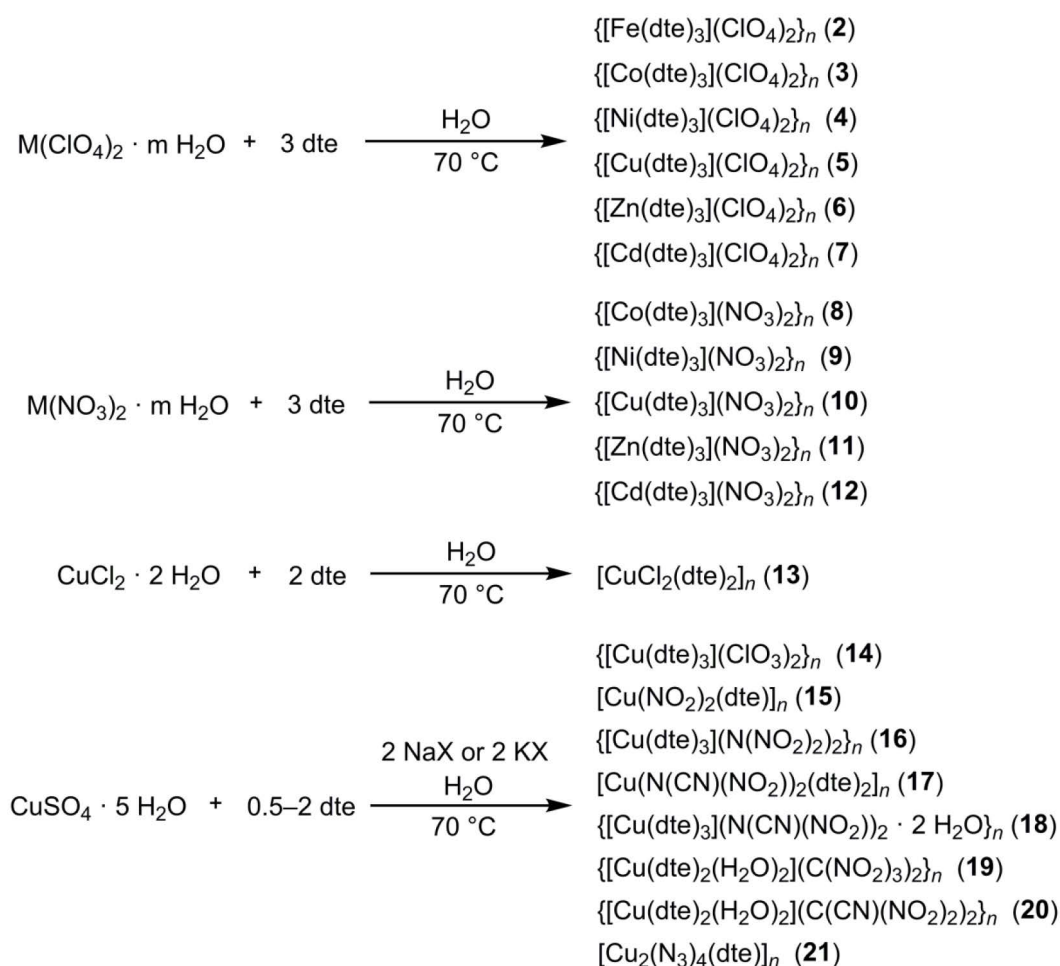
8.3. Results and Discussion

Syntheses: The ligand **1** was synthesized according to the method described by Saito and Kamiya (Scheme 1).^[15] The product was obtained as colorless plates of high purity and in a yield of 66 %.



Scheme 1. Synthesis of dte (1) by the method of Saito and Kamiya.^[15]

Warm aqueous solutions of **1** were combined with concentrated aqueous solutions of the appropriate metal(II) salt (Scheme 2). The resulting solutions were left for crystallization at room temperature. Single crystals suitable for X-ray diffraction were obtained within a few days except for **4**, **8**, **9**, and **13** which precipitated as powders or microcrystalline materials.



Scheme 2. Synthesis of the metal(II) complexes **2–21**.

Crystal structure: X-ray suitable single crystals were obtained directly from the mother liquor. Detailed X-ray data is available in the supporting information (Table S1–S3). The X-ray structures of **3–5**, **13** and **21** are literature known and not presented.^[14a,14b,16]

The bond lengths and angles of the tetrazole rings of the compounds **10–12**, **14–17** and **19–20** are in the typical range of the free ligand and other 1-substituted tetrazoles.^[17] Thus, they are not discussed in detail.

The copper(II) nitrate complex **10** crystallizes as pale blue blocks in the trigonal space group $P\bar{3}$ with one formula unit per unit cell and a calculated density of 1.869 g cm^{-3} at 173 K. The asymmetric unit consists of one-sixth of the sum formula. The copper(II) center is symmetrically surrounded by six tetrazole rings (Figure 1) and not Jahn-Teller distorted. This is in agreement with its symmetrical absorption band (${}^2T_{2g} \leftarrow {}^2E_g$) at 722 nm in the UV/Vis/NIR spectrum of **10** (Figure S2). The Cu1–N4 distance of **10** is with 2.149(2) Å between equatorial (about 2.0 Å) and axial (about 2.4 Å) Cu–N bond lengths of Jahn-Teller distorted complexes.^[14a] All dte ligands are *anti*-oriented ($\langle \text{N1-C2-C2}^i\text{-N1}^i \rangle = 180.0(3)^\circ$; symmetry code: i: $1-x, 1-y, 1-z$) in complex **10** and bridge one copper(II) center to six other. A three-dimensional coordination polymer is formed (Figure S3). In the gaps of this network, the nearly perfect trigonal planar ($\langle \text{O1-N5-O1}^{\text{viii}}\text{-O1}^{\text{ix}} \rangle = -178.5(4)^\circ$; symmetry codes: viii: $1-y, x-y, z$; ix: $1-x-y, 1-x, z$) nitrate anions are placed.

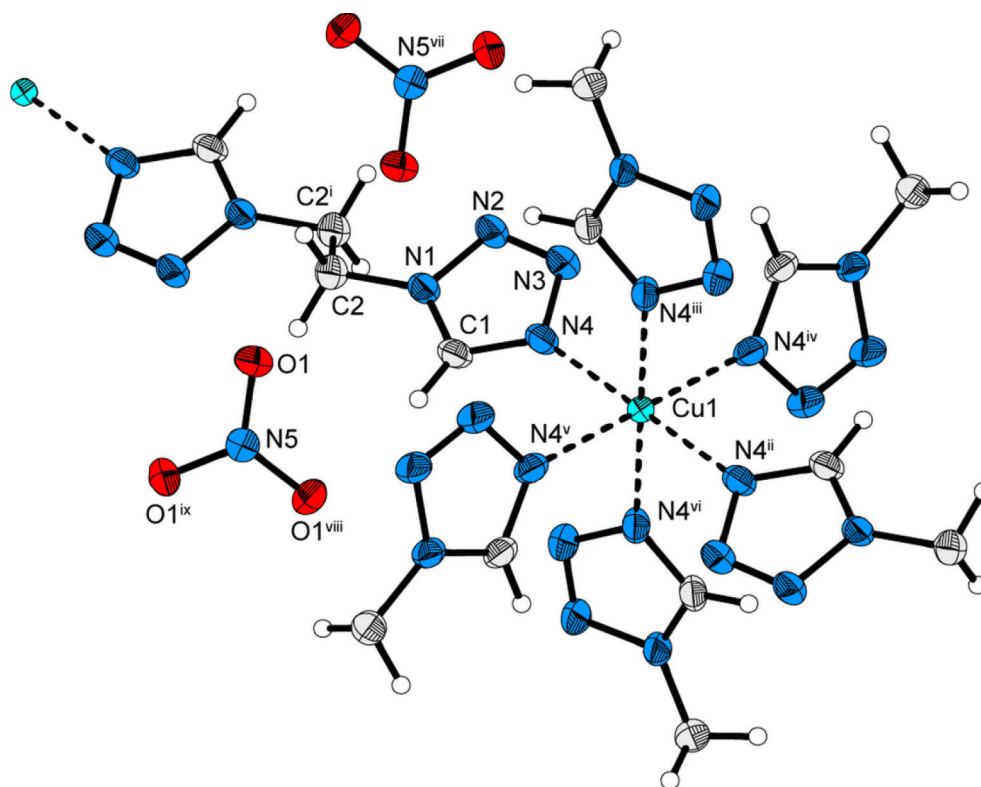


Figure 1. Octahedral coordination sphere of complex **10**. Thermal ellipsoids of non-hydrogen atoms are drawn at the 50 % probability level. Selected bond lengths [Å]: Cu1–N4 2.149(2), O1–N5 1.255(2), N1–C1 1.330(4), N1–N2 1.348(3), N1–C2 1.467(4), N4–C1 1.327(4), N4–N3 1.365(3), N2–N3 1.293(4); selected bond angles [°]: N4–Cu1–N4ⁱⁱ 180.0, N4–Cu1–N4ⁱⁱⁱ 87.7(1), C1–N4–Cu1 132.1(2), C1–N1–N2 108.7(2), C1–N1–C2 129.2(2), N3–N2–N1 107.0(2), O1–N5–O^{viii} 120.0(1); selected torsion angles [°]: N4–Cu1–N4ⁱⁱⁱ–N4^{iv} –92.4(1), N4–N4ⁱⁱⁱ–N4ⁱⁱ–N4^{vi} –0.0(1), Cu1–N4–N3–N2 178.3(2), C1–N1–N2–N3 0.8(3), N1–N2–N3–N4 0.7(3), N1–C2–C2ⁱ–N1ⁱ 180.0(3), O1–N5–O1^{viii}–O1^{ix} –178.5(4). Symmetry codes: i: $1-x, 1-y, 1-z$; ii: $-x, -y, -z$; iii: $x-y, x, -z$; iv: $-y, x-y, z$; v: $y, -x+y, -z$; vi: $-x+y, -x, z$; vii: $1-x, 1-y, -z$; viii: $1-y, x-y, z$; ix: $1-x-y, 1-x, z$.

The zinc(II) nitrate complex **11** crystallizes as colorless blocks in the trigonal space group $P\bar{3}$ with one formula unit per unit cell and a calculated density of 1.855 g cm^{-3} at 173 K. The crystal structure is similar to that of the copper complex **10**. The asymmetric unit consists of one-sixth of the sum formula. The zinc(II) center has an octahedral coordination sphere surrounded by six tetrazole rings with equivalent Zn1–N4 bonds of $2.176(1) \text{ \AA}$ (Figure 2).

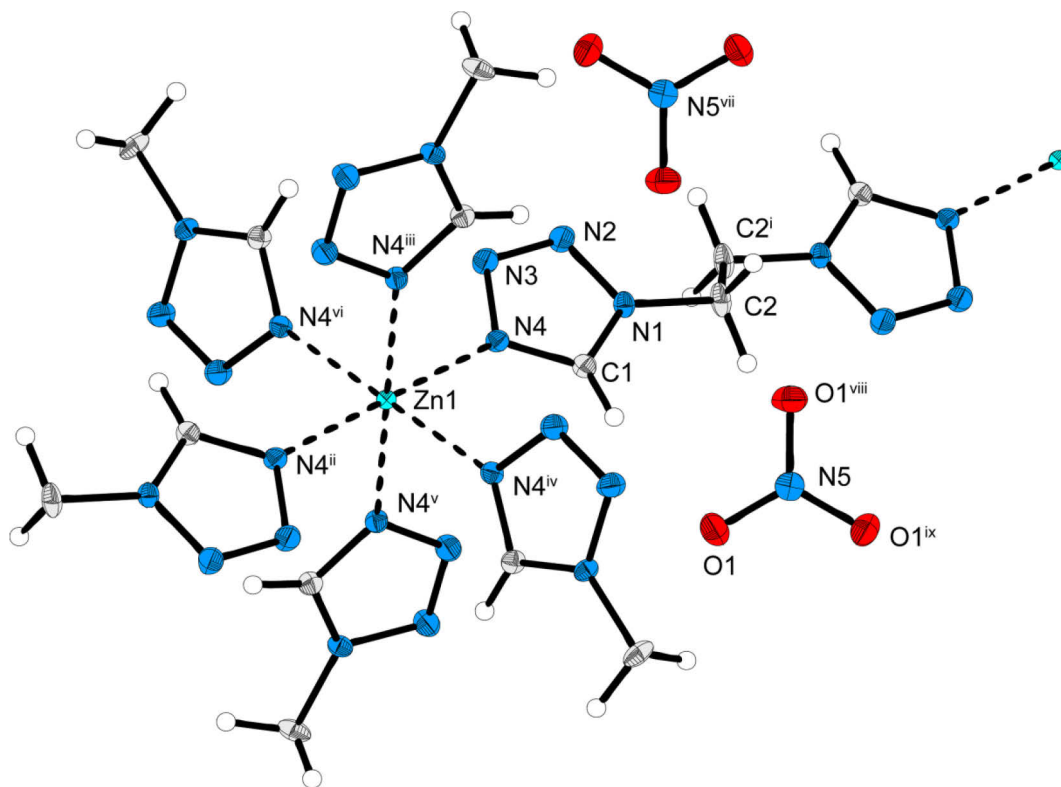


Figure 2. Octahedral coordination sphere of complex **11**. Thermal ellipsoids of non-hydrogen atoms are drawn at the 50 % probability level. Selected bond lengths [\AA]: Zn1–N4 $2.176(1)$, O1–N5 $1.254(1)$, N1–C1 $1.332(2)$, N1–N2 $1.345(1)$, N1–C2 $1.468(2)$, N4–C1 $1.320(2)$, N4–N3 $1.364(1)$, N2–N3 $1.294(2)$; selected bond angles [$^\circ$]: N4–Zn1–N4ⁱⁱ 180.0 , N4–Zn1–N4ⁱⁱⁱ $87.7(0)$, C1–N4–Zn1 $132.2(1)$, C1–N1–N2 $108.7(1)$, C1–N1–C2 $129.2(1)$, N3–N2–N1 $106.9(1)$, O1–N5–O^{viii} $120.0(1)$; selected torsion angles [$^\circ$]: N4–Zn1–N4ⁱⁱⁱ–N4^{iv} $-87.6(0)$, N4–N4ⁱⁱⁱ–N4ⁱⁱ–N4^v $-0.0(0)$, Zn1–N4–N3–N2 $178.1(1)$, C1–N1–N2–N3 $-0.6(1)$, N1–N2–N3–N4 $0.4(1)$, N1–C2–C2ⁱ–N1ⁱ $-180.0(1)$, O1–N5–O1^{viii}–O1^{ix} $-178.3(2)$. Symmetry codes: i: $-x, 1-y, 2-z$; ii: $-x, -y, 1-z$; iii: $-y, -x+y, 1-z$; iv: $x-y, x, 1-z$; v: $-y, x-y, z$; vi: $-x+y, -x, z$; vii: $-x, 1-y, 1-z$; viii: $-y, 1+x-y, z$; ix: $-1-x+y, -x, z$.

The cadmium(II) nitrate complex **12** crystallizes as colorless blocks in the trigonal space group $P\bar{3}$ with one formula unit per unit cell and a calculated density of 1.863 g cm^{-3} at 173 K. The structure is similar to that of **10** and **11**. However, the Cd1–N4 bond ($2.3584(13) \text{ \AA}$) is considerably longer than the corresponding copper ($d(\text{Cu1–N4}) = 2.149(2) \text{ \AA}$) and zinc ($d(\text{Zn1–N4}) = 2.176(1) \text{ \AA}$) bonds.

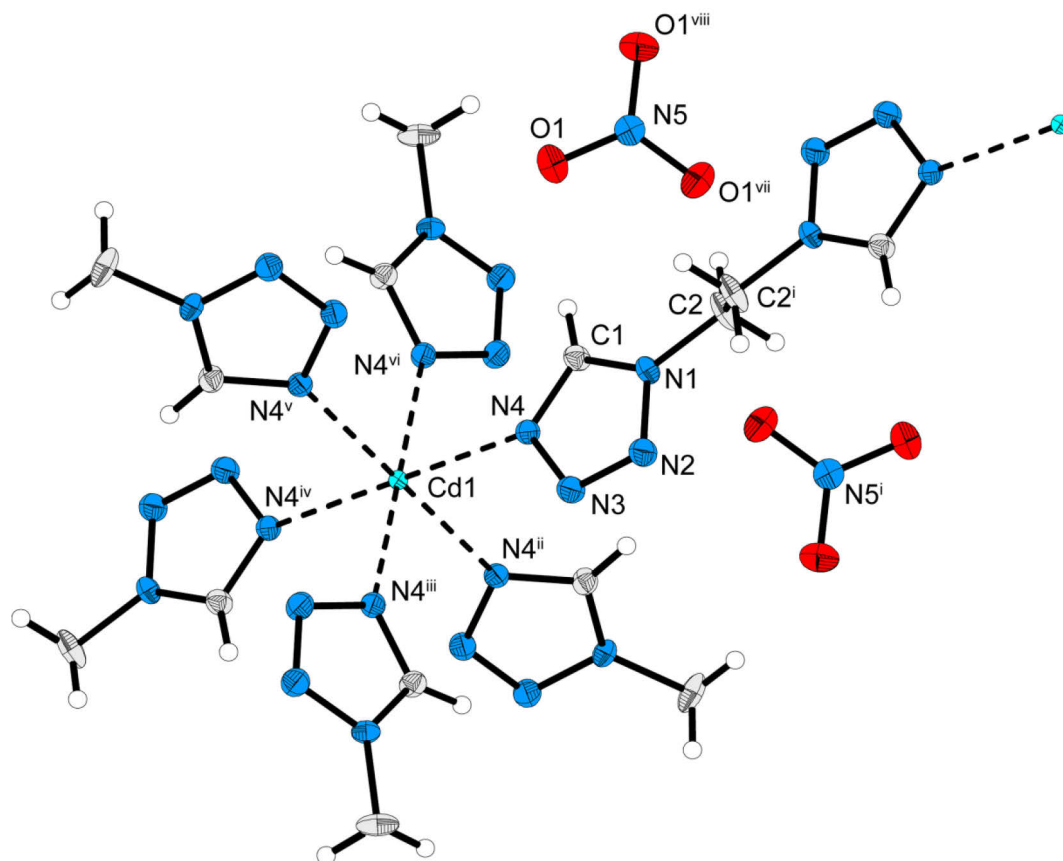


Figure 3. Octahedral coordination sphere of complex **12**. Thermal ellipsoids of non-hydrogen atoms are drawn at the 50 % probability level. Selected bond lengths [Å]: Cd1–N4 2.3584(13), O1–N5 1.2504(11), N1–C1 1.3305(16), N1–N2 1.3434(16), N1–C2 1.4643(16), N4–C1 1.3226(16), N4–N3 1.3616(15), N2–N3 1.2896(16); selected bond angles [°]: N4–Cd1–N4^{iv} 180.0, N4–Cd1–N4ⁱⁱ 85.7(0), C1–N4–Cd1 133.7(1), C1–N1–N2 108.8(1), C1–N1–C2 130.2(1), N3–N2–N1 107.0(1), O1–N5–O^{vii} 120.0(1); selected torsion angles [°]: Cd1–N4–N3–N2 175.8(1), C1–N1–N2–N3 –0.2(1), N1–N2–N3–N4 0.1(1), N1–C2–C2ⁱ–N1ⁱ 180.0(1), O1–N5–O1^{vii}–O1^{viii} 179.8(2). Symmetry codes: i: 1–x, 1–y, 1–z; ii: –y, –x+y, –z; iii: –x+y, –x, z; iv: –x, –y, –z; v: –y, x–y, z; vi: x–y, x, –z; vii: 1–y, 1+x–y, z; viii: –x+y, 1–x, z.

The chlorate complex **14** crystallizes as blue blocks in the trigonal space group $P\bar{3}c1$ with four formula units per unit cell and a calculated density of 1.838 g cm^{-3} at 293 K. The asymmetric unit consists of one-third of the formula unit. The copper(II) center has an octahedral coordination sphere which is not Jahn-Teller distorted (Figure 4). It is surrounded by six tetrazole rings which are coordinated to the metal center over the N4 and N8 position ($d(\text{Cu1–N4}) = 2.151(2) \text{ \AA}$ and $d(\text{Cu1–N8}) = 2.153(2) \text{ \AA}$). Comparable with complex **10**, the Cu1–N4 and Cu1–N8 distances are between equatorial (about 2.0 \AA) and axial (about 2.4 \AA) Cu–N bonds of Jahn-Teller distorted complexes. Half of the dte ligands have an *anti* conformation ($\angle(\text{N1–C2–C2}^{\text{iii}}\text{–N1}^{\text{iii}}) = 180.0(2)^\circ$; symmetry code: i: –y, x–y, z) while the other half shows a *gauche* conformation ($\angle(\text{N5–C4–C4}^{\text{iv}}\text{–N5}^{\text{iv}}) = -51.2(3)^\circ$; symmetry code: iv: –x, –x+y, 0.5–z). The three *gauche*-oriented dte-ligands bridge two copper(II) centers to each other similar to the literature known copper(II) perchlorate complexes,^[14a] while the three *anti*-oriented ligands bridge one copper(II) to three others by forming a three-dimensional

network (Figure S4, S5 and S6). The chlorate anions exhibit typical values for the Cl–O bonds ($d(\text{Cl1–O1}) = 1.478(2) \text{ \AA}$ and $d(\text{Cl2–O2}) = 1.467(2) \text{ \AA}$) and O–Cl–O angles ($\angle(\text{O1–Cl1–O1}^{\text{v}}) = 107.3(1)^\circ$; symmetry code: v: $1-x+y, 1-x, z$) compared to literature.^[18]

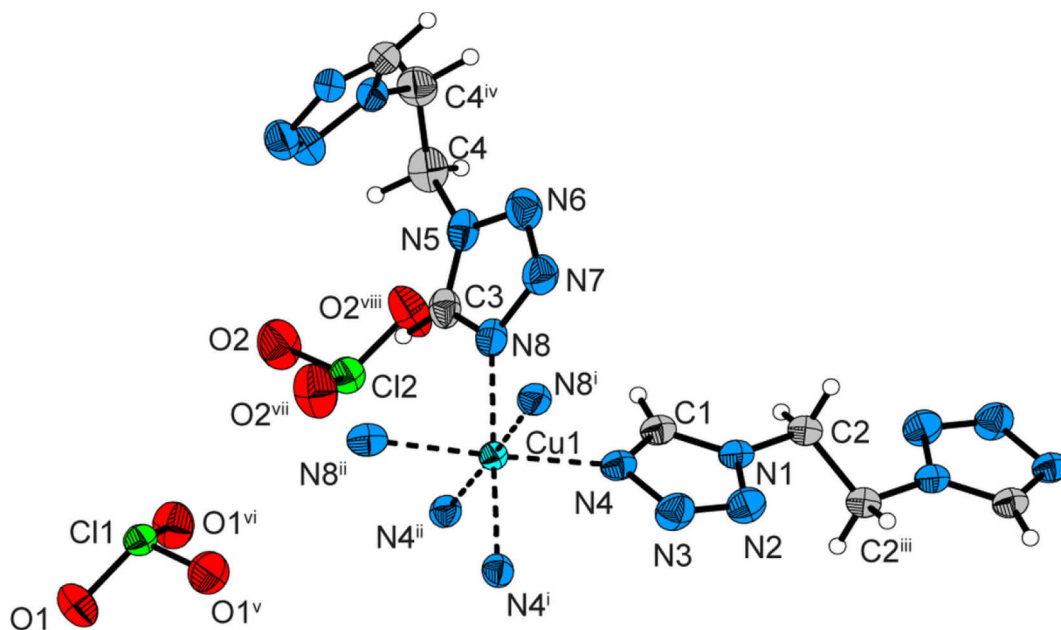


Figure 4. Octahedral coordination sphere of complex **14**. Thermal ellipsoids of non-hydrogen atoms are drawn at the 50 % probability level. Selected bond lengths [\AA]: Cu1–N4 2.151(2), Cu1–N8 2.153(2), Cl1–O1 1.478(2), Cl2–O2 1.467(2), N4–C1 1.322(3), N4–N3 1.358(3), N1–C1 1.327(3), N1–N2 1.351(3), N1–C2 1.464(3), N8–C3 1.314(3), N8–N7 1.361(3), N6–N7 1.293(3), N6–N5 1.353(3), N5–C3 1.320(3), N5–C4 1.472(3); selected bond angles [$^\circ$]: N4–Cu1–N8 86.6(7), N4–Cu1–N4ⁱ 93.3(8), N8ⁱ–Cu1–N8ⁱⁱ 90.3(8), C1–N4–Cu1 131.7(2), N3–N4–Cu1 122.1 (2), C3–N8–Cu1 131.4(2), N7–N8–Cu1 122.1(2), N4–C1–N1 108.7(2), N2–N3–N4 110.1(2), N8–C3–N5 108.6(2), N6–N7–N8 109.7(2), O1–Cl1–O1^v 107.3(1); selected torsion angles [$^\circ$]: N8–Cu1–N4–C1 $-24.1(2)$, N8–Cu1–N4–N3 153.4(2), N4–Cu1–N8ⁱ–N4ⁱⁱ 179.7(1), Cu1–N4–N3–N2 $-178.0(2)$, C1–N4–N3–N2 0.0(3), N1–C2–C2ⁱⁱⁱ–N1ⁱⁱⁱ 180.0(2), N7–N6–N5–C3 $-0.4(3)$, N5–C4–C4^{iv}–N5^{iv} $-51.2(3)$. Symmetry codes: i: $-y, x-y, z$; ii: $-x+y, -x, z$; iii: $-1-x, -y, 1-z$; iv: $-x, -x+y, 0.5-z$; v: $1-x+y, 1-x, z$; vi: $1-y, x-y, z$; vii: $-x+y, 1-x, z$; viii: $1-y, 1+x-y, z$.

The nitrito complex **15** crystallizes as dark green blocks in the monoclinic space group $P2_1/c$ with two formula units per unit cell and a calculated density of 2.012 g cm^{-3} at 293 K. The asymmetric unit consists of one-half of the formula unit. The copper(II) center is surrounded by two tetrazole rings and two nitrito anions (Figure 5). The bidentate nitrito anions are coordinating with both oxygen atoms ($\kappa^2\text{O1}, \text{O2}$) to the copper center. The complex shows a Jahn-Teller distortion of the octahedral coordination sphere along the Cu1–O2 bond with a length of $2.508(2) \text{ \AA}$. Due to the fixed geometry of the nitrito ligand, the O1–Cu1–O2 angle ($53.8(7)^\circ$) is strongly deviating from 90° . The N–O bond lengths ($d(\text{O1–N5}) = 1.270(3) \text{ \AA}$ and $d(\text{O2–N5}) = 1.236(3) \text{ \AA}$) are both elongated compared to uncoordinated nitrite anions ($d(\text{N–O}) = 1.12\text{--}1.17 \text{ \AA}$).^[19] However, the O1–N5 bond is longer and the O2–N5 bond shorter than the analogue bonds (N–O = $1.217(1)$ and $1.306(2) \text{ \AA}$) of a comparable bidentate nitrito complex.^[20] The μ -bridging dte ligand is *anti*-oriented ($\angle(\text{N1–C2–C2}^{\text{ii}}$

$\text{N1}^{\text{ii}}) = 180.0(2)^\circ$; symmetry code: ii: $-x, -y, 1-z$) and connects two copper(II) ions to a one-dimensional chain (Figure S7).

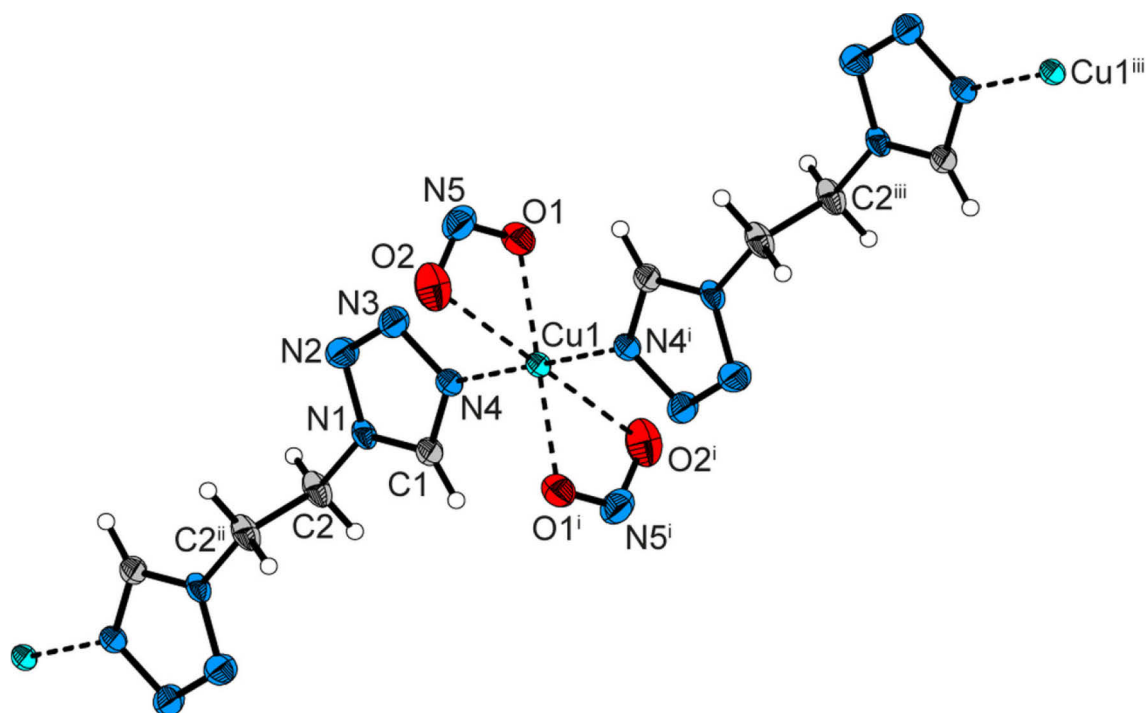


Figure 5. Octahedral coordination sphere of complex **15**. Thermal ellipsoids of non-hydrogen atoms are drawn at the 50 % probability level. Selected bond lengths [Å]: Cu1–N4 1.991(2), Cu1–O1 2.015(2), Cu1–O2 2.508(2), N1–C1 1.318(3), N1–N2 1.349(3), N1–C2 1.466(3), O1–N5 1.270(3), O2–N5 1.236(3); selected bond angles [°]: N4–Cu1–O1 91.6(8), O1–Cu1–O2 53.8(7), C1–N1–N2 108.8(2), C1–N1–C2 130.1(2), N2–N1–C1 121.1(2), C1–N4–Cu1 129.6(2), O2–N5–O1 113.2(2); selected torsion angles [°]: O1–Cu1–N4–C1 171.8(2), N4–Cu1–O2–N4ⁱ $-180.0(1)$, C1–N1–N2–N3 0.3(3), N1–C2–C2ⁱⁱ–N1ⁱⁱ 180.0(2). Symmetry codes: i: $1-x, -y, -z$; ii: $-x, -y, 1-z$; iii: $1+x, y, -1+z$.

The dinitramide complex **16** crystallizes as blue blocks in the triclinic space group $P1$ with one formula unit per unit cell and a calculated density of 1.748 g cm^{-3} at 173 K. The asymmetric unit is equivalent to the formula unit. The symmetry is reduced to the space group $P1$ due to a disorder of the dinitramide anions. The copper(II) center is surrounded by six tetrazole rings (Figure 6). The octahedral coordination sphere is Jahn-Teller distorted along the Cu1–N8 (2.414(7) Å) and Cu1–N24 (2.447(7) Å) bonds. Two types of dte ligands are observed. Four dte ligands are in a *gauche* conformation and always two of them bridge two copper centers with each other. In contrast, each one of the two *anti*-oriented dte ligands bridges one copper to another. Consequently, a two-dimensional coordination polymer is formed (Figure S8). The bond lengths and angles of the dinitramide anions are not discussed because of the isotropic refinement of N25–N30.

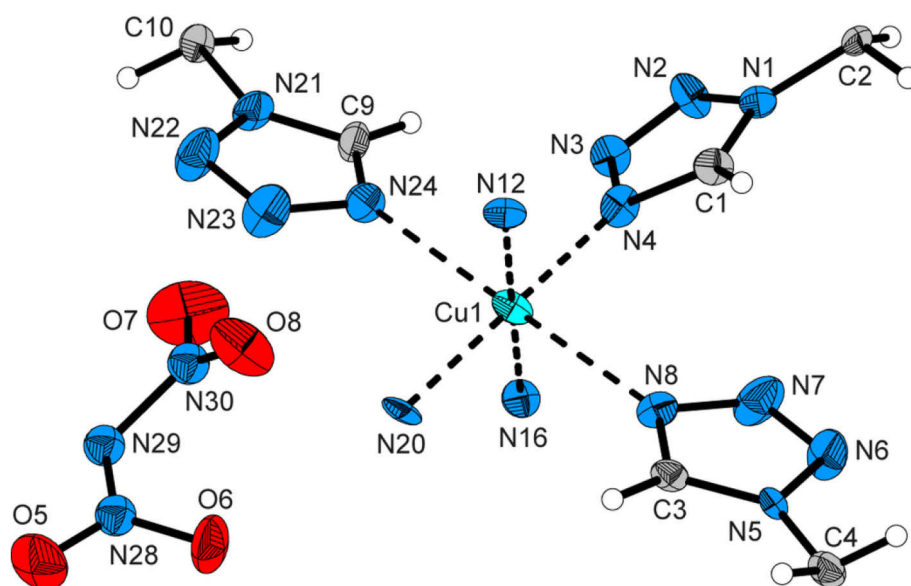


Figure 6. Octahedral coordination sphere of complex **16**. For clarity only the half of the asymmetric unit is presented. Thermal ellipsoids of non-hydrogen atoms are drawn at the 50 % probability level. The nitrogen atoms N25–N30 were refined isotropically due to a disorder of the dinitramide anions. Selected bond lengths [Å]: Cu1–N4 1.992(7), Cu1–N8 2.414(7), Cu1–N12 2.026(7), C1–N1 1.313(1), N1–N2 1.356(1), N1–C2 1.450(9), N28–N29 1.29(2), N29–N30 1.46(2), N28–O5 1.18(2), N28–O6 1.330(19); selected bond angles [°]: N4–Cu1–N8 89.2(3), N4–Cu1–N12 88.4(3), N4–Cu1–N20 179.4(3), C1–N1–C2 130.0(7), C1–N1–N2 107.7(6), N2–N1–C2 122.3(7); selected torsion angles [°]: N8–Cu1–N4–N24 $-179.2(3)$, C1–N1–N2–N3 $-0.9(9)$, C2–N1–N2–N3 $-178.7(7)$, N1–C2–C4ⁱ–N5ⁱ $-72.3(9)$, N9–C6–C8ⁱⁱ–N13ⁱⁱ $177.7(7)$, N29–N28–O5–O6 $176.9(3)$; symmetry codes: i: $x, -1+y, z$; ii: $1+x, y, 1+z$.

The waterfree nitrocyanamide complex **17** crystallizes as blue blocks in the triclinic space group $P\bar{1}$ with one formula unit per unit cell and a calculated density of 1.821 g cm^{-3} at 100 K. The asymmetric unit consists of one-half of the formula unit. The copper(II) center has a Jahn-Teller distorted octahedral coordination sphere ($d(\text{Cu1–N4}) = 2.0123(2) \text{ \AA}$, $d(\text{Cu1–N8}) = 2.034(2) \text{ \AA}$ and $d(\text{Cu1–N11}) = 2.409(2) \text{ \AA}$). The dte-ligand is oriented in a *gauche* conformation ($\langle(\text{N1–C2–C4}^{\text{ii}}\text{–N5}^{\text{ii}})\rangle = -62.1(3)^\circ$, symmetry code: ii: $x, -1+y, z$) and bridges the copper(II) centers to a one-dimensional chain (Figure 7 and Figure S9). The nitrocyanamido ligand coordinates in the axial positions to the copper(II). The bond lengths and values of the nitrocyanamido ligand are in the range of literature known nitrocyanamido compounds ($d(\text{N9–C5}) = 1.335(3) \text{ \AA}$, $d(\text{N11–C5}) = 1.157(3) \text{ \AA}$ and $\langle(\text{N11–C5–N9})\rangle = 172.0(2)^\circ$).^[21] However, no linear coordination of the nitrile unit to the copper center ($\langle(\text{C5–N11–Cu1})\rangle = 134.0(2)^\circ$) is observed as it would be expected for a nitrile with a triple bond. Similar to other nitrocyanamido complexes, a reason might be found in a delocalization of electron densities caused by electrostatic interactions (non-classic hydrogen bonds) between the dte-ligand and the nitrile unit.^[21b]

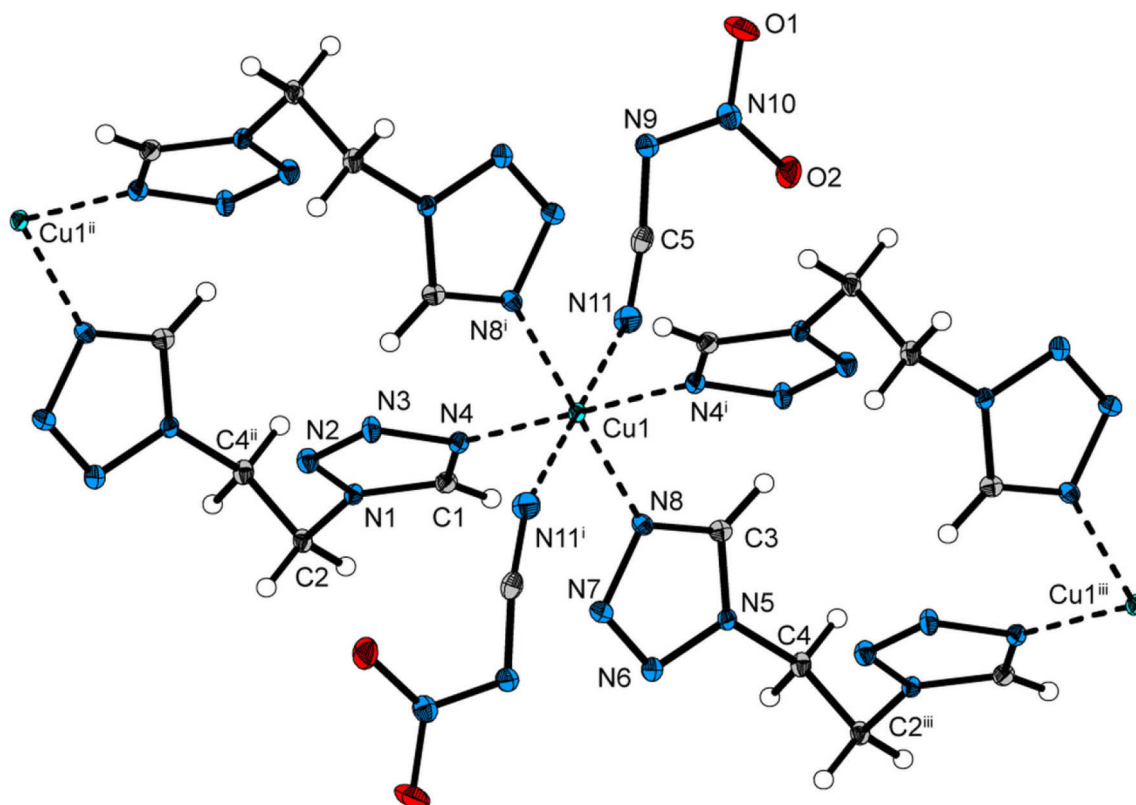


Figure 7. Octahedral coordination sphere of complex **17**. Thermal ellipsoids of non-hydrogen atoms are drawn at the 50 % probability level. Selected bond lengths [Å]: Cu1–N4 2.0123(2), Cu1–N8 2.034(2), Cu1–N11 2.409(2), C1–N1 1.330(2), N1–N2 1.356(2), N1–C2 1.465(2), N2–N3 1.292(2), N3–N4 1.364(2), N9–C5 1.335(3), N11–C5 1.157(3), N9–N10 1.344(2), O1–N10 1.251(2), O2–N10 1.246(2); selected bond angles [°]: N4–Cu1–N8 89.8(1), N4–Cu1–N11 88.3(1), N8–Cu1–N11 87.5(1), C1–N1–N2 108.7(2), C1–N1–C2 130.1(2), N2–N1–C2 121.2(2), N3–N2–N1 106.8(2), C5–N11–Cu1 134.0(2), N11–C5–N9 172.0(2), O2–N10–O1 122.0(2); selected torsion angles [°]: N4–Cu1–N8–N4ⁱ –180.0(1), N4–Cu1–N11–N4ⁱ 180.0(1), C1–N1–N2–N3 0.0(2), C2–N1–N2–N3 176.1(2), N1–C2–C4ⁱⁱ–N5ⁱⁱ –62.1(3), N9–N10–O1–O2 180.0(3); symmetry codes: i: 1–*x*, –*y*, –*z*; ii: *x*, –1+*y*, *z*; iii: *x*, 1+*y*, *z*.

The trinitromethanide complex **19** crystallizes as pale green blocks in the triclinic space group $P\bar{1}$ with one formula unit per unit cell and a calculated density of 1.842 g cm^{–3} at 293 K. The complex forms a similar structure than **17** with the difference that the trinitromethanide is not coordinating (Figure 8). Instead, aqua ligands occupy the axial positions ($d(\text{Cu1–O1}) = 2.415(2)$ Å). All bond lengths ($d(\text{Cu1–N4}) = 2.017(2)$ Å, $d(\text{N1–C1}) = 1.325(2)$ Å and $d(\text{N1–N2}) = 1.345(2)$ Å) and angles ($\angle(\text{N4–Cu1–N8}) = 91.5(1)^\circ$ and $\angle(\text{C1–N1–N2}) = 108.6(2)^\circ$) of the inner complex unit are in typical ranges compared to the other herein presented copper(II) complexes. The trinitromethanide anion shows values for the bond lengths ($d(\text{N9–C5}) = 1.364(3)$ Å, $d(\text{N10–C5}) = 1.448(3)$ Å and $d(\text{O2–N9}) = 1.254(3)$ Å) and angles ($\angle(\text{N9–C5–N10}) = 116.3(2)^\circ$ and $\angle(\text{O3–N9–O2}) = 122.0(2)^\circ$) which are similar to literature known compounds.^[22]

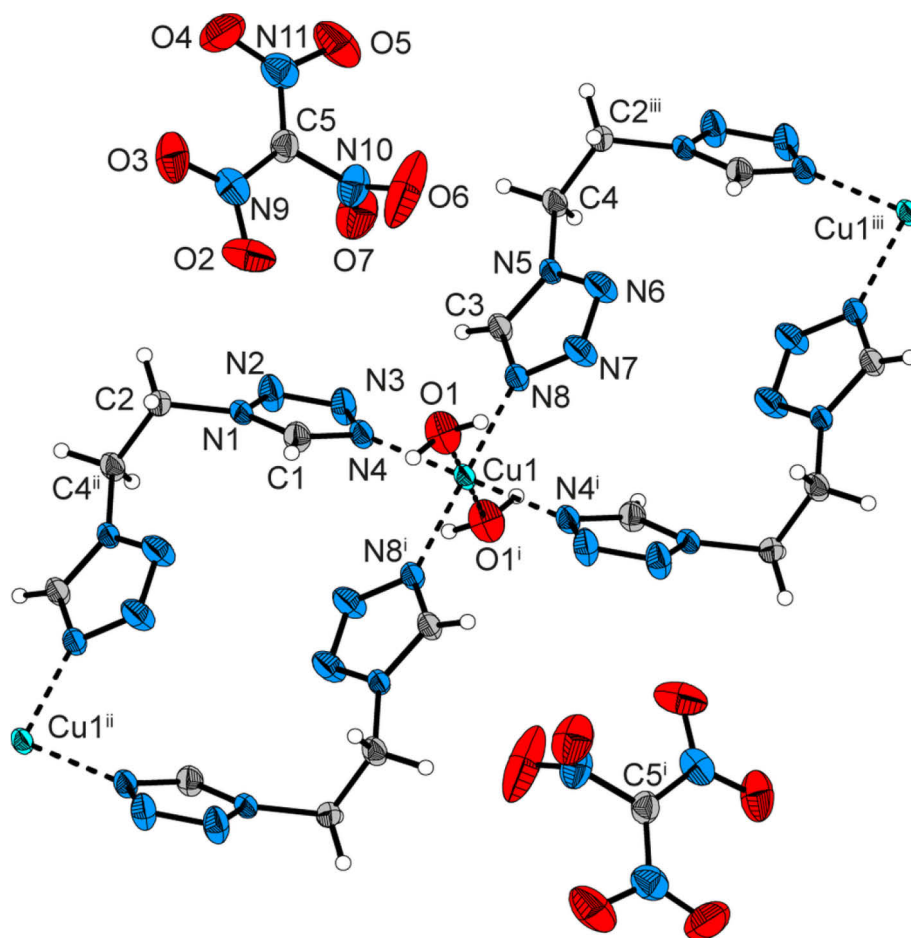


Figure 8. Octahedral coordination sphere of complex **19**. Thermal ellipsoids of non-hydrogen atoms are drawn at the 50 % probability level. Selected bond lengths [Å]: Cu1–N4 2.017(2), Cu1–N8 2.033(1), Cu1–O1 2.415(2), N1–C1 1.325(2), N1–N2 1.345(2), N1–C2 1.472(2), N2–N3 1.291(2), N3–N4 1.356(2), N9–C5 1.364(3), N10–C5 1.448(3), N11–C5 1.366(3), O2–N9 1.254(3), O3–N9 1.234(2); selected bond angles [°]: N4–Cu1–N8 91.5(1), N4–Cu1–O1 87.8(1), N8–Cu1–O1 91.6(1), C1–N1–N2 108.6(2), C1–N1–C2 131.4(2), N2–N1–C2 120.0(2), N3–N2–N1 107.0(2), N9–C5–N10 116.3(2), O3–N9–O2 122.0(2); selected torsion angles [°]: N4–Cu1–N8–N4ⁱ –180.0(1), N4–N8–N4ⁱ–N8ⁱ 0.0(1), C1–N1–N2–N3 0.3(2), C2–N1–N2–N3 –180.0(2), N1–C2–C4ⁱ–N5ⁱ 83.9(2), N9–C5–N10–N11 –177.9(3); symmetry codes: i: $-x, -y, 2-z$; ii: $1+x, y, z$; iii: $-1+x, y, z$.

The cyanodinitromethanide complex **20** crystallizes as pale green rods in the monoclinic space group $P2_1/n$ with two formula units per unit cell and a calculated density of 1.826 g cm^{-3} at 173 K. The asymmetric unit consists of one half of the formula unit. The coordination geometry is octahedral (Figure 9) and similar to that of complex **19** ($d(\text{Cu1–N4}) = 2.033(2) \text{ Å}$, $d(\text{Cu1–N8}) = 2.057(2) \text{ Å}$ and $d(\text{Cu1–O1}) = 2.317(2) \text{ Å}$). Like complex **17** and **19**, the dte ligand exhibits a *gauche* conformation ($\angle(\text{N1–C2–C4}^{\text{ii}}\text{–N5}^{\text{ii}}) = 70.6(2)^\circ$; symmetry code: ii: $1-x, y, z$) and bridges the copper(II) centers to one-dimensional chains. The bond lengths and angles of the cyanodinitromethanide anion are in a typical range.^[23] The anion is nearly planar ($\angle(\text{C6–C5–N9–N10}) = 176.9(2)^\circ$ and $\angle(\text{C5–N9–O2–O3}) = -179.6(3)^\circ$).

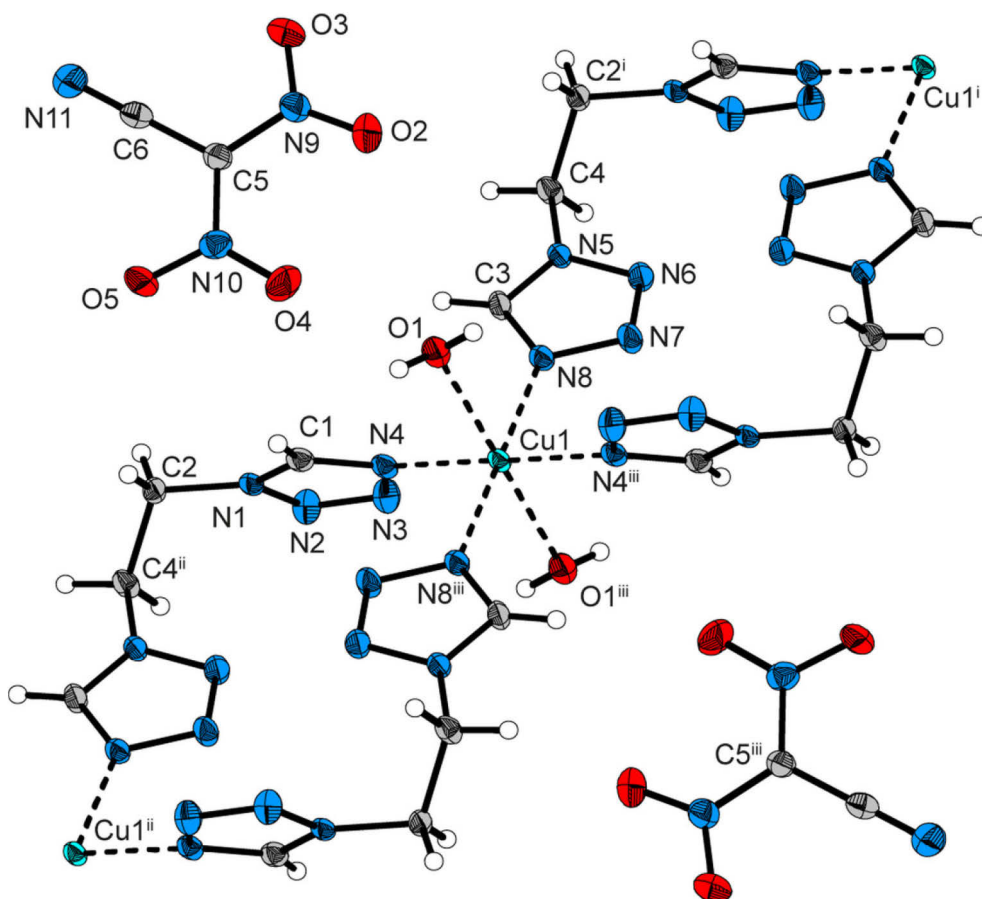


Figure 9. Octahedral coordination sphere of complex **20**. Thermal ellipsoids of non-hydrogen atoms are drawn at the 50 % probability level. Selected bond lengths [Å]: Cu1–N4 2.033(2), Cu1–N8 2.057(2), Cu1–O1 2.317(2), N1–C1 1.324(2), N1–N2 1.353(2), N1–C2 1.474(2), N2–N3 1.287(2), N3–N4 1.366(2), C5–C6 1.415(3), C5–N9 1.387(2), C5–N10 1.395(2), C6–N11 1.146(3), O2–N9 1.235(2); selected bond angles [°]: N4–Cu1–N8 89.7(1), N4–Cu1–O1 88.9(1), N8–Cu1–O1 86.4(1), C1–N1–N2 108.7(2), C1–N1–C2 131.1(2), N2–N1–C2 120.2(2), N11–C6–C5 178.6(2), N9–C5–N10 123.3(2), O2–N9–O3 122.5(2); selected torsion angles [°]: N4–Cu1–N8–N4ⁱⁱⁱ 180.0(1), N4–N8–N4ⁱⁱⁱ–N8ⁱⁱⁱ 0.0(1), C1–N1–N2–N3 0.4(2), C2–N1–N2–N3 –179.3(2), N1–C2–C4ⁱⁱ–N5ⁱⁱ 70.6(2), C6–C5–N9–N10 176.9(2), C5–N9–O2–O3 –179.6(3); symmetry codes: i: 1+x, y, z; ii: 1–x, y, z; iii: –x, 1–y, 1–z.

Infrared spectroscopy: Infrared spectra of all compounds **1–21** were recorded. Raman spectroscopy was not performed because of the potential photosensitivity of the synthesized metal complexes toward the Nd:YAG laser of the Raman spectrometer.

The neutral compound **1** shows sharp bands for the C–H stretching vibrations at 3119, 3025 and 2977 cm^{-1} . The C=N stretching vibration can be observed at 1576 cm^{-1} . Typical C–N, N–N and C–C stretching and deformation modes are found below 1500 cm^{-1} .^[24] These vibrations can also be found in the spectra of the investigated metal(II) complexes. However, the ligand vibrations can be blue or red shifted due to complexation. In the case of the metal(II) perchlorates **2–7**, an additional strong absorption band around 1083 cm^{-1} is observed and can be assigned to the perchlorate vibration. The perchlorate anion does not coordinate to the metal(II) center which is indicated by a single signal. In case of a coordination of the perchlorate to the metal center a splitting of the vibration band would be expected.^[25] The

infrared spectra of the perchlorates are similar and together with the results of elemental analysis, similar structures can be suggested for **2–7**. The nitrate complexes **8** and **10–12** showed very similar infrared spectra (e.g. two N–H valence vibrations at 3086–3094 cm^{-1} and 2985–2989 cm^{-1}) indicating similar structures, which is in agreement with the crystal structures of **10–12**. Only the nitrate compound **9** seems to have a slightly different structure indicated amongst others by additional N–H valence vibrations at 3132, 3034 and 2946 cm^{-1} . A strong vibration band of an uncoordinated nitrate can be observed for all five complexes **8–12** at typical values between 1354 and 1342 cm^{-1} .^[26] The infrared spectra of the copper(II) compounds **14–21** exhibit characteristic vibration modes for the corresponding anions: (i) the chlorate vibration at 957 cm^{-1} for **14**,^[27] (ii) a very strong nitrite vibration at 1364 cm^{-1} for **15**,^[28] (iii) the dinitramide vibration at 1514 cm^{-1} for **16**,^[1a,29] (iv) the nitrile vibration at 2183 cm^{-1} for **17** and at 2173 cm^{-1} for **18** as well as the nitramine vibration at 1264 cm^{-1} for **17** and 1259 cm^{-1} for **18**,^[21b] (v) one of the nitro vibrations at 1487 cm^{-1} for **19**,^[24,30] (vi) the nitrile vibration at 2216 cm^{-1} and the nitro vibration at 1254 cm^{-1} for **20**,^[24,30] (vii) the azide vibration at 2074 and 2044 cm^{-1} for **21**.^[31] However, not all vibrations modes of the anions could be assigned definitely because vibration bands of the dte ligand were observed in these regions, too. Furthermore, in the IR spectra of the complexes **18–20** can be observed the asymmetric and symmetric O–H-stretching modes around 3500 cm^{-1} .

Energetic properties and laser ignition: Determinations of the sensitivities toward friction, impact, and electrostatic discharge, as well as the temperature stability were performed for the free ligand **1** and for all coordination compounds **2–21**. Afterwards, the compounds were classified according to the UN Recommendations on the Transport of Dangerous Goods.^[32] An overview about the energetic properties and the laser ignition and initiation results is given in Tables 1–4.

The ligand **1** is classified as insensitive toward impact and friction. It further shows only a minor sensitivity toward electrostatic discharge with a value of 0.75 J. The perchlorate complexes **2–7** (Table 1) together with the copper(II) chlorate **14** (Table 3) and azide **21** (Table 4) showed the highest sensitivities of the herein investigated compounds. Compounds **3, 4, 5, 14, and 21** are classified as extremely sensitive toward friction and very sensitive toward impact. The perchlorates **2, 6, 7**, and the dinitramide **16** show lower sensitivities and are classified as very sensitive toward friction and impact. The nitrates **8–12** are all classified as sensitive toward impact and friction except **12**, which is further classified as less sensitive toward friction. The chloride **13**, the nitrocyanamide **18**, and the cyanodinitromethanide **20** are also sensitive toward impact and friction. The nitrite **15** is classified as very sensitive toward impact and sensitive toward friction. The nitrocyanamide **17** and the nitroformate **19**

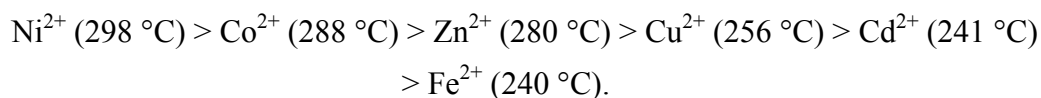
are both sensitive toward friction. However, **17** is very sensitive toward impact whereas **19** is classified as insensitive.

Table 1. Energetic properties of the $[M(dte)_3](ClO_4)_2$ complexes **2–7**.

	2	3	4	5	6	7
Metal cation	Fe ²⁺	Co ²⁺	Ni ²⁺	Cu ²⁺	Zn ²⁺	Cd ²⁺
T_{decomp} (onset) [°C]	240	288	298	256	280	241
IS [J]	2	1	1	1.5	2	4
FS [N]	14	6	6	10	42	60
ESD [J]	0.08	0.25	0.25	0.15	0.30	0.08
Grain size [μm]	< 100	100–500	100–500	< 100	100–500	100–500
$F(R)$ at 940 nm ^[a]	0.104	0.075	0.029	0.006	0.000	0.003
Laser ignition ^[b]	4	4	4	1	4	4

[a] Absorption intensity $F(R)$ at wavelength $\lambda = 940$ nm. [b] Parameters of the laser beam: $\lambda = 940$ nm, $\tau = 100$ μs, $\sigma = 105$ μm, $\Phi_e = \text{const}$. Results of irradiation with diode laser light: 1: detonation; 2: deflagration; 3: combustion or fragmentary decomposition; 4: no ignition.

Comparing the thermal stabilities of the perchlorates **2–7**, the nickel(II) complex **4** shows the highest decomposition point with a onset temperature of 298 °C and the iron(II) complex **2** the lowest with 240 °C. The decomposition temperatures (T_{decomp}) of the $[M(dte)_3](ClO_4)_2$ complexes decrease in the following sequence:



The nitrate complexes **8–12** are less temperature stable than the corresponding perchlorates. However, the decomposition temperatures (T_{decomp}) of the $[M(dte)_3](NO_3)_2$ complexes decrease in a sequence similar to the perchlorates:

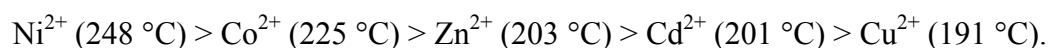


Table 2. Energetic properties of the $[M(dte)_3](NO_3)_2$ complexes **8–12**.

	8	9	10	11	12
Metal cation	Co ²⁺	Ni ²⁺	Cu ²⁺	Zn ²⁺	Cd ²⁺
T_{decomp} (onset) [°C]	225	248	191	203	201
IS [J]	12.5	7	7	5	10
FS [N]	288	240	160	240	360
ESD [J]	0.20	0.20	1.0	0.30	0.80
Grain size [μm]	< 100	< 100	500–100	100–500	100–500
$F(R)$ at 940 nm ^[a]	0.082	0.066	0.007	0.008	0.010
Laser ignition ^[b]	4	4	3	4	4

[a] Absorption intensity $F(R)$ at wavelength $\lambda = 940$ nm. [b] Parameters of the laser beam: $\lambda = 940$ nm, $\tau = 100$ μs, $\sigma = 105$ μm, $\Phi_e = \text{const}$. Results of irradiation with diode laser light: 1: detonation; 2: deflagration; 3: combustion or fragmentary decomposition; 4: no ignition.

The copper(II) complexes **13–21** are less temperature stable than 200 °C except **20** ($T_{\text{decomp}} = 212$ °C). Further, the aqua complexes **18** and **20** showed endothermic signals in the DTA measurements which indicated a loss of crystal water. The nitrocyanamide **18** loses its crystal water between 80 and 135 °C whereas **20** dehydrates between 75 and 100 °C. However, no attempts were made to dehydrate the compounds in the oven. Complex **19** cannot be dehydrated because exothermic decomposition starts at 83 °C.

Table 3. Energetic properties of the copper(II) complexes **13–16**.

	13	14	15	16
Anion	Cl ⁻	ClO ₃ ⁻	NO ₂ ⁻	N(NO ₂) ₂ ⁻
T_{decomp} (onset) [°C]	186	175	139	168
IS [J]	10	1.5	2	1
FS [N]	324	6	160	80
ESD [J]	1.0	0.015	1.0	0.25
Grain size [μm]	500–1000	< 100	500–100	< 100
Laser ignition ^[a]	3	1	4	2

[a] Parameters of the laser beam: $\lambda = 940$ nm, $\tau = 100$ μs, $\sigma = 105$ μm, $\Phi_e = \text{const}$. Results of irradiation with diode laser light: 1: detonation; 2: deflagration; 3: combustion or fragmentary decomposition; 4: no ignition.

The laser ignition experiments were made with a single pulsed diode laser at a wavelength of 940 nm and a pulse length of 100 μs. The radiant power (Φ_e) of the laser was kept constant. The samples, containing 5 % binder (PTFE), were pestled to powders with grain sizes smaller 100 μm and pressed to pellets of about 200 mg substance and pressing densities of 1.6 to 1.7 g cm⁻³ (except **21** which had a pressed density of 1.5 g cm⁻³). Summarizing the results (Table 1–4), it can be concluded that laser ignition and initiation was only successful for the copper compounds. Nearly all copper(II) compounds, except the nitrito complex **15** and the nitrocyanamido **17**, were ignited by the laser beam. As expected, the influence of the metal center on the laser ignitability seems to be much higher than that of the anion, which is in agreement with a thermal mechanism. Absorption of laser radiation leads to a heating and formation of hot spots. According to literature,^[33] it is supposed that only some spots and not the whole bulk are heated sufficient. Thus, self-sustained decomposition of the energetic material starts when the ignition temperature is reached within a few hot spots.

The ignition delay, defined as the time period from irradiating the sample to the beginning decomposition of the sample, depends on many parameters according to literature: (i) absorption intensity at the wavelength of the laser beam (mainly influenced by the metal), (ii) particle size, (iii) pressed density, (iv) ignition temperature and (v) thermal conductivity.^[9] Further, the ignition delay time correlates with the initiation energy threshold in the point that the ignition delay is also a function of the laser power density. For equal laser power

densities, a lower critical energy threshold for initiation implicates also a shorter ignition delay.

Concluding, on the assumption of a thermal mechanism, the initiation energy threshold of the coordination compounds is mainly influenced by the metal center and not by the anion, and in case of the dte complexes only for copper(II) low enough that initiation or ignition occurs at a 100 μ s pulse. However, when comparing the UV/Vis/NIR spectral data (Figure S1 and S2) and the decomposition temperatures of the perchlorate and nitrate compounds with the laser initiation results, it is not fully understood why compound **2** could not be initiated whereas initiation of e.g. **5** or ignition of e.g. **10** was successful. Compound **2** showed the highest absorption intensity at 940 nm and further the lowest thermal stability (lowest decomposition temperature) of the investigated perchlorates, thus, a successful initiation was expected. Therefore, it seems that the thermal stability and the absorption intensity do not have that supposed major influence on the laser ignitability. This also fits to the ignition results of the nitrate complexes. The copper(II) complex **10** showed the lowest absorption intensity at 940 nm, which is even lower than that of **11** and **12**. However, **10** was the only laser ignitable complex of the formula $[M(dte)_3](NO_3)_2$. An explanation might be found in the "hot spot" theory. During laser irradiation of the explosive, only small spots (caused by e.g. crystal defects or inhomogeneities) are heated sufficiently within the bulk and not the whole sample. The critical temperature for these hot spots is different from the ignition temperature of a sample bulk which was externally heated. Examples for external heat are DTA or DSC measurements of explosive samples and therefore, the obtained exothermic decomposition temperatures, at which a self-sustained decomposition reaction occurs, cannot be compared to the ignition temperatures which have to be reached within the hot spots. These critical temperatures depend on the material and its properties (e.g. thermal conductivity, heat of reaction, activation energy).

Table 4. Energetic properties of the copper(II) complexes **17–21**.

	17	18	19	20	21
Anion	$N(CN)(NO_2)^-$	$N(CN)(NO_2)^-$	$C(NO_2)_3^-$	$C(CN)(NO_2)_2^-$	N_3^-
T_{decomp} (onset) [$^{\circ}C$]	170	171	83	212	197
IS [J]	1	5	40	4	1
FS [N]	108	120	192	288	5
ESD [J]	0.5	0.7	0.2	0.1	0.014
Grain size [μ m]	< 100	< 100	< 100	< 100	500–100
Laser ignition ^[a]	4	3	3	3	1

[a] Parameters of the laser beam: $\lambda = 940$ nm, $\tau = 100$ μ s, $\sigma = 105$ μ m, $\Phi_e = \text{const}$. Results of irradiation with diode laser light: 1: detonation; 2: deflagration; 3: combustion or fragmentary decomposition; 4: no ignition.

Although the type of metal center is critical for the laser ignitability, the anion has a great influence on the power of the metal complex and the decomposition reaction. The anion influences e.g. if a detonation-to-deflagration transition (DDT) occurs or not. The perchlorate **5**, chlorate **14**, or azide **21** detonated whereas all other copper(II) compounds deflagrated, combusted, or even only partially decomposed.

8.4. Conclusion

The literature known ligand 1,2-di(1*H*-tetrazol-1-yl)ethane was applied as ligand for various metal(II) complexes. Perchlorates of the formula $[M(\text{dte})_3](\text{ClO}_4)_2$ with $M = \text{Fe}^{2+}$, Co^{2+} , Ni^{2+} , Cu^{2+} , Zn^{2+} , Cd^{2+} (**2–7**) and nitrates of the formula $[M(\text{dte})_3](\text{NO}_3)_2$ with $M = \text{Co}^{2+}$, Ni^{2+} , Cu^{2+} , Zn^{2+} , Cd^{2+} (**8–12**) were synthesized, characterized and tested toward laser irradiation. Because of their similar structures, a good comparability of the complexes was provided and the influence of the metal center on the laser ignitability could be investigated. To investigate the influence of the anion on laser ignition and initiation, additional copper(II) complexes with the following anions were prepared and characterized: chloride (**13**), chlorate (**14**), nitrite (**15**), dinitramide (**16**), nitrocyanamide (**17** and **18**), trinitromethanide (**19**), cyanodinitromethanide (**20**), and azide (**21**). The laser ignition tests showed that only the copper(II) compounds, except **15** and **17**, could be ignited by a 100 μs pulse. This means that the metal center mainly influences the laser ignitability. However, the anion delivers energy for the decomposition reaction and affects if a DDT occurs or not. The perchlorate **5**, the chlorate **14**, and the azide **21** showed a DDT after initiation by laser radiation and might be interesting for laser-ignitable detonator systems.

Assuming that laser initiation is a thermal mechanism, it is not understood which parameter mostly influences the initiation energy threshold when comparing the laser initiation results. As it was shown, complexes, e.g. $[\text{Fe}(\text{dte})_3](\text{ClO}_4)_2$, with lower decomposition temperatures and higher absorption intensities than the corresponding copper(II) compound could not be successfully ignited. Maybe, the thermal conductivity or another parameter which was not included yet plays an important role for the laser ignition and initiation process.

8.5. Experimental Section

Caution! All of the metal(II) complexes prepared herein are energetic materials that show sensitivities toward various stimuli. Proper protective measures (safety glasses, face shield, leather coat, earthed equipment, conductive floor and shoes, Kevlar gloves, and ear plugs) should be used when handling these compounds. Extra safety precautions should be taken when compounds **2–7**, **14** and **21** are handled. These compounds are extremely sensitive toward impact, friction, and electrostatic discharge.

General Methods. All chemicals were used as supplied by ABCR, Acros Organics, AppliChem, Fluka, Sigma-Aldrich, and VWR. The impact and friction sensitivity tests were performed according to standard methods by using a BAM (Bundesanstalt für Materialforschung und -prüfung) drop hammer and a BAM friction tester.^[34] The sensitivity toward electrostatic discharge was tested by using an OZM Research electric spark tester ESD 2010 EN.^[35] Decomposition temperatures were measured via differential thermal analysis (DTA) with an OZM Research DTA 552-Ex instrument at a heating rate of 5 °C min⁻¹ and in a range of room temperature to 400 °C.^[35-36]

Suitable single crystals of **10–12**, **14–17** and **19–20** were directly obtained from the mother liquor and mounted in Kel-F oil. The structures were determined on an Oxford Diffraction Xcalibur 3 diffractometer with a Sapphire CCD detector, four circle kappa platform, Enhance molybdenum K_α radiation source ($\lambda = 71.073$ pm) and Oxford Cryosystems Cryostream cooling unit.^[37] Data collection and reduction were performed with the CrysAlisPro software.^[38] The structures were solved with SIR97 or SIR2004.^[39] The refinement was performed with SHELXL-97.^[40] The CIF-files were checked at the checkCIF website.^[41] The non-hydrogen atoms were refined anisotropically and the hydrogen atoms isotropically if not calculated. The determination of the carbon, hydrogen and nitrogen contents was carried out by combustion analysis using an Elementar Vario EL.^[42] Infrared (IR) spectra were recorded on a Perkin-Elmer BXII FT-IR system with a Smith DuraSamplIR II diamond ATR unit.^[43] ¹H and ¹³C NMR spectra were recorded on a JEOL Eclipse 270 spectrometer.^[44] The UV/Vis/NIR reflectance of solid samples was determined with a Varian Cary 500 spectrometer in the wavelength range of 350–1300 nm.^[37] The reflectance *R* [%] was transformed by the Kubelka–Munk function to the absorption intensity *F(R)*.^[45]

Analytical data of all metal(II) complexes can be found in the Supporting Information.

1,2-Di(1*H*-tetrazol-1-yl)ethane (1): The ligand dte was synthesized similar to the method of Kamiya and Saito in a 500 mmol batch.^[15] Yield: 54.7 g (329 mmol, 66 %). DTA (5 °C min⁻¹) onset: 133 °C (melting), 194 °C (decomp.); ¹H NMR (270 MHz, [D₆]DMSO, 25 °C, TMS): 9.33 (s, 2 H, N₄CH), 5.04 ppm (s, 4 H, CH₂); ¹³C{¹H} NMR (68 MHz, [D₆]DMSO, 25 °C, TMS): 144.3 (N₄CH), 46.9 ppm (CH₂); IR (ATR): $\tilde{\nu} = 3119$ (m), 3025 (vw), 2977 (vw), 1811 (vw), 1576 (vw), 1506 (vw), 1480 (m), 1460 (vw), 1443 (m), 1428 (m), 1393 (vw), 1383 (vw), 1324 (w), 1303 (w), 1252 (m), 1169 (m), 1122 (m), 1092 (s), 1022 (m), 964 (s), 908 (s), 770 (m), 722 (w), 691 (m), 683 (m), 671 cm⁻¹ (vs); elemental analysis calcd (%) for C₄H₆N₈ (166.14 g mol⁻¹): C 28.92, H 3.64, N 67.44; found: C 28.80, H 3.49, N 66.41; BAM impact: 40 J; BAM friction 360 N; ESD: 0.75 J (at grain size 100–500 μm).

Metal(II) complexes (2–21): The complexes have been synthesized via three similar methods:

A) To a 70 °C warm solution of **1** (332 mg, 2 mmol) in water (20 mL) was added an aqueous solution of the corresponding metal(II) salt (**3–6**: 1.00 mmol of $M(\text{ClO}_4)_2 \cdot 6 \text{H}_2\text{O}$; **2, 7**: 1.00 mmol of $M(\text{ClO}_4)_2 \cdot x \text{H}_2\text{O}$; **10**: 1.00 mmol $\text{Cu}(\text{NO}_3)_2 \cdot 3 \text{H}_2\text{O}$; **11**: 1.00 mmol $\text{Zn}(\text{NO}_3)_2 \cdot 6 \text{H}_2\text{O}$; **12**: 1.00 mmol $\text{Cd}(\text{NO}_3)_2 \cdot 4 \text{H}_2\text{O}$; **13**: 1.00 mmol $\text{CuCl}_2 \cdot 2 \text{H}_2\text{O}$). The colored solution was left for crystallization. Within a few hours or days, the products precipitated from the mother liquor. The solids were filtered off, washed and dried in air.

B) To a 70 °C warm solution of **1** (**14, 15–20**: 332 mg, 2 mmol; **21**: 166 mg, 1 mmol) and copper(II) sulfate pentahydrate (**14, 16, 18–20**: 1.00 mmol; **15, 17, 21**: 2.00 mmol) in water (15 mL) was added an aqueous solution of an appropriate alkali-salt (**14**: 2.00 mmol of KClO_3 ; **15**: 4.00 mmol of NaNO_2 ; **16**: 2.00 mmol of $\text{KN}(\text{NO}_2)_2$; **17**: 6.00 mmol of $\text{NaN}(\text{CN})(\text{NO}_2)$; **18**: 2.00 mmol of $\text{NaN}(\text{CN})(\text{NO}_2)$; **19**: 2.00 mmol of $\text{KC}(\text{NO}_2)_3$; **20**: 2.00 mmol of $\text{KC}(\text{CN})(\text{NO}_2)_2$, **21**: 4.00 mmol of NaN_3). The clear solutions were left for crystallization until a crystalline solid appeared. The obtained single crystals were filtered off, washed with a small amount of water and then air dried.

C) To a 70 °C warm solution of **1** (332 mg, 2 mmol) in water (20 mL) was added an aqueous solution of the corresponding metal(II) salt (**8** and **9**: 1.00 mmol of $M(\text{NO}_3)_2 \cdot 6 \text{H}_2\text{O}$). The colored solution was left for crystallization. Within a day, the products precipitated as powders. The solids were filtered off, washed and dried at 120 °C in the oven to remove crystal water.

8.6. References

- [1] a) K. O. Christe, W. W. Wilson, M. A. Petrie, H. H. Michels, J. C. Bottaro, R. Gilardi, *Inorg. Chem.* **1996**, *35*, 5068–5071; b) T. M. Klapötke, D. G. Piercey, *Inorg. Chem.* **2011**, *50*, 2732–2734; c) Q. Zhang, J. n. M. Shreeve, *Angew. Chem., Int. Ed.* **2013**, *52*, 8792–8794; d) T. Klapötke, N. Fischer, D. Fischer, D. G. Piercey, J. Stierstorfer, M. Reymann, *DE 102011081254 A1*, February 21, **2013**; e) C. He, J. Zhang, D. A. Parrish, J. n. M. Shreeve, *J. Mater. Chem. A* **2013**, *1*, 2863–2868; f) D. E. Chavez, D. Parrish, D. N. Preston, I. W. Mares, *Propellants, Explos., Pyrotech.* **2012**, *37*, 647–652.
- [2] T. M. Klapötke, *Chemie der hochenergetischen Materialien*, 1. ed., Walter de Gruyter, Berlin, New York, **2009**.
- [3] R. Matyáš, J. Pachman, *Primary Explosives*, 1. ed., Springer, Heidelberg, New York, Dordrecht, London, **2013**.
- [4] a) J. Fronabarger, M. Williams, M. Bichay, *Joint Armaments Conference*, Dallas, USA, May 20, **2010**; b) J. W. Fronabarger, M. D. Williams, W. B. Sanborn, J. G. Bragg, D. A. Parrish, M. Bichay, *Propellants, Explos., Pyrotech.* **2011**, *36*, 541–550.

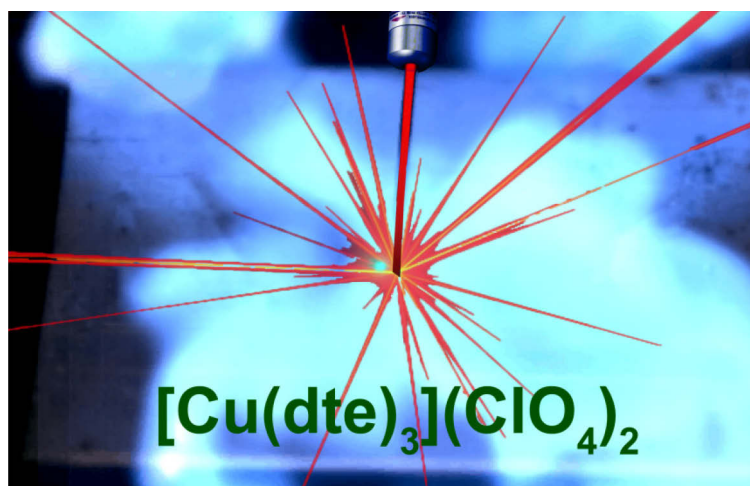
- [5] a) B. Morosin, R. G. Dunn, R. Assink, T. M. Massis, J. Fronabarger, E. N. Duesler, *Acta Crystallogr., Sect. C: Cryst. Struct. Commun.* **1997**, C53, 1609–1611; b) A. Y. Zhilin, M. A. Ilyushin, I. V. Tselinskii, A. S. Brykov, *Russ. J. Appl. Chem.* **2001**, 74, 99–102; c) M. B. Talawar, A. P. Agrawal, J. S. Chhabra, S. N. Asthana, *J. Hazard. Mater.* **2004**, 113, 57–65; d) S. Qi, Z. Li, T. Zhang, Z. Zhou, L. Yang, J. Zhang, X. Qiao, K. Yu, *Huaxue Xuebao* **2011**, 69, 987–992.
- [6] Q. Zhang, J. n. M. Shreeve, *Angew. Chem., Int. Ed.* **2014**, 53, 2540–2542.
- [7] S. G. Zhu, Y. C. Wu, W. Y. Zhang, J. Y. Mu, *Propellants, Explos., Pyrotech.* **1997**, 22, 317–320.
- [8] R. Varosh, *Propellants, Explos., Pyrotech.* **1996**, 21, 150–154.
- [9] E. S. Hafenrichter, B. W. Marshall, K. J. Fleming, *41st Aerospace Sciences Meeting and Exhibit*, Reno, USA, January 6–9, **2003**.
- [10] a) A. A. Brish, I. A. Galeeva, B. N. Zaitsev, E. A. Sbimev, L. V. Tararinstev, *Fiz. Goreniya Vzryva* **1966**, 2, 132; b) A. A. Brish, I. A. Galeeva, B. N. Zaitsev, E. A. Sbimev, L. V. Tararinstev, *Fiz. Goreniya Vzryva* **1969**, 5, 475; c) L. C. Yang, V. J. Menichelli, *Appl. Phys. Lett.* **1971**, 19, 473–475; d) L. C. Yang, J. Menichelli, *US 3812783*, May 28, **1974**.
- [11] a) M. A. Ilyushin, I. V. Tselinsky, I. A. Ugryumov, A. Y. Zhilin, A. S. Kozlov, *6th New Trends in Research of Energetic Materials Seminar*, Pardubice, Czech Republic, April 22–24, **2003**, 146–152; b) I. A. Ugryumov, M. A. Ilyushin, I. V. Tselinskii, A. S. Kozlov, *Russ. J. Appl. Chem.* **2003**, 76, 439–441; c) M. A. Ilyushin, I. V. Tselinskiy, A. V. Smirnov, I. V. Shigalei, *Cent. Eur. J. Energ. Mater.* **2012**, 9, 3–16.
- [12] V. P. Sinditskii, V. V. Seurshkin, *Defence Science Journal* **1996**, 46, 371–383.
- [13] a) M. Joas, T. M. Klapötke, J. Stierstorfer, N. Szimhardt, *Chem. - Eur. J.* **2013**, 19, 9995–10003; b) M. Joas, T. M. Klapötke, N. Szimhardt, *Eur. J. Inorg. Chem.* **2014**, 2014, 493–498; c) N. Fischer, M. Joas, T. M. Klapötke, J. Stierstorfer, *Inorg. Chem.* **2013**, 52, 13791–13802.
- [14] a) P. J. van Koningsbruggen, Y. Garcia, G. Bravic, D. Chasseau, O. Kahn, *Inorg. Chim. Acta* **2001**, 326, 101–105; b) P.-P. Liu, A.-L. Cheng, N. Liu, W.-W. Sun, E.-Q. Gao, *Chem. Mater.* **2007**, 19, 2724–2726; c) R.-Y. Li, X.-Y. Wang, T. Liu, H.-B. Xu, F. Zhao, Z.-M. Wang, S. Gao, *Inorg. Chem.* **2008**, 47, 8134–8142; d) R.-Y. Li, B.-W. Wang, X.-Y. Wang, X.-T. Wang, Z.-M. Wang, S. Gao, *Inorg. Chem.* **2009**, 48, 7174–7180.
- [15] T. Kamiya, Y. Saito, *DE 2147023*, March 29, **1973**.
- [16] a) P.-P. Liu, A.-L. Cheng, Q. Yue, N. Liu, W.-W. Sun, E.-Q. Gao, *Cryst. Growth Des.* **2008**, 8, 1668–1674; b) P. Weinberger, K. Mereiter, *CCDC Private Communication* **2007**, CCDC 658097; c) M. Joas, T. M. Klapötke, *Z. Anorg. Allg. Chem.* **2014**, 640, 1886–1891.

- [17] a) J. Schweifer, P. Weinberger, K. Mereiter, M. Boca, C. Reichl, G. Wiesinger, G. Hilscher, P. J. van Koningsbruggen, H. Kooijman, M. Grunert, W. Linert, *Inorg. Chim. Acta* **2002**, *339*, 297–306; b) K. Karaghiosoff, T. M. Klapötke, C. M. Sabate, *Chem. - Eur. J.* **2009**, *15*, 1164–1176.
- [18] R. Sharma, R. P. Sharma, R. Bala, B. M. Kariuki, *J. Mol. Struct.* **2007**, *826*, 177–184.
- [19] T.-H. Lu, S.-C. Lin, H. Aneetha, K. Panneerselvam, C.-S. Chung, *J. Chem. Soc., Dalton Trans.* **1999**, 3385–3391.
- [20] A. A. Holder, R. T. Stibrany, N. Bolotina, M. Hall, V. C. R. Payne, K. Kirschbaum, A. A. Pinkerton, A. M. Newton, *J. Chem. Crystallogr.* **2004**, *34*, 383–386.
- [21] a) L. He, G.-H. Tao, D. A. Parrish, J. n. M. Shreeve, *Chem. - Eur. J.* **2010**, *16*, 5736–5743, S5736/5731–S5736/5737; b) J. Kohout, M. Hvastijovi, J. Kozisek, D. J. Garcia, M. Valko, L. Jager, I. Svoboda, *Inorg. Chim. Acta* **1999**, *287*, 186–192.
- [22] N. V. Podberezkaya, N. V. Pervukhina, V. P. Doronina, *Zh. Strukt. Khim.* **1991**, *32*, 34–39.
- [23] a) B. Klewe, *Acta Chem. Scand.* **1972**, *26*, 1921–1930; b) R. Wang, H. Gao, C. Ye, B. Twamley, J. n. M. Shreeve, *Inorg. Chem.* **2007**, *46*, 932–938; c) Q. Qiu, K. Xu, S. Yang, Z. Gao, H. Zhang, J. Song, F. Zhao, *J. Solid State Chem.* **2013**, *205*, 205–210.
- [24] M. Hesse, H. Meier, B. Zeeh, *Spektroskopische Methoden der organischen Chemie*, 7. ed., Thieme, Stuttgart, New York, **2005**.
- [25] D. L. Lewis, E. D. Estes, D. J. Hodgson, *J. Cryst. Mol. Struct.* **1975**, *5*, 67–74.
- [26] F. A. Miller, C. H. Wilkins, *Anal. Chem.* **1952**, *24*, 1253–1294.
- [27] W. Sterzel, W. D. Schnee, *Z. Anorg. Allg. Chem.* **1971**, *383*, 231–239.
- [28] A. L. Lott, II, *J. Amer. Chem. Soc.* **1971**, *93*, 5313–5314.
- [29] H.-G. Ang, W. Fraenk, K. Karaghiosoff, T. M. Klapötke, P. Mayer, H. Nöth, J. Sprott, M. Warchhold, *Z. Anorg. Allg. Chem.* **2002**, *628*, 2894–2900.
- [30] V. V. Mel'nikov, I. V. Tselinskii, I. N. Shokhor, A. G. Gal'kovskaya, *Zh. Prikl. Spektrosk.* **1969**, *10*, 283–289.
- [31] a) I. Agrell, *Acta Chem. Scand.* **1971**, *25*, 2965–2974; b) K. Dehnicke, *Z. Anorg. Allg. Chem.* **1974**, *409*, 311–319.
- [32] Impact: insensitive > 40 J, less sensitive \geq 35 J, sensitive \geq 4 J, very sensitive \leq 3 J; Friction: insensitive > 360 N, less sensitive = 360 N, sensitive < 360 N and > 80 N, very sensitive \leq 80 N, extremely sensitive \leq 10 N, According to: *Recommendations on the Transport of Dangerous Goods, Manual of Tests and Criteria*, 4th edition, United Nations, New York - Geneva, **1999**.
- [33] N. K. Bourne, *Proc. R. Soc. A* **2001**, *457*, 1401–1426.
- [34] a) NATO Standardization Agreement 4489, September 17, **1999**; b) NATO Standardization Agreement 4487, October 29, **2009**.

-
- [35] <http://www.ozm.cz> (accessed March 13, **2014**).
- [36] NATO Standardization Agreement 4515, August 23, **2002**.
- [37] <http://www.agilent.com/> (accessed March 13, **2014**).
- [38] a) *CrysAlisPro 1.171.35.11*, Oxford Diffraction Ltd., Abingdon, UK, **2011**; b) *CrysAlisPro 1.171.36.21*, Oxford Diffraction Ltd., Abingdon, UK, **2012**; c) *CrysAlisPro 1.171.36.24*, Oxford Diffraction Ltd., Abingdon, UK, **2012**.
- [39] a) A. Altomare, M. C. Burla, M. Camalli, G. L. Casciarano, C. Giacovazzo, A. Guagliardi, A. G. G. Moliterni, G. Polidori, R. Spagna, *J. Appl. Cryst.* **1999**, *32*, 115–119; b) M. C. Burla, R. Calianro, M. Camalli, B. Carrozzini, G. L. Casciarano, L. De Caro, C. Giacovazzo, G. Polidori, R. Spagna, *J. Appl. Cryst.* **2005**, *38*, 381–388.
- [40] G. M. Sheldrick, *Acta Crystallogr. Sect. A* **2008**, *A64*, 112–122.
- [41] <http://journals.iucr.org/services/cif/checkcif.html> (accessed March 24, **2014**).
- [42] <http://www.elementar.de/> (accessed March 13, **2014**).
- [43] <http://www.perkinelmer.de/> (accessed March 13, **2014**).
- [44] <http://www.jeol.co.jp/en/> (accessed April 2, **2014**).
- [45] P. Kubelka, F. Munk, *Z. Tech. Phys.* **1931**, *1*, 593–601.

9. A Study on the Effect of the Metal Center, Ligand, and Anion on the Laser Ignitability of Energetic Coordination Compounds

Unpublished work.



9.1. Abstract

Various transition metal complexes of the nitrogen-rich ligands 1,2-di(1*H*-tetrazol-1-yl)ethane (**1**, dte), 1,2-di(1*H*-tetrazol-1-yl)propane (**2**, dtp), and 1,4-di(1*H*-tetrazol-1-yl)butane (**3**, dtb) were synthesized, characterized by infrared spectroscopy, and finally their behavior toward laser irradiation investigated. A diode laser emitting single pulses at 940 nm served as radiation source. Further, the ignitability, the function time, and the energy output of the samples were measured. It was shown that the copper compounds exhibited the highest sensitivity toward laser irradiation whereas zinc showed the lowest. The anion and the ligand do not have a great effect on the ignitability but strongly influence the function time and the type of decomposition reaction. While perchlorates and chlorates undergo a deflagration-to-detonation transition after successful initiation, dinitramides tend to deflagrate and nitrates only partially decompose. Finally, the tris(1,2-di(1*H*-tetrazol-1-yl)ethane)metal(II) perchlorates **4–8** were shown to be potential laser ignitable primary explosives.

9.2. Introduction

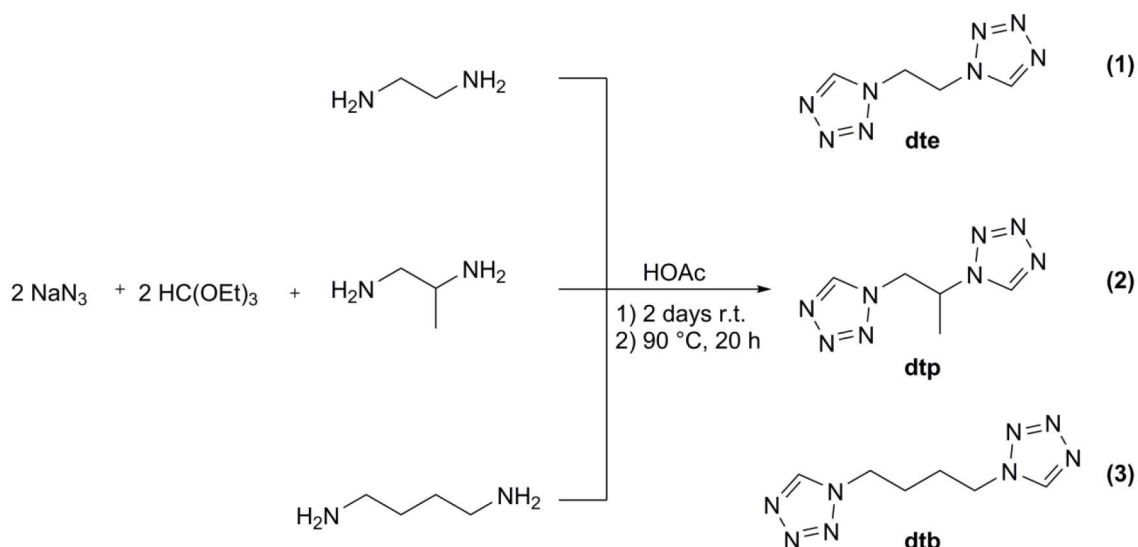
Because of several advantages over electric (e.g. hot-wire, exploding-bridgewire, or exploding foil initiator) or mechanical initiation (e.g. stab),^[1] the ignition and initiation of energetic materials by laser irradiation represents a recent and intensive investigated technique.^[2] It ensures a high level of safety due to its good isolation of the initiating substance from undesired stimulating impulses. However, to be a potential replacement for

the very accurate and fast-functioning exploding-bridgewire (EBW) and exploding foil initiators (EFI), it is necessary to exhibit a low ignition delay in the range of microseconds and a fast deflagration-to-detonation transition (DDT).^[1] One approach to reduce the ignition delay time is the use of high-power short-pulsed laser radiation sources like neodymium or ruby glass lasers, which enable power densities in the order of GW cm^{-2} and act in the nanosecond range. But laser diodes are much more capable for practical use although they provide a lower energy output.^[1] To compensate the low power, investigation and development of photosensitive energetic materials has started. Especially complex perchlorates with hydrazinoazoles (e.g. 3-hydrazino-5-aminopyrazole, 3-hydrazino-4-amino-1,2,4-triazole, or 5-hydrazino-1*H*-tetrazole) as ligands represent a novel class of explosives providing a high susceptibility to laser radiation.^[3] For example, 5-hydrazino-1*H*-tetrazolemercury(II) perchlorate (HTMP) exhibits one of the lowest initiation energies with a value of $1 \cdot 10^{-5}$ J.^[3a] Further, hydrazinoazoles (5-(1-methylhydrazinyl)-1*H*-tetrazole and 1,2-bis[5-(1-methylhydrazinyl)tetrazol-1-yl]ethane) containing complexes were investigated upon their behavior toward laser irradiation by our research group.^[4]

Due to the fact that the laser initiation mechanism is not completely understood,^[2a,2b,5] systematic design of new photosensitive energetic materials is difficult. The first step to facilitate the design would be to investigate the influence of the individual components of the photosensitive coordination compounds on the laser ignitability. To achieve a good comparability, it is necessary to investigate complexes which exhibit identical structures and only differ in the analyzed component. The three components to be analyzed are the metal center, the energetic ligand and the anion. A first qualitative study about the influence of the metal center and the anion was done by our research group with the nitrogen-rich ligand 1,2-di(1*H*-tetrazol-1-yl)ethane (dte).^[6] But to perform a quantitative analysis and investigate also the ligands role, in this work metal(II) complexes of the form $[\text{M}(1,2\text{-di}(1\text{H-tetrazol-1-yl})\text{alkane})_3]\text{X}_2$ ($\text{M} = \text{Fe}^{2+}$, Co^{2+} , Ni^{2+} , Cu^{2+} , and Zn^{2+} ; ligand = ethane (dte), propane (dtp), and butane (dtb); $\text{X} = \text{ClO}_4^-$, ClO_3^- , NO_3^- , and $\text{N}(\text{NO}_2)_2^-$) were prepared and investigated quantitatively on their behavior toward laser irradiation by measuring their function times. As laser radiation source, a diode laser at a wavelength of 940 nm was used. Some of the investigated complexes have been partly described in literature,^[7] but none of them characterized as energetic materials until now.

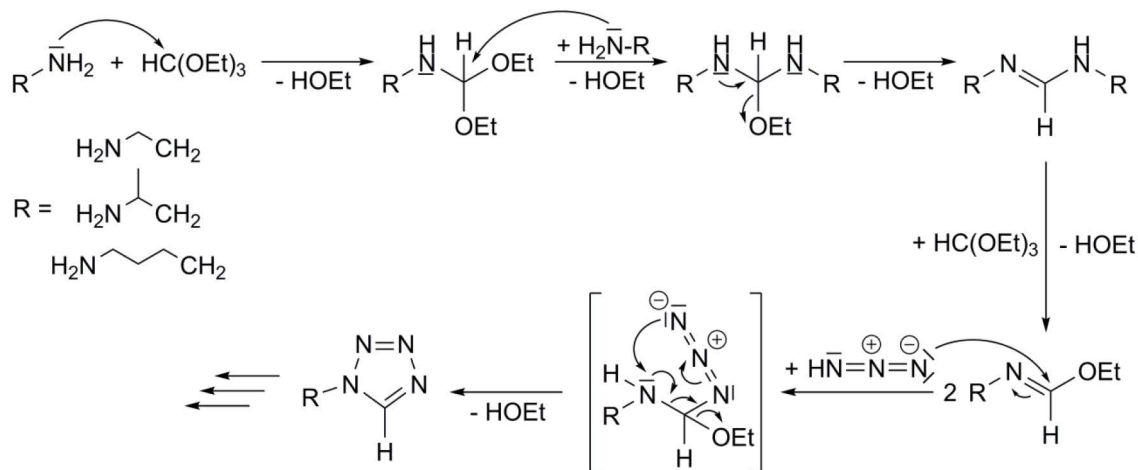
9.3. Results and Discussion

Synthesis: The nitrogen-rich ligands dte (**1**), dtp (**2**), and dtb (**3**) were prepared in a slightly modified way similar to the method for 1*H*-tetrazoles by Kamiya and Saito (Scheme 1).^[8] A possible reaction mechanism (see Scheme 2) for the cyclization reaction of primary amines with azide and triethylorthoformate was suggested by Gaponik *et al.*^[9]



Scheme 1. Synthesis of dte (1), dtp (2), and dtb (3) by a procedure slightly modified to the method of Saito and Kamiya.^[8]

The suggested mechanism fits to the observed increase of yield when stirring the reaction mixture for two days at room temperature before heating up to 90 °C. During this time, the nucleophilic attack of the amine to the orthoester and the further reaction occur. It seems that the subsequent attack of the azide and the ring closure firstly proceeds with heating the reaction mixture to 80–90 °C for several hours. In the case of **1**, previous stirring of the reaction mixture for two days increased the yield from ~40 to 66 % in contrast to direct heating.

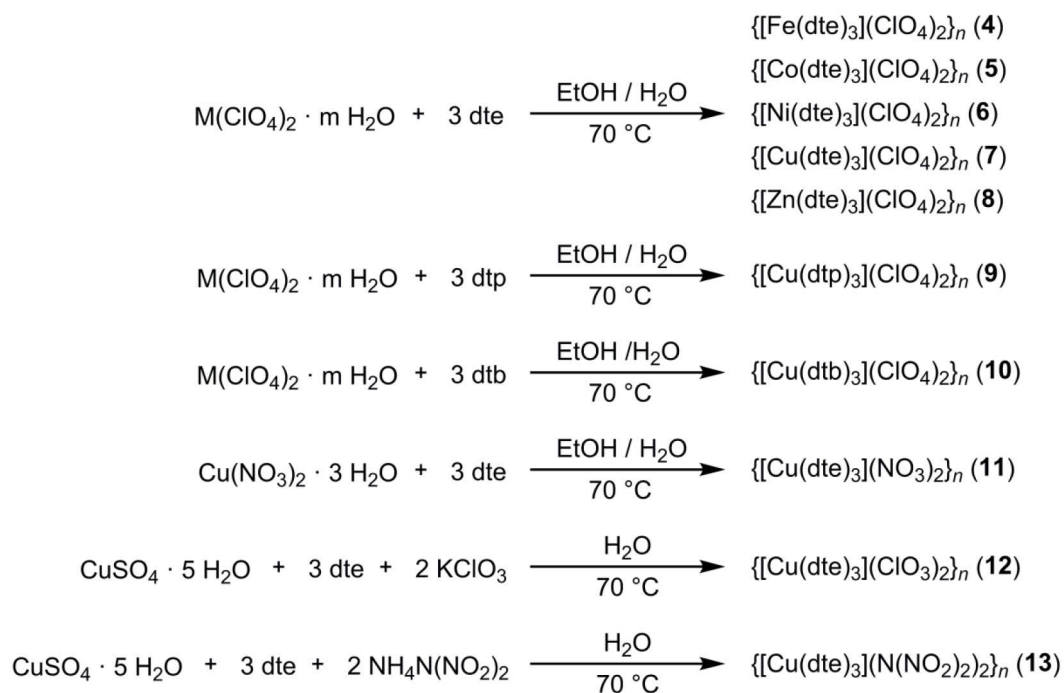


Scheme 2. Possible reaction mechanism suggested by Gaponik *et al.*^[9]

The complexes were prepared via two ways:

(i) The ligand was solved in hot ethanol and a concentrated aqueous metal(II) perchlorate or nitrate solution added (Scheme 2). Cooling the solutions under stirring to room temperature yielded fine powders with grain sizes smaller 100 μm .

(ii) The ligand was solved in hot water and a concentrated aqueous copper(II) sulfate solution added (Scheme 3). Addition of potassium chlorate or ammonium dinitramide to the reaction mixture yielded the corresponding copper(II) complexes after a few days. The filtered complexes were solved in hot water and added to an excess of ice-cooled propan-2-ol to precipitate the product as fine powder.



Scheme 3. Synthesis of the metal complexes 4–13.

Infrared spectroscopy: The ligand 1–3 and all complexes 4–13 were characterized by infrared spectroscopy. Characteristic vibrations were assigned referring to literature.^[10] The $\nu(\text{C-H})$ vibration is nearly identical for 1 (3119 cm^{-1}) and 3 (3116 cm^{-1}) whereas it is splitted and shifted to higher wavenumbers for 2 (3136 and 3125 cm^{-1}) owing to its asymmetric structure. In the spectrum of 1 are four $\nu(\text{C-H}_2)$ vibrations observed (3025, 2988, 2977, and 2947 cm^{-1}) which are shifted to higher wavenumbers compared to 3 (2961, 2947, 2926, and 2872 cm^{-1}).

Table 1. Wavenumbers [cm^{-1}] of selected infrared active vibrations for 1–3.

	1	2	3
$\nu(\text{C-H})$	3119	3136 + 3125	3116
$\nu(\text{N}_2=\text{N}_3)$	1480	1484 + 1473 + 1465	1491
$\delta(\text{CH}_2)$	1443 + 1428	1435 + 1423	1450 + 1422
$\nu(\text{C}_1=\text{N}_4, \text{N}_1-\text{N}_2)$	1169	1177 + 1161	1172
$\nu(\text{C-C})$	1092	1104 + 1095 + 1086	1106

Absorption bands between 3016 and 2895 cm^{-1} can be assigned to the C–H valence vibrations of the CH, CH₂ and CH₃ group of 2. Further, the infrared spectra of 1 and 3 exhibit an

identical number of bands for the $\nu(\text{N2=N3})$, $\delta(\text{CH}_2)$, $\nu(\text{C1=N4, N1-N2})$, and $\nu(\text{C-C})$ vibrations whereas they are partly splitted for **2**. This is again the result of the asymmetry of **2**. The IR spectra of **1–3** are shown in Figure 1 and selected vibrations in Table 1.

All investigated complexes **4–13** exhibit a typical coordination induced shifting compared to the free ligand. An overview of selected vibrations is given in Table 2 and 3. The anion vibrations were assigned referring to literature.^[11]

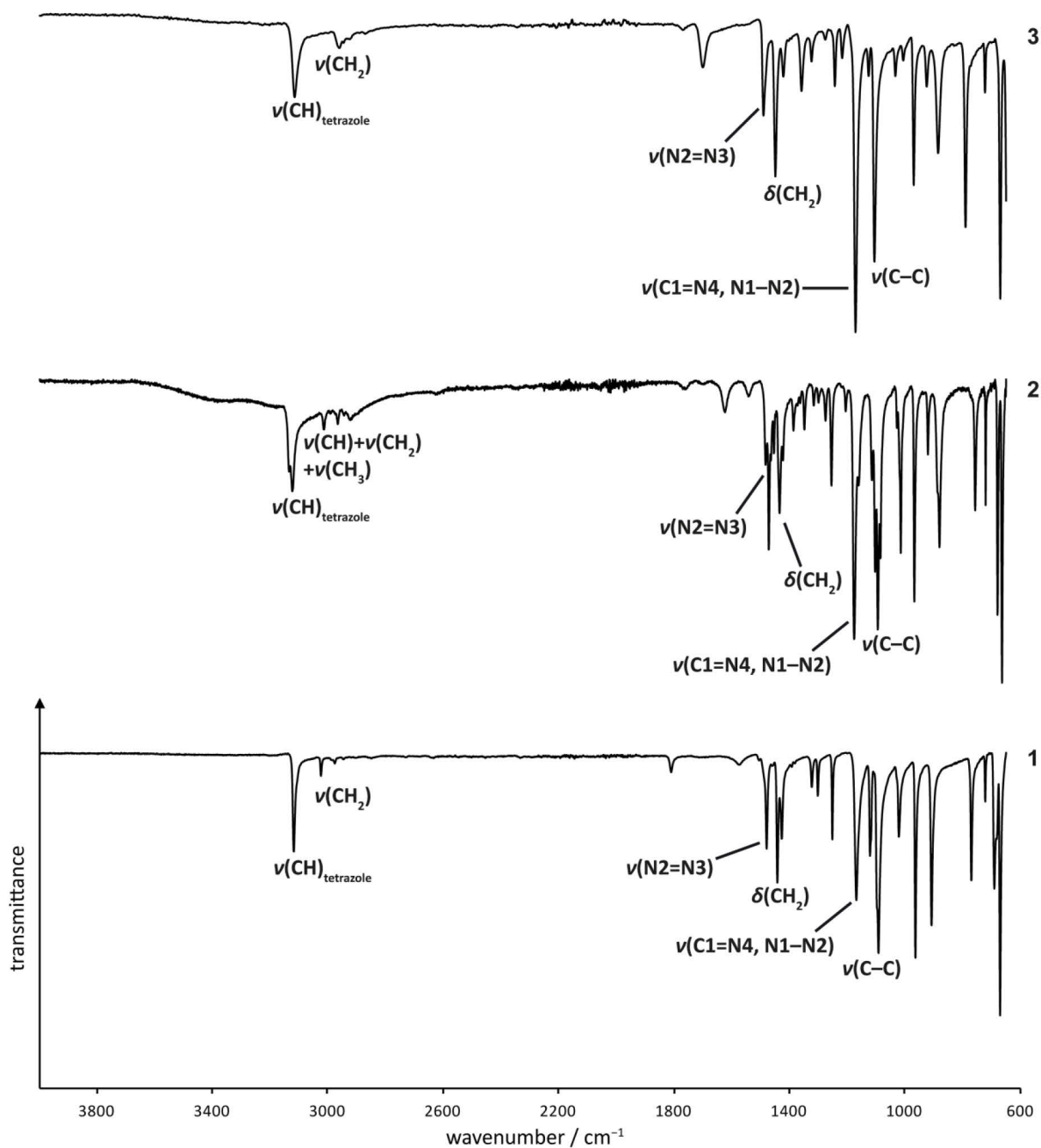


Figure 1. Infrared spectra of **1–3**.

Table 2. Wavenumbers [cm^{-1}] of selected infrared active vibrations for **4–6** and **8**.

	4	5	6	8
$\nu(\text{C-H})$	3132	3135	3140	3134
$\nu(\text{N2=N3})$	1507 + 1497	1508 + 1497	1509 + 1497	1507 + 1497
$\nu(\text{C1=N4, N1-N2})$	1182	1182	1184	1182
$\nu(\text{ClO}_4)$	1083	1083	1083	1083

As expected, the infrared spectra of the perchlorates **4–8** are nearly identical and the wavenumbers only differ slightly. This is an indication that **4–8** exhibit similar structures implicating a good comparability of the metal centers for the laser initiation experiments.

Interestingly, all three different copper(II) perchlorate complexes **7**, **9** and **10** show only one C–H valence vibration for the tetrazole ring and this vibration is further observed at nearly the same wavenumber ($3137\text{--}3136\text{ cm}^{-1}$). Thus it can be concluded that the tetrazole ring coordinates to the copper(II) center over the same nitrogen position (N4 according to literature)^[7b] for all three. This coordination strengthens the C–H valence vibration and influences it more than the kind of alkyl moiety (ethyl, 1-methylethyl, or butyl) at the N1 position. The C–H valence vibrations of the perchlorates **4–6** and **8** were also detected in a range of $3140\text{--}3132\text{ cm}^{-1}$ explained by the same reason. In contrast, $\nu(\text{C-H})$ is observed at lower wavenumbers for the nitrate (3096 and 3087 cm^{-1}) and chlorate (3098 cm^{-1}) complexes **11** and **12** as a result of different structures compared to **4–8**. Whereas in complex **7** all dte ligands are existent in a *gauche* conformation, the dte is *anti*-oriented in **11** and half *gauche*, half *anti* in **12** according to literature.^[6,7b]

The very strong absorption in the spectrum of **11** at 1350 cm^{-1} can be assigned to the nitrate, the strong one in the spectrum of **12** at 964 cm^{-1} to the chlorate and the two strong bands at 1514 and 1175 cm^{-1} in the spectrum of **13** to the dinitramide anion.

Table 3. Wavenumbers [cm^{-1}] of selected infrared active vibrations for **7** and **9–13**.

	7	9	10
$\nu(\text{C-H})$	3136	3136	3137
$\nu(\text{N2=N3})$	1500 + 1491	1498	1510 + 1498
$\nu(\text{C1=N4, N1-N2})$	1179	1184	1181 + 1176
$\nu(\text{ClO}_4)$	1081	1080	1088
	11	12	13
$\nu(\text{C-H})$	3096 + 3087	3098	3134 + 3124
$\nu(\text{N2=N3})$	1505 + 1492	1504	1492
$\nu(\text{C1=N4, N1-N2})$	1189	1189	1191
$\nu(\text{NO}_3)$	1350	-	-
$\nu(\text{ClO}_3)$	-	964	-
$\nu(\text{N}(\text{NO}_2)_2)$	-	-	1514 + 1175

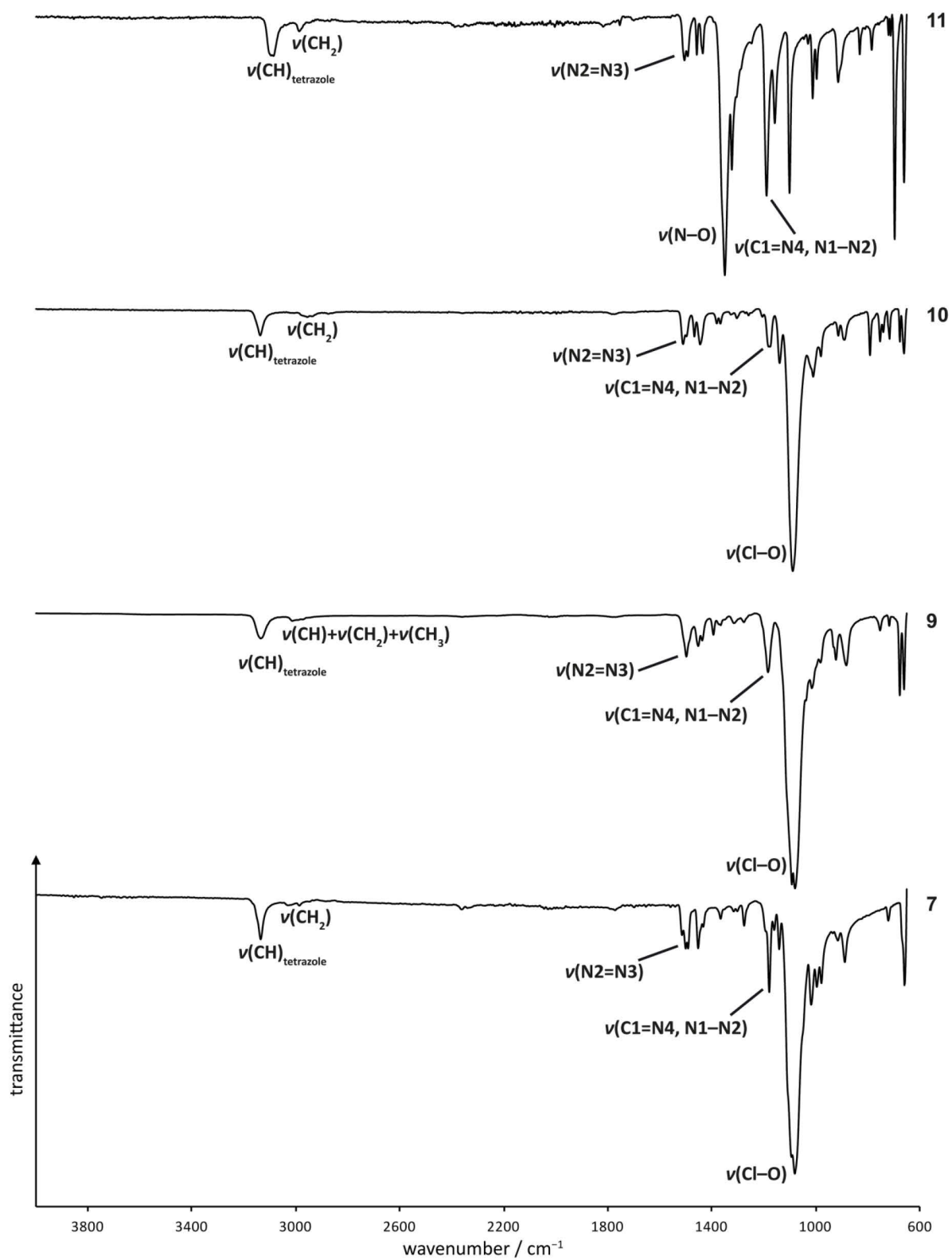


Figure 2. Infrared spectra of 7 and 9–11.

Energetic properties and laser ignition: The mechanical and thermal stabilities of the investigated complexes **4–13** were determined and classified according the UN Recommendations on the Transport of Dangerous Goods.^[12] An overview about the energetic properties and laser ignition and initiation results is given in Table 4 and 5.

Table 4. Energetic properties and laser initiation results of the perchlorate complexes **4–8**.

	4	5	6	7	8
Metal cation	Fe ²⁺	Co ²⁺	Ni ²⁺	Cu ²⁺	Zn ²⁺
T_{decomp} (onset) [°C]	240	288	298	256	280
IS [J]	2	1	1	1.5	2
FS [N]	14	6	6	10	42
ESD [J]	0.08	0.25	0.25	0.15	0.30
Grain size [μm]	< 100	100–500	100–500	< 100	100–500
$F(R)$ at 940 nm ^[a]	0.104	0.075	0.029	0.006	0.000
ρ_{pellet} [g cm ⁻³] ^[b]	1.4	1.4	1.4	1.4	1.4
Laser ignition ^[c]	detonation	detonation	detonation	detonation	-
t_f [10 ⁻⁵ s] ^[d]	16.8±1.9	19.3±2.1	12.9±0.5	9.3±0.2	-

[a] Absorption intensity $F(R)$ at wavelength $\lambda = 940$ nm. [b] Density of sample pellets. [c] Parameters of the laser beam: $\lambda = 940$ nm, $\tau = 500$ μs, $\sigma = 105$ μm, $\Phi_e = 14$ W. [d] Average function time.

Table 5. Energetic properties and laser initiation results of the copper(II) complexes **9–13**.

	9	10	11	12	13
Ligand	ntp	ntb	nte	nte	nte
Anion	ClO ₄ ⁻	ClO ₄ ⁻	NO ₃ ⁻	ClO ₃ ⁻	N(NO ₂) ₂ ⁻
T_{decomp} (onset) [°C]	235	230	191	175	168
IS [J]	4	12.5	7	1.5	1
FS [N]	20	120	160	6	80
ESD [J]	0.15	0.25	1.0	0.015	0.25
Grain size [μm]	< 100	< 100	100–500	< 100	< 100
$F(R)$ at 940 nm ^[a]	0.019	-	0.007	0.001	0.026
ρ_{pellet} [g cm ⁻³] ^[b]	1.3	1.4	1.4	1.4	1.4
Laser ignition ^[c]	detonation	deflagration	combustion	detonation	deflagration
t_f [10 ⁻⁵ s] ^[d]	10.6 ^[f]	- ^[e]	3938.6 ^[f]	6.7±0.1	28.8 ^[f]

[a] Absorption intensity $F(R)$ at wavelength $\lambda = 940$ nm. [b] Density of sample pellets. [c] Parameters of the laser beam: $\lambda = 940$ nm, $\tau = 500$ μs, $\sigma = 105$ μm, $\Phi_e = 14$ W. [d] Average function time. [e] No function time determined due to incomplete reaction. [f] Only one value for function time measured due to problems with detection of the optical stop signal. Measurement of function time was not successful in every case.

The perchlorate complexes **4–8**, the chlorate **12**, and the dinitramide **13** are all very sensitive toward impact whereas **9–11** are classified as sensitive. Further, the complexes **5–7** and **12** are extremely sensitive toward friction. Very sensitive toward friction are the complexes **4, 8, 9**, and **13** whereas **10** and **11** are classified only as sensitive. The mechanical

stability of the $[\text{CuL}_3](\text{ClO}_4)_2$ complexes increases with the chain length of the alkyl-bridge and the carbon content in the following order:

dte (FS: 10 N, IS: 1.5 J) < dtp (FS: 20 N, IS: 4 J) < dtb (FS: 120 N, IS: 12.5 J)

However, the performance decreases in the same order. Therefore, it is necessary to make a compromise between performance and safety. For example, unconfined samples of **4–13** all deflagrate when touched with the tip of a hot needle. But the compounds **4–9** and **12** exhibit a better performance than the compounds **10**, **11** and **13**.

As expected, the perchlorates exhibit a higher thermal stability than the other investigated anions. The thermal stability of the $[\text{Cu}(\text{dte})_3]\text{X}_2$ complexes decreases in the following order: ClO_4^- (256 °C) > NO_3^- (191 °C) > ClO_3^- (175 °C) > $\text{N}(\text{NO}_2)_2^-$ (168 °C)

Varying the ligand also influences the thermal stability. Thus, a decrease of the decomposition temperature from dte (**7**: $T_{\text{decomp}} = 256$ °C) over dtp (**9**: $T_{\text{decomp}} = 235$ °C) to dtb (**10**: $T_{\text{decomp}} = 230$ °C) is observed for the corresponding $[\text{CuL}_3](\text{ClO}_4)_2$ complexes.

The laser initiation experiments were performed with a diode laser as radiation source emitting single pulses at 940 nm. The pulse length was set to 500 μs at a surface power density (also called irradiance) of 0.161 MW cm^{-2} . The laser radiation was brought onto the surface of the sample pellets by an optical fiber without focusing. The samples ($m = 0.15\text{--}0.20$ g) containing of 95 % coordination compound (powders with grain size < 100 μm) + 5 % polyethylene as binder were prepared by the following procedure: Polyethylene was solved in boiling *n*-hexane and the coordination compound (**4–13**) added under vigorous stirring. The suspension was slowly cooled to room temperature while stirring was maintained. After precipitation of polyethylene ceased, the solid was filtered off and dried under ambient conditions for several hours. Finally, the samples were pressed to pellets of a defined density and loaded into an aluminum cap, fixed on a witness plate, and connected to the optical fiber (Figure 3).

In case of a successful initiation, the function time (t_f , eq. 1) as the sum of the ignition delay time (t_i) and the transit time (t_t ; time for propagation of the reaction zone until breakout at the end of the device), was measured.

$$t_f = t_i + t_t \quad (1)$$

For function times in an order of 10^{-4} s and under the assumption of a transit time for DDT and propagation of the reaction of $2\text{--}10 \cdot 10^{-6}$ s, the measured function time can be equated to the ignition delay time in approximation.^[1] For faster function times in order of 10^{-6} s, it would be necessary to directly measure the ignition delay time similar to the method described by Hafenrichter *et al.*^[1]

For every complex, several samples were measured and the average value of the function times with its standard deviations (σ , equation 2) calculated.

$$\sigma = \sqrt{\frac{\sum(x-\bar{x})^2}{n}} \quad (2)$$

Where x is the sample mean value and n the number of samples.

Under the assumption of a process time for DDT of $2\text{--}10 \cdot 10^{-6}$ s, it is within the order of the standard deviation (e.g. $\pm 2.1 \cdot 10^{-5}$ s for **5** or $\pm 0.2 \cdot 10^{-5}$ s for **7**).

Based on previous results (e.g. positive influence of light absorbing additives on initiation threshold), it is supposed that the initiation mechanism is thermal.^[4c,6,13]

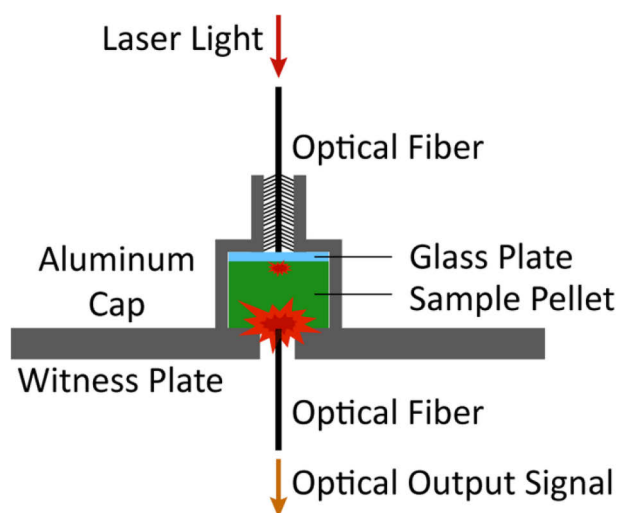


Figure 3. Schematic set up of the laser initiation experiments.

For a thermal mechanism according to literature,^[1,14] the laser initiation threshold, and correlated the ignition delay, depends on many parameters e.g. absorption intensity at the laser wavelength, mean particle size, sample density, thermal conductivity, and ignition temperature. To ensure a high comparability of the samples and for investigation of the samples influence depending on the cation, anion, and ligand it is necessary to keep as many parameters as possible constant. Thus, the power density, wavelength and pulse length of laser radiation, the mean particle size ($< 100 \mu\text{m}$), and the pressed density were kept constant. As it is literature known,^[14] every material has one specific density optimum for the best laser ignitability and one for the ability to undergo DDT. However, there is a trade-off problem because in many cases the two optimum densities do not converge and a compromise has to be made. To ascertain the optimum, the function time of **7** was determined for four different densities. A pressed density of 1.4 g cm^{-3} seems to be ideal for the similar $[\text{M}(\text{dte})_3](\text{ClO}_4)_2$ complexes and provided an average function time of $9.3 \pm 0.2 \cdot 10^{-5}$ s for **7**. For a density of 1.3 ($t_f = 12.6 \cdot 10^{-5}$ s), 1.5 ($t_f = 21.4 \cdot 10^{-5}$ s), and 1.6 g cm^{-3} ($t_f = 22.4 \cdot 10^{-5}$ s) not only the function time increased, also firing failures occurred and only one value was obtained respectively for these three densities. The increasing function time for higher densities might be explained by an increased thermal conductivity (particles are closer and in a better contact to each other; less isolating air pockets). The heat is superiorly conducted away from the

irradiated and heated increment. Thus, more energy is required to reach the ignition temperature. Additionally, the light reflection at the surface of the sample pellet is increased by a higher density. In contrast, lower densities influence the DDT process and not the ignition delay because propagation of the reaction front or shockwave is hindered. Furthermore, diffuse light scattering might be increased at low densities.

Comparing the laser initiation results leads to the conclusion that for similar complex structures mainly the type of metal cation influences the laser ignitability. Under the assumption that the perchlorate complexes **4–8** undergo DDT at a similar rate, the measured function times are an indicator for the ignitability. Thus, a lower value for the function time means also a lower value for the ignition delay and correlated to it a lower initiation energy threshold. In agreement with previous measurement data,^[6,13] copper(II) exhibits the lowest ignition delay of the investigated $[M(dte)_3](ClO_4)_2$ complexes with an average value for the function time of $9.3 \pm 0.2 \cdot 10^{-5}$ s. The second shortest function time is obtained for nickel (**6**), followed by iron (**4**) and cobalt (**5**). Zinc could not be initiated with a pulse length of 500 μ s. However, it is not understood which parameter mainly influences the initiation threshold. Comparing the function times to the absorption intensities at 940 nm (Table 4 and Figure 4), there is no simple relation even not in consideration of the decomposition temperatures. For example, the cobalt complex **5** exhibits a two and half times higher absorption intensity and a 10 °C lower decomposition temperature than the nickel compound **6** but its function time is one and a half times higher. It is also interestingly that the iron complex **4** exhibits the lowest decomposition temperature combined with the highest absorption intensity of the $[M(dte)_3](ClO_4)_2$ complexes although a higher value for the function time was measured than for copper **7** and nickel **6**.

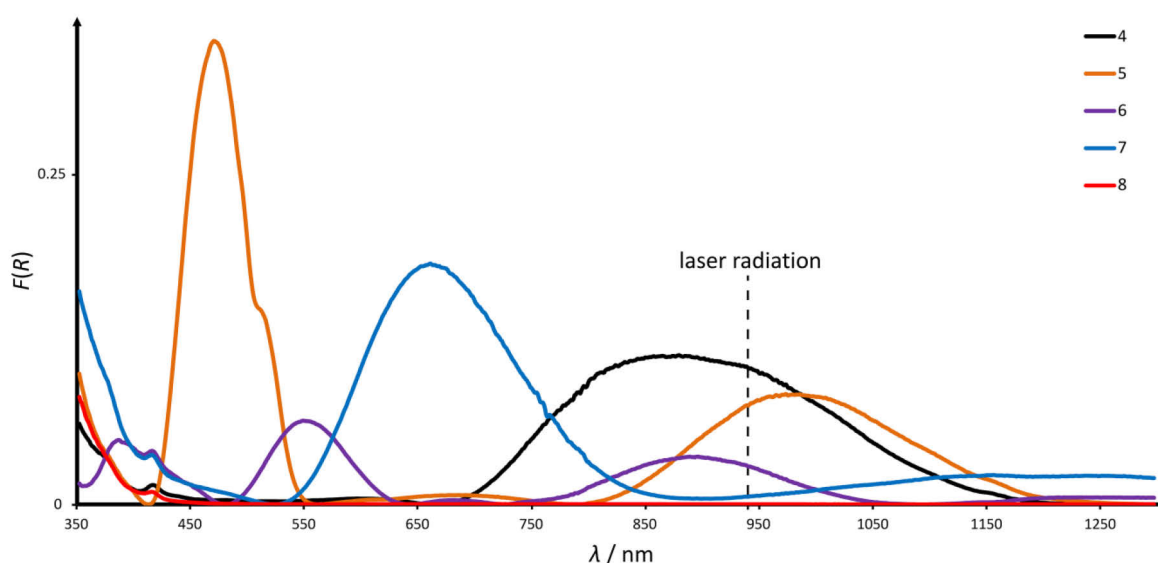


Figure 4. UV/Vis/NIR spectra of complexes **4–8**.

Further investigations are necessary but it might be possible that the material specific thermal conductivity plays an important role even though the influence of further parameters (e.g. temperature dependency of light absorption, ionization potential of the metal cation)^[3b,15] cannot be excluded.

Regarding the laser initiation results of the complexes **7** and **11–13** (see Table 4 and 5), it seems there are no major effects of the anion on the ignition threshold what also fits to previous experimental data (independent of the anion, nearly all copper(II) complexes could be initiated with a single laser pulse at $\tau = 100 \mu\text{s}$).^[4a,6] The increase of function time can be explained by the decrease of explosive power and burning rate as well as the decrease of the sensitivities in the order of: chlorate (**12**: detonation; $t_f = 6.7 \pm 0.1 \cdot 10^{-5} \text{ s}$; FS: 6 N) > perchlorate (**7**: detonation; $t_f = 9.3 \pm 0.2 \cdot 10^{-5} \text{ s}$; FS: 10 N) > dinitramide (**13**: deflagration; $t_f = 28.8 \cdot 10^{-5} \text{ s}$; FS: 80 N) > nitrate (**11**: combustion; $t_f = 39.4 \cdot 10^{-3} \text{ s}$; FS: 160 N) for the complexes of the form $[\text{M}(\text{dte})_3]\text{X}_2$. Depending on the anion, the DDT is slowed or even not undergone.

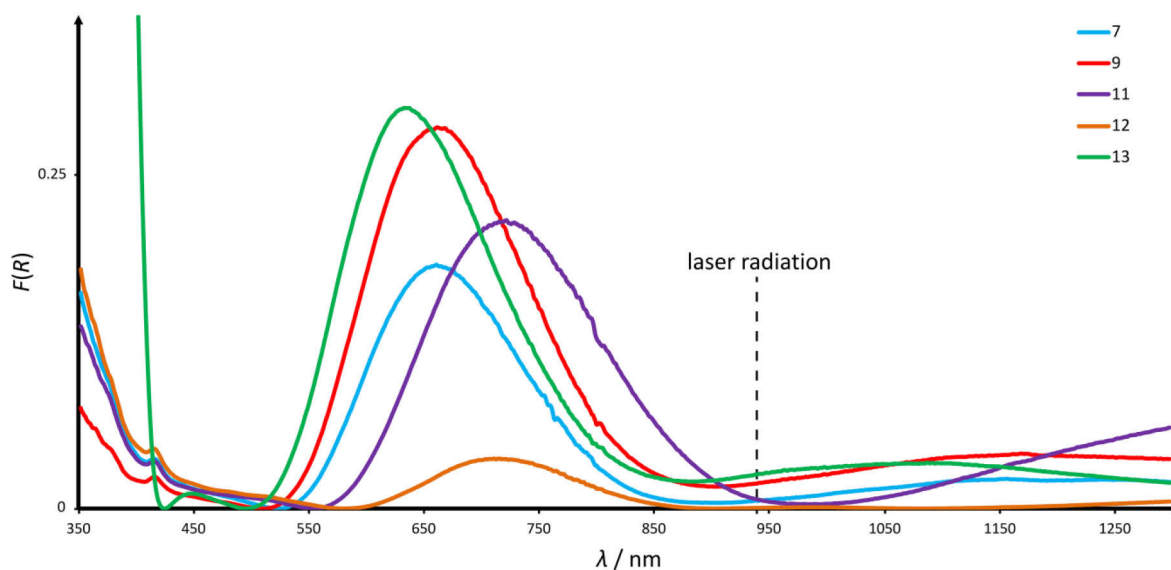


Figure 5. UV/Vis/NIR spectra of complexes **7**, **9** and **11–13**.

As already shown in literature,^[4c,16] the type of ligand has an effect on the initiation threshold if the structure is fundamental different (e.g. hydrazino-moieties can decrease the initiation threshold compared to non-hydrazine containing derivatives). However, the length of the alkyl chain of the herein investigated ditetrazoles mostly influences the performance (burning rate, power) of the complexes and not the initiation threshold. Thus, in agreement with their similar structures, complex **7** and **9** for example show nearly identical UV/Vis/NIR absorptions and only slightly differ in intensity. They further exhibit very similar function times with $93 \mu\text{s}$ for **7** and $106 \mu\text{s}$ for **9** explained by a slower DDT.

9.4. Conclusion

The synthesis and characterization (elemental analysis, IR and UV/Vis/NIR spectroscopy) of the following metal(II) perchlorate complexes of the formula $[ML_3]X_2$ with 1,2-di(1*H*-tetrazol-1-yl)ethane (**1**, dte), 1,2-di(1*H*-tetrazol-1-yl)propane (**2**, dtp), and 1,4-di(1*H*-tetrazol-1-yl)butane (**3**, dtb) as ligand is presented: $[Fe(dte)_3](ClO_4)_2$ (**4**), $[Co(dte)_3](ClO_4)_2$ (**5**), $[Ni(dte)_3](ClO_4)_2$ (**6**), $[Cu(dte)_3](ClO_4)_2$ (**7**), $[Zn(dte)_3](ClO_4)_2$ (**8**), $[Cu(dtp)_3](ClO_4)_2$ (**9**), $[Cu(dtb)_3](ClO_4)_2$ (**10**), $[Cu(dte)_3](NO_3)_2$ (**11**), $[Cu(dte)_3](ClO_3)_2$ (**12**), and $[Cu(dte)_3](N(NO_2)_2)_2$ (**13**). Owing to the similar structures, a high degree of comparability is provided and the influence of the cation, anion, and ligand on the laser ignitability could be investigated by measuring the function times. It was shown that the initiation threshold is mainly influenced by the metal center whereas the length of the alkyl-chain and the type of anion affects the rate of DDT. The copper(II) chlorate complex **12** exhibited the lowest value for the function time ($t_f = 6.7 \pm 0.1 \cdot 10^{-5}$ s) whereas the zinc(II) complex **8** was the only one which could not be initiated by a 500 μ s pulse at an irradiance (surface power density) of 0.161 MW cm^{-2} . Further, the sensitivities toward friction, impact, and electrostatic discharge as well as the temperature stabilities were determined for all complexes **4–13** and the following conclusions can be drawn: (i) the perchlorate complexes exhibited the highest temperature stabilities of the investigated compounds but are considerably more sensitive toward mechanical stimuli than nitrate and dinitramide, (ii) the thermal stability and the sensitivity toward mechanical stimuli decreases with increasing length of the alkyl chain, and (iii) the thermal stability decreases from nickel (**6**) over cobalt (**5**), zinc (**8**), and copper (**7**) to iron (**4**).

Finally it can be concluded that the perchlorate complexes **4–7** are interesting for laser initiated safe priming charges due to their good energetic properties and their facile and cheap synthesis.

9.5. Experimental Section

Caution! All of the metal(II) complexes prepared herein are energetic materials that show sensitivities toward various stimuli. Proper protective measures (safety glasses, face shield, leather coat, earthed equipment, conductive floor and shoes, Kevlar gloves, and ear plugs) should be used when handling these compounds. Extra safety precautions should be taken when compounds **4–9** and **12** are handled. These compounds are extremely sensitive toward impact, friction, and electrostatic discharge.

General Methods. All chemicals were used as supplied by ABCR, Acros Organics, AppliChem, Fluka, Sigma-Aldrich, and VWR. The impact and friction sensitivity tests were performed according to standard methods by using a BAM (Bundesanstalt für

Materialforschung und -prüfung) drop hammer and a BAM friction tester.^[17] The sensitivity toward electrostatic discharge was tested by using an OZM Research electric spark tester ESD 2010 EN.^[18] Decomposition temperatures were measured via differential thermal analysis (DTA) with an OZM Research DTA 552-Ex instrument at a heating rate of 5 °C min⁻¹ and in a range of room temperature to 400 °C.^[18-19]

The determination of the carbon, hydrogen and nitrogen contents was carried out by combustion analysis using an Elementar Vario EL.^[20] Infrared (IR) spectra were recorded on a Perkin-Elmer BXII FT-IR system with a Smith DuraSamplIR II diamond ATR unit.^[21] ¹H and ¹³C NMR spectra were recorded on a JEOL Eclipse 270 or a JEOL Eclipse 400 spectrometer.^[22] The UV/Vis/NIR reflectance of solid samples was determined with a Varian Cary 500 spectrometer in the wavelength range of 350–1300 nm.^[23] The reflectance *R* [%] was transformed by the Kubelka–Munk function to the absorption intensity *F(R)*.^[24]

1,2-Di(1*H*-tetrazol-1-yl)ethane (1): The ligand **1** was synthesized similar to the method of Kamiya and Saito in a 500 mmol batch.^[8] Yield: 54.7 g (329 mmol, 66 %). DTA (5 °C min⁻¹) onset: 133 °C (melting), 194 °C (decomp.); ¹H NMR (270 MHz, [D₆]DMSO, 25 °C, TMS): 9.33 (s, 2 H, N₄CH), 5.04 ppm (s, 4 H, CH₂); ¹³C{¹H} NMR (68 MHz, [D₆]DMSO, 25 °C, TMS): 144.3 (N₄CH), 46.9 ppm (CH₂); IR (ATR): $\tilde{\nu}$ = 3119 (m), 3025 (vw), 2988 (vw), 2977 (vw), 1811 (vw), 1576 (vw), 1506 (vw), 1480 (m), 1460 (vw), 1443 (m), 1428 (m), 1393 (vw), 1383 (vw), 1324 (w), 1303 (w), 1252 (m), 1169 (m), 1122 (m), 1092 (s), 1022 (m), 964 (s), 908 (s), 770 (m), 722 (w), 691 (m), 683 (m), 671 cm⁻¹ (vs); elemental analysis calcd (%) for C₄H₆N₈ (166.14 g mol⁻¹): C 28.92, H 3.64, N 67.44; found: C 28.80, H 3.49, N 66.41; BAM impact: 40 J; BAM friction 360 N; ESD: 0.75 J (at grain size 100–500 μm).

1,2-Di(1*H*-tetrazol-1-yl)propane (2): The ligand **2** was synthesized similar to the method of Kamiya and Saito in a 200 mmol batch.^[8] Yield: 18.1 g (100 mmol, 50 %). DTA (5 °C min⁻¹) onset: 93 °C (melting), 189 °C (decomp.); ¹H NMR (270 MHz, [D₆]DMSO, 25 °C, TMS): 9.40 (s, 1 H, N₄CH), 9.28 (s, 1 H, N₄CH), 5.47–5.35 (m, 1 H, CH₃CH), 5.11–4.96 (m, 2 H, CH₂), 1.65 ppm (d, *J* = 6.9, 3 H, CH₃); ¹³C{¹H} NMR (68 MHz, [D₆]DMSO, 25 °C, TMS): 144.5 (N₄CH), 143.3 (N₄CH), 54.7 (CH₃CH), 51.5 (CH₂), 17.4 ppm (CH₃); IR (ATR): $\tilde{\nu}$ = 3136 (m), 3125 (m), 3016 (w), 2991 (w), 2967 (w), 2946 (w), 2925 (w), 2895 (vw), 1761 (vw), 1699 (vw), 1624 (w), 1543 (vw), 1484 (w), 1473 (m), 1465 (w), 1455 (w), 1435 (m), 1423 (w), 1387 (w), 1373 (vw), 1364 (vw), 1349 (w), 1317 (vw), 1300 (vw), 1276 (w), 1255 (m), 1206 (w), 1177 (s), 1161 (m), 1115 (m), 1104 (s), 1095 (s), 1086 (m), 1028 (w), 1015 (m), 968 (s), 921 (w), 881 (m), 757 (m), 721 (m), 680 (s), 664 cm⁻¹ (vs); elemental analysis calcd (%) for C₅H₈N₈ (180.18 g mol⁻¹): C 33.33, H 4.48, N 62.19; found: C 33.15, H 4.62, N 60.28; BAM impact: 30 J; BAM friction 360 N (at grain size 500–1000 μm).

1,4-Di(1*H*-tetrazol-1-yl)butane (3): The ligand **3** was synthesized similar to the method of Kamiya and Saito in a 100 mmol batch.^[8] Yield: 4.1 g (21.3 mmol, 21 %). ¹H NMR

(400 MHz, [D₆]DMSO, 25 °C, TMS): 9.40 (s, 2 H, N₄CH), 4.54–4.47 (m, 4 H, CN₄CH₂CH₂), 1.86–1.81 ppm (m, 4 H, CN₄CH₂CH₂); ¹³C{¹H} NMR (100 MHz, [D₆]DMSO, 25 °C, TMS): 144.0 (N₄CH), 46.8 (CN₄CH₂CH₂), 26.1 ppm (CN₄CH₂CH₂); IR (ATR): $\tilde{\nu}$ = 3116 (w), 2961 (w), 2947 (vw), 2926 (vw), 2872 (vw), 1771 (vw), 1701 (w), 1491 (m), 1450 (m), 1422 (w), 1359 (w), 1324 (w), 1277 (vw), 1244 (w), 1218 (w), 1172 (vs), 1126 (w), 1106 (s), 1034 (w), 1006 (w), 970 (m), 925 (w), 886 (m), 791 (s), 723 (w), 670 cm⁻¹ (s); elemental analysis calcd (%) for C₆H₁₀N₈ (194.20 g mol⁻¹): C 37.11, H 5.19, N 57.70; found: C 37.10, H 5.21, N 55.14.

{[Fe(dte)₃](ClO₄)₂]_n (4): To a hot solution of **1** (0.66 g, 4.00 mmol) in ethanol (30 mL) and water (2.0 mL) was added an aqueous solution of iron(II) perchlorate hydrate (0.56 g, 2.20 mmol) and ascorbic acid (0.18 g, 1.00 mmol). Under stirring, the solution was cooled down to room temperature. Within a few minutes, the product precipitated from the reaction mixture as a fine colorless powder. The solid was filtered off, washed with ethanol and dried in air. Yield: 0.85 g (1.13 mmol, 85 %). DTA (5 °C min⁻¹) onset: 240 °C (decomp.); IR (ATR): $\tilde{\nu}$ = 3132 (w), 3035 (vw), 2987 (vw), 1507 (w), 1497 (w), 1451 (w), 1366 (vw), 1312 (vw), 1269 (w), 1182 (m), 1157 (w), 1141 (w), 1094 (vs), 1083 (vs), 1019 (w), 1005 (w), 991 (m), 919 (w), 891 (w), 720 (vw), 664 (w), 656 cm⁻¹ (m); UV/Vis/NIR: λ_{max} = 879 nm; elemental analysis calcd. (%) for C₁₂H₁₈Cl₂FeN₂₄O₈ (753.18 g mol⁻¹): C 19.14, H 2.41, N 44.63; found: C 19.31, H 2.39, N 44.56; BAM impact: 2 J; BAM friction 14 N; ESD: 80 mJ (at grain size < 100 μm).

{[Co(dte)₃](ClO₄)₂]_n (5): To a hot warm solution of **1** (0.66 g, 4.00 mmol) in ethanol (30 mL) and water (2.0 mL) was added a concentrated aqueous solution of cobalt(II) perchlorate hexahydrate (0.73 g, 2.00 mmol). Under stirring, the solution was cooled down to room temperature. Within a few minutes, the product precipitated from the reaction mixture as a fine orange powder. The solid was filtered off, washed with ethanol and dried in air. Yield: 0.96 g (1.27 mmol, 95 %). DTA (5 °C min⁻¹) onset: 288 °C (decomp.); IR (ATR): $\tilde{\nu}$ = 3135 (w), 3032 (vw), 2990 (vw), 1508 (w), 1497 (w), 1451 (w), 1366 (vw), 1313 (vw), 1270 (vw), 1182 (w), 1158 (w), 1141 (w), 1093 (vs), 1083 (vs), 1019 (w), 1007 (w), 995 (m), 919 (w), 891 (w), 720 (vw), 665 (w), 656 cm⁻¹ (m); UV/Vis/NIR: λ_{max} = 471, 974 nm; elemental analysis calcd. (%) for C₁₂H₁₈Cl₂CoN₂₄O₈ (756.27 g mol⁻¹): C 19.06, H 2.40, N 44.45; found: C 19.28, H 2.38, N 44.32; BAM impact: 1 J; BAM friction 6 N; ESD: 0.25 J (at grain size 100–500 μm).

{[Ni(dte)₃](ClO₄)₂]_n (6): To a hot solution of **1** (0.66 g, 4.00 mmol) in ethanol (30 mL) and water (2.0 mL) was added a concentrated aqueous solution of nickel(II) perchlorate hexahydrate (0.73 g, 2.00 mmol). Under stirring, the solution was cooled to room temperature. Within a few minutes, the product precipitated from the reaction mixture as a fine violet powder. The solid was filtered off, washed with ethanol and dried under ambient

conditions. Yield: 0.97 g (1.28 mmol, 96 %). DTA (5 °C min⁻¹) onset: 298 °C (decomp.); IR (ATR): $\tilde{\nu}$ = 3140 (w), 3033 (vw), 2986 (vw), 1509 (w), 1497 (w), 1451 (w), 1367 (w), 1314 (vw), 1271 (w), 1184 (w), 1160 (w), 1143 (w), 1093 (vs), 1083 (vs), 1019 (w), 1000 (m), 919 (w), 891 (w), 721 (vw), 657 cm⁻¹ (m); UV/Vis/NIR: λ_{max} = 387, 549, 896 nm; elemental analysis calcd. (%) for C₁₂H₁₈Cl₂N₂₄NiO₈ (756.03 g mol⁻¹): C 19.06, H 2.40, N 44.46; found: C 19.11, H 2.32, N 44.21; BAM impact: 1 J; BAM friction 6 N; ESD: 0.25 J (at grain size 100–500 μm).

{[Cu(dte)₃](ClO₄)₂]_n (7): To a 70 °C warm solution of **1** (0.66 g, 4.00 mmol) in ethanol (30 mL) and water (2.0 mL) was added a concentrated aqueous solution of copper(II) perchlorate hexahydrate (0.74 g, 2.00 mmol). The solution was cooled to room temperature under stirring. Within a few minutes, the product precipitated as fine blue needles. The solid was filtered off, washed with ethanol and dried under ambient conditions. Yield: 1.00 g (1.32 mmol, 99 %). DTA (5 °C min⁻¹) onset: 256 °C (decomp.); IR (ATR): $\tilde{\nu}$ = 3136 (w), 3030 (vw), 2987 (vw), 1515 (w), 1500 (w), 1491 (w), 1452 (w), 1433 (w), 1366 (w), 1316 (vw), 1302 (vw), 1276 (w), 1179 (m), 1160 (w), 1141 (w), 1093 (vs), 1081 (vs), 1018 (m), 996 (m), 978 (m), 915 (w), 888 (w), 721 (w), 659 cm⁻¹ (m); UV/Vis/NIR: λ_{max} = 661 nm; elemental analysis calcd. (%) for C₁₂H₁₈Cl₂CuN₂₄O₈ (760.88 g mol⁻¹): C 18.94, H 2.38, N 44.18; found: C 19.07, H 2.29, N 43.90; BAM impact: 1.5 J; BAM friction 10 N; ESD: 0.15 J (at grain size < 100 μm).

{[Zn(dte)₃](ClO₄)₂]_n (8): To a 70 °C warm solution of **1** (0.66 g, 4.00 mmol) in ethanol (30 mL) and water (2.0 mL) was added a conc. aqueous solution of zinc(II) perchlorate hexahydrate (0.74 g, 2.00 mmol). The solution was cooled to room temperature under stirring. Within a few minutes, the product precipitated as a colorless solid. The solid was filtered off, washed with ethanol and dried in air. Yield: 0.92 g (1.20 mmol, 90 %). DTA (5 °C min⁻¹) onset: 280 °C (decomp.); IR (ATR): $\tilde{\nu}$ = 3134 (w), 3033 (vw), 2986 (vw), 1507 (w), 1497 (w), 1451 (w), 1366 (vw), 1313 (vw), 1269 (vw), 1182 (m), 1158 (w), 1141 (w), 1093 (vs), 1083 (vs), 1020 (w), 1008 (w), 994 (m), 918 (w), 892 (w), 720 (vw), 656 cm⁻¹ (m); UV/Vis/NIR: λ_{max} = none; elemental analysis calcd. (%) for C₁₂H₁₈Cl₂N₂₄O₈Zn (762.71 g mol⁻¹): C 18.90, H 2.38, N 44.07; found: C 19.11, H 2.30, N 43.99; BAM impact: 2 J; BAM friction 42 N; ESD: 0.30 J (at grain size 100–500 μm).

{[Cu(dtp)₃](ClO₄)₂]_n (9): To a solution of **2** (0.72 g, 4.00 mmol) in hot ethanol (25 mL) was added a concentrated aqueous solution of copper(II) perchlorate hexahydrate (0.74 g, 2.00 mmol) under stirring. The solution was cooled to room temperature under stirring and the product started to precipitate within a few minutes as fine blue powder. The powder was filtered off and dried under ambient conditions. Yield: 1.02 g (1.27 mmol, 95 %). DTA (5 °C min⁻¹) onset: 235 °C (decomp.); IR (ATR): $\tilde{\nu}$ = 3136 (vw), 3014 (vw), 2990 (vw), 2973 (vw), 1498 (w), 1452 (w), 1394 (vw), 1373 (vw), 1366 (vw), 1315 (vw), 1277 (vw), 1184 (w),

1092 (vs), 1080 (vs), 1038 (m), 1015 (w), 982 (w), 922 (w), 882 (w), 752 (vw), 717 (vw), 677 (w), 660 cm^{-1} (w); UV/Vis/NIR: $\lambda_{\text{max}} = 662\text{ nm}$; elemental analysis calcd (%) for $\text{C}_{15}\text{H}_{24}\text{Cl}_2\text{CuN}_{24}\text{O}_8$ (802.96 g mol^{-1}): C 22.44, H 3.01, N 41.87; found: C 22.41, H 2.98, N 41.32; BAM impact: 4 J; BAM friction 20 N; ESD: 0.15 J (at grain size $< 100\ \mu\text{m}$).

$\{\{\text{Cu}(\text{dtb})_3\}(\text{ClO}_4)_2\}_n$ (10): To a solution of **3** (0.78 g, 4.00 mmol) in hot ethanol (25 mL) was added a concentrated aqueous solution of copper(II) perchlorate hexahydrate (0.74 g, 2.00 mmol) under stirring. The solution was cooled to room temperature under stirring and the product started to precipitate within a few minutes as fine blue powder. The powder was filtered off and dried under ambient conditions. Yield: 1.10 g (1.30 mmol, 97.4 %). DTA ($5\text{ }^\circ\text{C min}^{-1}$) onset: $230\text{ }^\circ\text{C}$ (decomp.); IR (ATR): $\tilde{\nu} = 3137$ (w), 2956 (vw), 2940 (vw), 2875 (vw), 1510 (w), 1498 (w), 1467 (w), 1445 (w), 1381 (vw), 1367 (vw), 1326 (vw), 1304 (vw), 1271 (vw), 1258 (vw), 1205 (vw), 1181 (w), 1176 (w), 1139 (w), 1088 (vs), 1010 (w), 980 (w), 913 (w), 890 (w), 791 (w), 752 (w), 740 (vw), 716 (w), 676 (w), 660 cm^{-1} (w); elemental analysis calcd (%) for $\text{C}_{18}\text{H}_{30}\text{Cl}_2\text{CuN}_{24}\text{O}_8$ (845.04 g mol^{-1}): C 25.58, H 3.58, N 39.78; found: C 25.70, H 3.54, N 39.65; BAM impact: 12.5 J; BAM friction 120 N; ESD: 0.25 J (at grain size $< 100\ \mu\text{m}$).

$\{\{\text{Cu}(\text{dte})_3\}(\text{NO}_3)_2\}_n$ (11): To a hot solution of **1** (0.66 g, 4.00 mmol) in ethanol (30 mL) and water (2.0 mL) was added a conc. aqueous solution of copper(II) nitrate trihydrate (0.48 g, 2.00 mmol). The solution was cooled to room temperature under stirring. Within a few minutes, the product precipitated as a blue powder. The solid was filtered off, washed with ethanol and dried in the open air. Yield: 0.75 g (1.10 mmol, 83 %). DTA ($5\text{ }^\circ\text{C min}^{-1}$) onset: $191\text{ }^\circ\text{C}$ (decomp.); IR (ATR): $\tilde{\nu} = 3087$ (w), 2987 (vw), 1505 (w), 1492 (w), 1458 (w), 1435 (w), 1350 (vs), 1323 (m), 1189 (s), 1158 (m), 1101 (s), 1030 (w), 1012 (m), 996 (w), 914 (w), 831 (w), 785 (w), 720 (vw), 712 (vw), 696 (s), 660 cm^{-1} (s); UV/Vis/NIR: $\lambda_{\text{max}} = 722\text{ nm}$; elemental analysis calcd. (%) for $\text{C}_{12}\text{H}_{18}\text{CuN}_{26}\text{O}_6$ (685.99 g mol^{-1}): C 21.01, H 2.64, N 53.09; found: C 21.16, H 2.59, N 52.97; BAM impact: 7 J; BAM friction 160 N; ESD: 1.0 J (at grain size $100\text{--}500\ \mu\text{m}$).

$\{\{\text{Cu}(\text{dte})_3\}(\text{ClO}_3)_2\}_n$ (12): To a $70\text{ }^\circ\text{C}$ warm solution of **1** (0.66 g, 4.00 mmol) and copper(II) sulfate pentahydrate (0.50 g, 2.00 mmol) in water (30 mL) was added an aqueous solution of potassium chlorate (0.49 g, 4.00 mmol). The clear solution was left for crystallization for two days until blue crystals precipitated. The obtained X-ray suitable single crystals were filtered off and washed with a small amount of ethanol / water. The product was solved again in hot water and poured into ice-cooled isopropyl alcohol under stirring. The product immediately precipitated as fine powder which was filtered off and dried in air. Yield: 0.64 g (0.88 mmol, 66 %). DTA ($5\text{ }^\circ\text{C min}^{-1}$) onset: $175\text{ }^\circ\text{C}$ (decomp.); IR (ATR): $\tilde{\nu} = 3098$ (w), 2983 (vw), 1818 (vw), 1504 (w), 1459 (w), 1448 (w), 1438 (w), 1357 (vw), 1324 (vw), 1299 (vw), 1265 (vw), 1249 (vw), 1216 (vw), 1189 (m), 1156 (m), 1109 (m), 1102 (m), 1095 (m), 1013 (w), 998 (w),

964 (vs), 957 (vs), 938 (m), 934 (m), 926 (m), 913 (m), 842 (w), 837 (w), 824 (vw), 817 (vw), 806 (vw), 777 (w), 720 (w), 695 (m), 668 (m), 659 cm^{-1} (s); UV/Vis/NIR: $\lambda_{\text{max}} = 715 \text{ nm}$; elemental analysis calcd. (%) for $\text{C}_{12}\text{H}_{18}\text{Cl}_2\text{CuN}_{24}\text{O}_6$ ($728.88 \text{ g mol}^{-1}$): C 19.77, H 2.49, N 46.12; found: C 19.96, H 2.39, N 46.05; BAM impact: 1.5 J; BAM friction 6 N; ESD: 15 mJ (at grain size $< 100 \mu\text{m}$).

{[Cu(dte)₃](N(NO₂)₂)₂]_n (13): To a 70 °C warm solution of **1** (0.66 g, 4.00 mmol) and copper(II) sulfate pentahydrate (0.50 g, 2.00 mmol) in water (30 mL) was added an aqueous solution of ammonium dinitramide (0.50 g, 4.00 mmol). The clear solution was left for crystallization for three days until large blue crystals precipitated. The obtained X-ray suitable single crystals were filtered off and washed with a small amount of ethanol. The product was solved again in a small amount of hot water and poured into ice-cooled isopropyl alcohol under stirring. The product immediately precipitated as fine powder which was filtered off and dried in air. Yield: 0.90 g (1.16°mmol, 87 %). DTA (5 °C min^{-1}) onset: 168 °C (decomp.); IR (ATR): $\tilde{\nu} = 3134$ (w), 3124 (w), 3023 (vw), 2979 (vw), 1514 (s), 1492 (m), 1439 (m), 1366 (w), 1326 (w), 1317 (w), 1287 (vw), 1268 (w), 1191 (s), 1175 (vs), 1167 (vs), 1145 (m), 1097 (s), 1088 (m), 1051 (vw), 1015 (m), 993 (s), 974 (m), 936 (w), 895 (m), 879 (w), 825 (w), 818 (w), 757 (m), 721 (m), 696 (w), 684 (m), 672 (w), 658 cm^{-1} (s); UV/Vis/NIR: $\lambda_{\text{max}} = 633 \text{ nm}$; elemental analysis calcd. (%) for $\text{C}_{12}\text{H}_{18}\text{CuN}_{30}\text{O}_8$ ($774.01 \text{ g mol}^{-1}$): C 18.62, H 2.34, N 54.29; found: C 18.89, H 2.37, N 54.04; BAM impact: 1 J; BAM friction 80 N; ESD: 0.25 J (at grain size $< 100 \mu\text{m}$).

9.6. References

- [1] E. S. Hafenrichter, B. W. Marshall, K. J. Fleming, *41st Aerospace Sciences Meeting and Exhibit*, Reno, USA, January 6–9, **2003**.
- [2] a) A. A. Brish, I. A. Galeeva, B. N. Zaitsev, E. A. Sbimev, L. V. Tararinstev, *Fiz. Goreniya Vzryva* **1966**, 2, 132; b) A. A. Brish, I. A. Galeeva, B. N. Zaitsev, E. A. Sbimev, L. V. Tararinstev, *Fiz. Goreniya Vzryva* **1969**, 5, 475; c) L. C. Yang, V. J. Menichelli, *Appl. Phys. Lett.* **1971**, 19, 473–475; d) L. C. Yang, J. Menichelli, *US 3812783*, May 28, **1974**; e) S. C. Kunz, F. J. Salas, *13th International Pyrotechnics Seminar*, Grand Junction, USA, July 11–15, **1988**, 505–523; f) M. A. Ilyushin, I. V. Tselinskii, A. V. Chernai, *Ross. Khim. Zh.* **1997**, 41, 81–88; g) L. Strakovskiy, A. Cohen, R. Fifer, R. Beyer, B. Forch, *Laser Ignition of Propellants and Explosives*, ARL-TR-1699, Army Research Laboratory, Aberdeen Proving Ground, **1998**; h) J. E. Kennedy, *Spie 6287, Optical Technologies for Arming, Safing, Fuzing, and Firing II*, 628708, San Diego, USA, August 13, **2006**, 628708/1–628708/9; i) G. Damamme, V. M. Lisitsyn, D. Malis, V. P. Tsipilev, *Condens. Matter* **2010**, 1–14.
- [3] a) M. A. Ilyushin, I. V. Tselinsky, I. A. Ugryumov, A. Y. Zhilin, A. S. Kozlov, *6th New Trends in Research of Energetic Materials Seminar*, Pardubice, Czech Republic, April 22–24, **2003**,

- 146–152; b) I. A. Ugryumov, M. A. Ilyushin, I. V. Tselinskii, A. S. Kozlov, *Russ. J. Appl. Chem.* **2003**, *76*, 439–441; c) A. Y. Zhilin, M. A. Ilyushin, I. V. Tselinskii, A. S. Kozlov, I. S. Lisker, *Russ. J. Appl. Chem.* **2003**, *76*, 572–576; d) M. A. Ilyushin, I. V. Tselinskii, *8th New Trends in Research of Energetic Materials Seminar*, Pardubice, Czech Republic, April 19–21, **2005**, 213–221.
- [4] a) M. Joas, T. M. Klapötke, J. Stierstorfer, N. Szimhardt, *Chem. - Eur. J.* **2013**, *19*, 9995–10003; b) M. Joas, T. M. Klapötke, N. Szimhardt, *16th New Trends in Research of Energetic Materials Seminar*, Pardubice, Czech Republic, April 10–12, **2013**, 708–721; c) M. Joas, T. M. Klapötke, N. Szimhardt, *Eur. J. Inorg. Chem.* **2014**, *2014*, 493–498.
- [5] a) E. D. Aluker, A. G. Krechetov, A. Y. Mitrofanov, D. R. Nurmukhametov, M. M. Kuklja, *J. Phys. Chem. C* **2011**, *115*, 6893–6901; b) E. D. Aluker, A. G. Krechetov, A. Y. Mitrofanov, A. S. Zverev, M. M. Kuklja, *J. Phys. Chem. C* **2012**, *116*, 24482–24486.
- [6] M. Joas, T. M. Klapötke, *unpublished work*: Investigations to the Laser Initiation of Various Metal(II) Complexes with 1,2-Di(1*H*-tetrazol-1-yl)ethane as Ligand and a Large Set of Anions, **2014**.
- [7] a) P. J. van Koningsbruggen, Y. Garcia, O. Kahn, L. Fournes, H. Kooijman, A. L. Spek, J. G. Haasnoot, J. Moscovici, K. Provost, A. Michalowicz, F. Renz, P. Guetlich, *Inorg. Chem.* **2000**, *39*, 1891–1900; b) P. J. van Koningsbruggen, Y. Garcia, G. Bravic, D. Chasseau, O. Kahn, *Inorg. Chim. Acta* **2001**, *326*, 101–105; c) P. J. van Koningsbruggen, Y. Garcia, H. Kooijman, A. L. Spek, J. G. Haasnoot, O. Kahn, J. Linares, E. Codjovi, F. Varret, *J. Chem. Soc., Dalton Trans.* **2001**, 466–471.
- [8] T. Kamiya, Y. Saito, *DE 2147023*, March 29, **1973**.
- [9] P. N. Gaponik, V. P. Karavai, Y. V. Grigor'ev, *Khim. Geterotsykl. Soedin.* **1985**, 1521–1524.
- [10] a) M. Hesse, H. Meier, B. Zeeh, *Spektroskopische Methoden der organischen Chemie*, 7. ed., Thieme, Stuttgart, New York, **2005**; b) C. M. Grunert, P. Weinberger, J. Schweifer, C. Hampel, A. F. Stassen, K. Mereiter, W. Linert, *J. Mol. Struct.* **2004**, *733*, 41–52; c) M. Joas, T. M. Klapötke, *Z. Anorg. Allg. Chem.* **2014**, *640*, 1886–1891.
- [11] a) D. L. Lewis, E. D. Estes, D. J. Hodgson, *J. Cryst. Mol. Struct.* **1975**, *5*, 67–74; b) F. A. Miller, C. H. Wilkins, *Anal. Chem.* **1952**, *24*, 1253–1294; c) W. Sterzel, W. D. Schnee, *Z. Anorg. Allg. Chem.* **1971**, *383*, 231–239; d) K. O. Christe, W. W. Wilson, M. A. Petrie, H. H. Michels, J. C. Bottaro, R. Gilardi, *Inorg. Chem.* **1996**, *35*, 5068–5071; e) H.-G. Ang, W. Fraenk, K. Karaghiosoff, T. M. Klapötke, P. Mayer, H. Nöth, J. Sprott, M. Warchhold, *Z. Anorg. Allg. Chem.* **2002**, *628*, 2894–2900.
- [12] Impact: insensitive > 40 J, less sensitive ≥ 35 J, sensitive ≥ 4 J, very sensitive ≤ 3 J; Friction: insensitive > 360 N, less sensitive = 360 N, sensitive < 360 N and > 80 N, very sensitive ≤ 80 N, extremely sensitive ≤ 10 N, According to: *Recommendations on the Transport of Dangerous Goods, Manual of Tests and Criteria*, 4th edition, United Nations, New York - Geneva, **1999**.

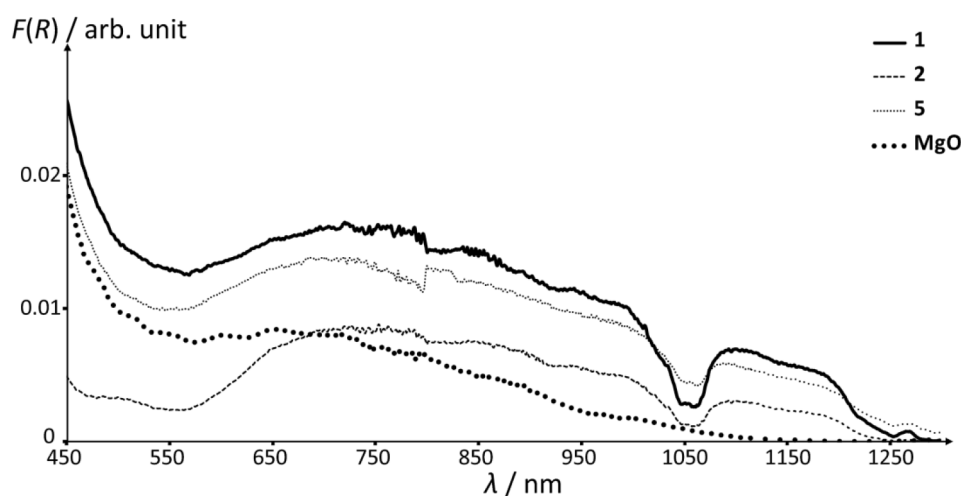
- [13] M. Joas, T. M. Klapötke, *Propellants Explos. Pyrotech.* **2014**, DOI: 10.1002/prop.201400142.
- [14] N. K. Bourne, *Proc. R. Soc. A* **2001**, *457*, 1401–1426.
- [15] E. V. Duginov, A. V. Khanefit, *Fiz. Goreniya Vzryva* **2011**, *47*, 127–135.
- [16] N. Fischer, M. Joas, T. M. Klapötke, J. Stierstorfer, *Inorg. Chem.* **2013**, *52*, 13791–13802.
- [17] a) NATO Standardization Agreement 4489, September 17, **1999**; b) NATO Standardization Agreement 4487, October 29, **2009**.
- [18] <http://www.ozm.cz> (accessed March 13, **2014**).
- [19] NATO Standardization Agreement 4515, August 23, **2002**.
- [20] <http://www.elementar.de/> (accessed March 13, **2014**).
- [21] <http://www.perkinelmer.de/> (accessed March 13, **2014**).
- [22] <http://www.jeol.co.jp/en/> (accessed April 2, **2014**).
- [23] <http://www.agilent.com/> (accessed March 13, **2014**).
- [24] P. Kubelka, F. Munk, *Z. Tech. Phys.* **1931**, *1*, 593–601.

10. Laser Initiation of Tris(carbohydrazide)metal(II) Perchlorates and Bis(carbohydrazide)diperchloratocopper(II)

Reproduced with permission from M. Joas, T. M. Klapötke, *Propellants, Explosives, Pyrotechnics* **2014**, DOI: 10.1002/prop.201400142.

Online: <http://dx.doi.org/10.1002/prop.201400142>.

Copyright 2014 Wiley-VCH Verlag GmbH & Co. KGaA, Weinheim.



10.1. Abstract

The literature-known tris(carbohydrazide)metal(II) perchlorates $[M(\text{CHZ})_3](\text{ClO}_4)_2$ ($M = \text{Mg}^{2+}$ (1), Mn^{2+} (2), Co^{2+} (3), Ni^{2+} (4), and Zn^{2+} (5)) and the bis(carbohydrazide)diperchloratocopper(II) (6) were prepared and characterized by elemental analysis, IR and Vis/NIR spectroscopy. The sensitivities toward mechanical, thermal, and electrical stimuli were determined for all complexes 1–6. Following, confined samples of 1–6 were irradiated with a monopulsed laser beam at a wavelength of 940 nm. The function times between beginning irradiation and complete decomposition (“breakout” at the end of the device) were measured. Further, the influence of light-absorbing additives was investigated to proof if the laser initiation mechanism might be photothermal or photochemical. Addition of 1% active carbon to the samples decreased the function time and the correlated initiation threshold enormously. This was an indication that the initiation mechanism seems to be thermal.

10.2. Introduction

The main topics in the recent research of energetic materials are safety, environmental acceptability, and high performance. Thus, the development of new materials, which achieve the desired requirements, is necessary. Promising primary and secondary explosives, oxidizers and pyrotechnics have been presented in the last years.^[1] However, there has always been a demand for safe initiation methods to improve and facilitate the handling of explosives, too. While classic primary explosives are stimulated by e.g. impact, friction or heat and consequently susceptible to undesired initiation,^[2] exploding bridgewire (EBW) and foil initiators (EFI) represent a class of safe non-primary explosive detonators.^[3] These type of electric detonators is considerably less susceptible toward unintended initiation by electric impulses than simple hot-wire initiators,^[3a] however, they are improper for some applications due to several other reasons e.g. large size of the required power sources.^[4]

As a consequence, laser initiation was suggested as an alternative. In the late 1960s and early 1970s, the first laser initiation experiments were made by Brish *et al.* as well as Menichelli and Yang.^[5] Common primary (lead azide) as well as secondary explosives (like pentaerythritol tetranitrate, cyclotrimethylenetrinitramine, and *N*-methyl-*N*-2,4,6-tetranitroaniline) were irradiated by Q-switched neodymium glass and ruby lasers of high power. In the work of Menichelli and Yang for example, the energy of the Q-switched ruby laser ranged from 0.8 to 4.0 J for a pulse width of 25 ns.^[5c] Owing to high costs and large size, the practical use of neodymium or ruby lasers for initiation was very limited. The practical application of laser radiation as initiation source firstly received importance in the 1980s by the introduction of laser diodes, which were smaller and cheaper.^[4a] However, the energy output of laser diodes was much lower than that of high-power Nd:YAG or ruby lasers. But for an alternative to fast-functioning detonators like EBWs and EFIs, it is necessary to exhibit a short ignition delay, which can be achieved by direct shock initiation of the explosive with a high laser power. Another possibility for short ignition delay times is the use of energetic materials, which show a high susceptibility to laser radiation and are ignited by low laser power densities. Complex perchlorates with hydrazinoazoles as ligands were presented as a novel class of explosives, which exhibited a high sensitivity to laser radiation.^[6] The 5-hydrazino-1*H*-tetrazolemercury(II) perchlorate (HTMP) is one example for such a laser-sensitive explosive with an initiation energy of 1×10^{-5} J at a pulse length of 30 ns.^[6] Other interesting complexes with low initiation thresholds are the bis(3-hydrazino-4-amino-1,2,4-triazole)metal(II) perchlorates, whereas especially copper(II) showed a very high photosensitivity.^[7] Metal(II) complexes with 5-(1-methylhydrazinyl)-1*H*-tetrazole (HMHT) and 1,2-bis[5-(1-methylhydrazinyl)tetrazol-1-yl]-ethane (BMHTE) as ligand have been synthesized and investigated toward laser irradiation by our research group.^[8] Amongst

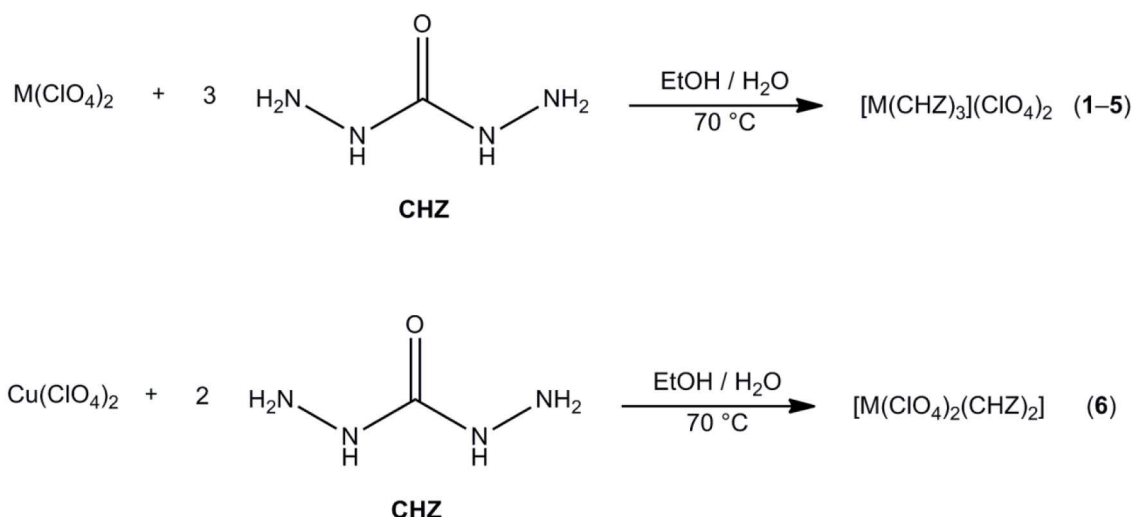
others, it was shown that the metal(II) perchlorates (Co, Ni, and Cu) with BMHTE showed a high sensitivity to laser radiation and could all be initiated by a 100 μs pulse of a common diode laser at 940 nm. But not only hydrazinoazoles are suitable ligands for laser-sensitive coordination compounds. For example, various metal perchlorates (Co^{2+} , Ni^{2+} , Cu^{2+} , and Ag^+) with the hydrazine-derivative 3-amino-1-nitroguanidine as ligand were prepared and their behavior upon laser irradiation tested by our research group.^[9] In the case of cobalt, copper, and silver, the initiation by a 100 μs pulse at 940 nm was successful.

Although laser initiation of energetic materials is extensively investigated, the initiation mechanism is still not completely understood. A photothermal mechanism and a photochemical one are discussed in literature, though the thermal one is the most prominent.^[5b, 10] According to literature,^[4a,11] it is stated that in case of a photothermal mechanism, light absorbing particles like carbon black decrease the initiation energy threshold.

Based on the previous results, further investigations to the laser initiation mechanism are necessary. To investigate the influence of the metal center on the laser ignitability it would be wise to have complexes of same formula and structure. Suitable energetic coordination compounds are the literature-known tris(carbohydrazide)metal(II) perchlorate complexes $[\text{M}(\text{CHZ})_3](\text{ClO}_4)_2$,^[12] which all crystallize in the monoclinic space group $P2_1/n$ and the bis(carbohydrazide) diperchloratocopper(II), whose crystal structure is still unknown. In this work, the literature known carbohydrazide perchlorate complexes with Mg^{2+} , Mn^{2+} , Co^{2+} , Ni^{2+} , Zn^{2+} , and Cu^{2+} were tested upon laser irradiation. Further, the influence of activated carbon as light absorbing additive and magnesium oxide as light scattering additive was investigated.

10.3. Results and Discussion

Synthesis: Carbohydrazide was synthesized according to the literature procedure from dimethylcarbonate and hydrazine.^[13] Further, aqueous metal(II) perchlorate solutions were combined with hot carbohydrazide solutions in ethanol. Owing to the use of ethanol as solvent, the products precipitated fast and as fine powders from the reaction mixture. The prepared coordination compounds **1–6** (Scheme 1) are all literature-known.^[12]

**Scheme 1.** Synthesis of 1–6.

Infrared spectroscopy: IR spectra of the ligand CHZ and all perchlorate complexes 1–6 were recorded. Carbohydrazide vibrations were assigned according to Ref.^[14]. The free ligand exhibits typical N–H valence vibrations in the range between 3353 and 3094 cm^{-1} . The absorption bands are sharp due to the formation of hydrogen bonds in the solid state. Further, a very strong band at 1629 cm^{-1} , with shoulders at 1681, 1648, and 1637 cm^{-1} , can be observed for the N–H deformation vibrations and the C=O stretching vibration. The very strong band at 1531 cm^{-1} is a vibrational combination of an N–H bend and a C–N stretching vibration. At 1447 cm^{-1} an N–H bend vibration and at 1340 and 1318 cm^{-1} rocking vibrations are observed in strong intensity. Between 1209 and 693 cm^{-1} further vibrational combinations of carbohydrazide are detected.

Table 1. Wavenumbers [cm^{-1}] of selected infrared active vibrations for the complexes 1–6.

Vibration ^{a)}	1 ^{b)}	2 ^{b)}	3 ^{b)}	4 ^{b)}	5 ^{b)}	6 ^{b)}
$\nu(\text{N-H})$	3405			3405		
	3392	3391	3389	3389	3389	
	3353	3348	3350	3344	3350	3368
	3317	3324	3327	3328	3329	
	3307	3308	3299	3308	3304	3303
	3232	3235	3228	3232	3225	3263
						3187
						1670
$\delta(\text{N-H})$ + $\nu(\text{C=O})$	1645	1645	1645	1645	1645	1635
						1616
$\delta(\text{N-H})$ + $\nu(\text{C-N})$	1546	1548	1541	1544	1541	1503
	1544	1541			1538	
$\nu(\text{Cl-O})$	1066	1062	1066	1065	1067	1075
						1061

a) Vibration assignment according to Refs. ^[14, 15]. b) Experimental data.

Compared to the free carbohydrazide, the CHZ ligand vibrations are shifted and changed in the complexes due to coordination. An overview is given in Table 1. The vibrations of the

complexes **1–5** are nearly identical which is in agreement with the crystal structures. In contrast, the structure and formula of the copper complex **6** is different, which is also indicated by the deviating wavenumbers and the presence of different vibrations than in the spectra of **1–5**.

Energetic properties and laser initiation: The sensitivities toward impact, friction, and electrostatic discharge were determined for the complexes **1–6** via standard methods. Further, the temperature stability was determined with differential thermal analysis. The compounds were classified according to the UN Recommendations on the Transport of Dangerous Goods.^[16] An overview about the sensitivities and temperature stabilities is given in Table 2.

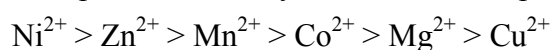
All complexes **1–6** are classified as very sensitive in terms of impact. Further, the magnesium (**1**), manganese (**2**) and zinc (**5**) complexes are classified as very sensitive toward friction, whereas the cobalt (**3**), nickel (**4**), and copper (**6**) compounds are extremely sensitive. Complex **6** showed the highest friction sensitivity and once detonated accidentally by positioning a small amount on the porcelain plate during the preparation for the friction test.

Table 2. Sensitivities and thermal stabilities of complexes **1–6**.

	T_{onset} [°C]	IS ^{a, b)} [J]	FS ^{a, b)} [N]	ESD ^{a)} [J]
[Mg(CHZ) ₃](ClO ₄) ₂	239	2.5	60	0.20
[Mn(CHZ) ₃](ClO ₄) ₂	263	2	24	0.50
[Co(CHZ) ₃](ClO ₄) ₂	243	1	≤ 5	0.035
[Ni(CHZ) ₃](ClO ₄) ₂	273	1	≤ 5	0.30
[Zn(CHZ) ₃](ClO ₄) ₂	268	1.5	20	0.70
[Cu(ClO ₄) ₂ (CHZ) ₂]	186	3	<< 5	0.02

a) At grain sizes < 100 μm for all samples. b) According to BAM standard methods (IS: BAM Drophammer; FS: BAM friction tester).

The copper complex **6** further shows the highest sensitivity toward electrostatic discharge followed by cobalt compound **3**. The zinc compound **5** exhibited the lowest ESD sensitivity. The temperature stability of the metal complexes **1–6** decreases in the following series:



The low temperature stability of copper (**6**) may also be a result of its different structure ([Cu(ClO₄)₂(CHZ)₂]) compared to **1–5**.

Laser initiation tests were performed with a single-pulsed diode laser at a wavelength of 940 nm and a pulse length of 400 μs. The laser power was in the order of 10⁵ W cm⁻² and kept constant for all tests. Multiple samples of each complex were tested under constant parameters. The samples consisted of powders of the complexes **1–6** and 5 wt% polyethylene as binder. Additionally, to half of the samples 1 wt% powdered activated carbon was added to investigate the influence of light absorbing particles on the initiation threshold. Sample bulks of 180 mg were further pressed to pellets of a bulk-density of 1.5 g cm⁻³, confined with an

aluminum shell and placed on an aluminum witness plate for detection of detonation. In case of a successful initiation, the function time as the sum of the ignition delay time (time from beginning irradiation to beginning of decomposition) and the propagation of the reaction zone (time from beginning of the self-sustained decomposition reaction until 'breakout' at the end of the device) was measured.^[3b] Thereby, the beginning of irradiation was detected by an electric signal and the end of reaction by an optical output signal due to a light emission accompanied with the detonation. For function times in the order of 10^{-4} s and under the assumption of a process time for DDT of $2-10 \times 10^{-6}$ s, the measured function time can nearly be supposed as the ignition delay time.^[4a] For faster function times in magnitude of $10^{-6}-10^{-5}$ s, it would be necessary to directly measure the ignition delay time similar to the method by Hafenrichter *et al.*^[4a] However, under the assumption that the required time for the DDT process is similar in magnitude for the complexes **1-6**, it would be sufficient to measure the function time to obtain a trend for the laser ignitability related to the metal cation

Table 3. Laser initiation results and average function times t_f of complexes **1-6**.

	$F(R)$ at 940 nm	$t_f^a)$ [s]	$t_f^b)$ [s]
[Mg(CHZ) ₃](ClO ₄) ₂	0.01	no init.	no init.
[Mn(CHZ) ₃](ClO ₄) ₂	< 0.01	no init.	no init.
[Co(CHZ) ₃](ClO ₄) ₂	0.03	40.1×10^{-5}	4.3×10^{-5}
[Ni(CHZ) ₃](ClO ₄) ₂	0.37	13.6×10^{-5}	1.7×10^{-5}
[Zn(CHZ) ₃](ClO ₄) ₂	0.01	no init.	no init.
[Cu(ClO ₄) ₂](CHZ) ₂	< 0.01	6.5×10^{-5}	0.8×10^{-5}

a) No addition of activated carbon. b) Addition of 1 % activated carbon ($F(R)_{@940 \text{ nm}} = 0.76$).

The results of the laser initiation are listed in Table 3. The complexes **1**, **2**, and **5** could not be initiated by the laser pulse in our experiments what is in agreement with the Vis/NIR spectra, which show nearly no absorption (Figure 1). Even under addition of 1 wt% activated carbon, the samples of the complexes **1**, **2**, and **5** could not be initiated. Contrary, the complexes **3** (401 μ s), **4** (136 μ s) and **6** (65 μ s) were successfully initiated and the function times measured. Regarding the solid Vis/NIR spectra (Figure 2), it appears plausible that the nickel compound **4** has a lower initiation energy threshold according to its higher light absorption at 940 nm than the cobalt compound **3**. However, the copper(II) complex **6** exhibits nearly no absorption at 940 nm but showed the lowest ignition delay of the undoped samples. One reason might be the found in the lowest auto-ignition temperature ($T_{\text{onset}} = 186$ °C) for **6** of the herein investigated complexes, although this could not be the only explanation under the assumption that the initiation follows a thermal mechanism. Further parameters like thermal conductivity, heat capacity or other yet disregarded might play an important role.

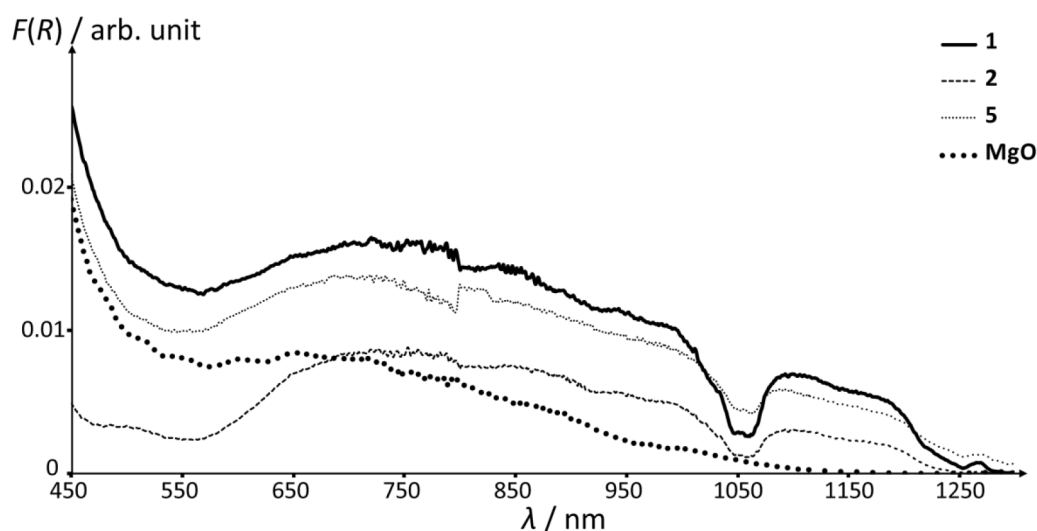


Figure 1. Vis/NIR spectra of the colorless complexes **1**, **2**, **5**, and MgO.

By adding 1 wt% activated carbon ($R_{@940\text{ nm}} = 31\%$) to the samples to decrease the light reflection R [%], the function time and correlated to it the energy threshold could be decreased by approximately factor ten for **3**, **4**, and **6**. Thus it can be concluded, that the main amount of laser radiation is absorbed by the carbon particles independent of the absorptivity of the metal complex itself and that heating of carbon particles and heat transfer to energetic particles is the influential process. This is also an indication for a thermal initiation mechanism.

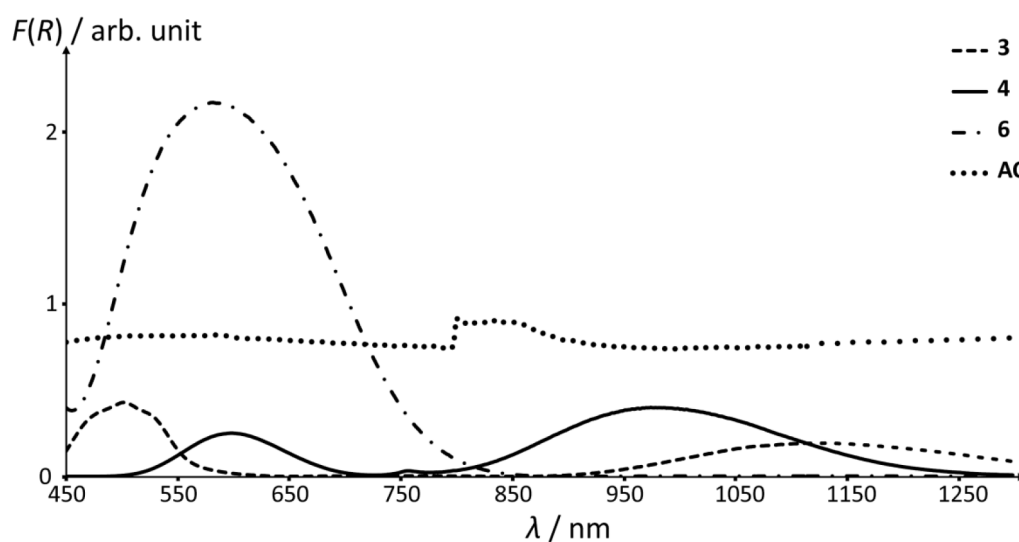


Figure 2. Vis/NIR spectra of the colored complexes **3**, **4**, **6**, and activated carbon (AC).

A further proof for a thermal mechanism and not a photochemical one was given by mixing 1 wt% of magnesium oxide ($R_{@940\text{ nm}} = 107\%$) instead of carbon to a sample of **6**. In case of a photochemical process according to literature,^[10a] light scattering particles like MgO should decrease the initiation energy threshold by an increase of irradiated volume resulting in an enhancement of probability for electronic excitation. However, the opposite is observed.

The function time of **6** is lengthened from 65 μs to 126 μs . This can be explained by the increase of reflection and the enlargement of irradiated volume by light scattering. Due to the consequential lowering of energy density, more energy is necessary to reach the auto-ignition temperature, which is finally achieved by a longer irradiation time at constant power P .

10.4. Experimental Section

Caution! The perchlorate complexes **1–6** are energetic materials, which show increased sensitivities toward various stimuli (e.g. impact, friction, electrostatic discharge, heat). Proper protective measures (safety glasses, face shield, leather coat, earthed equipment, conductive floor and shoes, Kevlar gloves, and ear plugs) are recommended when handling these materials.^[17] The handled scales should be kept small. Especially, the cobalt (**3**), nickel (**4**) and copper (**6**) compounds are extremely sensitive toward impact and friction.

All chemicals were used as supplied by ABCR, Acros Organics, AppliChem, Fluka, Sigma-Aldrich, and VWR. The impact and friction sensitivity tests were performed according to standard methods by using a BAM (Bundesanstalt für Materialforschung und -prüfung) drop hammer and a BAM friction tester.^[18] The sensitivity toward electrostatic discharge was tested by using an OZM Research electric spark tester ESD 2010 EN.^[19] Decomposition temperatures were determined by differential thermal analysis (DTA) with an OZM Research DTA 552-Ex instrument at a heating rate of 5 °C min⁻¹ and in a range of room temperature to 400 °C.^[19–20] The determination of the carbon, hydrogen and nitrogen contents was carried out by combustion analysis using an Elementar Vario EL.^[21] IR spectra were recorded with a Perkin-Elmer BXII FT-IR system with a Smith DuraSAMPLIR II diamond ATR unit.^[22] The Vis/NIR reflectance of solid samples (powders) was determined with a Varian Cary 500 spectrometer in the wavelength range of 450–1300 nm.^[23] The relative reflectance R [%] was transformed by the Kubelka–Munk equation to the absorption intensity $F(R)$ [arbitrary units]. A reflectance of $R > 100$ % is possible because the values are relative to the background reflection of blank samples.^[24]

The tris(carbohydrazide)metal(II) perchlorates **1–5** and the bis(carbohydrazide)diperchloratocopper(II) (**6**) have all been prepared in a similar way. A concentrated aqueous solution of the corresponding metal(II) perchlorate (2.2 mmol) was added to a 70 °C warm solution of carbohydrazide (**1–5**: 6.0 mmol, 0.54 g; **6**: 4.0 mmol, 0.36 g) in ethanol (45 mL) whilst stirring. The resulting clear solution was cooled down to room temperature whilst stirring. The product precipitated in form of a fine powder (**1**: colorless; **2**: colorless; **3**: intense red; **4**: intense blue; **5**: colorless; **6**: dark blue) within 1 h. Detailed experimental data can be found in the supporting information.

10.5. Conclusion

The literature known carbohydrazide (CHZ) complexes with perchlorate as anion and magnesium (**1**), manganese (**2**), cobalt (**3**), nickel (**4**), zinc (**5**), and copper (**6**) as metal(II) cations were synthesized by fast precipitation from ethanol solutions. The complexes were characterized by Vis/NIR and infrared spectroscopy as well as elemental analysis. Further, the sensitivities toward mechanical, electrical, and thermal stimuli were determined. Especially the copper(II) complex **6** was extremely sensitive toward friction, whereas the magnesium complex exhibited the lowest mechanical sensitivity. Additional, laser initiation experiments were made. The copper (**6**) compound exhibited the shortest ignition delay time followed by nickel (**4**) and cobalt (**3**). The complexes **1**, **2**, and **5** could not be ignited. By addition of powdered activated carbon (decrease of initiation threshold) and alternatively magnesium oxide (increase of initiation threshold), it could be shown that the initiation of explosives by monopulsed diode laser radiation presumably is a thermal process which is also in agreement with the literature.^[4a,5b,25] However, it is not understood, which parameter mainly influences the initiation energy threshold.

Future investigations should proof if the initiation energy threshold is decreased for laser wavelengths, at which the absorptance of the corresponding coordination compound is higher e.g. for **6** ($F(R)_{@635\text{ nm}} = 1.94$) under use of a AlGaInP diode laser or for **3** ($F(R)_{@1064\text{ nm}} = 0.17$) under use of a Nd:YAG laser.

10.6. References

- [1] a) G. Steinhauser, T. M. Klapötke, "Green" Pyrotechnics: a Chemists' Challenge, *Angew. Chem., Int. Ed.* **2008**, *47*, 3330–3347; b) M. B. Talawar, R. Sivabalan, T. Mukundan, H. Muthurajan, A. K. Sikder, B. R. Gandhe, A. S. Rao, Environmentally Compatible Next Generation Green Energetic Materials (GEMs), *J. Hazard. Mater.* **2009**, *161*, 589–607; c) J. Fronabarger, M. Williams, M. Bichay, Environmentally Acceptable Alternatives To Existing Primary Explosives, *Joint Armaments Conference*, Dallas, USA, May 20, **2010**; d) H. Gao, J. M. Shreeve, Azole-Based Energetic Salts, *Chem. Rev.* **2011**, *111*, 7377–7436; e) Q. J. Axthammer, M. A. Kettner, T. M. Klapötke, R. Moll, S. F. Rest, Progress in the Development of High Energy Dense Oxidizers Based on CHNO(F) Materials, *16th New Trends in Research of Energetic Materials Seminar*, Pardubice, Czech Republic, April 10–12, **2013**, 29–39.
- [2] R. Matyáš, J. Pachman, *Primary Explosives*, 1. ed., Springer, Heidelberg, **2013**.
- [3] a) R. Varosh, Electric Detonators: EBW and EFI, *Propellants Explos. Pyrotech.* **1996**, *21*, 150–154; b) P. W. Cooper, *Explosives Engineering*, Wiley-VCH, Weinheim, **1996**.
- [4] a) E. S. Hafenrichter, B. W. Marshall, K. J. Fleming, Fast Laser Diode Ignition of Confined BNCP, *41st Aerospace Sciences Meeting and Exhibit*, Reno, NV, USA, January 6–9, **2003**; b) J. E. Kennedy, Motivations for Laser Detonator and Firing System Developments, *Spie* *6287*,

Optical Technologies for Arming, Safing, Fuzing, and Firing II, 628708, San Diego, CA, USA, August 13, **2006**, 628708/1–628708/9.

- [5] a) A. A. Brish, I. A. Galeeva, B. N. Zaitsev, E. A. Sbimev, L. V. Tararinstev, Laser-Excited Detonation of Condensed Explosives, *Fiz. Goreniya Vzryva* **1966**, 2, 132; b) A. A. Brish, I. A. Galeeva, B. N. Zaitsev, E. A. Sbimev, L. V. Tararinstev, Mechanism of Initiation of Condensed Explosives by Laser Radiation, *Fiz. Goreniya Vzryva* **1969**, 5, 475; c) L. C. Yang, V. J. Menichelli, Detonation of Insensitive High Explosives by a Q-Switched Ruby Laser, *Appl. Phys. Lett.* **1971**, 19, 473–475; d) L. C. Yang, J. Menichelli, Optically Detonated Explosive Device, *US 3812783*, May 28, **1974**.
- [6] M. A. Ilyushin, I. V. Tselinsky, I. A. Ugryumov, A. Y. Zhilin, A. S. Kozlov, Coordination Complexes as Inorganic Primary Explosives, *6th New Trends in Research of Energetic Materials Seminar*, Pardubice, Czech Republic, April 22–24, **2003**, 146–152.
- [7] I. A. Ugryumov, M. A. Ilyushin, I. V. Tselinskii, A. S. Kozlov, Synthesis and Properties of Photosensitive Complex Perchlorates of d Metals with 3(5)-Hydrazino-4-amino-1,2,4-triazole as Ligand, *Russ. J. Appl. Chem.* **2003**, 76, 439–441.
- [8] a) M. Joas, T. M. Klapötke, J. Stierstorfer, N. Szimhardt, Synthesis and Characterization of Various Photosensitive Copper(II) Complexes with 5-(1-Methylhydrazinyl)-1H-tetrazole as Ligand and Perchlorate, Nitrate, Dinitramide, and Chloride as Anions, *Chem. - Eur. J.* **2013**, 19, 9995–10003; b) M. Joas, T. M. Klapötke, N. Szimhardt, Photosensitive Metal(II) Perchlorates with 1,2-Bis[5-(1-methylhydrazinyl)tetrazol-1-yl]ethane as Ligand: Synthesis, Characterization and Laser Ignition, *Eur. J. Inorg. Chem.* **2014**, 2014, 493–498.
- [9] N. Fischer, M. Joas, T. M. Klapötke, J. Stierstorfer, Transition Metal Complexes of 3-Amino-1-nitroguanidine as Laser Ignitable Primary Explosives: Structures and Properties, *Inorg. Chem.* **2013**, 52, 13791–13802.
- [10] a) E. D. Aluker, A. G. Krechetov, A. Y. Mitrofanov, D. R. Nurmukhametov, M. M. Kuklja, Laser Initiation of Energetic Materials: Selective Photoinitiation Regime in Pentaerythritol Tetranitrate, *J. Phys. Chem. C* **2011**, 115, 6893–6901; b) E. D. Aluker, A. G. Krechetov, A. Y. Mitrofanov, A. S. Zverev, M. M. Kuklja, Understanding Limits of the Thermal Mechanism of Laser Initiation of Energetic Materials, *J. Phys. Chem. C* **2012**, 116, 24482–24486.
- [11] a) S. C. Kunz, F. J. Salas, Diode Laser Ignition of High Explosives and Pyrotechnics, *13th International Pyrotechnics Seminar*, Grand Junction, USA, July 11–15, **1988**, 505–523; b) Y.-h. Zhu, D.-l. Sheng, B. Yang, L.-k. Chen, F.-e. Ma, Synthesis and Properties of Laser Sensitivity Primary Explosive 5-Hydrazinotetrazole Mercury Perchlorate, *Hanneng Cailiao* **2009**, 17, 169–172.
- [12] a) V. P. Sinditskii, A. E. Fogel'zang, M. D. Dutov, V. V. Serushkin, S. P. Yarkov, B. S. Svetlov, Carbohydrazide Complexes of Copper(II) Salts, *Zh. Neorg. Khim.* **1986**, 31, 1759–1765; b) V. P. Sinditskii, A. E. Fogel'zang, M. D. Dutov, V. I. Sokol, V. V. Serushkin, B. S. Svetlov, M. A.

- Porai-Koshits, Structure of Transition Metal Chloride, Sulfate, Nitrate and Perchlorate Complexes with Carbohydrazide, *Zh. Neorg. Khim.* **1987**, *32*, 1944–1949; c) J.-G. Zhang, T.-L. Zhang, Z.-R. Wei, K.-B. Yu, Studies on Preparation, Crystal Structure and Application of $[\text{Mn}(\text{CHZ})_3](\text{ClO}_4)_2$, *Gaodeng Xuexiao Huaxue Xuebao* **2001**, *22*, 895–897; d) M. B. Talawar, A. P. Agrawal, J. S. Chhabra, S. N. Asthana, Studies on Lead-free Initiators: Synthesis, Characterization and Performance Evaluation of Transition Metal Complexes of Carbohydrazide, *J. Hazard. Mater.* **2004**, *113*, 57–65; e) M. B. Talawar, A. P. Agrawal, C. K. Ghatak, N. Asthana, B. R. Gandhe, T. Mukundan, Tris(carbohydrazide) Nickel Perchlorate (NCP) as Detonators for Explosives, *IN 2005DE01093A*, June 19, **2009**; f) S. Qi, Z. Li, T. Zhang, Z. Zhou, L. Yang, J. Zhang, X. Qiao, K. Yu, Crystal Structure, Thermal Analysis and Sensitivity Property of $[\text{Zn}(\text{CHZ})_3](\text{ClO}_4)_2$, *Huaxue Xuebao* **2011**, *69*, 987–992; g) Z.-M. Li, T.-L. Zhang, L. Yang, Z.-N. Zhou, J.-G. Zhang, Synthesis, Crystal Structure, Thermal Decomposition, and Non-isothermal Reaction Kinetic Analysis of an Energetic Complex: $[\text{Mg}(\text{CHZ})_3](\text{ClO}_4)_2$ (CHZ = carbohydrazide), *J. Coord. Chem.* **2012**, *65*, 143–155.
- [13] Z. Li, W. Zhu, J. Yu, X. Ma, Z. Lu, S. Xiao, Green Synthetic Method for 1,5-Disubstituted Carbohydrazones, *Synth. Commun.* **2006**, *36*, 2613–2619.
- [14] a) H. M. Badawi, W. Forner, A Study of the H-bonded Structures and Infrared and Raman Spectral Analysis of Carbohydrazide and Thiocarbohydrazide, *J. Mol. Struct.* **2013**, *1037*, 218–224; b) M. Hesse, H. Meier, B. Zeeh, *Spektroskopische Methoden der organischen Chemie*, 7. ed., Thieme, Stuttgart, **2005**.
- [15] D. L. Lewis, E. D. Estes, D. J. Hodgson, The Infrared Spectra of Coordinated Perchlorates, *J. Cryst. Mol. Struct.* **1975**, *5*, 67–74.
- [16] Impact: insensitive > 40 J, less sensitive ≥ 35 J, sensitive ≥ 4 J, very sensitive ≤ 3 J; Friction: insensitive > 360 N, less sensitive = 360 N, sensitive < 360 N and > 80 N, very sensitive ≤ 80 N, extremely sensitive ≤ 10 N, According to: *Recommendations on the Transport of Dangerous Goods, Manual of Tests and Criteria*, 4th edition, United Nations, New York - Geneva, **1999**.
- [17] T. M. Klapötke, B. Krumm, F. Xaver Steemann, G. Steinhauser, Hands on explosives: Safety Testing of Protective Measures, *Safety Science* **2010**, *48*, 28–34.
- [18] a) NATO Standardization Agreement 4489, September 17, **1999**; b) NATO Standardization Agreement 4487, October 29, **2009**.
- [19] <http://www.ozm.cz> (accessed March 13, **2014**).
- [20] NATO Standardization Agreement 4515, August 23, **2002**.
- [21] <http://www.elementar.de/> (accessed March 13, **2014**).
- [22] <http://www.perkinelmer.de/> (accessed March 13, **2014**).
- [23] <http://www.agilent.com/> (accessed March 13, **2014**).
- [24] P. Kubelka, F. Munk, Ein Beitrag zur Optik der Farbanstriche, *Z. Tech. Phys.* **1931**, *1*, 593–601.

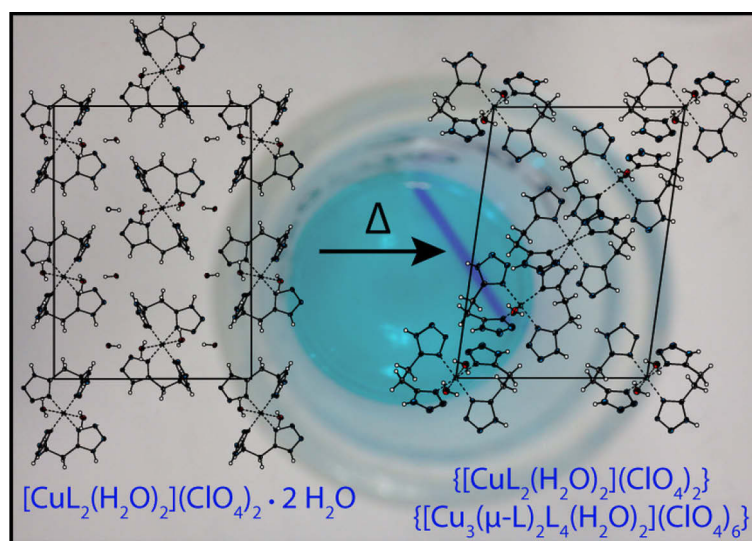
- [25] N. K. Bourne, On the Laser Ignition and Initiation of Explosives, *Proc. R. Soc. Lond. A* **2001**, 457, 1401–1426.

11. Cocrystallization of Photosensitive Energetic Copper(II) Perchlorate Complexes with the Nitrogen-rich Ligand 1,2-Di(1*H*-tetrazol-5-yl)ethane

Reproduced with permission from J. Evers, I. Gospodinov, M. Joas, T. M. Klapötke, J. Stierstorfer, *Inorganic Chemistry* **2014**, 53, 11749–11756.

Online: <http://pubs.acs.org/articlesonrequest/AOR-zg4Xzfnbr2dDG9EuzbMx>.

Copyright 2014 American Chemical Society.



11.1. Abstract

Two recently introduced concepts in the design of new energetic materials, namely complexation and cocrystallization, have been applied in the synthesis and characterization of the energetic copper(II) compound “[Cu(dt-5-e)₂(H₂O)](ClO₄)₂”, which consists of two different complex cations and can be described as a model energetic ionic cocrystal. The presence of both the N-rich 1,2-di(1*H*-tetrazol-5-yl)ethane ligand and oxidizing perchlorate counterion results in a new type of energetic material. The ionic complex cocrystal consists of a mononuclear and a trinuclear complex unit. It can be obtained by precipitation from perchloric acid or by dehydration of the related mononuclear coordination compound [Cu(dt-5-e)₂(H₂O)](ClO₄)₂·2H₂O at 70 °C in the solid state. The transformation starting at 60 °C was monitored by X-ray powder diffraction and thermal analysis. The energetic ionic cocrystal was shown to be a new primary explosive suitable for laser ignition. The different coordination spheres within the ionic cocrystal (octahedral and square pyramidal) were shown by UV/vis/NIR spectroscopy to result in excellent light absorption.

11.2. Introduction

The improvement of the performance, safety, and environmental compatibility of energetic materials (EMs) is a major goal for energetic material researchers around the world.^[1-4] Not only due to the European REACH regulations from 2007, the replacement of toxic, carcinogenic, and hazardous energetic materials like 1,3,5-trinitroperhydro-1,3,5-triazine (RDX), monomethylhydrazine (MMH), or lead azide (LA) by “green” alternatives is a main object.^[5-7] Strategies for the development of new EMs include increasing the nitrogen content, introducing ring strain, or oxidation of the molecule backbone.^[8] An interesting and recent approach is the synthesis of energetic coordination compounds (ECCs), which offers the advantage of allowing selective design, since the metal center, energetic ligand, and oxidizing anion can be varied.^[9] This is an extremely important possibility since it allows the development of EMs with specific, defined, and targeted properties. Two of the most powerful coordination compounds of this type which have been reported are tris(hydrazine)cobalt(II) perchlorate (CHP) and tris(hydrazine)nickel(II) perchlorate (NHP), which show detonation energies in the range of those of secondary explosives.^[10] Unfortunately, both of these compounds are too sensitive and not suitable for any application. Probably the best investigated and most promising ECC is tetraammine-cis-bis(5-nitro-2*H*-tetrazolato)cobalt(III) perchlorate (BNCP).^[11]

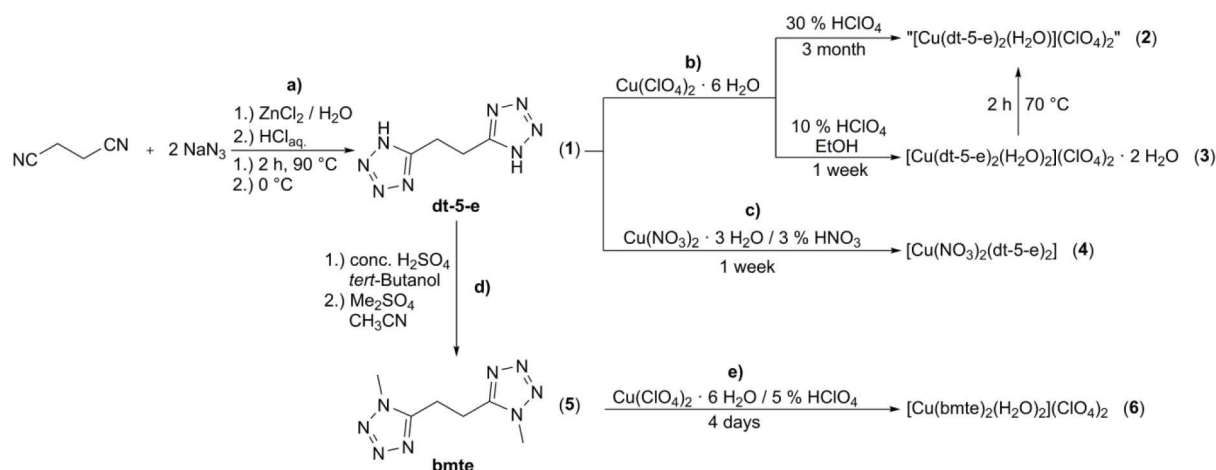
Another trend in the improvement of EMs is the synthesis and investigation of energetic cocrystals. In such compounds, usually secondary explosives such as 2,4,6-trinitrotoluene (TNT),^[12] octahydro-1,3,5,7-tetranitro-1,3,5,7-tetrazocine (HMX),^[13] or 2,4,6,8,10,12-hexanitro-2,4,6,8,10,12-hexaazaisowurtzitane (CL-20)^[12,13] are used for cocrystallization. Investigations have shown that the cocrystallization of two energetic compounds can decrease the sensitivity but (crucially) maintain the performance. An important example of this are 2:1 cocrystals of Cl-20/HMX.^[13]

While cocrystals of (nonenergetic) coordination compounds are well-known in inorganic chemistry,^[14] to the best of our knowledge, cocrystals of compounds containing energetic complexes have not yet been described. The concept of combining both the formation of a coordination compound and the introduction of an ionic cocrystal to develop a new class of EMs has been used in this work, and the synthesis and characterization of the energetic ionic complex cocrystal abbreviated as “[Cu(dt-5-e)₂(H₂O)](ClO₄)₂” (**2**) containing 1,2-di(1*H*-tetrazol-5-yl)ethane (dt-5-e, **1**)^[15-17] as a neutral coordinating ligand and the perchlorate anion as a counterion has been achieved. The ionic cocrystal (**2**) consists of a mononuclear ([Cu(dt-5-e)₂(H₂O)](ClO₄)₂) and a trinuclear ([[(dt-5-e)(H₂O)Cu(μ-dt-5-e)Cu(dt-5-e)₂(μ-dt-5-e)Cu(dt-5-e)(H₂O)](ClO₄)₆) complex unit. Additionally, two mononuclear coordination compounds with dt-5-e as a ligand and perchlorate (**3**) and nitrate (**4**) as counterions as well as the

mononuclear perchlorate coordination compound with 1,2-bis(1-methyltetrazol-5-yl)ethane as a ligand (**6**) were prepared, characterized, and compared to the ionic cocrystal **2**.

11.3. Results and Discussion

Synthesis: Preparation of ligand **1** (dt-5-e) was similar to the method of Demko and Sharpless in yields of 30%.^[15] Compound **2** can be obtained two ways (Scheme 1a,b): (i) by extremely slow evaporation (three months) of a concentrated solution of $\text{Cu}(\text{ClO}_4)_2 \cdot 6\text{H}_2\text{O}$ and **1** in perchloric acid or (ii) by dehydration of the similar – but more accessible – mononuclear coordination compound $[\text{Cu}(\text{dt-5-e})_2(\text{H}_2\text{O})_2](\text{ClO}_4)_2 \cdot 2\text{H}_2\text{O}$ (**3**) in the solid state at 70 °C. The mononuclear coordination compound **3** is obtained within a few days by precipitation of the product due to the addition of ethanol to the reaction mixture (diluted perchloric acid). Treating **1** with copper(II) nitrate in nitric acid yields the nitrato compound **4** with the formula $[\text{Cu}(\text{NO}_3)_2(\text{dt-5-e})_2]$ (Scheme 1c). Methylation of **1** using the method of Ivashkevich *et al.* resulted in the formation of 1,2-bis(1-methyltetrazol-5-yl)ethane (bmte, **5**),^[18] which can react with $\text{Cu}(\text{ClO}_4)_2 \cdot 6\text{H}_2\text{O}$ to form the mononuclear coordination compound **6** (Scheme 1d,e).



Scheme 1. a) Literature synthesis of the ligand 1,2-di(1*H*-tetrazol-5-yl)ethane,^[15] b) Reaction of dt-5-e forming the copper(II) compounds **2** and **3**, c) Reaction of **1** forming the nitrato compound **4**, d) Methylation of **1** according to literature,^[18] e) Further reaction of **5** forming compound **6**.

Crystal Structures: The structures of **2**, **3**, **4**, and **6** were determined using single crystal X-ray diffraction. In contrast to **3**, compound **2** does not only show a mononuclear octahedral coordination sphere. Instead, an atypical and rare energetic ionic cocrystal consisting of a mononuclear and a trinuclear complex unit is formed (Figure 1). Compound **2** crystallized as blue rod ($20 \times 2 \times 1 \text{ mm}^3$) in the triclinic space group $P\bar{1}$ with a density of 1.908 cm^{-3} at 173 K. The mononuclear unit shows the expected Jahn–Teller distorted octahedral coordination sphere, as is also observed for compound **3**.

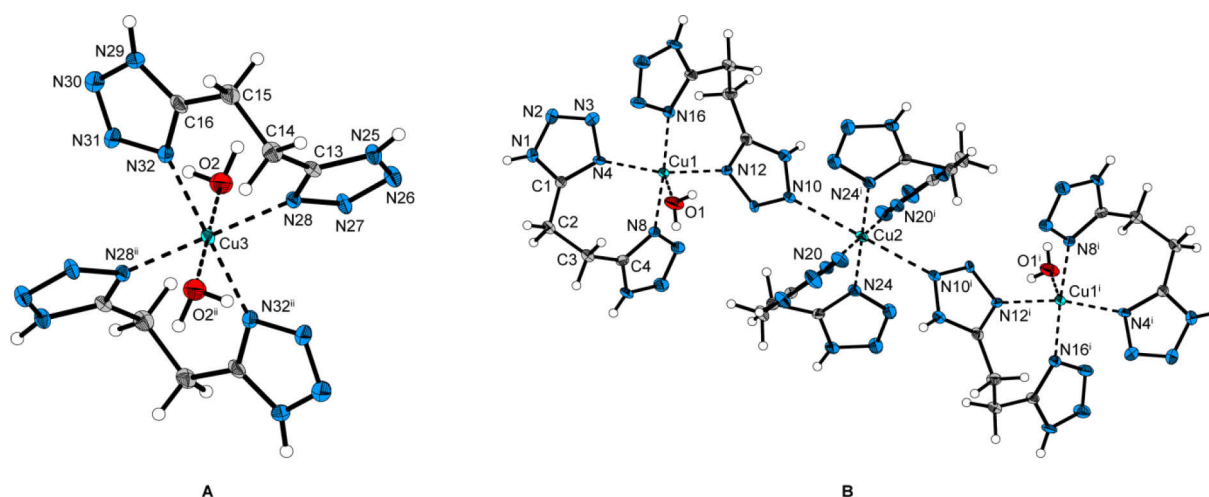


Figure 1. Crystal structures of the ionic cocrystal **2** showing the mononuclear (**A**) and trinuclear (**B**) copper units. Thermal ellipsoids of non-hydrogen atoms are drawn at the 50 % probability level. The perchlorates counterions were omitted for clarity. Selected bond lengths [\AA] and angles [deg]: Cu1–N4 2.006(3), Cu1–N8 2.009(3), Cu1–N12 2.002(3), Cu1–N16 2.022(3), Cu1–O1 2.172(3), Cu2–N10 2.5674(31), Cu2–N20 2.013(3), Cu2–N24 2.014(3), Cu3–N28 1.997(3), Cu3–N32 2.049(3), Cu3–O2 2.411(3), N25–C13 1.328(5), C11–O3 1.411(4), N4–Cu1–N8 87.58(12), N12–Cu1–N8 91.89(12), N8–Cu1–N16 176.15(12), N4–Cu1–O1 98.35(13), N8–Cu1–O1 91.84(13), N12–Cu1–N4 149.41(13), N20–Cu1–N24 88.09(12), N10–Cu2–N20 85.94(11), N10–Cu1–N10ⁱ 180.00, N20–Cu2–N20ⁱ 180.00, N24–Cu1–N24ⁱ 180.00, N28–Cu3–N32 89.97(12), N28–Cu3–O2 83.94(12), N28–Cu3–N28ⁱⁱ 180.00, N32–Cu3–N32ⁱⁱ 180.00, O2–Cu3–O2ⁱⁱ 180.00, C13–N25–N26–N27 0.1(4), C1–C2–C3–C4 $-57.2(4)$, C13–C14–C15–C16 67.1(4). Symmetry code: i: $1-x, 1-y, 1-z$; ii: $1-x, 2-y, -z$.

The angles and Cu–N and Cu–O bond lengths of the mononuclear unit are in the expected range for typical Jahn–Teller distorted octahedral copper(II) complexes.^[19] The trinuclear copper complex consists of two pentacoordinated copper centers which are connected through a six-coordinated octahedral unit. The coordination sphere of the pentacoordinated copper center is between those of a trigonal-bipyramid and a square-pyramid (Addison parameter $\tau = 0.45$).^[20] Due to the similar N positions and an Addison parameter $\tau < 0.5$, the structure is described as square-pyramidal. All of the equatorial positions of the two symmetric square-pyramids are occupied by nitrogen atoms (Cu–N 2.00–2.02 \AA similar to literature values)^[14,18] of two bidentate dt-5-e ligands (N12–Cu1–N4 149.41(13) $^\circ$ and N8–Cu1–N16 176.15(12) $^\circ$). The apical position is occupied by the oxygen atom of an aqua ligand. The Cu–O bond (Cu1–O1 2.172(3) \AA) is slightly elongated compared to the equatorial Cu–N bonds but is still shorter than the values reported for Cu–O bonds in similar square-pyramidal copper complexes in the literature.^[14] The two dt-5-e ligands differ in their coordination mode. One is bidentate only, whereas the other is bidentate and additionally μ -bridging at the N10 position to Cu2. The copper center Cu2 is surrounded by six nitrogen atoms arranged in a Jahn–Teller distorted octahedron (Cu2–N20 2.013(3), Cu2–N24 2.014(3), and Cu2–N10 2.5674(31) \AA). Two dt-5-e ligands coordinate in a terminal bidentate mode (equatorial positions), while the axial positions are occupied by N atoms of μ -bridging dt-5-e ligands of neighboring copper

In compound **2**, numerous hydrogen bonds are formed between the neutral dt-5-e ligands of the mononuclear and trinuclear unit, the aqua ligands, and the perchlorate counterions (Figure 2). The distances and angles of selected hydrogen bonds are given in Table 1. Most notable are the hydrogen bonds between N1 and N27^{vi}, N21ⁱ and N26, as well as N22ⁱ and N25, which clearly show the connections between the mononuclear and the trinuclear complex units (symmetry codes: i: 1-x, 1-y, 1-z; vi: 1+x, -1+y, z).

Table 1. Distances and angles of selected hydrogen bonds in **2**.

D-H...A ^a	D-H / Å	H...A / Å	D...A / Å	D-H...A / deg
N1-H1...N27 ^{vi}	0.76(5)	2.12(5)	2.878(5)	175(6)
O2-H2C...N4 ^v	0.79(7)	2.06(7)	2.829(5)	166(7)
O2-H2D...N4	0.87(7)	2.19(6)	2.922(5)	141(5)
N5-H5...O14 ^{iv}	0.73(4)	2.12(4)	2.824(5)	161(4)
N17-H17...O7	0.89(4)	1.97(4)	2.855(6)	170(4)
N21 ⁱ -H21 ⁱ ...N26	0.75(4)	2.49(4)	2.969(5)	123(4)
N21 ⁱ -H21 ⁱ ...O9 ⁱⁱⁱ	0.75(4)	2.34(4)	3.022(7)	152(4)
N25-H25...N22 ⁱ	0.84(4)	2.46(4)	3.000(4)	123(3)

^a Symmetry codes: i: 1-x, 1-y, 1-z; iii: x, 1+y, z; iv: 1-x, -y, 1-z; v: -x, 2-y, -z; vi: 1+x, -1+y, z.

The mononuclear coordination compound **3** crystallizes in the orthorhombic space group $Pbc2_1$ with four formula units per unit cell and a calculated density of 1.881 g cm⁻³ at 173 K. The copper(II) center is coordinated by two bidentate dt-5-e ligands at the equatorial positions and by two aqua ligands at the axial positions (Figure 3). The coordination sphere is octahedral and similar to the mononuclear complex unit of compound **2**. Jahn-Teller distortion can be observed along the O1-Cu1-O2 axis. Further, the structure contains two crystal water molecules which are disordered. The bond lengths and angles are in a typical range.

Coordination compound **4** crystallizes in the triclinic space group $P\bar{1}$ with a calculated density of 1.948 g cm⁻³ (at 100 K). Compound **4** is the only compound of the herein investigated ones which crystallizes in a water-free form. As expected, the copper center exhibits a Jahn-Teller distorted octahedral coordination sphere with nitrate anions in the axial position and bidentate dt-5-e ligands in the equatorial (Figure 4). The equatorial positions are occupied by the N4 atoms of the two bidentate dt-5-e ligands with typical Cu-N bond lengths of 1.9672(16) and 2.0856(16) Å. The bidentate dt-5-e forms a seven-membered ring with the copper center. The axial positions are occupied by the O1 atoms of the two nitrate ligands. The Cu-O bond is strongly elongated with 2.4180(14) Å.

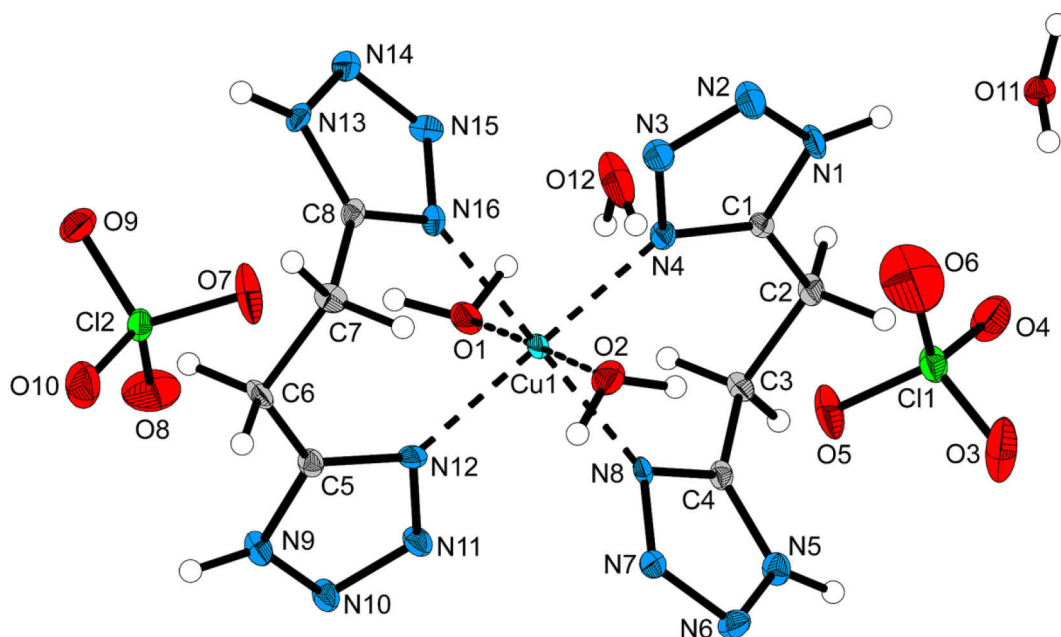


Figure 3. Crystal structure of the mononuclear coordination compound **3**. Thermal ellipsoids of non-hydrogen atoms are drawn at the 50 % probability level. Selected bond lengths [Å] and angles [deg]: Cu1–N4 2.016(3), Cu1–N8 1.992(3), Cu1–N12 2.009(3), Cu1–N16 1.993(3), Cu1–O1 2.7471(28), Cu1–O2 2.6453(29), N1–C1 1.320(5), C11–O3 1.432(3), N8–Cu1–N4 90.86(11), N8–Cu1–N12 89.45(13), N12–Cu1–N4 179.68(14), N8–Cu1–N16 178.01(14), O2–Cu1–O1 178.76(9), O3–C11–O4 108.43(17), N1–C1–N4 107.4(3), C4–C3–C2–C1 –62.5(4).

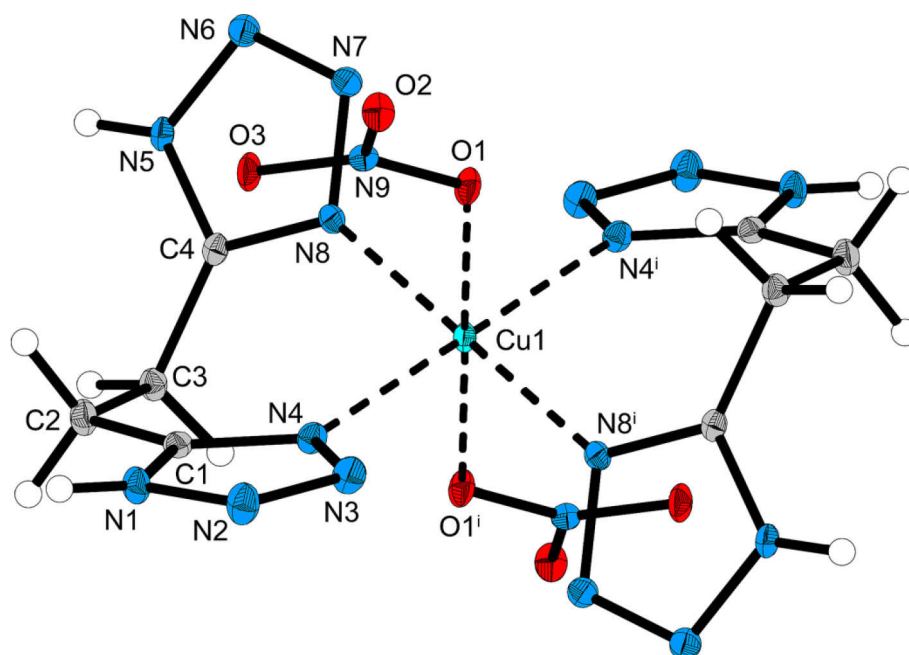


Figure 4. Crystal structure of the mononuclear coordination compound **4**. Thermal ellipsoids of non-hydrogen atoms are drawn at the 50 % probability level. Selected bond lengths [Å] and angles [deg]: Cu1–N8 1.9672(16), Cu1–N4 2.0856(16), Cu1–O1 2.4180(14), N1–C1 1.332(2), O1–N9 1.262(2), N8–Cu1–N4 90.75(6), N8–Cu1–O1 88.84(6), O1–Cu1–O1ⁱ 180.00, N4–Cu1–N4ⁱ 180.00, N8–Cu1–N8ⁱ 180.00(7). Symmetry code: *i*: $-x, 1-y, 1-z$.

The obtained copper(II) perchlorate coordination compound **6** with **5** as a ligand forms the expected mononuclear octahedron with two bidentate bmte ligands in the equatorial and two

aqua ligands in the axial positions (Figure 5) showing the typical Jahn–Teller distortion (Cu1–O1 2.4387(13) Å). The bond lengths and angles are very similar to the mononuclear complex unit of compound **2**. The ECC **6** crystallizes in the monoclinic space group $P2_1/c$ with two formula units per unit cell and a calculated density of 1.790 g cm⁻³ (at 100 K).

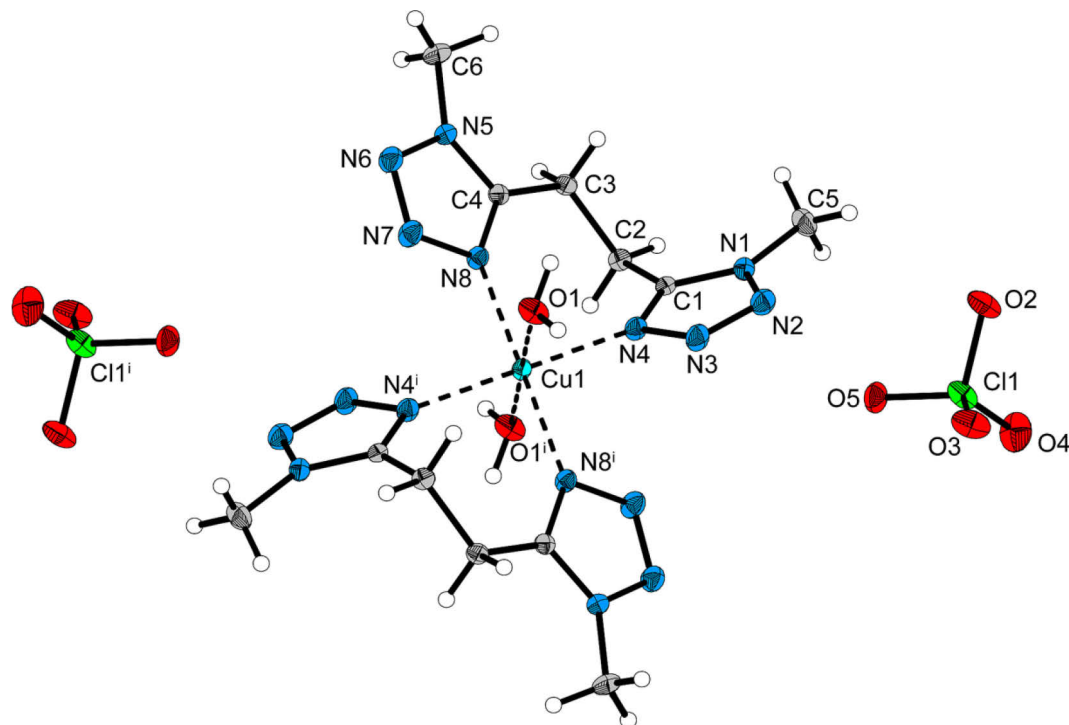


Figure 5. Crystal structure of the mononuclear coordination compound **6**. Thermal ellipsoids of non-hydrogen atoms are drawn at the 50 % probability level. Selected bond lengths [Å] and angles [deg]: Cu1–N4 1.9998(14), Cu1–N8 2.0294(14), Cu1–O1 2.4387(13), N1–C1 1.335(2), N4–Cu1–N8 89.66(6), N4–Cu1–O1 85.91(5), O1–Cu1–O1ⁱ 180.00, N4–Cu1–N4ⁱ 180.00(6), N8–Cu1–N8ⁱ 180.00, C1–N1–N2–N3 –0.40(18), C1–C2–C3–C4 –62.7(2). Symmetry code: i: $-x, -y, -z$.

Powder Diffraction: Due to the mixed coordination mode, compound **2** shows superior laser absorption. Therefore, the formation of **2** by thermal transition of the mononuclear coordination compound **3** was investigated by X-ray powder diffraction. Gunier diffractograms (Figures S1 and S2) with MoK α 1 radiation ($\lambda = 0.7093$ Å) were performed in the 2θ range between 4 and 34° with **3** (orthorhombic) and **2** (triclinic). In addition, a series of Gunier diffractograms was obtained for orthorhombic **3**, which was heated for 2 h at 50, 60, 70, and 80 °C. At 50 °C the diffractogram showed only the phase-pure diffraction pattern of **3**. At 60 °C, equal amounts of **3** and **2** were observed, whereas at 70 °C, a diffraction pattern containing only phase-pure **2** was obtained. In addition to infrared spectroscopy and elemental analysis, powder diffraction proved that the mononuclear, octahedral compound **3** transforms into the mono- and trinuclear coordination compound **2** by a solid state thermal dehydration and migration process.

Due to the dehydration which occurs, the copper centers rearrange within the unit cell to saturate the free coordination sites which arise and which were originally occupied by aqua

ligands. Saturation of the copper coordination sites is achieved by the new coordination modes of the dt-5-e ligand which are observed ($\mu_2, \kappa^3 N^2, N^4, N^4$ instead of only $\kappa^2 N^4, N^4$) and the new coordination spheres which are formed (square-pyramidal instead of only octahedral). The cell parameters (see Table S1) change slightly due to the loss of water (e.g., **3**, $V = 2355.3 \text{ \AA}^3 \rightarrow 2, V = 2132.9 \text{ \AA}^3$).

Infrared Spectroscopy: In addition to the powder diffractions of **2** and **3**, infrared spectra were recorded for all compounds **1–6**. A comparison of the infrared spectra of the free ligand **1** with the coordination compounds **2** and **3** shows that both coordination compounds exhibit the ligand vibrations of **1**, although in **2** and **3** they are shifted owing to coordination to the Cu^{2+} center (Figure S3 and S4). For example, the C=N stretching vibration of the free ligand **1** at 1583 cm^{-1} is shifted to 1564 cm^{-1} for **3** and to $1571, 1562,$ and 1557 cm^{-1} for **2**. The three C=N vibration bands in the spectra of **2** also indicate that different coordination modes of ligand **1** are present in compound **2**, which is in agreement with the crystal structure. The IR spectra of the mononuclear octahedral coordination compounds **3** and **6** show similar vibration bands and agree with the crystal structures of $[\text{CuL}_2(\text{H}_2\text{O})_2](\text{ClO}_4)_2$. For compound **3**, an additional broad vibration band at approximately 3490 cm^{-1} is observed which can be assigned to uncoordinated crystal water. The spectra of compounds **2, 3,** and **6** also show the typical perchlorate vibration bands (**2**, 1071 cm^{-1} ; **3**, 1073 cm^{-1} ; **6**, 1087 cm^{-1}), while in the spectrum of **4** split nitrate vibrations are observed, which is due to the coordination of the nitrate ion (**4**, 1333 and 1323 cm^{-1}).

Energetic Properties and Laser Ignition: The metal coordination compounds were also investigated for their potential use as primary explosives, and selected parameters are summarized in Table 2. As expected (in contrast to the nitrate coordination compound **4**), the perchlorate compounds show an increased sensitivity toward mechanical stimuli.

Table 2. Energetic properties of **2, 3, 4** and **6**.

	2	3	4	6
IS / J^a	1	3	4	4
FS / N^a	5	14	160	80
grain size / μm	100–500	500–1000	< 100	500–1000
hot needle ^b	det. ^c	defl. ^d	decomp. ^e	defl. ^d
laser init. ^f	det. ^c	-	-	defl. ^d
function time / μs	67	-	-	292
$F(R)_{@940 \text{ nm}}^g$	1.35	0.04	-	0.09

^a According to BAM standard methods. ^b The hot needle test was performed by penetrating the sample, which is confined by adhesive tape, with the hot tip of a needle. ^c Detonation. ^d Deflagration. ^e Decomposition. ^f Wavelength of the diode laser $\lambda = 940 \text{ nm}$ at constant power density in the order of 10^5 W cm^{-2} . ^g Relative light absorption [arbitrary units] as function of the reflectance at 940 nm .

The coordination compound **2** in particular shows sensitivities and performance corresponding to that of a primary explosive. Despite this, however, it can be handled appropriately. The thermal stabilities of the compounds were determined by differential thermal analysis using a heating rate of $5\text{ }^{\circ}\text{C min}^{-1}$. The mononuclear compound **3** can be dehydrated at about $70\text{ }^{\circ}\text{C}$ and is transformed to **2** in the solid state. Compound **2** is thermally stable up to $188\text{ }^{\circ}\text{C}$ at which temperature dehydration occurs followed by exothermic decomposition. The dehydration of **6** occurs in a similar range, although the resulting compound is stable up to $278\text{ }^{\circ}\text{C}$. However, only compound **2** shows energetic properties comparable with those of a primary explosive. Without confinement, **2** only deflagrates by thermal ignition while with confinement it detonates if exposed to shock, thermal, or laser ignition. Due to the high light absorption over a broad range (500 to 1200 nm; Figure 6) compound **2** shows an outstanding response toward laser radiation.

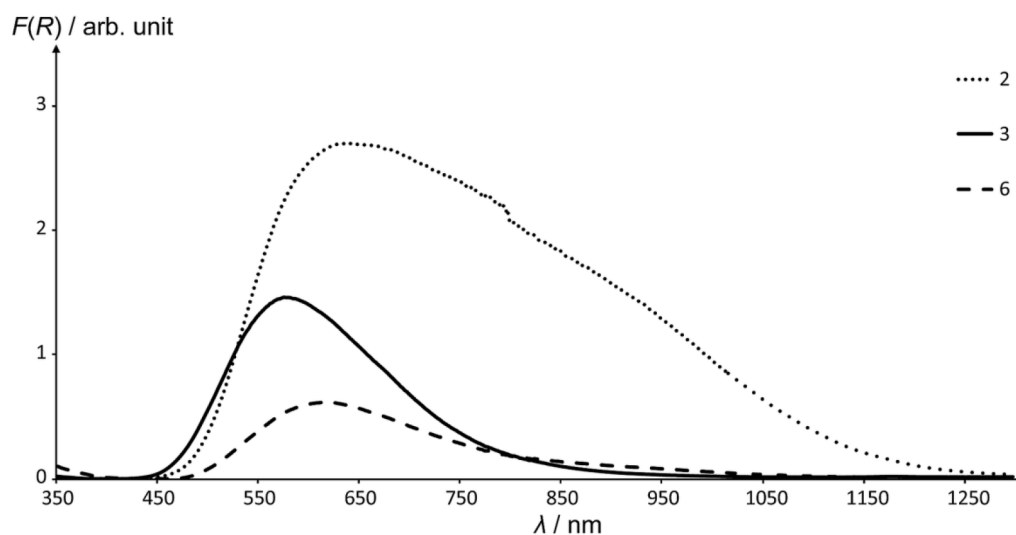


Figure 6. UV/Vis/NIR spectra of compounds **2**, **3**, and **6**.

The UV/Vis/NIR spectra of **3** and **6** are very similar, indicating the same electronic transitions occur (from the xy orbital to the x^2-y^2 and from xz/yz to x^2-y^2), which are typical for a Jahn–Teller distorted d^9 -complex. Owing to the different coordination spheres present in the compound **2** (octahedral and square-pyramidal), **2** absorbs in a much larger range than the mononuclear, octahedral coordination compounds **3** and **6**. Compound **2** is therefore more suitable for laser ignition because the use of radiation sources emitting in the near infrared ($\sim 800\text{--}1100\text{ nm}$) are preferred for technical reasons. Confined samples of **2** and **6** were irradiated with a monopulsed laser beam at 940 nm and a pulse length of $400\text{ }\mu\text{s}$. Compound **2** detonated, while the less powerful compound **6** only deflagrated. The energy output was measured qualitatively by an aluminum witness plate (Figure 7) and indicated detonation for **2**. For compound **6**, no dent was observed in the witness plate. Furthermore, the function times t_f (time delay between beginning irradiation and complete reaction) were determined

and showed a 4 times faster value for **2** ($t_f = 67 \mu\text{s}$) than for **6** ($t_f = 292 \mu\text{s}$). This is in agreement with the higher absorption by **2** at 940 nm (Table 2). Values for the function time in the low-microsecond range are essential for potential alternatives for fast-functioning electric type detonators such as exploding-bridge-wires.^[21]

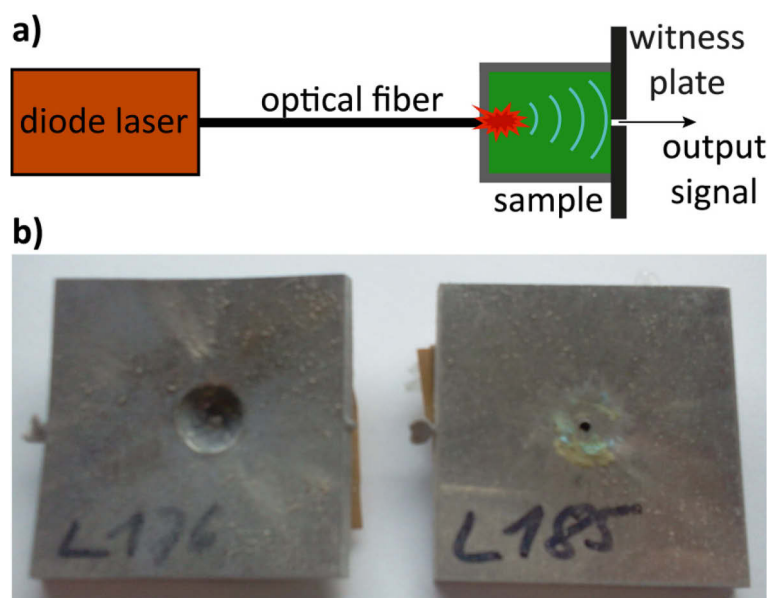


Figure 7. a) Laser ignition setup. b) Witness plates after laser ignition of coordination compounds **2** (left) and **6** (right).

11.4. Conclusion

In conclusion, the successful combination of the synthesis of energetic coordination compounds with the concept of cocrystallization was achieved in the synthesis and characterization of the mono- and trinuclear copper(II) perchlorate coordination compound **2** using dt-5-e as flexible ligand. This represents a new concept in the design of energetic materials and offers the possibility to prepare highly photosensitive explosives. Furthermore, it was shown that the mono- and trinuclear coordination compound **2** can be obtained in a facile method by the dehydration of its mononuclear homologue **3** in the solid state. Due to the three different copper(II) coordination spheres in **2**, light is absorbed over a broad range with high intensity making **2** suitable for advanced laser initiated explosive devices.

11.5. Experimental Section

CAUTION! The prepared copper(II) compounds are energetic materials with increased sensitivity to various stimuli (e.g., friction, impact, or heat). Proper protective measures (face shield, ear protection, leather coat, earthed equipment, conductive floor and shoes, Kevlar gloves) should be used at all time. Only small scales of the compounds **2** and **3** should be handled.

The impact and friction sensitivity tests were performed according to standard methods by using a BAM (Bundesanstalt für Materialforschung und -prüfung) drop hammer and a BAM friction tester.^[22,23] Decomposition temperatures were measured via differential thermal analysis (DTA) with an OZM Research DTA 552-Ex instrument at a heating rate of 5 °C min^{-1} and in a range of room temperature to 400 °C .^[24,25] The determination of the carbon, hydrogen and nitrogen contents was carried out by combustion analysis using an Elementar Vario EL.^[26] Infrared (IR) spectra were recorded on a PerkinElmer BXII FT-IR system with a Smith DuraSamplIR II diamond ATR unit.^[27] The UV/Vis/NIR reflectance of solid samples (powders) was determined with a Varian Cary 500 spectrometer in the wavelength range of 350–1300 nm.^[28] The relative reflectance R [%] was transformed by the Kubelka–Munk equation to the absorption intensity $F(R)$ [arbitrary units]. A reflectance of $R > 100\%$ is possible because the values are relative to the background reflection of blank samples.^[29]

The crystal structures were determined on an Oxford Diffraction Xcalibur 3 diffractometer with a Sapphire CCD detector, four circle kappa platform, Enhance molybdenum $K\alpha$ radiation source ($\lambda = 71.073\text{ pm}$), and Oxford Cryosystems Cryostream cooling unit.^[28] Data collection and reduction were performed with the CrysAlisPro software.^[30,31] The structures were solved with SIR97 or SIR2004.^[32,33] The refinement was performed with SHELXL-97.^[34] The CIF-files were checked at the checkCIF website.^[35] The non-hydrogen atoms were refined anisotropically and the hydrogen atoms isotropically if not calculated.

X-ray powder experiments were performed on a Guinier diffractometer (Huber G644) with Mo $K\alpha_1$ radiation ($\lambda = 0.7093\text{ Å}$) (quartz monochromator) in Lindemann capillaries (0.7 mm diameter). The angle calibration was performed with electronic grade germanium. In the 2θ range between 4 and 34° with an increment of 0.04° , 750 data points were collected with a counting rate of 10 s for each increment. The Rietveld parameters were analyzed with the program FullProf.^[36] The Rietveld data set contained 106 crystallographic independent atoms for the triclinic compound **2** and 59 crystallographic independent atoms for the orthorhombic compound **3**. Due to excessive peak overlapping, calculating diffractograms with FullProf was only possible in the 2θ range between 4 and 16° .

All chemicals were used as purchased. The ligands 1,2-di(1*H*-tetrazol-5-yl)ethane (dt-5-e, **1**) and 1,2-bis(1-methyltetrazol-5-yl)ethane (bmte, **5**) were synthesized similar to the literature procedures.^[15,18]

{[Cu(dt-5-e)₂(H₂O)₂](ClO₄)₂}{[(dt-5-e)(H₂O)Cu(μ-dt-5-e)Cu(dt-5-e)₂(μ-dt-5-e)Cu(dt-5-e)(H₂O)](ClO₄)₆} (**2**) abbreviated as "[Cu(dt-5-e)₂(H₂O)](ClO₄)₂".

a) The ligand **1** (166 mg, 1.00 mmol) was dissolved in perchloric acid (30 %, 5.0 mL) at 60 °C . Under stirring, a solution of copper(II) perchlorate hexahydrate (186 mg, 0.5 mmol) in perchloric acid (30 %, 1.0 mL) was added, and the resulting blue reaction mixture cooled to

room temperature and left for crystallization. After three months, one single crystal in form of a blue rod ($20 \times 2 \times 1 \text{ mm}^3$) suitable for X-ray diffraction was obtained. The crystal was filtered off and dried under ambient conditions for 1 h. Yield: 76 mg (0.04 mmol, 12 %).

b) Drying of compound **3** (333 mg, 0.50 mmol) at $70 \text{ }^\circ\text{C}$ in the oven for 2 h yielded 306 mg (0.13 mmol, 100 %) of **2**. DTA ($5 \text{ }^\circ\text{C min}^{-1}$) onset: $188 \text{ }^\circ\text{C}$ (dehydration), $206 \text{ }^\circ\text{C}$ (decomposition). IR (ATR): $\tilde{\nu} = 3527$ (w), 3476 (vw), 3317 (w), 3153 (w), 1571 (w), 1562 (m), 1557 (m), 1415 (w), 1394 (w), 1101 (s), 1091 (s), 1071 (s), 1051 cm^{-1} (vs). Elem anal. ($\text{C}_{32}\text{H}_{56}\text{Cl}_8\text{Cu}_4\text{N}_{64}\text{O}_{36}$, $2451.17 \text{ g mol}^{-1}$) calcd.: C 15.68, H 2.30, N 36.57 %. Found: C 15.98, H 2.44, N 36.29 %. BAM impact: 1 J. BAM friction: $\leq 5 \text{ N}$ (at grain size 100–500 μm).

[Cu(dt-5-e)₂(H₂O)₂](ClO₄)₂·2H₂O (3). Compound **1** (330 mg, 2.00 mmol) was dissolved in diluted perchloric acid (10 %, 6.0 mL) at $60 \text{ }^\circ\text{C}$. A solution of copper(II) perchlorate hexahydrate (372 mg, 1.00 mmol) in water was added under stirring and the blue reaction mixture cooled to room temperature. After 2 days, ethanol (3.0 mL) was added and the solution left for crystallization for further 3 days. Single crystals in the form of violet blocks were obtained, filtered off, washed with a small amount of ether, and dried under ambient conditions. Yield: 454 mg (0.68 mmol, 68 %). DTA ($5 \text{ }^\circ\text{C min}^{-1}$) onset: $77 \text{ }^\circ\text{C}$ (dehydration). IR (ATR): $\tilde{\nu} = 3490$ (m), 3153 (w), 1564 (m), 1417 (w), 1403 (w), 1071 (vs), 1054 cm^{-1} (vs). Elem anal. ($\text{C}_8\text{H}_{20}\text{Cl}_2\text{CuN}_{16}\text{O}_{12}$, $666.80 \text{ g mol}^{-1}$) calcd.: C 14.41, H 3.02, N 33.61 %. Found: C 14.68, H 3.17, N 33.22 %. BAM impact: 3 J. BAM friction: 14 N (at grain size 500–1000 μm).

[Cu(NO₃)₂(dt-5-e)₂] (4). Compound **1** (330 mg, 2.00 mmol) was dissolved in 0.5 M nitric acid (7.0 mL) at $60 \text{ }^\circ\text{C}$. A solution of copper(II) nitrate trihydrate (247 mg, 1.00 mmol) in water (1.0 mL) was added under stirring. The blue solution was cooled to room temperature and left for crystallization. After 1 week, X-ray suitable single crystals in the form of blue blocks were obtained. The crystals were filtered off, washed with a small amount of ethanol, and air-dried. Yield: 495 mg (0.95 mmol, 95 %). DTA ($5 \text{ }^\circ\text{C min}^{-1}$) onset: $180 \text{ }^\circ\text{C}$ (decomposition). IR (ATR): $\tilde{\nu} = 3177$ (w), 3136 (w), 1559 (s), 1426 (s), 1390 (s), 1333 (vs), 1323 (vs), 1051 cm^{-1} (vs). Elem anal. ($\text{C}_8\text{H}_{12}\text{CuN}_{18}\text{O}_6$, $519.84 \text{ g mol}^{-1}$) calcd.: C 18.48, H 2.33, N 48.50 %. Found: C 18.74, H 2.32, N 47.95 %. BAM impact: 4 J. BAM friction: 160 N (at grain size $< 100 \mu\text{m}$).

[Cu(bmte)₂(H₂O)₂](ClO₄)₂ (6). The nitrogen-rich compound **5** (390 mg, 2.00 mmol) was dissolved in diluted perchloric acid (5 %, 8.0 mL) at $60 \text{ }^\circ\text{C}$. A solution of copper(II) perchlorate hexahydrate (372 mg, 1.00 mmol) in diluted perchloric acid (5 %, 1.0 mL) was added under stirring. The reaction mixture was cooled to room temperature and left for crystallization. Within 4 days, X-ray suitable single crystals were obtained in the form of blue blocks. The crystals were filtered off, washed with a small amount of water, and dried at ambient conditions. Yield: 428 mg (0.62 mmol, 62 %). DTA ($5 \text{ }^\circ\text{C min}^{-1}$) onset: $190 \text{ }^\circ\text{C}$

(dehydration), 278 °C (decomposition). IR (ATR): $\tilde{\nu}$ = 3593 (vw), 3509 (vw), 1619 (w), 1543 (w), 1420 (w), 1087 cm^{-1} (vs). Elem anal. ($\text{C}_{12}\text{H}_{24}\text{Cl}_2\text{CuN}_{16}\text{O}_{10}$, 686.87 g mol^{-1}) calcd.: C 20.98, H 3.52, N 32.63 %. Found: C 21.11, H 3.43, N 32.70 %. BAM impact: 4 J. BAM friction: 80 N (at grain size 500–1000 μm).

11.6. References

- [1] Haiges, R.; Schneider, S.; Schroer, T.; Christe, K. O. *Angew. Chem. Int. Ed.* **2004**, *43*, 4919.
- [2] Gao, H.; Shreeve, J. M. *Chem. Rev.* **2011**, *111*, 7377.
- [3] Fronabarger, J. W.; Williams, M. D.; Sanborn, W. B.; Bragg, J. G.; Parrish, D. A.; Bichay, M. *Propellants Explos. Pyrotech.* **2011**, *36*, 541.
- [4] Sabatini, J. J.; Moretti, J. D. *Chem. - Eur. J.* **2013**, *19*, 12839.
- [5] Giles, J. *Nature* **2004**, *427*, 580.
- [6] Vogel, S. Defense Dept. Standards On Lead Exposure Faulted. *Washington Post*, Dec 4, 2012; p 23.
- [7] Brinck, T. *Green Energetic Materials*; 1st ed.; John Wiley & Sons Ltd: Chichester, U. K., 2014.
- [8] Klapötke, T. M. *Chemie der hochenergetischen Materialien*; 1st ed.; Walter de Gruyter: Berlin, 2009.
- [9] Sinditskii, V. P.; Seurshkin, V. V. *Defence Science Journal* **1996**, *46*, 371.
- [10] Bushuyev, O. S.; Brown, P.; Maiti, A.; Gee, R. H.; Peterson, G. R.; Weeks, B. L.; Hope-Weeks, L. J. *J. Am. Chem. Soc.* **2012**, *134*, 1422.
- [11] Fronabarger, J. W.; Sanborn, W. B.; Massis, T. *Proceedings of the 22nd International Pyrotechnics Seminar*; Fort Collins, CO, Jul 15–19, 1996; p 645.
- [12] Bolton, O.; Matzger, A. J. *Angew. Chem., Int. Ed.* **2011**, *50*, 8960.
- [13] Bolton, O.; Simke, L. R.; Pagoria, P. F.; Matzger, A. J. *Cryst. Growth Des.* **2012**, *12*, 4311.
- [14] El Bakkali, H.; Choquesillo-Lazarte, D.; Dominguez-Martin, A.; Perez-Toro, M. I.; Lezama, L.; Gonzalez-Perez, J. M.; Castineiras, A.; Niclos-Gutierrez, J. *Cryst. Growth Des.* **2014**, *14*, 889.
- [15] Demko, Z. P.; Sharpless, K. B. *J. Org. Chem.* **2001**, *66*, 7945.
- [16] Shen, L.; Yang, J.; Yang, G.-W.; Li, Q.-Y.; Tang, X.-Y.; Zhou, F.; Miao, Z.-F.; Jin, J.-N.; Shen, W. *Inorg. Chim. Acta* **2011**, *370*, 150.
- [17] Qiao, C.-F.; Zhou, C.-S.; Wei, Q.; Xia, Z.-Q. *Acta Crystallogr., Sect. E: Struct. Rep. Online* **2012**, *68*, o989.
- [18] Ivashkevich, D. O.; Lyakhov, A. S.; Pytleva, D. S.; Voitekhovich, S. V.; Gaponik, P. N. *Acta Crystallogr., Sect. C: Cryst. Struct. Commun.* **2003**, *C59*, m221.

- [19] Joas, M.; Klapötke, T. M.; Stierstorfer, J.; Szimhardt, N. *Chem. - Eur. J.* **2013**, *19*, 9995.
- [20] Addison, A. W.; Rao, T. N.; Reedijk, J.; Van Rijn, J.; Verschoor, G. C. *J. Chem. Soc., Dalton Trans.* **1984**, 1349.
- [21] Hafenrichter, E. S.; Marshall, B. W.; Fleming, K. J. *41st Areospace Sciences Meeting and Exhibit*, Reno, NV, Jan 6–9, 2003; pp 1–11.
- [22] NATO *Standardization Agreement 4489*, September 17, 1999.
- [23] NATO *Standardization Agreement 4487*, October 29, 2009.
- [24] OZM Research s.r.o. Home Page. <http://www.ozm.cz> (accessed March 13, 2014).
- [25] NATO *Standardization Agreement 4515*, August 23, 2002.
- [26] Elementar Analysensysteme GmbH Home Page. <http://www.elementar.de/> (accessed March 13, 2014).
- [27] PerkinElmer Inc. Home Page. <http://www.perkinelmer.de/> (accessed March 13, 2014).
- [28] Agilent Technologies Inc. Home Page. <http://www.agilent.com/> (accessed March 13, 2014).
- [29] P. Kubelka; Munk, F. *Z. Tech. Physik* **1931**, *1*, 593.
- [30] *CrysAlisPro 1.171.36.24*, Oxford Diffraction Ltd., Abingdon, U. K., 2012.
- [31] *CrysAlisPro 1.171.37.31*, Oxford Diffraction Ltd., Abingdon, U. K., 2014.
- [32] Altomare, A.; Burla, M. C.; Camalli, M.; Cascarano, G. L.; Giacovazzo, C.; Guagliardi, A.; Moliterni, A. G. G.; Polidori, G.; Spagna, R. *J. Appl. Cryst.* **1999**, *32*, 115.
- [33] Burla, M. C.; Caliendo, R.; Camalli, M.; Carrozzini, B.; Cascarano, G. L.; De Caro, L.; Giacovazzo, C.; Polidori, G.; Spagna, R. *J. Appl. Cryst.* **2005**, *38*, 381.
- [34] Sheldrick, G. M. *Acta Crystallogr., Sect. A* **2008**, *A64*, 112.
- [35] checkCIF/PLATON Home Page.
<http://journals.iucr.org/services/cif/checkcif.html> (accessed June 27, 2014).
- [36] Rodriguez-Carvajal, J.R. *Abstracts of the Satellite Meeting on Powder Diffraction of XV Congress of the IUCr*, Toulouse, France, 1990; p127.

12. Summary

12.1. Summary and Conclusion

In this thesis, the preparation and characterization (by infrared and UV/Vis/NIR spectroscopy, elemental and ICP-AES analysis, single crystal X-ray and powder diffraction, differential thermal analysis, impact and friction test, ESD test, laser ignition) of various energetic coordination compounds (ECCs) as laser ignitable materials was presented. The preparation of the complexes followed the general rules for designing ECCs.^[1] The ECCs were tested toward laser irradiation and their potential as environmentally acceptable primary explosives was studied. With exceptions (e.g. content of crystal water), the general constitution of the ECCs was $[\text{Metal}(\text{Nitrogen-rich Ligand})_n](\text{Oxidizing Anion})_m$. The following nitrogen-rich compounds (see Figure 1 for molecular structures) served as ligands: 3-amino-1-nitroguanidine (anq), carbohydrazide (chz), 5-(1-methylhydrazinyl)-1*H*-tetrazole (hmht), 1,2-di(1*H*-tetrazol-5-yl)ethane (dt-5-e), 1,2-di(1*H*-tetrazol-1-yl)ethane (dte), 1,2-bis[5-(1-methylhydrazinyl)tetrazol-1-yl]ethane (bmhte), 1,2-bis(1-methyl-1*H*-tetrazol-5-yl)ethane (bmte), 1,2-di(1*H*-tetrazol-1-yl)propane (dtp), and 1,2-di(1*H*-tetrazol-1-yl)butane (dtb).

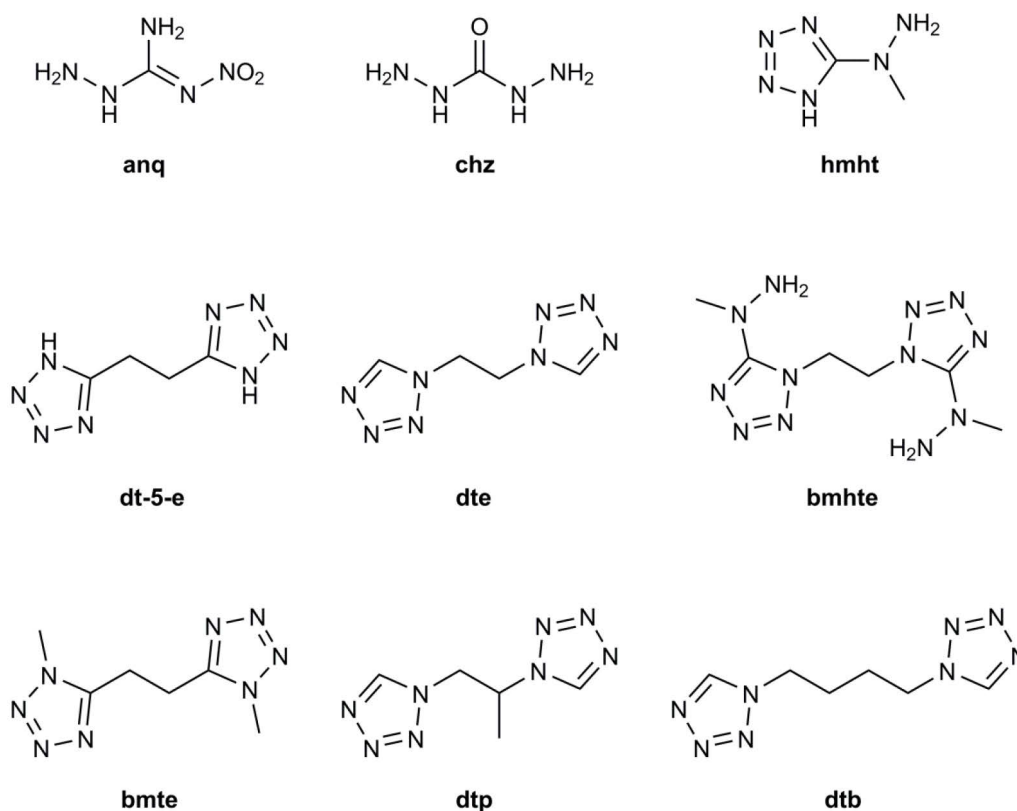


Figure 1. Molecular structures of the used ligands.

The investigated ECCs included magnesium(II), manganese(II), iron(II), cobalt(II), nickel(II), copper(II), zinc(II), silver(I), and cadmium(II) as metal cations. Except silver(I), all metal cations were present in the oxidation state +II and therefore, a good comparability of the cations was provided. Further, the following list of anions was investigated: perchlorate, chlorate, chloride, nitrate, nitrite, dinitramide, trinitromethanide, cyanodinitromethanide, nitrocyanamide, and azide.

When comparing (Figure 2–4) the investigated ECCs, it is possible to summarize subsequently some trends for the energetic properties.

In general, the decomposition temperatures decrease in the following order for the metal center (Figure 2 and 4): $\text{Ni}^{2+} > \text{Co}^{2+} \approx \text{Zn}^{2+} \approx \text{Mn}^{2+} > \text{Mg}^{2+} > \text{Cu}^{2+} \geq \text{Fe}^{2+} \approx \text{Cd}^{2+}$.

The highest sensitivity toward mechanical stimulation is observed for complexes with the transition metals Ag^+ , Cu^{2+} , Ni^{2+} , and Co^{2+} . In the most cases, complexes with Fe^{2+} as cation tend to be less sensitive than Cu^{2+} , Ni^{2+} , and Co^{2+} but considerable more sensitive than Zn^{2+} , Mn^{2+} , and the alkaline earth metal Mg^{2+} . Especially complexes with Mg^{2+} are remarkably less sensitive than the corresponding transition metal ones (Figure 4). However, synthesis of energetic magnesium complexes is not always possible and therefore, zinc and manganese seem to be the metals of choice for explosives with a decreased sensitivity.

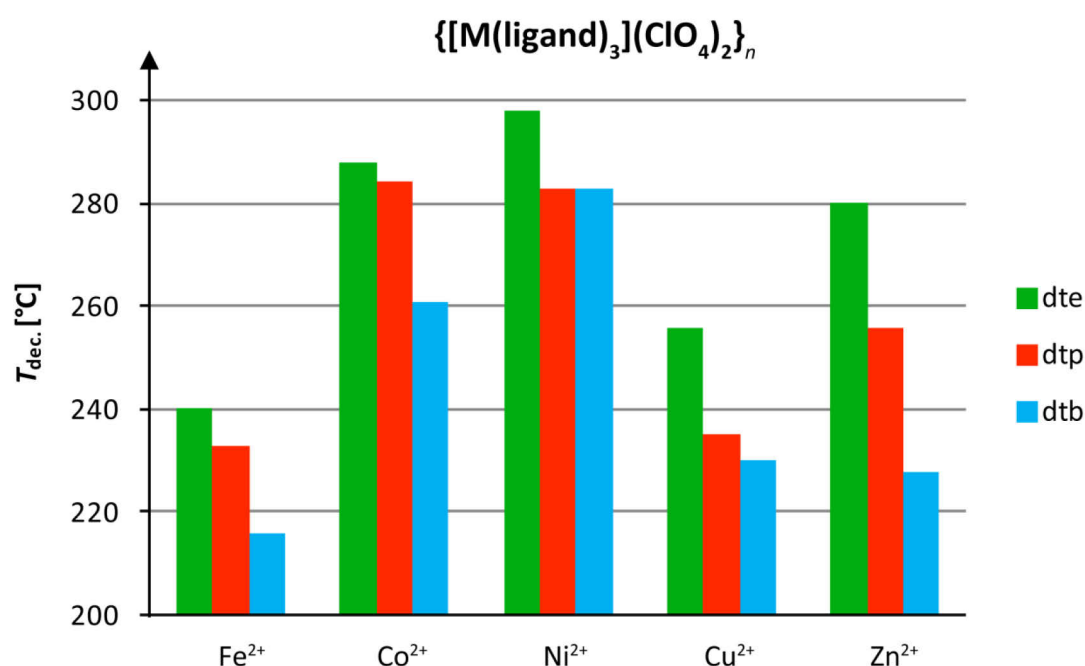


Figure 2. Decomposition temperatures of the metal(II) perchlorate complexes with dte, dtp, and dtb as ligand.

A further parameter which influences the stability of ECCs is the type of ligand. E.g. the thermal stability (Figure 2) decreases with the length of the alkyl-chain of ditetrazoles while the mechanical stability is considerably increased (Figure 3). Reducing moieties like the hydrazino group of hmht, bmhte, anq, or chz increase the sensitivity of the metal complexes

(e.g. the FS is increased from 10 N for $\{[\text{Cu}(\text{dte}_3)](\text{ClO}_4)_2\}_n$ to 5 N for $\{[\text{Cu}(\text{ClO}_4)(\text{bmhte})(\text{H}_2\text{O})](\text{ClO}_4)(\text{H}_2\text{O})\}_n$). This appears plausible because together with the oxidizing anion and the catalytic metal center a suitable redox system is present.

The connection of the tetrazole ring to the alkyl-chain of ditetrazoles also affects the stability. For example, the N1 connected complex $[\text{Cu}(\text{dte})_3](\text{ClO}_4)_2$ (FS: 10 N; IS: 1.5 J) is less sensitive toward mechanical stimuli than the C5 connected one $[\text{Cu}(\text{dt-5-e})_2(\text{H}_2\text{O})](\text{ClO}_4)_2$ (FS: 5 N; IS: 1 J). On the other hand, methylation of the ligand stabilizes the complexes as exemplary shown for $[\text{Cu}(\text{dt-5-e})_2(\text{H}_2\text{O})_2](\text{ClO}_4)_2 \cdot 2 \text{H}_2\text{O}$ (FS: 14 N; IS: 3 J) and its homologue $[\text{Cu}(\text{bmte})_2(\text{H}_2\text{O})_2](\text{ClO}_4)_2$ (FS: 80 N; IS: 4 J).

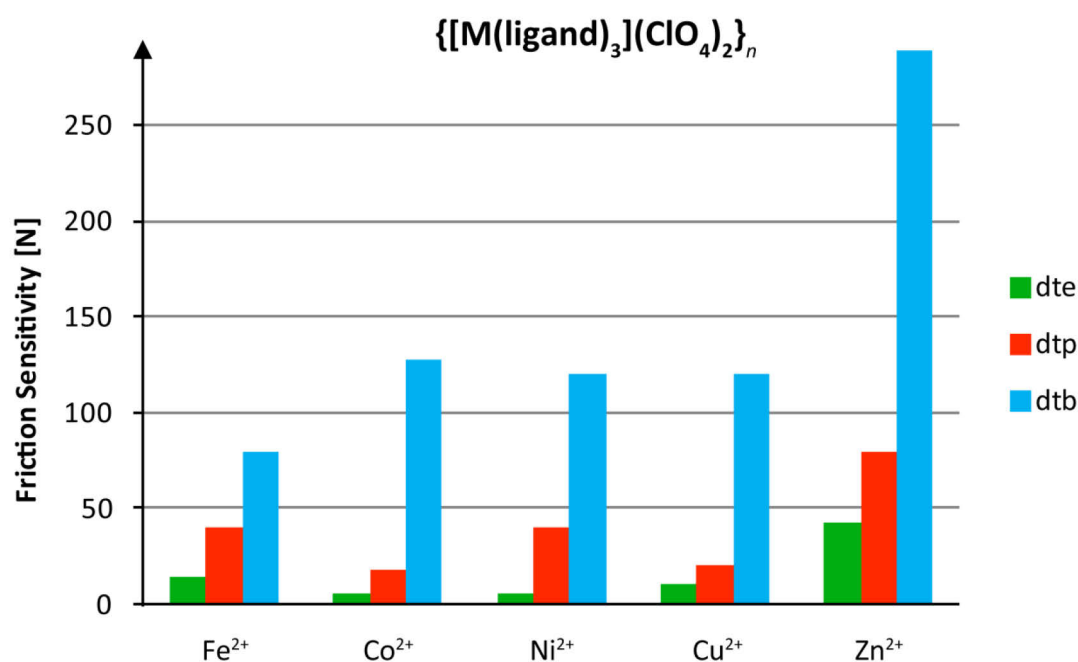


Figure 3. Friction sensitivity of the metal(II) perchlorate complexes with dte, dtp, and dtb as ligand.

According to literature,^[1] the type of anion plays an important role for the stability and performance of an ECC. For the copper(II) complexes with dte as ligand, for example, the friction and impact sensitivity as well as the thermal stability decrease in the following order:

FS: N_3^- (5 N) > ClO_3^- (6 N) > ClO_4^- (10 N) > $\text{N}(\text{NO}_2)_2^-$ (80 N) > $\text{N}(\text{CN})(\text{NO}_2)^-$ (108 N) > NO_2^- (160 N) = NO_3^- (160 N) > $\text{C}(\text{NO}_2)_3^-$ (192 N) > $\text{C}(\text{CN})(\text{NO}_2)_2^-$ (288 N) > Cl^- (324 N).

IS: N_3^- (1 J) > $\text{N}(\text{NO}_2)_2^-$ (1 J) > $\text{N}(\text{CN})(\text{NO}_2)^-$ (1 J) > ClO_3^- (1.5 J) > ClO_4^- (1.5 J) > NO_2^- (2 J) > $\text{C}(\text{CN})(\text{NO}_2)_2^-$ (4 J) > NO_3^- (7 J) > Cl^- (10 N) > $\text{C}(\text{NO}_2)_3^-$ (40 J).

$T_{\text{dec.}}$: ClO_4^- (256 °C) > $\text{C}(\text{CN})(\text{NO}_2)_2^-$ (212 °C) > N_3^- (197 °C) > NO_3^- (191 °C) > Cl^- (186 °C) > ClO_3^- (175 °C) > $\text{N}(\text{CN})(\text{NO}_2)^-$ (170 °C) > $\text{N}(\text{NO}_2)_2^-$ (168 °C) > NO_2^- (139 °C) > $\text{C}(\text{NO}_2)_3^-$ (83 °C).

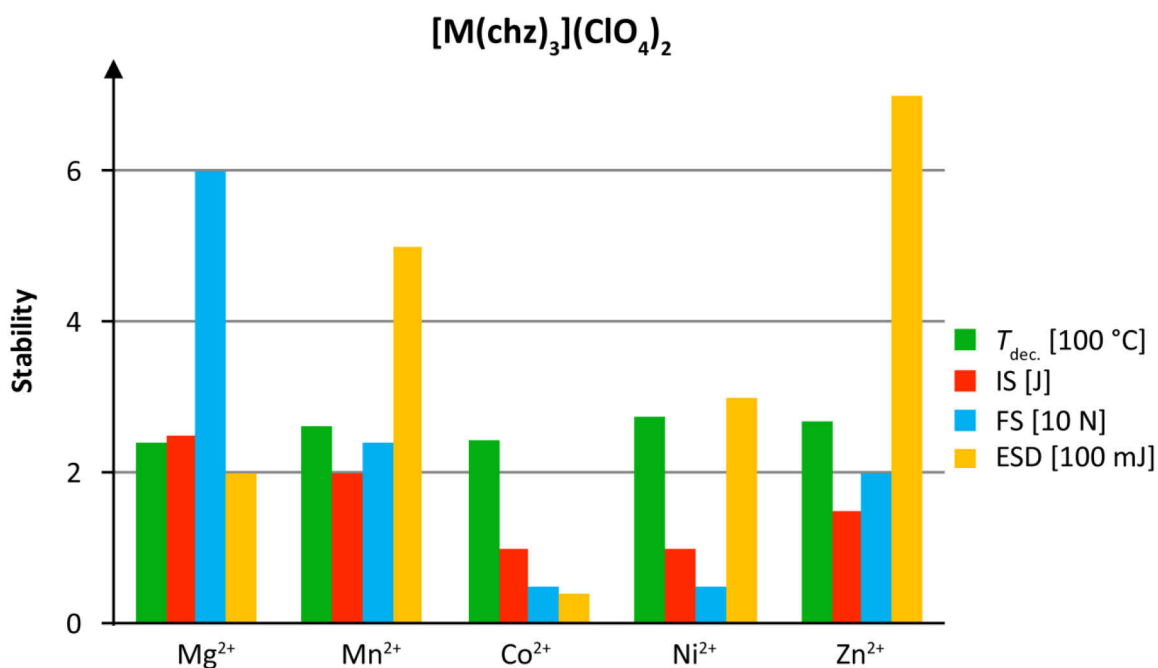


Figure 4. Stabilities of the metal(II) perchlorate complexes with chz as ligand.

However, a trade-off problem exists between performance and stability. The compounds with a good performance e.g. $[\text{Cu}(\text{dte})_3](\text{ClO}_4)_2$ or $[\text{Cu}_2(\text{N}_3)_4(\text{dte})]$ undergo the DDT in a short time but are considerably more sensitive than $[\text{Cu}(\text{dte})_3](\text{NO}_3)_2$ or $[\text{Cu}(\text{dtb})_3](\text{ClO}_4)_2$, which only deflagrate even under confinement. Concluding, the border between detonation and deflagration has been determined for sensitivities around 60 N and 4 J for the investigated compounds. Above these values, the compounds generally do not undergo detonation although there exist some exceptions like the $\{[\text{Cu}(\text{mht})(\text{N}(\text{NO}_2)_2)(\text{hmht})] \cdot \text{H}_2\text{O}\}_2$ complex (FS: 120 N; IS: 10 J). This aspect had to be considered for the laser initiation experiments and for evaluation of an explosive as possible BNCP or CP replacement.

Additional to the standard tests for primary explosives (hot needle, hot plate, electric match blasting caps), almost all investigated complexes were tested on their behavior toward single-pulsed diode laser irradiation. As laser radiation source an InGaAs laser diode ($\lambda = 940\text{ nm}$, $\tau_{\text{max}} = 600\ \mu\text{s}$, $E_{\text{e,max}} = 0.23\ \text{MW cm}^{-2}$) was used. The samples (about 0.2 g ECC containing 2–5 % binder) were pressed to pellets and confined with aluminum caps. The following conclusion can be drawn from the results of diode laser ignition:

- (i) As already demonstrated by previous works of various research groups,^[2] diode laser ignition of explosives is possible and the explosives undergo a deflagration-to-detonation transition (see Figure 5).
- (ii) ECCs are suitable explosives for laser ignited DDT actuators.
- (iii) In agreement with literature,^[2c,2e] function times (t_f) in the lower microsecond range are possible for diode laser ignition (Table 1).

- (iv) The laser initiation threshold of the ECCs strongly depends on the type of metal cation (Table 1 and Figure 6). Copper(II) represented the best ignitable metal(II) center. Other good metal cations might be silver(I) and cobalt(III). However, this remains to be seen by extensive investigations.
- (v) The high influence of the metal center on the laser ignitability might be explained by a decrease of the activation energy by noble metals for the redox reaction between the oxidizing anion and the energetic ligand. The oxidation of the ligand might be favored by a noble central metal ion which itself is reduced in this step.
- (vi) The type of ligand influences the performance and also the initiation threshold (Figure 6). Reducing moieties e.g. hydrazino groups exhibited a positive effect on the initiation threshold in agreement with a redox mechanism for the decomposition process. However, these moieties also increased the mechanical sensitivity and decreased the thermal stability.
- (vii) The type of anion might have only a minor effect on the initiation threshold (Figure 6), however, it strongly influences the performance and stability of the ECC, which is in agreement to literature.^[1]
- (viii) Addition of light absorbing particles considerably decreases the laser initiation threshold (Table 1), which was an indication for a thermal mechanism.
- (ix) Although laser ignition and initiation is a thermal process, it is not understood which parameters mainly influence the threshold energy. The investigations showed that the ignitability cannot be described exclusively by the absorptance at the wavelength of the laser (Figure 6) and the thermal stability of the ECC. Further parameters (e.g. thermal conductivity, ionization potential, capability for self-sustaining reaction) might play an important role for laser ignition and initiation. Further investigations would be necessary for identification.



Figure 5. Series of images showing the laser ignited DDT of $[\text{Cu}(\text{H}_2\text{BTA})](\text{NO}_3)_2 \cdot 0.5 \text{H}_2\text{O}$.^[2f] Picture 1 shows the moment before and picture 2 shows the moment of ignition. Pictures 3–5 show the propagation of deflagration and picture 6 is finally showing the detonation. Time period 0.63 s. Laser parameters: $\lambda = 940 \text{ nm}$, $\tau = 100 \mu\text{s}$, $E_e = 0.14 \text{ MW cm}^{-2}$.

Some of the investigated ECCs exhibited very good energetic properties making them capable as initiating explosives. The most interesting and suitable compounds are listed in Table 2 together with their possible application. The crystal structures of three of them

$[\text{Cu}(\text{ClO}_4)(\mu\text{-MHT})(\text{HMHT})]_2$, $\{[\text{Cu}(\text{dte})_3](\text{ClO}_3)_2\}_n$, and the cocrystal $[\text{Cu}(\text{dt-5-e})_2(\text{H}_2\text{O})](\text{ClO}_4)_2$ are shown in Figure 7.

In addition, thermally stable compounds, for example $\{[\text{Ni}(\text{dte})_3](\text{ClO}_4)_2\}_n$ ($T_{\text{dec.}} = 298\text{ }^\circ\text{C}$) or $\{[\text{Co}(\text{dte})_3](\text{ClO}_4)_2\}_n$ ($T_{\text{dec.}} = 288\text{ }^\circ\text{C}$), might be interesting for special applications like the initiation of low sensitive, thermally stable secondary explosives like 2,6-bis(picrylamino)-3,5-dinitropyridine (Pyx).

Table 1. Properties and laser ignition results of several carbohydrazone complexes of the formula $[\text{M}(\text{chz})_3](\text{ClO}_4)_2$ and $[\text{Cu}(\text{ClO}_4)_2(\text{chz})_2]$.

Cation	Mg ²⁺	Mn ²⁺	Co ²⁺	Ni ²⁺	Cu ²⁺	Zn ²⁺
$M_r / \text{g mol}^{-1}$	493.46	524.09	528.09	527.85	442.62	534.53
Crystal system	monoclinic ^[3]	monoclinic ^[4]	monoclinic ^[5]	monoclinic ^[5]	unknown	monoclinic ^[6]
Space group	$P2_1/n$ ^[3]	$P2_1/n$ ^[4]	$P2_1/n$ ^[5]	$P2_1/n$ ^[5]	unknown	$P2_1/n$ ^[6]
$\rho / \text{g cm}^{-3}$	1.837 ^[3]	1.889 ^[4]	1.941 ^[5]	1.973 ^[5]	n. d.	2.021 ^[6]
$T_{\text{dec.}} / ^\circ\text{C}$	239	263	243	273	186	268
$F(R)_{@940\text{ nm}}$ ^[a]	0.01	< 0.01	0.03	0.37	< 0.01	0.01
$t_f / \mu\text{s}$ ^[b]	no ignition	no ignition	401	136	65	no ignition
$t_f / \mu\text{s}$ ^[c]	no ignition	no ignition	43	17	8	no ignition

[a] Absorption intensity $F(R)$ at 940 nm in arbitrary units. The absorption intensity $F(R)$ is calculated by the Kubelka-Munk equation from the reflectance R [%].^[7] [b] Function time t_f for pure samples. Laser parameters: $\lambda = 940\text{ nm}$, $\tau = 400\text{ }\mu\text{s}$, $E_e = 0.085\text{ MW cm}^{-2}$. [c] Function time t_f under addition of 1 % activated carbon to the sample. Laser parameters: $\lambda = 940\text{ nm}$, $\tau = 400\text{ }\mu\text{s}$, $E_e = 0.085\text{ MW cm}^{-2}$.

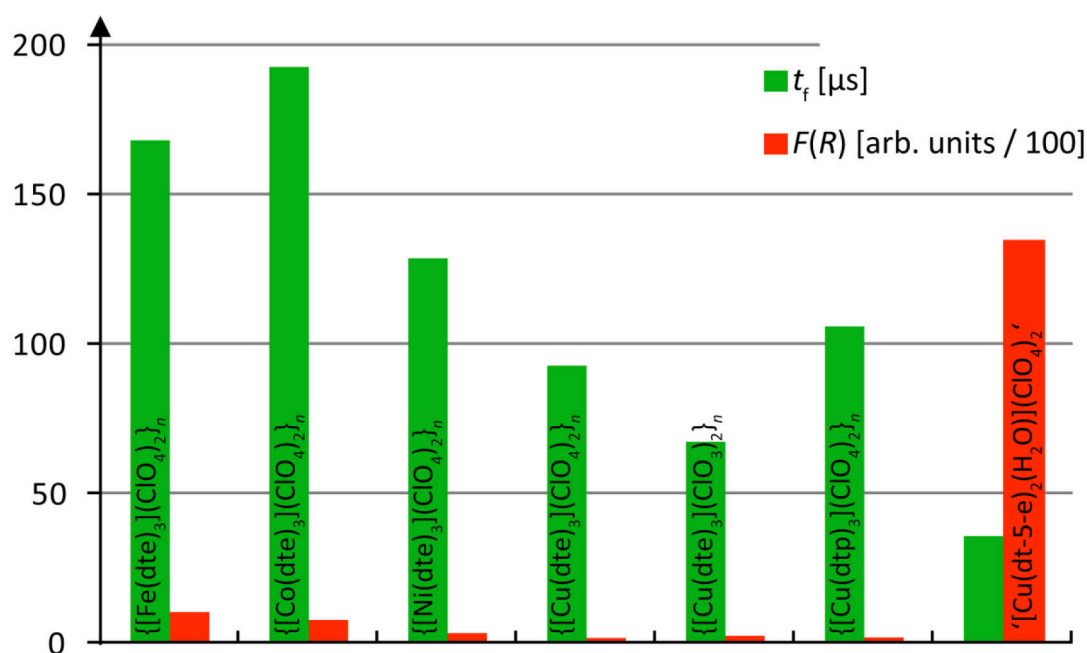


Figure 6. Function time t_f for laser ignition and absorption intensity $F(R)$ at 940 nm of several metal(II) complexes (+ 5 % polyethylene as binder). Laser parameters: $\lambda = 940\text{ nm}$, $\tau = 400\text{ }\mu\text{s}$, $E_e = 0.16\text{ MW cm}^{-2}$. The absorption intensity $F(R)$ was calculated by the Kubelka-Munk equation from the reflectance R [%].^[7]

Table 2. Potential replacements for common initiating explosives.

Application:	Stab or hot-wire detonator	Percussion cap	Laser initiator
Replacement for:	Lead azide	Lead styphnate	BNCP / CP
Compound	$[\text{Cu}(\text{ClO}_4)(\mu\text{-mht})(\text{hmht})]_2$	$[\text{Cu}_2(\text{N}_3)_4(\text{dte})]_n$	$\{\text{Cu}(\text{dte})_3(\text{ClO}_4)_2\}_n$
$T_{\text{dec.}} [^\circ\text{C}]$	217	197	256
IS [J] ^[a]	1	1	1.5
FS [N] ^[a]	5	< 5	10
ESD [mJ]	10	14	150
Compound	$[\text{Cu}(\text{ClO}_4)(\mu\text{-mht})(\text{H}_2\text{O})]_n$	$\{\text{Cu}(\text{dte})_3(\text{ClO}_3)_2\}_n$	' $[\text{Cu}(\text{dt-5-e})_2(\text{H}_2\text{O})(\text{ClO}_4)_2]$ '
$T_{\text{dec.}} [^\circ\text{C}]$	206	175	188
IS [J] ^[a]	1	1.5	1
FS [N] ^[a]	5	6	5
ESD [mJ]	7	15	-

[a] Impact and friction sensitivity determined by BAM standard methods.

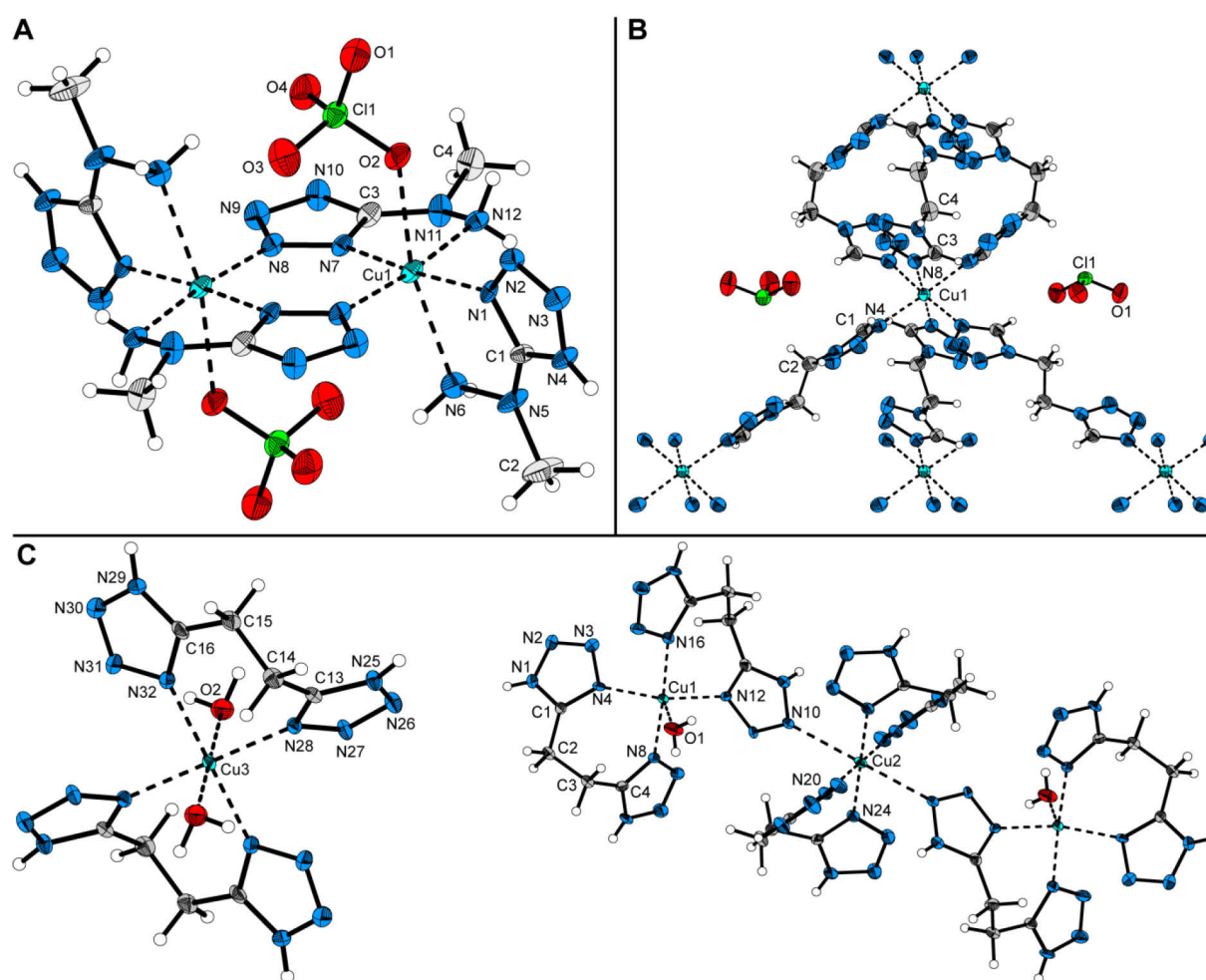


Figure 7. Crystal structures of the dinuclear copper(II) complex $[\text{Cu}(\text{ClO}_4)(\mu\text{-MHT})(\text{HMHT})]_2$ (A), the polynuclear copper(II) complex $\{\text{Cu}(\text{dte})_3(\text{ClO}_3)_2\}_n$ (B) and the copper(II) complex cocrystal ' $[\text{Cu}(\text{dt-5-e})_2(\text{H}_2\text{O})(\text{ClO}_4)_2]$ ' (C).

Contrary to the copper(II) compounds listed in Table 2, which are laser ignitable but extremely sensitive toward mechanical stimuli, two compounds nearly achieve the required sensitivities for a booster-explosive together with a satisfying performance although they only deflagrated after laser ignition: $\{[\text{Cu}(\text{dte})_3](\text{N}(\text{NO}_2)_2)_2\}_n$ ($T_{\text{dec.}} = 168\text{ }^\circ\text{C}$, IS: 1 J; FS: 80 N) and $\{[\text{Fe}(\text{dtb})_3](\text{ClO}_4)_2\}_n$ ($T_{\text{dec.}} = 216\text{ }^\circ\text{C}$, IS: 1 J; FS: 80 N). Various other investigated ECCs (e.g. $\{[\text{Cu}(\text{dte})_3](\text{NO}_3)_2\}_n$ and $\{[\text{Cu}(\text{dtb})_3](\text{ClO}_4)_2\}_n$) with decreased sensitivities exhibited a significant lower performance and only combusted or partially decomposed after ignition by laser irradiation and are consequently rather useless for applications.

However, the potential of $\{[\text{Cu}(\text{dte})_3](\text{N}(\text{NO}_2)_2)_2\}_n$ and $\{[\text{Fe}(\text{dtb})_3](\text{ClO}_4)_2\}_n$ for laser diode initiators is high although their capability of initiating secondary explosives has to be investigated in future works.

12.2. References

- [1] V. P. Sinditskii, V. V. Seurshkin, *Defence Science Journal* **1996**, *46*, 371–383.
- [2] a) S. C. Kunz, F. J. Salas, *13th International Pyrotechnics Seminar*, Grand Junction, USA, July 11–15, **1988**, 505–523; b) W. J. Kass, L. A. Andrews, C. M. Boney, W. W. Chow, J. W. Clements, J. A. Merson, F. J. Salas, R. J. Williams, *2nd NASA Aerospace Pyrotechnic Systems Workshop*, Albuquerque, USA, **1994**; c) J. A. Merson, F. J. Salas, J. G. Harlan, *19th International Pyrotechnics Seminar*, Christchurch, New Zealand, Februar 21–25, **1994**, 191–206; d) E. S. Hafenrichter, B. Marshall, Jr., K. J. Fleming, *29th International Pyrotechnics Seminar*, Westminster, USA, July 14–19, **2002**, 787–793; e) E. S. Hafenrichter, B. W. Marshall, K. J. Fleming, *41st Aerospace Sciences Meeting and Exhibit*, Reno, USA, January 6–9, **2003**; f) M. Joas, Master Thesis, Ludwig-Maximilian University (Munich), **2011**; g) N. K. Bourne, *Proc. R. Soc. A* **2001**, *457*, 1401–1426.
- [3] Z.-M. Li, T.-L. Zhang, L. Yang, Z.-N. Zhou, J.-G. Zhang, *J. Coord. Chem.* **2012**, *65*, 143–155.
- [4] J.-G. Zhang, T.-L. Zhang, Z.-R. Wei, K.-B. Yu, *Gaodeng Xuexiao Huaxue Xuebao* **2001**, *22*, 895–897.
- [5] V. P. Sinditskii, A. E. Fogel'zang, M. D. Dutov, V. I. Sokol, V. V. Serushkin, B. S. Svetlov, M. A. Porai-Koshits, *Zh. Neorg. Khim.* **1987**, *32*, 1944–1949.
- [6] S. Qi, Z. Li, T. Zhang, Z. Zhou, L. Yang, J. Zhang, X. Qiao, K. Yu, *Huaxue Xuebao* **2011**, *69*, 987–992.
- [7] P. Kubelka, F. Munk, *Z. Tech. Phys.* **1931**, *1*, 593–601.

Appendix

A1. Supporting Information Chapter 4

Transition Metal Complexes of 3-Amino-1-nitroguanidine as Laser Ignitable Primary Explosives: Structures and Properties

Table of Content

1. X-ray Diffraction

X-ray Diffraction

Table S1. Crystallographic data of 3–7.

	3	4	5	6	7
Formula	C ₂ Cl ₂ CoH ₁₄ N ₁₀ O ₁₄	C ₂ Cl ₂ H ₁₄ N ₁₀ NiO ₁₄	C ₂ Cl ₂ CuH ₁₄ N ₁₀ O ₁₄	C ₂ Cl ₂ H ₁₄ N ₁₀ O ₁₄ Zn	AgC ₂ ClH ₁₀ N ₁₀ O ₈
FW [g mol ⁻¹]	532.06	531.82	536.68	538.52	445.52
Crystal system	Monoclinic	Orthorhombic	Triclinic	Monoclinic	Triclinic
Space Group	<i>P2₁/c</i>	<i>Pca2₁</i>	<i>P-1</i>	<i>P2₁/c</i>	<i>P$\bar{1}$</i>
Color / Habit	Red block	Light purple block	Blue Block	Colorless Block	Colorless Plate
Size [mm]	0.16 x 0.19 x 0.25	0.32 x 0.28 x 0.18	0.20 x 0.15 x 0.08	0.35 x 0.26 x 0.23	0.50 x 0.40 x 0.02
<i>a</i> [Å]	8.827(3)	16.0756(5)	7.5926(6)	7.9056(5)	8.4231(4)
<i>b</i> [Å]	10.020(2)	8.3203(3)	7.7551(6)	12.5134(6)	9.8158(4)
<i>c</i> [Å]	10.316(3)	12.2323(4)	7.8619(6)	10.1931(7)	15.6296(6)
α [°]	90	90	72.087(7)	90	89.133(4)
β [°]	110.54(4)	90	74.101(7)	126.024(4)	86.745(4)
γ [°]	90	90	77.206(7)	90	82.022(4)
<i>V</i> [Å ³]	854.4(5)	1636.12(9)	418.84(6)	815.53(10)	1277.64(9)
<i>Z</i>	2	4	1	2	4
ρ_{calc} [g cm ⁻³]	2.068	2.159	2.128	2.193	2.316
μ [mm ⁻¹]	1.416	1.616	1.724	1.937	1.854
<i>F</i> (000)	538	1080	271	544	880
$\lambda_{\text{MoK}\alpha}$ [Å]	0.71073	0.71073	0.71073	0.71073	0.71073
<i>T</i> [K]	173	173	173	173	173
θ Min–Max [°]	4.3, 27.3	4.1, 30.1	4.3, 26.0	4.2, 26.5	4.2, 25.8
Dataset	-10:11; -12:9 ; -13:12	-22:21; -11:11; -15: 17	-9:9; -9:9; -9:9	-9:7 ; -15:13 ; -11:12	-10:10; -11:11; -19:19
Reflections collected	4763	10824	4252	4341	12241
Independent refl.	1898	4556	1648	1686	4860
<i>R</i> _{int}	0.051	0.041	0.032	0.038	0.032
Observed reflections	1164	3495	1282	1256	3363
Parameters	189	194	161	161	477
<i>R</i> ₁ (obs) ^a	0.0406	0.0327	0.0285	0.0294	0.0289
<i>wR</i> ₂ (all data) ^b	0.0890	0.0563	0.0718	0.0617	0.0654
Goof ^c	0.85	0.88	0.96	0.91	0.89
Resd. Dens. [e Å ⁻³]	-0.34, 0.56	-0.41, 0.57	-0.43, 0.46	-0.50, 0.40	-0.51, 0.57
Absorption correction	multi-scan	multi-scan	multi-scan	multi-scan	multi-scan
CCDC	900148	900144	900147	900149	900143

a) $R_1 = \frac{\sum ||F_o| - |F_c||}{\sum |F_o|}$; b) $wR_2 = \frac{[\sum [w(F_o^2 - F_c^2)^2]]^{1/2}}{[\sum [w(F_o^2)]]^{1/2}}$; $w = [\sigma^2(F_o^2) + (xP)^2 + yP]^{-1}$ and $P = (F_o^2 + 2F_c^2)/3$; c) $\text{Goof} = \{[\sum [w(F_o^2 - F_c^2)^2]] / (n-p)\}^{1/2}$ (n = number of reflections; p = total number of parameters).

Table S2. Crystallographic data of **8–13**.

	8	9	10	11	12	13
Formula	C ₂ CoH ₁₄ N ₁₂ O ₁₂	C ₂ H ₁₄ N ₁₂ NiO ₁₂	C ₂ CuH ₁₀ N ₁₂ O ₁₀	C ₂ H ₁₄ N ₁₂ O ₁₂ Zn	AgC ₂ H ₁₀ N ₁₁ O ₇	C ₂ CoH ₁₈ N ₁₆ O ₁₆
FW [g mol ⁻¹]	457.07	456.94	425.76	463.62	408.08	581.25
Crystal system	Triclinic	Triclinic	Monoclinic	Triclinic	Orthorhombic	Monoclinic
Space Group	<i>P</i> $\bar{1}$	<i>P</i> $\bar{1}$	<i>C2/c</i>	<i>P</i> $\bar{1}$	<i>Pbca</i>	<i>P2₁/c</i>
Color / Habit	Light red block	Light purple block	Blue Block	Colorless Block	Colorless block	Orange block
Size [mm]	0.35 x 0.20 x 0.10	0.36 x 0.24 x 0.05	0.20 x 0.10 x 0.05	0.28 x 0.25 x 0.20	0.35 x 0.15 x 0.11	0.30 x 0.30 x 0.15
<i>a</i> [Å]	6.8524(4)	7.1453(6)	13.9605(8)	7.0614(5)	7.2936(5)	12.2271(4)
<i>b</i> [Å]	6.9311(4)	7.1712(7)	7.3636(4)	7.1953(4)	13.1752(10)	6.5441(2)
<i>c</i> [Å]	9.1821(5)	8.4053(7)	25.8007(15)	8.8214(5)	25.2461(13)	13.1602(5)
α [°]	86.232(5)	94.582(7)	90	94.681(5)	90	90
β [°]	79.608(5)	94.334(7)	100.759(5)	94.130(5)	90	111.047(4)
γ [°]	62.648(6)	117.057(9)	90	119.274(7)	90	90
<i>V</i> [Å ³]	380.92(4)	379.28(7)	2605.7(3)	386.42(5)	2426.0(3)	982.77(6)
<i>Z</i>	1	1	8	1	8	2
ρ_{calc} [g cm ⁻³]	1.993	2.001	2.171	1.992	2.235	1.964
μ [mm ⁻¹]	1.225	1.378	1.771	1.686	1.725	0.993
<i>F</i> (000)	233	234	1720	236	1616	594
$\lambda_{\text{MoK}\alpha}$ [Å]	0.71073	0.71073	0.71073	0.71073	0.71073	0.71073
<i>T</i> [K]	173	173	173	173	173	173
θ Min–Max [°]	4.4, 26.0	4.3, 26.5	4.1, 26.5	4.3, 24.0	4.3, 26.0	4.2, 26.2
Dataset	-8:8 ; -8:8; -11:11	-8:8; -9:8; -10:10	-17:17; -9:9; -32:32	-6:6; -8:8; -10:10	-7:8; -16:15; -19:31	-15:15; -8:8; -16:16
Reflections collected	3852	2975	13224	3096	11798	9596
Independent refl.	1499	1539	2689	1144	2373	1980
<i>R</i> _{int}	0.018	0.048	0.054	0.018	0.064	0.037
Observed reflections	1379	1267	1904	1091	1360	1744
Parameters	132	152	266	152	230	196
<i>R</i> ₁ (obs) ^a	0.0215	0.0304	0.0285	0.0184	0.0279	0.0249
<i>wR</i> ₂ (all data) ^b	0.0589	0.0680	0.0541	0.0468	0.0492	0.0633
GooF ^c	1.05	0.94	0.85	1.09	0.78	1.09
Resd. Dens. [e Å ⁻³]	-0.34, 0.31	-0.34, 0.43	-0.26, 0.48	-0.20, 0.24	-0.41, 0.72	-0.29, 0.26
Absorption correction	multi-scan	multi-scan	multi-scan	multi-scan	multi-scan	multi-scan
CCDC	900142	900139	900141	900146	900140	900155

a) $R_1 = \frac{\sum ||F_o| - |F_c||}{\sum |F_o|}$; b) $wR_2 = \frac{[\sum [w(F_o^2 - F_c^2)^2]]^{1/2}}{[\sum [w(F_o^2)]]^{1/2}}$; $w = [\sigma^2(F_o^2) + (xP)^2 + yP]^{-1}$ and $P = (F_o^2 + 2F_c^2)/3$; c) $\text{GooF} = \{[\sum [w(F_o^2 - F_c^2)^2]] / (n-p)\}^{1/2}$ (n = number of reflections; p = total number of parameters).

Table S3. Crystallographic data of 14–19.

	14	15	16	17	18	19
Formula	C ₂ H ₁₈ N ₁₆ NiO ₁₆	AgCH ₇ N ₈ O ₇	C ₂ Cl ₂ CoH ₁₄ N ₁₀ O ₆	C ₂ Cl ₂ H ₁₄ N ₁₀ NiO ₆	C ₂ Cl ₂ CuH ₁₄ N ₁₀ O ₆	C ₂ Cl ₂ H ₁₄ N ₁₀ O ₆ Zn
FW [g mol ⁻¹]	581.01	351.02	404.06	403.84	408.67	410.50
Crystal system	Monoclinic	Monoclinic	Monoclinic	Monoclinic	Monoclinic	Monoclinic
Space Group	<i>P</i> 2 ₁ / <i>c</i>	<i>P</i> 2 ₁ / <i>c</i>	<i>P</i> 2 ₁ / <i>n</i>	<i>P</i> 2 ₁ / <i>n</i>	<i>P</i> 2 ₁ / <i>c</i>	<i>P</i> 2 ₁ / <i>n</i>
Color / Habit	Light purple plate	Colorless block	Light red block	Light blue block	Blue block	Colorless block
Size [mm]	0.30 x 0.20 x 0.03	0.15 x 0.15 x 0.10	0.35 x 0.35 x 0.10	0.20 x 0.15 x 0.10	0.15 x 0.10 x 0.05	0.20 x 0.15 x 0.10
<i>a</i> [Å]	12.1641(4)	7.2076(9)	7.7202(3)	7.7086(2)	7.8539(8)	7.8148(3)
<i>b</i> [Å]	6.5297(2)	22.159(2)	13.1080(4)	13.0721(3)	12.9734(10)	13.0922(3)
<i>c</i> [Å]	13.1323(4)	5.9489(9)	7.8612(3)	7.8241(2)	7.7625(8)	7.8655(3)
α [°]	90	90	90	90	90	90
β [°]	111.038(3)	92.240(13)	118.913(6)	119.253(4)	118.106(13)	119.386(5)
γ [°]	90	90	90	90	90	90
<i>V</i> [Å ³]	973.54(6)	949.4(2)	696.37(6)	687.87(4)	697.67(14)	701.20(5)
<i>Z</i>	2	4	2	2	2	2
ρ_{calc} [g cm ⁻³]	1.982	2.456	1.927	1.950	1.945	1.944
μ [mm ⁻¹]	1.117	2.174	1.663	1.846	1.995	2.179
<i>F</i> (000)	596	688	410	412	414	416
$\lambda_{\text{MoK}\alpha}$ [Å]	0.71073	0.71073	0.71073	0.71073	0.71073	0.71073
<i>T</i> [K]	173	173	173	173	173	173
θ Min–Max [°]	4.2, 26.3	4.4, 26.1	4.3, 25.5	4.3, 25.5	4.3, 25.5	4.3, 25.5
Dataset	-15:15; -8:8; -16:16	-8:8; -27:13; -7:6	-9:9; -15:15; -9:9	-9:9; -15:15; -9:9	-9:8; -15:13; -6:9	-9:9; -15:15; -9:9
Reflections collected	9660	3662	6608	6505	2831	6638
Independent refl.	1972	1837	1299	1285	1295	1309
<i>R</i> _{int}	0.032	0.048	0.029	0.021	0.036	0.034
Observed reflections	1805	1196	1199	1216	1141	1197
Parameters	196	164	125	125	125	125
<i>R</i> ₁ (obs) ^a	0.0224	0.0850	0.0198	0.0171	0.0286	0.0202
<i>wR</i> ₂ (all data) ^b	0.0570	0.2130	0.0498	0.0424	0.0683	0.0525
Goof ^c	1.05	0.95	1.09	1.06	1.05	1.05
Resd. Dens. [e Å ⁻³]	-0.25, 0.34	-1.74, 6.82	-0.25, 0.24	-0.26, 0.26	-0.52, 0.42	-0.22, 0.36
Absorption correction	multi-scan	multi-scan	multi-scan	multi-scan	multi-scan	multi-scan
CCDC	900154	900138	900152	900153	900151	900156

a) $R_1 = \sum ||F_o| - |F_c|| / \sum |F_o|$; b) $wR_2 = [\sum [w(F_o^2 - F_c^2)^2] / \sum [w(F_o^2)]]^{1/2}$; $w = [\sigma^2(F_o^2) + (xP)^2 + yP]^{-1}$ and $P = (F_o^2 + 2F_c^2) / 3$; c) $\text{Goof} = \{\sum [w(F_o^2 - F_c^2)^2] / (n-p)\}^{1/2}$ (n = number of reflections; p = total number of parameters).

A2. Supporting Information Chapter 5

Synthesis and Characterization of Various Photosensitive Copper(II) Complexes with 5-(1-Methylhydrazinyl)-1H-tetrazole as Ligand and Perchlorate, Nitrate, Dinitramide, and Chloride as Anions

Table of Content

1. Crystal Structures
2. X-ray Data
3. UV-Vis-NIR Spectra
4. Ignition Test
5. Experimental

Crystal Structures

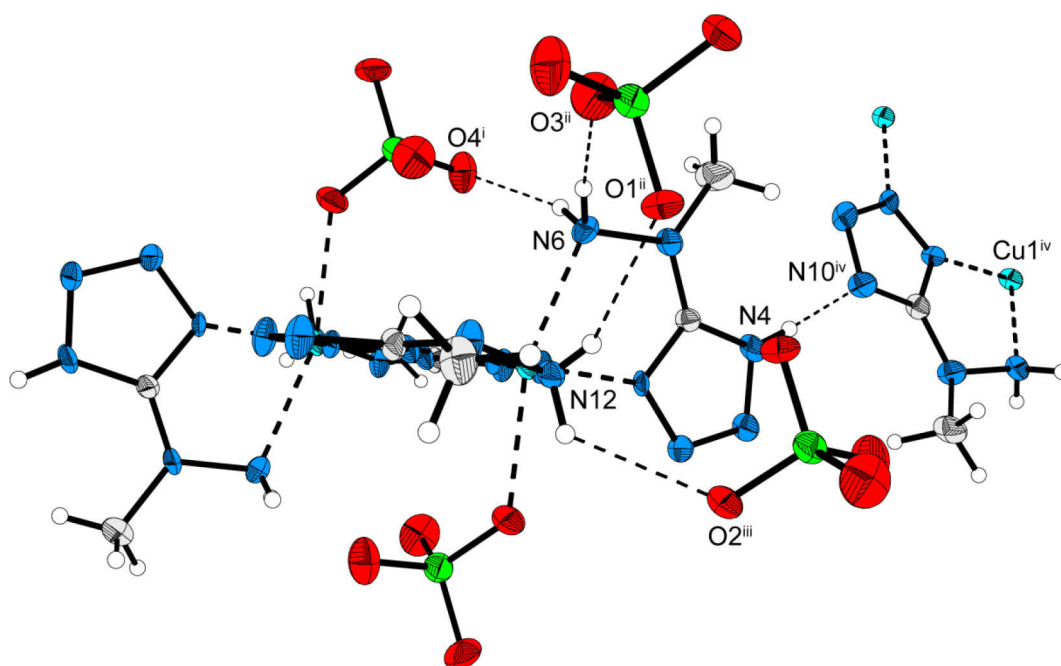


Figure S1. Selected hydrogen bonds of $[\text{Cu}(\text{ClO}_4)(\mu\text{-MHT})(\text{HMHT})]_2$ (**2**). Symmetry codes: (i) $1-x, 1-y, 2-z$; (ii) $x, -1+y, z$; (iii) $-x, 1-y, 2-z$; (iv) $-0.5+x, 0.5-y, 0.5+z$.

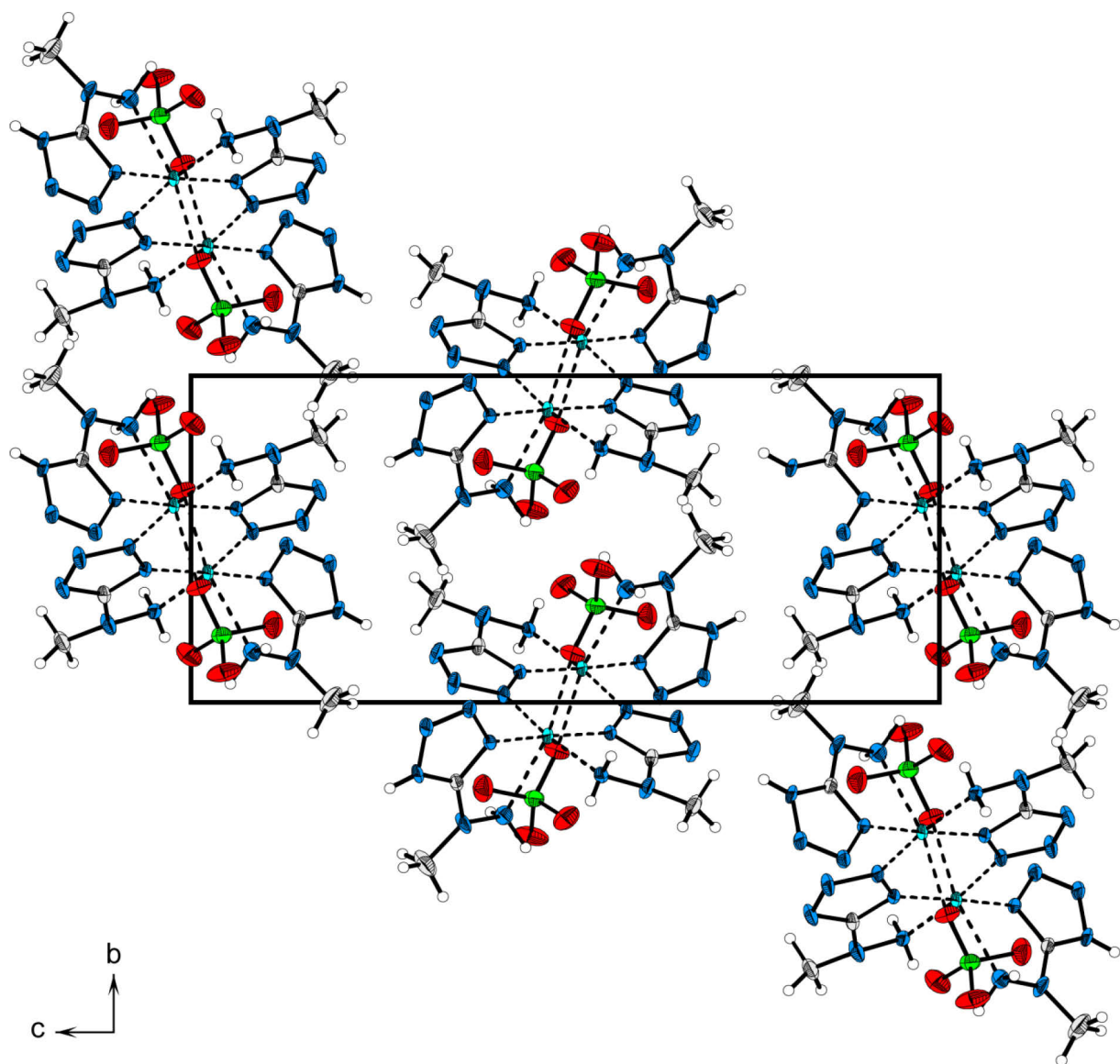


Figure S2. Packing scheme of $[\text{Cu}(\text{ClO}_4)(\mu\text{-MHT})(\text{HMHT})]_2$ (**2**). View along the a -axis.

Table S1. Distances and angles of selected hydrogen bonds in **2**.

D–H···A	D–H / Å	H···A / Å	D···A / Å	D–H···A / °
N4–H4···N10 ^{iv}	0.82(6)	1.95(6)	2.763(5)	171(6)
N6–H6A···O3 ⁱⁱ	0.99(3)	1.95(3)	2.930(6)	174(3)
N6–H6B···O4 ⁱ	0.88(5)	2.35(5)	3.188(6)	159(4)
N12–H12A···N2 ⁱⁱⁱ	0.91(4)	2.24(5)	3.072(5)	153(4)
N12–H12B···O1 ⁱⁱ	0.76(5)	2.44(5)	3.118(5)	150(4)
N12–H12A···O2 ⁱⁱⁱ	0.91(4)	2.50(4)	3.086(6)	150(4)

Symmetry codes: i: $1-x, 1-y, 2-z$; ii: $x, -1+y, z$; iii: $-x, 1-y, 2-z$; iv: $-0.5+x, 0.5-y, 0.5+z$.

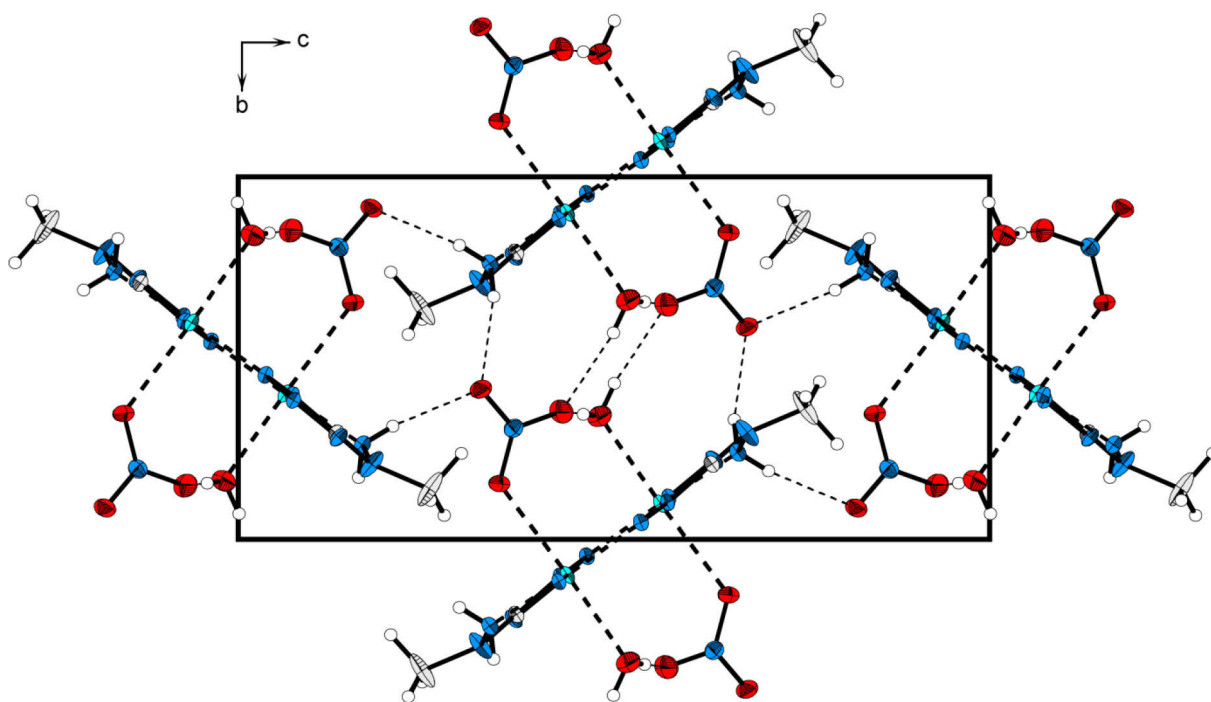


Figure S3. Packing scheme of $[\text{Cu}(\mu_3\text{-MHT})(\text{NO}_3)(\text{H}_2\text{O})]_\infty$ (**6**) with selected hydrogen bonds between the linear chains. View along the a -axis.

Table S2. Distances and angles of selected hydrogen bonds in **6**.

D–H···A	D–H / Å	H···A / Å	D···A / Å	D–H···A / °
O4–H4A···O1 ^v	0.80(3)	2.10(3)	2.867(2)	163(3)
O4–H4B···O1 ^{iv}	0.72(4)	2.19(4)	2.886(3)	163(4)
N6–H6A···O2 ^v	0.85(2)	2.13(2)	2.943(2)	159(2)
N6–H6B···O2 ^{vi}	0.81(2)	2.16(2)	2.967(2)	172(2)

Symmetry codes: iv: $-x, -y, 1-z$; v: $x, 1+y, z$; vi: $0.5-x, 0.5+y, 0.5-z$.

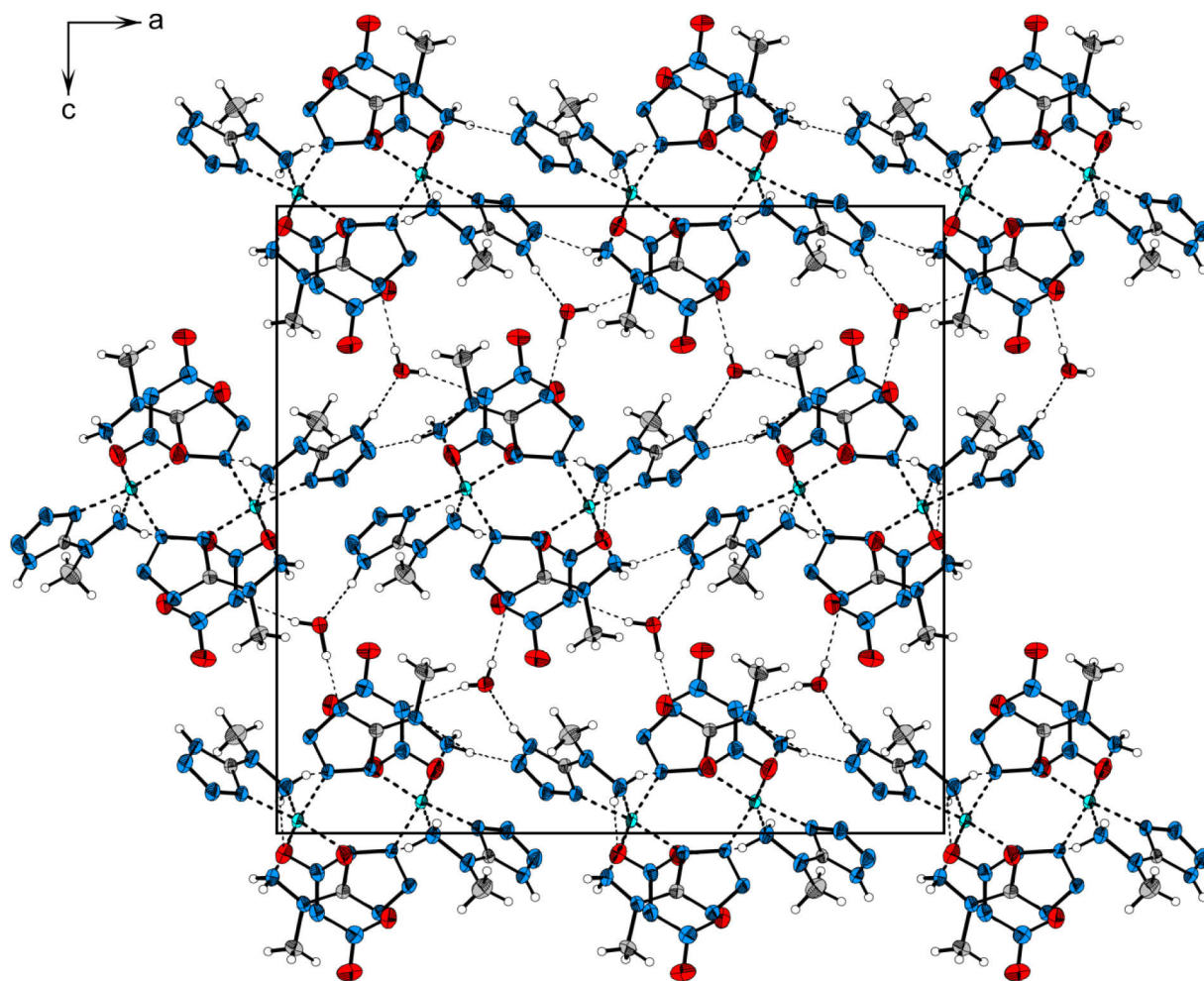


Figure S4. Packing scheme of $[\text{Cu}(\mu\text{-MHT})(\text{N}(\text{NO}_2)_2)(\text{HMHT})]_2 \cdot 2 \text{H}_2\text{O}$ (**7**) with selected hydrogen bonds between the complex dimers. View along the b -axis.

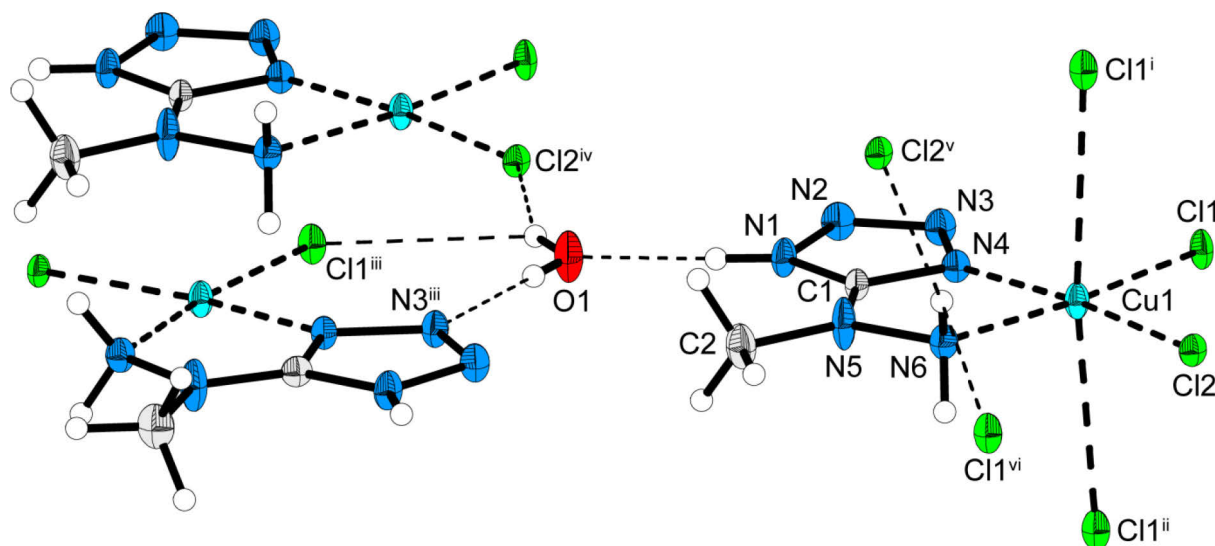


Figure S5. Selected hydrogen bonds of $[\text{CuCl}(\mu_3\text{-Cl})(\text{HMHT})]_\infty \cdot \text{H}_2\text{O}$ (**8**). Symmetry codes: i: $x, 0.5-y, -z$; ii: $x, 0.5-y, 1-z$; iii: $1-x, -0.5+y, 0.5-z$; iv: $1+x, y, z$; v: $-x, -y, -0.5+z$; vi: $-x, -0.5+y, 0.5-z$.

Table S3. Distances and angles of hydrogen bonds and electrostatic interactions in **8**.

D–H···A	D–H / Å	H···A / Å	D···A / Å	D–H···A / °
N1–H1···O1	0.84(6)	1.82(6)	2.661(5)	176(6)
O1–H1A···N3 ⁱⁱⁱ	0.78(8)	2.11(8)	2.884(5)	178(9)
O1–H1B···Cl2 ^{iv}	0.84(6)	2.58(7)	3.369(4)	156(6)
O1–H1B···Cl1 ⁱⁱⁱ	0.84(6)	2.76(6)	3.231(4)	117(5)
N6–H6···Cl2 ^v	0.89(4)	2.57(4)	3.410(2)	159(3)
N6–H6···Cl1 ^{vi}	0.89(4)	2.80(4)	3.197(4)	109(3)

Symmetry codes: i: $x, 0.5-y, -z$; ii: $x, 0.5-y, 1-z$; iii: $1-x, -0.5+y, 0.5-z$; iv: $1+x, y, z$; v: $-x, -y, -0.5+z$; vi: $-x, -0.5+y, 0.5-z$.

X-ray data

X-ray data of complexes **2** and **4–8** is summarized in Table S4.

Table S4. X-ray data of complexes **2** and **4–8**.

	2	4	5	6	7	8
formula	C ₈ H ₂₂ Cl ₂ Cu ₂ N ₂₄ O ₈	C ₄ H ₁₂ CuN ₁₄ O ₆	C ₄ H ₁₆ CuN ₁₄ O ₈	C ₂ H ₇ CuN ₇ O ₄	C ₈ H ₂₆ Cu ₂ N ₃₀ O ₁₀	C ₂ H ₈ Cl ₂ CuN ₆ O
<i>M_r</i> / g mol ⁻¹	780.48	415.82	451.85	256.69	829.67	266.58
color	green	blue	blue	dark green	green	green
habit	plate	block	block	block	plate	rod
crystal size / mm	0.15 × 0.10 × 0.05	0.35 × 0.30 × 0.20	0.08 × 0.06 × 0.04	0.10 × 0.10 × 0.05	0.22 × 0.20 × 0.11	0.40 × 0.03 × 0.03
crystal system	monoclinic	monoclinic	triclinic	monoclinic	orthorhombic	orthorhombic
space group	<i>P2₁/n</i>	<i>P2₁/c</i>	<i>P</i> $\bar{1}$	<i>P2₁/n</i>	<i>Pca2₁</i>	<i>Pbcm</i>
<i>a</i> / Å	8.7114(9)	7.5018(5)	5.7654(5)	6.1807(2)	21.3122(4)	10.8838(3)
<i>b</i> / Å	8.3337(8)	12.0996(7)	7.8993(7)	7.9197(3)	6.9575(2)	12.7348(4)
<i>c</i> / Å	19.0899(17)	8.0010(5)	8.9781(9)	16.6645(6)	20.0488(5)	6.0901(3)
α / °	90	90	75.057(8)	90	90	90
β / °	92.799(8)	101.967(6)	89.012(7)	100.400(3)	90	90
γ / °	90	90	86.621(7)	90	90	90
<i>V</i> / Å ³	1384.2(2)	710.46(8)	394.37(6)	802.31(5)	2972.83(13)	844.11(5)
<i>Z</i>	2	2	1	4	4	4
ρ_{calc} / g cm ⁻³	1.873	1.944	1.903	2.125	1.854	2.098
<i>T</i> / K	173(2)	293(2)	173(2)	173(2)	293(2)	100(2)
λ (Mo K α) / Å	0.71073	0.71073	0.71073	0.71073	0.71073	0.71073
<i>F</i> (000)	788	422	231	516	1688	532
μ / mm ⁻¹	1.81	1.61	1.46	2.73	1.53	3.18
θ range / °	4.3–25.0	4.3–26.0	4.3–27.9	4.2–26.0	4.2–26.4	4.2–26.0
dataset (<i>h</i> ; <i>k</i> ; <i>l</i>)	–9 ≤ <i>h</i> ≤ 10; –9 ≤ <i>k</i> ≤ 8; –22 ≤ <i>l</i> ≤ 16	–9 ≤ <i>h</i> ≤ 6; –14 ≤ <i>k</i> ≤ 13; –9 ≤ <i>l</i> ≤ 9	–7 ≤ <i>h</i> ≤ 3; –10 ≤ <i>k</i> ≤ 9; –11 ≤ <i>l</i> ≤ 10	–7 ≤ <i>h</i> ≤ 7; –9 ≤ <i>k</i> ≤ 9; –20 ≤ <i>l</i> ≤ 20	–26 ≤ <i>h</i> ≤ 24; –8 ≤ <i>k</i> ≤ 8; –25 ≤ <i>l</i> ≤ 22	–13 ≤ <i>h</i> ≤ 13; –15 ≤ <i>k</i> ≤ 15; –7 ≤ <i>l</i> ≤ 7
measured reflections	5005	3598	2385	7839	15067	8122
independent reflections	2426	1384	1856	1576	5692	909
observed reflections	1963	1209	1621	1490	5006	806
<i>R</i> _{int}	0.065	0.026	0.085	0.028	0.028	0.037
parameters	220	139	145	155	507	86
restraints	1	0	2	0	3	0
<i>R</i> ₁ (obs.)	0.049	0.030	0.055	0.020	0.028	0.025
<i>wR</i> ₂ (all data)	0.138	0.077	0.141	0.052	0.073	0.069
<i>S</i>	1.07	1.07	1.07	1.06	1.03	1.11
resd. dens. / e Å ⁻³	–1.04, 1.22	–0.31, 0.31	–1.41, 1.36	–0.30, 0.38	–0.29, 0.35	–0.76, 0.49
solution	SIR97	SIR97	SIR2004	SIR97	SIR92	SIR97
refinement	SHELXL-97	SHELXL-97	SHELXL-97	SHELXL-97	SHELXL-97	SHELXL-97
absorption correction	multi-scan	multi-scan	multi-scan	multi-scan	multi-scan	multi-scan
CCDC	917943	917944	917945	917946	922700	917947

UV-Vis-NIR Spectra

The UV-VIS-NIR reflectance of solid samples was measured with a *Varian Cary 500* spectrometer in a wavelength range of 350–1300 nm. The reflectance R [%] was transformed by the Kubelka–Munk function to the absorption intensity $F(R)$. The step in the absorption intensity $F(R)$ at 800 nm is caused by a detector change. The spectra have only qualitative character. Due to technical limitations no quantitative information about the absorption intensity could be obtained from the spectra. Commonly, R_∞ is technically approximated by a sample layer thick enough that the measuring instrument cannot detect differences in the thickness-dependent diffuse reflectance. However, not all samples could be coated on the object plate thick enough that there were no differences detectable anymore.

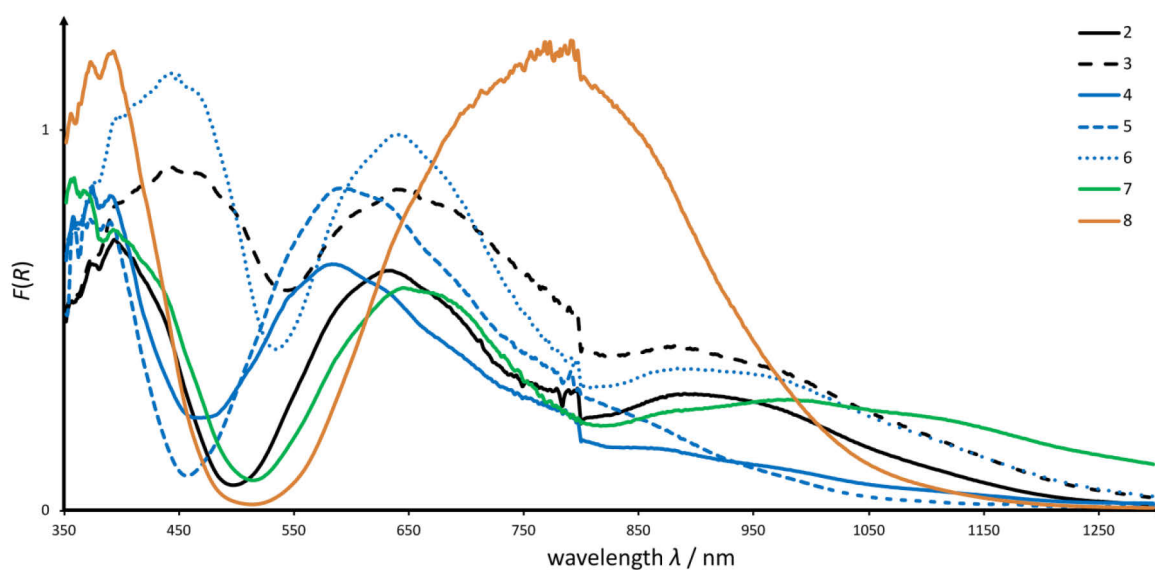


Figure S6. UV-Vis-NIR spectra of the copper(II) complexes 2–8.

Ignition Test



Figure S7. Ignition of same amounts of the perchlorate complexes **3** (left) and **2** (right) under confinement on an aluminum plate. The water containing complex **3** induced a slightly deeper dent in the aluminum plate than the water free compound **2**.

Experimental

Caution! All of the herein prepared copper(II) complexes and the free ligand **1** are energetic materials which show sensitivities towards various stimuli. Proper protective measures (safety glasses, face shield, leather coat, earthed equipment, conductive floor and shoes, Kevlar gloves and ear plugs) should be used when handling these compounds. Extra safety precautions should be taken when compound **2** and **3** are handled. **2** and the **3** are extremely sensitive towards impact, friction and electrostatic discharge. The handled scale of the compounds **2** and **3** should not be higher than 50–100 mg.

Poly[aqua(5-(1-methylhydrazinyl)tetrazolato)perchloratocopper(II)] (3): To a warm (70 °C) solution of **1** (132 mg, 1.00 mmol) in water (15 mL) was added a solution of copper(II) perchlorate hexahydrate (371 mg, 1.00 mmol) in water (2 mL). The green solution was left for crystallization at room-temperature. A green solid started to precipitate after a few hours. The solid was filtered off, washed with water and dried in air. Yield: 152 mg (0.52 mmol, 52 %). DTA (5 °C min⁻¹) onset: 206 °C (dec.); IR (ATR): $\tilde{\nu}$ = 3546 (vw), 3489 (vw), 3267 (w), 3217 (vw), 3188 (vw), 3133 (vw), 1637 (m), 1574 (m), 1449 (w), 1427 (w), 1296 (w), 1256 (w), 1214 (w), 1201 (w), 1159 (w), 1071 (vs), 966 (m), 934 (w), 746 (m), 673 (w), 668 (w), 652 (w) cm⁻¹; elemental analysis calc. (%) for C₂H₇O₅ClCuN₆ (294.11 g mol⁻¹): C 8.17, H 2.40, N 28.57; found: C 9.35, H 2.58, N 28.18; BAM impact: 1 J; BAM friction: 5 N; ESD: 0.007 J (at grain size < 100 μm).

Bis(5-(1-methylhydrazinyl)-1H-tetrazole-κ²N⁴,N⁶)dinitratocopper(II) (4): A warm (70 °C) solution of **1** (264 mg, 1.00 mmol) in 2 M nitric acid (10 mL) and a warm (70 °C) solution of

copper(II) nitrate trihydrate (242 mg, 1.00 mmol) in 2 M nitric acid (2 mL) were combined under stirring. The resulting deep blue solution was left for crystallization at room-temperature. Dark blue blocks crystallized after one day and were filtered off. The product was air dried. Yield: 285 mg (0.69 mmol, 69 %). DTA (5 °C min⁻¹) onset: 163 °C (dec.); IR (ATR): $\tilde{\nu}$ = 3200 (w), 3102 (w), 2948 (w), 2921 (w), 2792 (w), 2742 (w), 2675 (w), 2634 (w), 2482 (w), 2452 (w), 1758 (vw), 1681 (s), 1601 (w), 1442 (m), 1403 (s), 1331 (s), 1300 (vs), 1258 (s), 1133 (w), 1104 (m), 1097 (m), 1040 (s), 994 (w), 952 (s), 823 (m), 719 (s), 690 (w), 674 (w) cm⁻¹; elemental analysis calc. (%) for C₄H₁₂CuN₁₄O₆ (415.77 g mol⁻¹): C 11.56, H 2.91, N 47.16; found: C 11.86, H 2.77, N 46.88; BAM impact: 2 J; BAM friction: 32 N; ESD: 0.09 J (at grain size < 100 μm).

Diaquabis(5-(1-methylhydrazinyl)-1H-tetrazole-κ²N⁴,N⁶)copper(II) nitrate (5): A warm (70 °C) solution of **1** (264 mg, 2.00 mmol) in 2 M nitric acid (20 mL) and a warm (70 °C) solution of copper(II) nitrate trihydrate (242 mg, 1.00 mmol) in 2 M nitric acid (10 mL) were combined under stirring. The resulting blue solution was left for crystallization at room-temperature. Blue blocks crystallized after one week and were filtered off. The product was air dried. Yield: 393 mg (0.87 mmol, 87 %). DSC (5 °C min⁻¹) onset: 160 °C (dec.); DTA (5 °C min⁻¹) onset: 163 °C (dec.); IR (ATR): $\tilde{\nu}$ = 3540 (w), 3356 (vw), 3194 (w), 3128 (w), 3106 (w), 2946 (w), 2795 (w), 2653(w), 2613 (w), 2441 (w), 2454 (w), 1751 (vw), 1669 (s), 1637 (m), 1589 (w), 1443 (m), 1426 (m), 1402 (s), 1353 (vs), 1298 (vs), 1260 (m), 1172 (w), 1131 (w), 1106 (w), 1091 (m), 1054 (m), 1045 (s), 993 (w), 960 (m), 881 (w), 814 (w) cm⁻¹; elemental analysis calc. (%) for C₄H₁₆CuN₁₄O₈ (451.80 g mol⁻¹): C 10.63, H 3.57, N 43.40; found: C 11.02, H 3.30, N 43.38; BAM impact: 2 J; BAM friction: 96 N; ESD: 0.15 J (at grain size < 100 μm).

Poly[aqua(μ₃-5-(1-methylhydrazinyl)tetrazolato-κ⁴N¹,N²,N³,N⁶)nitratocopper(II)] (6): Compound **1** (132 mg, 1.00 mmol) was dissolved in 70 °C warm water under stirring and a solution of copper(II) nitrate trihydrate (242 mg, 1.00 mmol) was added. The green solution was left for crystallization and after one day the product was obtained as dark green blocks, which were filtered off and dried at ambient conditions. Yield: 200 mg (0.78 mmol, 78 %). DTA (5 °C min⁻¹) onset: 163 °C (dec.); IR (ATR): $\tilde{\nu}$ = 3437 (w), 3175 (w), 3099 (w), 2950 (w), 2822 (vw), 2734 (vw), 2634 (vw), 2478 (vw), 1755 (vw), 1655 (s), 1591 (m), 1474 (vw), 1450 (w), 1424 (w), 1342 (vs), 1307 (s), 1270 (s), 1219 (s), 1200 (m), 1183 (m), 1171 (m), 1125 (m), 1101 (m), 1050 (m), 974 (m), 921 (w), 824 (m), 745 (m), 716 (w), 697 (m), 689 (m), 656 (m) cm⁻¹; elemental analysis calc. (%) for C₂H₇CuN₇O₄ (256.69 g mol⁻¹): C 9.36, H 2.75, N 38.20; found: C 9.57, H 2.67, N 37.51; BAM impact: 3 J; BAM friction: 108 N; ESD: 0.80 J (at grain size < 100 μm).

Bis(dinitramido- κO)bis(μ -5-(1-methylhydrazinyl)tetrazolato- $1\kappa^2 N^1, N^6$ - $2\kappa N^2$)bis(5-(1-methylhydrazinyl)-1*H*-tetrazole- $1\kappa^2 N^4, N^6$)dicopper(II) dihydrate (7): To a solution of **1** (264 mg, 2.00 mmol) and ammonium dinitramide (372 mg, 3.00 mmol) in diluted sulfuric acid (3.3 %, 12 mL) was added copper(II) sulfate pentahydrate (250 mg, 1.00 mmol) at 50 °C under stirring. The solution turned dark green and after 5 min a green solid started to precipitate. The solid was filtered off, washed with a small amount of the mother liquor and air dried. Yield: 286 mg (0.69 mmol, 69 %). DTA (5 °C min⁻¹) onset: 145 °C (dec.); IR (ATR): $\tilde{\nu}$ = 3490 (w), 3374 (w), 3298 (w), 3226 (w), 3182 (w), 3149 (w), 3141 (w), 2811 (w), 2798 (w), 1678 (m), 1633 (m), 1600 (w), 1555 (w), 1538 (m), 1512 (m), 1454 (w), 1428 (m), 1417 (m), 1311 (w), 1291 (vw), 1279 (vw), 1247 (m), 1228 (w), 1200 (w), 1163 (vs), 1097 (m), 1070 (m), 1039 (w), 1032 (w), 1011 (s), 956 (w), 932 (m), 820 (vw), 754 (m), 733 (m), 683 (vw) cm⁻¹; elemental analysis calc. (%) for C₄H₁₃CuN₁₅O₅ (414.79 g mol⁻¹): C 11.58, H 3.16, N 50.65; found: C 11.97, H 3.05, N 50.59; BAM impact: 10 J; BAM friction: 120 N; ESD: 0.17 J (at grain size < 100 μ m).

Poly[chlorido- μ_3 -chlorido(5-(1-methylhydrazinyl)-1*H*-tetrazole- $\kappa^2 N^4, N^6$)copper(II)] monohydrate (8): Copper(II) chloride dihydrate (170 mg, 1.00 mmol) was added under stirring to a solution of **1** (132 mg, 1.00 mmol) in 1 M hydrochloric acid (5 mL) at 70 °C. The green solution was left for crystallization and after a few days the product was obtained in form of green rods. The crystals were filtered off and dried at ambient conditions. Yield: 90 mg (0.34 mmol, 34 %). DTA (5 °C min⁻¹) onset: 185 °C (dec.); IR (ATR): $\tilde{\nu}$ = 3509 (w), 3271 (w), 3192 (w), 3174 (w), 3166 (w), 1684 (w), 1638 (m), 1575 (m), 1545 (w), 1458 (w), 1450 (w), 1428 (w), 1416 (w), 1313 (vw), 1296 (vw), 1275 (w), 1256 (w), 1215 (w), 1202 (w), 1152 (w), 1082 (vs), 1060 (vs), 1005 (w), 967 (w), 955 (w), 942 (w), 834 (w), 755 (w), 746 (w), 724 (vw), 674 (w) cm⁻¹; elemental analysis calc. (%) for C₂H₈Cl₂CuN₆O (266.58 g mol⁻¹): C 9.01, H 3.02, N 31.53; found: C 9.05, H 2.97, N 29.27; BAM impact: 40 J; BAM friction: 252 N; ESD: 1.5 J (at grain size < 100 μ m).

A3. Supporting Information Chapter 8

Investigations Concerning the Laser Ignition and Initiation of Various Metal(II) Complexes with 1,2-Di(1H-tetrazol-1-yl)ethane as Ligand and a Large Set of Anions

Table of Content

1. Experimental
2. Solid UV/Vis/NIR spectroscopy
3. X-ray data
4. Additional X-ray illustrations

Experimental

{[Fe(dte)₃](ClO₄)₂]_n (2): Yield: 0.39 g (0.51 mmol, 77 %). DTA (5 °C min⁻¹) onset: 240 °C (decomp.); IR (ATR): $\tilde{\nu}$ = 3132 (w), 3035 (vw), 2987 (vw), 1507 (w), 1497 (w), 1451 (w), 1366 (vw), 1312 (vw), 1269 (w), 1182 (m), 1157 (w), 1141 (w), 1094 (vs), 1083 (vs), 1019 (w), 1005 (w), 991 (m), 919 (w), 891 (w), 720 (vw), 664 (w), 656 cm⁻¹ (m); UV/Vis/NIR: λ_{max} = 879 nm; elemental analysis calcd. (%) for C₁₂H₁₈Cl₂FeN₂₄O₈ (753.18 g mol⁻¹): C 19.14, H 2.41, N 44.63; found: C 19.31, H 2.39, N 44.56; BAM impact: 2 J; BAM friction 14 N; ESD: 80 mJ (at grain size < 100 μm).

{[Co(dte)₃](ClO₄)₂]_n (3): Yield: 0.29 g (0.39 mmol, 58 %). DTA (5 °C min⁻¹) onset: 288 °C (decomp.); IR (ATR): $\tilde{\nu}$ = 3135 (w), 3032 (vw), 2990 (vw), 1508 (w), 1497 (w), 1451 (w), 1366 (vw), 1313 (vw), 1270 (vw), 1182 (w), 1158 (w), 1141 (w), 1093 (vs), 1083 (vs), 1019 (w), 1007 (w), 995 (m), 919 (w), 891 (w), 720 (vw), 665 (w), 656 cm⁻¹ (m); UV/Vis/NIR: λ_{max} = 471, 974 nm; elemental analysis calcd. (%) for C₁₂H₁₈Cl₂CoN₂₄O₈ (756.27 g mol⁻¹): C 19.06, H 2.40, N 44.45; found: C 19.28, H 2.38, N 44.32; BAM impact: 1 J; BAM friction 6 N; ESD: 0.25 J (at grain size 100–500 μm).

{[Ni(dte)₃](ClO₄)₂]_n (4): Yield: 0.44 g (0.58 mmol, 86 %). DTA (5 °C min⁻¹) onset: 298 °C (decomp.); IR (ATR): $\tilde{\nu}$ = 3140 (w), 3033 (vw), 2986 (vw), 1509 (w), 1497 (w), 1451 (w), 1367 (w), 1314 (vw), 1271 (w), 1184 (w), 1160 (w), 1143 (w), 1093 (vs), 1083 (vs), 1019 (w), 1000 (m), 919 (w), 891 (w), 721 (vw), 657 cm⁻¹ (m); UV/Vis/NIR: λ_{max} = 387, 549, 896 nm; elemental analysis calcd. (%) for C₁₂H₁₈Cl₂N₂₄NiO₈ (756.03 g mol⁻¹): C 19.06, H 2.40, N 44.46; found: C 19.11, H 2.32, N 44.21; BAM impact: 1 J; BAM friction 6 N; ESD: 0.25 J (at grain size 100–500 μm).

{[Cu(dte)₃](ClO₄)₂]_n (5): Yield: 0.46 g (0.60 mmol, 90 %). DTA (5 °C min⁻¹) onset: 256 °C (decomp.); IR (ATR): $\tilde{\nu}$ = 3136 (w), 3030 (vw), 2987 (vw), 1515 (w), 1500 (w), 1491 (w), 1452 (w), 1433 (w), 1366 (w), 1316 (vw), 1302 (vw), 1276 (w), 1179 (m), 1160 (w), 1141

(w), 1093 (vs), 1081 (vs), 1018 (m), 996 (m), 978 (m), 915 (w), 888 (w), 721 (w), 659 cm⁻¹ (m); UV/Vis/NIR: λ_{\max} = 661 nm; elemental analysis calcd. (%) for C₁₂H₁₈Cl₂CuN₂₄O₈ (760.88 g mol⁻¹): C 18.94, H 2.38, N 44.18; found: C 19.07, H 2.29, N 43.90; BAM impact: 1.5 J; BAM friction 10 N; ESD: 0.15 J (at grain size < 100 μ m).

{[Zn(dte)₃](ClO₄)₂]_n (6): Yield: 0.35 g (0.46 mmol, 70 %). DTA (5 °C min⁻¹) onset: 280 °C (decomp.); IR (ATR): $\tilde{\nu}$ = 3134 (w), 3033 (vw), 2986 (vw), 1507 (w), 1497 (w), 1451 (w), 1366 (vw), 1313 (vw), 1269 (vw), 1182 (m), 1158 (w), 1141 (w), 1093 (vs), 1083 (vs), 1020 (w), 1008 (w), 994 (m), 918 (w), 892 (w), 720 (vw), 656 cm⁻¹ (m); UV/Vis/NIR: λ_{\max} = none; elemental analysis calcd. (%) for C₁₂H₁₈Cl₂N₂₄O₈Zn (762.71 g mol⁻¹): C 18.90, H 2.38, N 44.07; found: C 19.11, H 2.30, N 43.99; BAM impact: 2 J; BAM friction 42 N; ESD: 0.30 J (at grain size 100–500 μ m).

{[Cd(dte)₃](ClO₄)₂]_n (7): Yield: 0.40 g (0.49 mmol, 74 %). DTA (5 °C min⁻¹) onset: 241 °C (decomp.); IR (ATR): $\tilde{\nu}$ = 3133 (w), 3030 (vw), 2984 (vw), 1500 (w), 1463 (vw), 1451 (w), 1433 (vw), 1365 (vw), 1329 (vw), 1303 (vw), 1274 (vw), 1182 (m), 1153 (vw), 1138 (w), 1108 (s), 1093 (vs), 1082 (vs), 1048 (m), 1016 (w), 1003 (w), 985 (m), 973 (w), 923 (w), 895 (w), 888 (w), 720 (vw), 694 (m), 669 (w), 662 (w), 654 cm⁻¹ (m); UV/Vis/NIR: λ_{\max} = 374 nm; elemental analysis calcd. (%) for C₁₂H₁₈Cl₂CdN₂₄O₈ (809.74 g mol⁻¹): C 17.80, H 2.44, N 41.51; found: C 17.94, H 2.19, N 41.33; BAM impact: 4 J; BAM friction 60 N; ESD: 80 mJ (at grain size 100–500 μ m).

{[Co(dte)₃](NO₃)₂]_n (8): Yield: 0.33 g (0.49 mmol, 74 %). DTA (5 °C min⁻¹) onset: 225 °C (decomp.); IR (ATR): $\tilde{\nu}$ = 3094 (w), 2985 (vw), 1814 (vw), 1754 (vw), 1503 (w), 1458 (w), 1436 (w), 1351 (vs), 1322 (s), 1300 (m), 1248 (w), 1190 (s), 1157 (m), 1102 (s), 1046 (vw), 1032 (w), 1005 (m), 912 (m), 830 (w), 784 (w), 721 (vw), 712 (vw), 696 (s), 660 cm⁻¹ (s); UV/Vis/NIR: λ_{\max} = 475, 1007 nm; elemental analysis calcd. (%) for C₁₂H₁₈CoN₂₆O₆ (681.38 g mol⁻¹): C 21.15, H 2.66, N 53.45; found: C 21.02, H 2.64, N 52.70; BAM impact: 12.5 J; BAM friction 288 N; ESD: 0.2 J (at grain size < 100 μ m).

{[Ni(dte)₃](NO₃)₂]_n (9): Yield: 0.35 g (0.51 mmol, 77 %). DTA (5 °C min⁻¹) onset: 248 °C (decomp.); IR (ATR): $\tilde{\nu}$ = 3132 (vw), 3096 (w), 3034 (vw), 2992 (vw), 2946 (vw), 1506 (w), 1452 (w), 1342 (vs), 1316 (m), 1263 (w), 1223 (vw), 1182 (m), 1157 (w), 1112 (s), 1096 (m), 1047 (vw), 1023 (w), 1007 (m), 897 (w), 830 (w), 786 (vw), 722 (vw), 698 (w), 669 (m), 661 cm⁻¹ (s); UV/Vis/NIR: λ_{\max} = 543, 876 nm; elemental analysis calcd. (%) for C₁₂H₁₈N₂₆NiO₆ (681.14 g mol⁻¹): C 21.16, H 2.66, N 53.47; found: C 21.35, H 2.61, N 53.34; BAM impact: 7 J; BAM friction 240 N; ESD: 0.2 J (at grain size < 100 μ m).

{[Cu(dte)₃](NO₃)₂]_n (10): Yield: 0.38 g (0.55 mmol, 83 %). DTA (5 °C min⁻¹) onset: 191 °C (decomp.); IR (ATR): $\tilde{\nu}$ = 3087 (w), 2987 (vw), 1505 (w), 1492 (w), 1458 (w), 1435 (w), 1350 (vs), 1323 (m), 1189 (s), 1158 (m), 1101 (s), 1030 (w), 1012 (m), 996 (w), 914 (w), 831 (w), 785 (w), 720 (vw), 712 (vw), 696 (s), 660 cm⁻¹ (s); UV/Vis/NIR: λ_{\max} = 722 nm;

elemental analysis calcd. (%) for $C_{12}H_{18}CuN_{26}O_6$ ($685.99 \text{ g mol}^{-1}$): C 21.01, H 2.64, N 53.09; found: C 21.16, H 2.59, N 52.97; BAM impact: 7 J; BAM friction 160 N; ESD: 1.0 J (at grain size 100–500 μm).

{[Zn(dte)₃](NO₃)₂]_n (11): Yield 0.45 g (0.65 mmol, 98 %). DTA ($5 \text{ }^\circ\text{C min}^{-1}$) onset: 203 $^\circ\text{C}$ (decomp.); IR (ATR): $\tilde{\nu} = 3093$ (m), 2989 (w), 1505 (w), 1458 (w), 1436 (w), 1352 (vs), 1322 (s), 1300 (m), 1248 (w), 1190 (s), 1156 (m), 1102 (s), 1046 (vw), 1032 (vw), 1005 (m), 913 (m), 831 (w), 799 (vw), 784 (w), 750 (vw), 721 (w), 712 (w), 696 (s), 668 (w), 660 cm^{-1} (s); UV/Vis/NIR: $\lambda_{\text{max}} = \text{none}$; elemental analysis calcd. (%) for $C_{12}H_{18}N_{26}O_6Zn$ ($687.82 \text{ g mol}^{-1}$): C 20.95, H 2.64, N 52.95; found: C 20.99, H 2.58, N 52.48; BAM impact: 5 J; BAM friction 240 N; ESD: 0.3 J (at grain size 100–500 μm).

{[Cd(dte)₃](NO₃)₂]_n (12): Yield 0.40 g (0.54 mmol, 81 %). DTA ($5 \text{ }^\circ\text{C min}^{-1}$) onset: 201 $^\circ\text{C}$ (decomp.); IR (ATR): $\tilde{\nu} = 3086$ (m), 3032 (vw), 2986 (vw), 1828 (vw), 1753 (vw), 1509 (w), 1496 (w), 1463 (w), 1442 (w), 1436 (w), 1420 (vw), 1354 (vs), 1324 (m), 1304 (w), 1261 (vw), 1186 (s), 1146 (m), 1101 (s), 1046 (vw), 1029 (vw), 1000 (m), 920 (w), 830 (w), 720 (vw), 710 (vw), 696 (s), 664 cm^{-1} (s); UV/Vis/NIR: $\lambda_{\text{max}} = \text{none}$; elemental analysis calcd. (%) for $C_{12}H_{18}CdN_{26}O_6$ ($734.85 \text{ g mol}^{-1}$): C 19.61, H 2.47, N 49.56; found: C 19.67, H 2.42, N 48.80; BAM impact: 10 J; BAM friction 360 N; ESD: 0.8 J (at grain size 100–500 μm).

[CuCl₂(dte)₂]_n (13): Yield: 0.36 g (0.77 mmol, 77 %). DTA ($5 \text{ }^\circ\text{C min}^{-1}$) onset: 151 $^\circ\text{C}$ (melting), 186 $^\circ\text{C}$ (decomp.); IR (ATR): $\tilde{\nu} = 3132$ (w), 3109 (m), 3023 (vw), 2992 (w), 1804 (vw), 1743 (vw), 1504 (m), 1490 (m), 1451 (w), 1441 (m), 1422 (w), 1371 (w), 1357 (w), 1311 (vw), 1287 (w), 1275 (vw), 1259 (w), 1190 (m), 1176 (vs), 1148 (m), 1119 (m), 1112 (m), 1092 (vs), 1052 (w), 1033 (w), 1015 (w), 1005 (s), 974 (w), 954 (m), 907 (s), 890 (w), 873 (m), 721 (w), 703 (vw), 688 (m), 668 (m), 658 cm^{-1} (vs); elemental analysis calcd. (%) for $C_8H_{12}Cl_2CuN_{16}$ ($466.74 \text{ g mol}^{-1}$): C 20.59, H 2.59, N 48.02; found: C 20.59, H 2.50, N 47.33; BAM impact: 10 J; BAM friction 324 N; ESD: 1.0 J (at grain size 500–1000 μm).

{[Cu(dte)₃](ClO₃)₂]_n (14): Yield: 0.32 g (0.44 mmol, 66 %). DTA ($5 \text{ }^\circ\text{C min}^{-1}$) onset: 175 $^\circ\text{C}$ (decomp.); IR (ATR): $\tilde{\nu} = 3098$ (w), 2983 (vw), 1818 (vw), 1504 (w), 1459 (w), 1448 (w), 1438 (w), 1357 (vw), 1324 (vw), 1299 (vw), 1265 (vw), 1249 (vw), 1216 (vw), 1189 (m), 1156 (m), 1109 (m), 1102 (m), 1095 (m), 1013 (w), 998 (w), 964 (vs), 957 (vs), 938 (m), 934 (m), 926 (m), 913 (m), 842 (w), 837 (w), 824 (vw), 817 (vw), 806 (vw), 777 (w), 720 (w), 695 (m), 668 (m), 659 cm^{-1} (s); elemental analysis calcd. (%) for $C_{12}H_{18}Cl_2CuN_{24}O_6$ ($728.88 \text{ g mol}^{-1}$): C 19.77, H 2.49, N 46.12; found: C 19.96, H 2.39, N 46.05; BAM impact: 1.5 J; BAM friction 6 N; ESD: 15 mJ (at grain size < 100 μm).

[Cu(NO₂)₂(dte)]_n (15): Yield: 0.45 g (1.4 mmol, 70 %). DTA ($5 \text{ }^\circ\text{C min}^{-1}$) onset: 139 $^\circ\text{C}$ (decomp.); IR (ATR): $\tilde{\nu} = 3156$ (m), 3030 (w), 2983 (vw), 2960 (vw), 2705 (vw), 1777 (vw), 1519 (w), 1506 (w), 1451 (w), 1364 (s), 1328 (w), 1285 (w), 1186 (m), 1160 (vs), 1137 (vs), 1095 (vs), 1015 (s), 891 (m), 848 (m), 778 (w), 718 (vw), 696 (s), 660 cm^{-1} (s); elemental

analysis calcd. (%) for $C_4H_6CuN_{10}O_4$ ($321.70 \text{ g mol}^{-1}$): C 14.93, H 1.88, N 43.54; found: C 15.29, H 1.88, N 43.19; BAM impact: 2 J; BAM friction 160 N; ESD: 1.0 J (at grain size 100–500 μm).

$\{[\text{Cu}(\text{dte})_3](\text{N}(\text{NO}_2)_2)_2\}_n$ (16): Yield: 0.45 g (0.59 $^\circ$ mmol, 88 %). DTA ($5 \text{ }^\circ\text{C min}^{-1}$) onset: 168 $^\circ\text{C}$ (decomp.); IR (ATR): $\tilde{\nu} = 3134$ (w), 3124 (w), 3023 (vw), 2979 (vw), 1514 (s), 1492 (m), 1439 (m), 1366 (w), 1326 (w), 1317 (w), 1287 (vw), 1268 (w), 1191 (s), 1175 (vs), 1167 (vs), 1145 (m), 1097 (s), 1088 (m), 1051 (vw), 1015 (m), 993 (s), 974 (m), 936 (w), 895 (m), 879 (w), 825 (w), 818 (w), 757 (m), 721 (m), 696 (w), 684 (m), 672 (w), 658 cm^{-1} (s); elemental analysis calcd. (%) for $C_{12}H_{18}CuN_{30}O_8$ ($774.01 \text{ g mol}^{-1}$): C 18.62, H 2.34, N 54.29; found: C 18.89, H 2.37, N 54.04; BAM impact: 1 J; BAM friction 80 N; ESD: 0.25 J (at grain size $< 100 \mu\text{m}$).

$[\text{Cu}(\text{N}(\text{CN})(\text{NO}_2))_2(\text{dte})_2]_n$ (17): Yield: 0.37 g (0.65 mmol, 65 %). DTA ($5 \text{ }^\circ\text{C min}^{-1}$) onset: 170 $^\circ\text{C}$ (decomp.); IR (ATR): $\tilde{\nu} = 3117$ (w), 3027 (w), 3012 (w), 2979 (vw), 2333 (vw), 2221 (vw), 2183 (s), 2168 (w), 1802 (vw), 1550 (vw), 1535 (vw), 1512 (w), 1502 (w), 1458 (w), 1440 (m), 1422 (s), 1383 (w), 1368 (m), 1324 (vw), 1286 (s), 1264 (vs), 1187 (m), 1175 (s), 1151 (s), 1093 (vs), 1058 (w), 1024 (m), 1021 (m), 1012 (m), 1003 (m), 958 (m), 952 (m), 930 (w), 906 (m), 773 (m), 762 (w), 719 (w), 688 (w), 670 (s), 656 cm^{-1} (s); elemental analysis calcd. (%) for $C_{10}H_{12}CuN_{22}O_4$ ($567.89 \text{ g mol}^{-1}$): C 21.15, H 2.13, N 54.26; found: C 21.39, H 2.18, N 53.90; BAM impact: 1 J; BAM friction 108 N; ESD: 0.50 J (at grain size $< 100 \mu\text{m}$).

$\{[\text{Cu}(\text{dte})_3](\text{N}(\text{CN})(\text{NO}_2))_2 \cdot 2 \text{H}_2\text{O}\}_n$ (18): Yield: 0.29 g (0.38 $^\circ$ mmol, 57 %). DTA ($5 \text{ }^\circ\text{C min}^{-1}$) onset: 123 $^\circ\text{C}$ (dehydration), 171 $^\circ\text{C}$ (decomp.); IR (ATR): $\nu = 3574$ (vw), 3491 (vw), 3423 (vw), 3165 (vw), 3145 (vw), 3120 (w), 3033 (vw), 3016 (vw), 2225 (vw), 2173 (m), 1654 (vw), 1630 (vw), 1516 (w), 1452 (m), 1426 (s), 1329 (vw), 1317 (vw), 1259 (vs), 1186 (m), 1158 (m), 1140 (m), 1090 (s), 1012 (w), 999 (m), 983 (w), 952 (w), 876 (m), 772 (w), 719 (vw), 697 (s), 662 cm^{-1} (s); elemental analysis calcd. (%) for $C_{14}H_{22}CuN_{30}O_6$ ($770.07 \text{ g mol}^{-1}$): C 21.84, H 2.88, N 54.57; found: C 22.11, H 2.88, N 54.35; BAM impact: 5 J; BAM friction 120 N; ESD: 0.70 J (at grain size $< 100 \mu\text{m}$).

$\{[\text{Cu}(\text{dte})_2(\text{H}_2\text{O})_2](\text{C}(\text{NO}_2)_3)_2\}_n$ (19): Yield: 0.56 g (0.77 $^\circ$ mmol, 77 %). DTA ($5 \text{ }^\circ\text{C min}^{-1}$) onset: 83 $^\circ\text{C}$ (decomp.); IR (ATR): $\tilde{\nu} = 3559$ (w), 3506 (w), 3164 (w), 3124 (w), 3030 (vw), 3015 (vw), 2967 (vw), 1621 (w), 1526 (m), 1514 (m), 1508 (m), 1487 (s), 1456 (w), 1442 (m), 1425 (w), 1392 (w), 1374 (m), 1367 (m), 1303 (s), 1290 (s), 1211 (w), 1188 (w), 1176 (w), 1151 (vs), 1104 (m), 1098 (s), 1034 (m), 1019 (m), 1008 (m), 964 (w), 926 (w), 902 (w), 893 (m), 866 (w), 784 (s), 736 (m), 717 (w), 681 (m), 661 (m), 654 cm^{-1} (w); elemental analysis calcd. (%) for $C_{10}H_{16}CuN_{22}O_{14}$ ($731.92 \text{ g mol}^{-1}$): C 16.41, H 2.20, N 42.10; found: C 16.70, H 2.17, N 41.87; BAM impact: 40 J; BAM friction 192 N; ESD: 0.20 J (at grain size $< 100 \mu\text{m}$).

{[Cu(dte)₂(H₂O)₂](C(CN)(NO₂)₂)₂]_n (20): Yield: 0.22 g (0.32°mmol, 32 %). DTA (5 °C min⁻¹) onset: 212 °C (decomp.); IR (ATR): $\tilde{\nu}$ = 3550 (m), 3396 (s), 3141 (s), 3040 (w), 3014 (w), 2973 (w), 2216 (m), 1771 (vw), 1630 (w), 1510 (vs), 1451 (w), 1431 (m), 1414 (m), 1378 (vw), 1362 (w), 1322 (w), 1296 (m), 1254 (vs), 1244 (vs), 1192 (s), 1186 (s), 1180 (s), 1147 (s), 1097 (vs), 1055 (m), 1024 (w), 1006 (m), 943 (w), 935 (w), 888 (s), 848 cm⁻¹ (w); elemental analysis calcd. (%) for C₁₂H₁₆CuN₂₂O₁₀ (691.94 g mol⁻¹): C 20.83, H 2.33, N 44.53; found: C 21.06, H 2.40, N 44.46; BAM impact: 4 J; BAM friction 288 N; ESD: 0.10 J (at grain size < 100 μm).

[Cu₂(N₃)₄(dte)]_n (21): Yield: 0.39 g (0.85°mmol, 85 %). DTA (5 °C min⁻¹) onset: 197 °C (decomp.); IR (ATR): $\tilde{\nu}$ = 3365 (w), 3319 (w), 3122 (m), 3018 (w), 2976 (w), 2953 (w), 2074 (m), 2044 (vs), 1809 (w), 1513 (m), 1499 (m), 1454 (m), 1449 (m), 1387 (w), 1339 (w), 1290 (s), 1274 (m), 1183 (s), 1135 (m), 1092 (s), 1007 (m), 907 (s), 845 (w), 806 (w), 696 (s), 664 cm⁻¹ (s); elemental analysis calcd. (%) for C₄H₆Cu₂N₂₀ (461.32 g mol⁻¹): C 10.41, H 1.31, N 60.72; found: C 11.01, H 1.32, N 59.45; BAM impact: 1 J; BAM friction 5 N; ESD: 14 mJ (at grain size 100–500 μm).

Solid UV/Vis/NIR spectroscopy

UV/Vis/NIR spectra were recorded of solid samples for compounds **2–12** on a Varian Cary 500 spectrometer in the wavelength range of 350–1300 nm. The detected reflectance R [%] was transformed by the Kubelka-Munk equation to the absorption intensity $F(R)$. The absorption spectra of the perchlorates are shown in Figure S1 and for the nitrates in Figure S2.

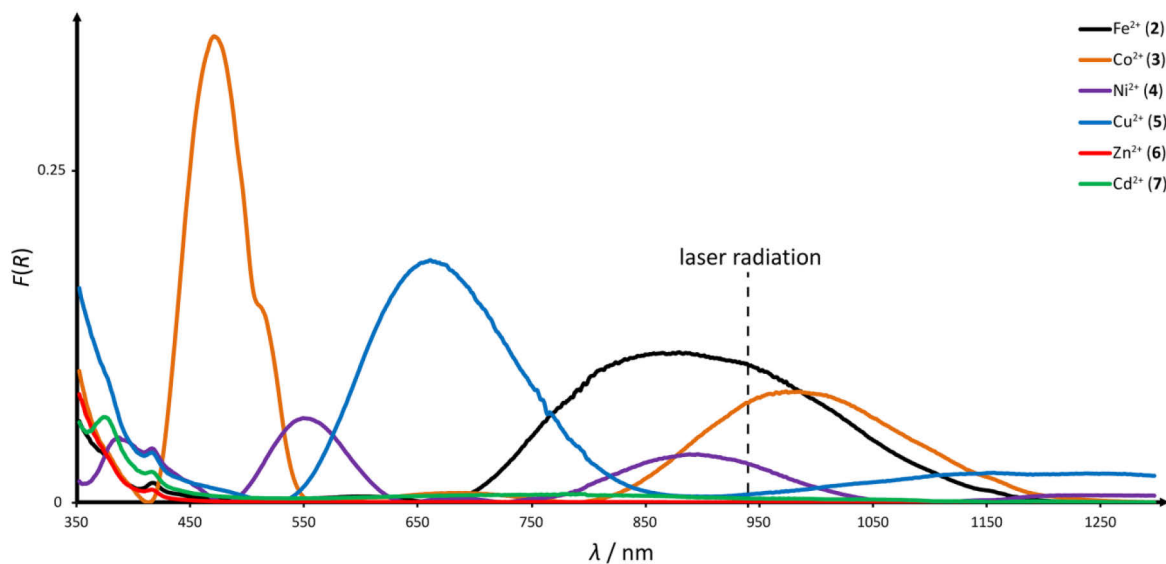


Figure S1. UV/Vis/NIR spectra of $[M(dte)_3](ClO_4)_2$ **2–7**.

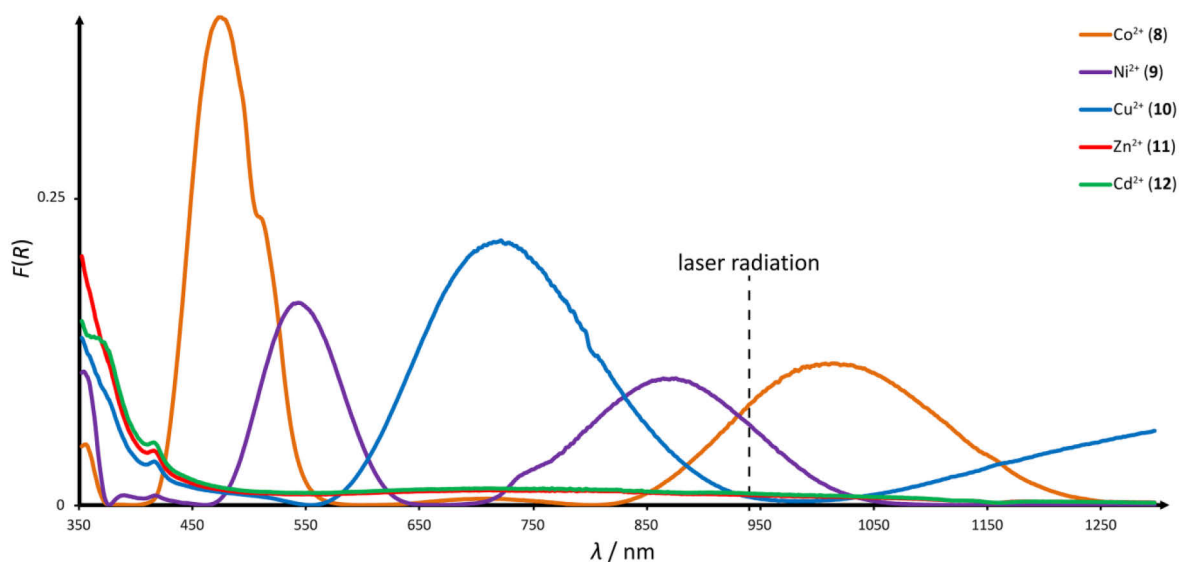


Figure S2. UV/Vis/NIR spectra of $[M(dte)_3](NO_3)_2$ **8–12**.

X-ray data

Table S1. X-ray data of complexes 10–12.

	10	11	12
Formula	C ₁₂ H ₁₈ CuN ₂₆ O ₆	C ₁₂ H ₁₈ N ₂₆ O ₆ Zn	C ₁₂ H ₁₈ CdN ₂₆ O ₆
<i>M</i> _r / g mol ⁻¹	686.06	687.89	734.92
Color	pale blue	colorless	colorless
Habit	block	block	block
Crystal size / mm	0.15 × 0.1 × 0.1	0.58 × 0.45 × 0.40	0.56 × 0.41 × 0.40
Crystal system	trigonal	trigonal	trigonal
Space group	<i>P</i> $\bar{3}$	<i>P</i> $\bar{3}$	<i>P</i> $\bar{3}$
<i>a</i> / Å	10.2767(17)	10.3245(2)	10.815(5)
<i>b</i> / Å	10.2767(17)	10.3245(2)	10.815(5)
<i>c</i> / Å	6.663(2)	6.6707(2)	6.467(5)
α / °	90	90	90
β / °	90	90	90
γ / °	120	120	120
<i>V</i> / Å ³	609.4(2)	615.80(3)	655.1(7)
<i>Z</i>	1	1	1
$\rho_{\text{calc.}}$ / g cm ⁻³	1.869	1.855	1.863
<i>T</i> / K	173(2)	173(2)	173(2)
λ (Mo K α) / Å	0.71073	0.71073	0.71073
<i>F</i> (000)	349	350	368
μ / mm ⁻¹	0.99	1.09	0.92
θ range / °	4.6–27.0	4.6–26.8	4.4–27.0
Dataset (<i>h</i> ; <i>k</i> ; <i>l</i>)	-11 ≤ <i>h</i> ≤ 13 -13 ≤ <i>k</i> ≤ 6 -8 ≤ <i>l</i> ≤ 8	-13 ≤ <i>h</i> ≤ 10 -13 ≤ <i>k</i> ≤ 12 -7 ≤ <i>l</i> ≤ 8	-13 ≤ <i>h</i> ≤ 13 -13 ≤ <i>k</i> ≤ 12 -8 ≤ <i>l</i> ≤ 8
Measured reflections	3371	3430	3684
Independent reflections	896	895	953
Observed reflections	737	867	950
<i>R</i> _{int}	0.061	0.019	0.021
Parameters	81	81	81
Restraints	0	0	0
<i>R</i> ₁ (obs.)	0.044	0.020	0.014
<i>wR</i> ₂ (all data)	0.110	0.047	0.036
<i>S</i>	1.06	1.11	1.12
Resd. dens. / e Å ⁻³	-0.85, 0.61	-0.28, 0.26	-0.19, 0.27
Solution	SIR97	SIR97	SIR97
Refinement	SHELXL-97	SHELXL-97	SHELXL-97
Absorption correction	multi-scan	multi-scan	multi-scan
CCDC	891889	891890	891892

Table S2. X-ray data of complexes **14–16**.

	14	15	16
Formula	C ₁₂ H ₁₈ Cl ₂ CuN ₂₄ O ₆	C ₄ H ₆ CuN ₁₀ O ₄	C ₁₂ H ₁₈ CuN ₃₀ O ₈
$M_r / \text{g mol}^{-1}$	728.94	321.73	774.10
Color	blue	dark green	blue
Habit	block	block	block
Crystal size / mm	0.38 × 0.25 × 0.25	0.45 × 0.40 × 0.20	0.17 × 0.12 × 0.08
Crystal system	trigonal	monoclinic	triclinic
Space group	$P\bar{3}c1$	$P2_1/c$	$P1$
$a / \text{Å}$	10.3438(3)	5.7809(3)	7.6855(6)
$b / \text{Å}$	10.3438(3)	9.6882(5)	8.7967(6)
$c / \text{Å}$	28.4362(12)	9.5123(5)	11.5671(9)
$\alpha / ^\circ$	90	90	90.040(6)
$\beta / ^\circ$	90	94.530(5)	109.044(7)
$\gamma / ^\circ$	120	90	95.627(6)
$V / \text{Å}^3$	2634.89(16)	531.09(5)	735.21
Z	4	2	1
$\rho_{\text{calc.}} / \text{g cm}^{-3}$	1.838	2.012	1.748
T / K	293(2)	293(2)	173(2)
$\lambda (\text{Mo K}\alpha) / \text{Å}$	0.71073	0.71073	0.71073
$F(000)$	1476	322	393
μ / mm^{-1}	1.12	2.09	0.84
θ range / °	4.2–26.4	4.2–25.2	4.3–28.3
Dataset ($h; k; l$)	$-12 \leq h \leq 11$ $-12 \leq k \leq 11$ $-35 \leq l \leq 35$	$-5 \leq h \leq 6$ $-9 \leq k \leq 11$ $-11 \leq l \leq 11$	$-10 \leq h \leq 10$ $-11 \leq k \leq 9$ $-15 \leq l \leq 15$
Measured reflections	12920	2450	4598
Independent reflections	1797	952	4156
Observed reflections	1533	848	3645
R_{int}	0.033	0.025	0.013
Parameters	160	93	532
Restraints	0	0	3
R_1 (obs.)	0.034	0.028	0.036
wR_2 (all data)	0.081	0.076	0.097
S	1.14	1.11	1.05
Resd. dens. / e Å ⁻³	-0.44, 0.39	-0.61, 0.34	-0.34, 0.34
Solution	SIR2004	SIR2004	SIR97
Refinement	SHELXL-97	SHELXL-97	SHELXL-97
Absorption correction	multi-scan	multi-scan	multi-scan
CCDC	920471	920472	969651

Table S3. X-ray data of complexes **17**, **19** and **20**.

	17	19	20
Formula	C ₁₀ H ₁₂ CuN ₂₂ O ₄	C ₁₀ H ₁₆ CuN ₂₂ O ₁₄	C ₁₂ H ₁₆ CuN ₂₂ O ₁₀
$M_r / \text{g mol}^{-1}$	567.96	731.99	692.01
Color	blue	pale green	pale green
Habit	block	block	rod
Crystal size / mm	0.41 × 0.27 × 0.12	0.3 × 0.15 × 0.1	0.20 × 0.05 × 0.05
Crystal system	triclinic	triclinic	monoclinic
Space group	$P\bar{1}$	$P\bar{1}$	$P2_1/n$
$a / \text{Å}$	7.8602(6)	9.1100(5)	8.8206(3)
$b / \text{Å}$	8.4767(6)	9.2603(8)	10.4813(6)
$c / \text{Å}$	9.1326(9)	9.4235(7)	13.6447(6)
$\alpha / ^\circ$	112.584(8)	68.346(7)	90
$\beta / ^\circ$	110.939(8)	63.502(6)	93.834(4)
$\gamma / ^\circ$	90.100(6)	83.682(6)	90
$V / \text{Å}^3$	517.87(7)	659.83(8)	1258.63(10)
Z	1	1	2
$\rho_{\text{calc.}} / \text{g cm}^{-3}$	1.821	1.842	1.826
T / K	100(2)	293(2)	173(2)
$\lambda (\text{Mo K}\alpha) / \text{Å}$	0.71073	0.71073	0.71073
$F(000)$	287	371	702
μ / mm^{-1}	1.13	0.94	0.97
θ range / °	4.4–26.4	4.3–26.4	4.1–26.0
Dataset ($h; k; l$)	$-7 \leq h \leq 9$ $-10 \leq k \leq 10$ $-11 \leq l \leq 11$	$-11 \leq h \leq 11$ $-11 \leq k \leq 11$ $-11 \leq l \leq 11$	$-10 \leq h \leq 10$ $-11 \leq k \leq 12$ $-16 \leq l \leq 13$
Measured reflections	3882	6954	6392
Independent reflections	2122	2696	2456
Observed reflections	1932	2469	2145
R_{int}	0.024	0.026	0.028
Parameters	193	246	237
Restraints	0	2	0
R_1 (obs.)	0.0030	0.030	0.029
wR_2 (all data)	0.070	0.079	0.077
S	1.09	1.06	1.06
Resd. dens. / e Å ⁻³	-0.41, 0.40	-0.40, 0.43	-0.39, 0.33
Solution	SIR2004	SIR2004	SIR2004
Refinement	SHELXL-97	SHELXL-97	SHELXL-97
Absorption correction	multi-scan	multi-scan	multi-scan
CCDC	969650	920473	920474

Additional X-ray illustrations

An exemplary illustration of a three-dimensional coordination polymer structure with anti-oriented dte units is given for compound **10** in Figure S3. The nitrate anions are placed in the voids which are formed by the Cu-dte-network.

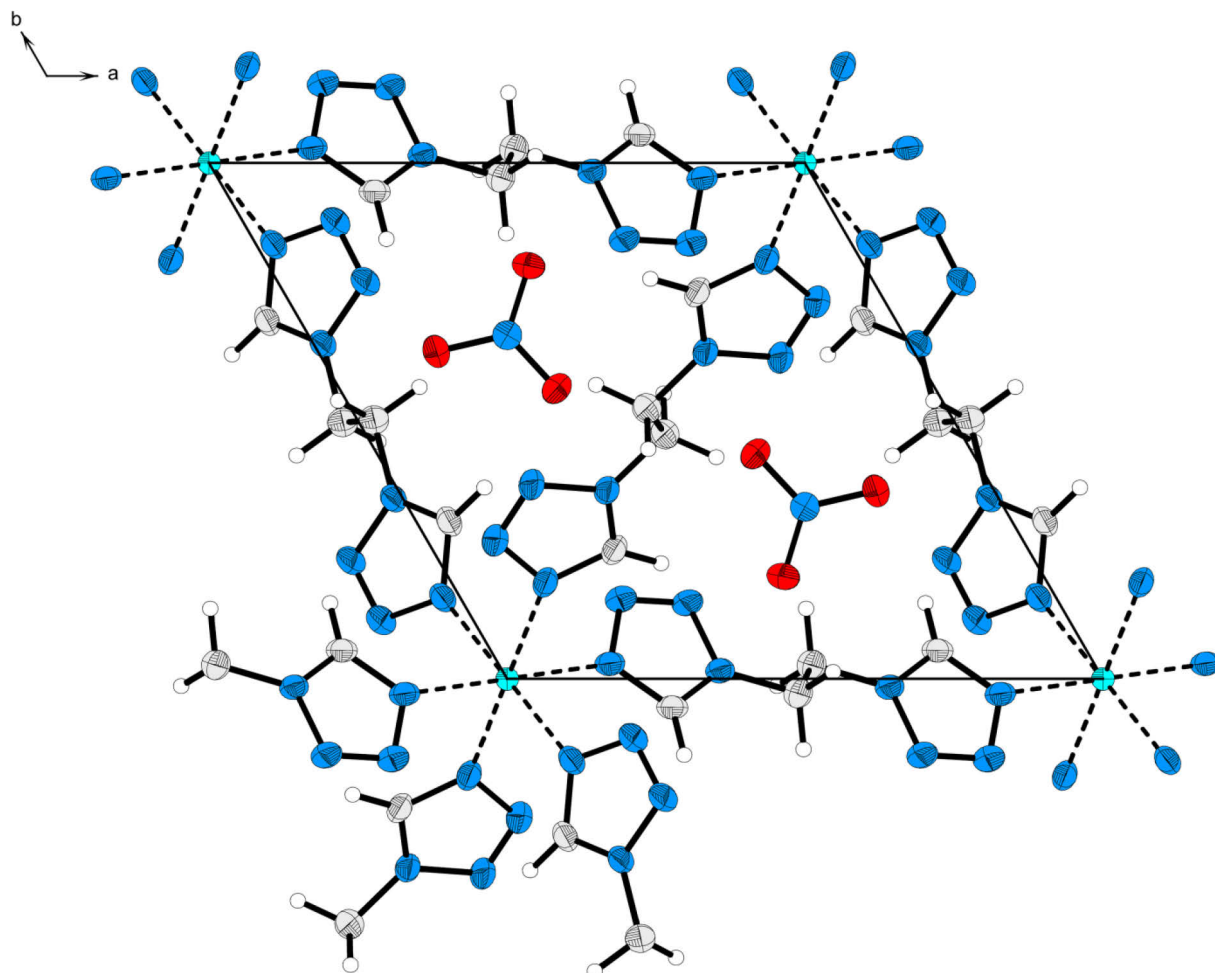


Figure S3. Unit cell of polynuclear complex **10** with view along the *c*-axis

An exemplary illustration of a three-dimensional coordination polymer structure with *gauche*- and *anti*-oriented dte units is given for compound **14** in Figure S4, S5 and S6.

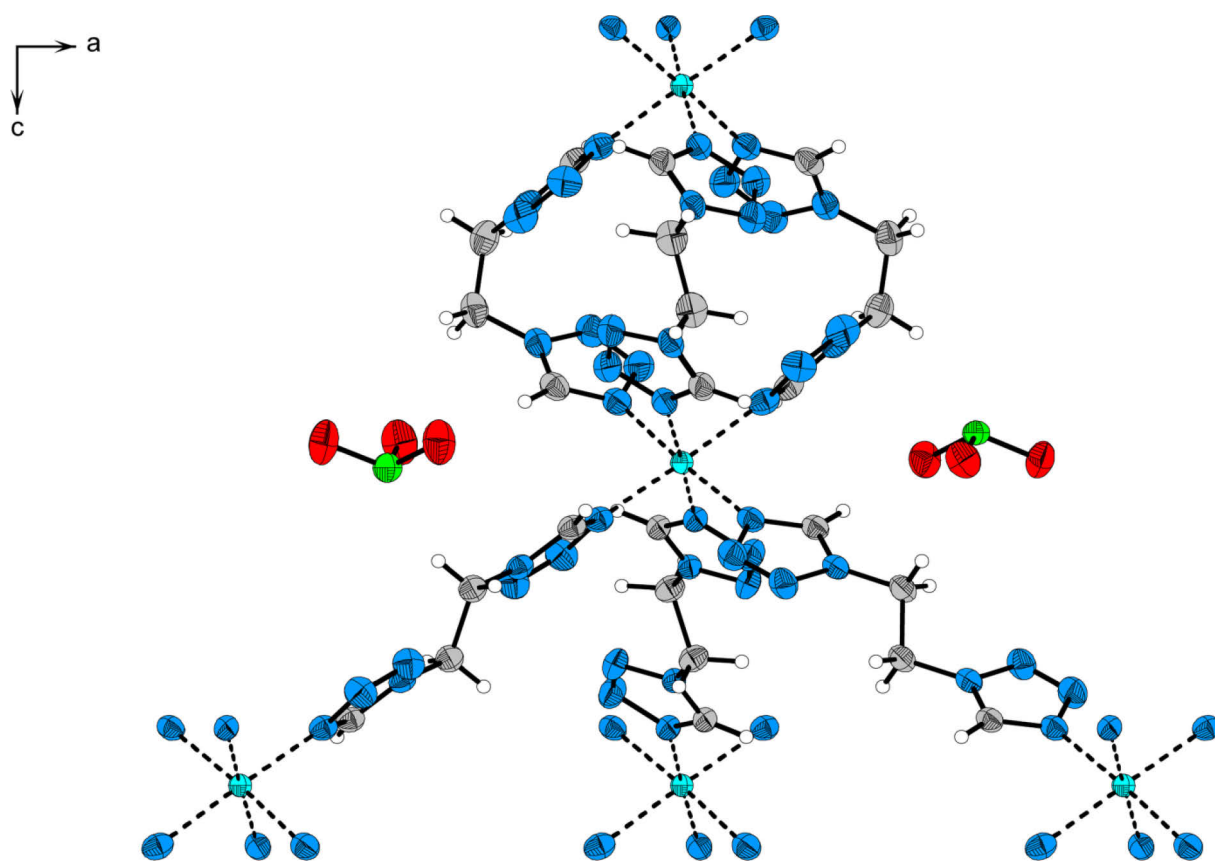


Figure S4. Cutout of the three-dimensional structure of **14** with view along the *b*-axis.

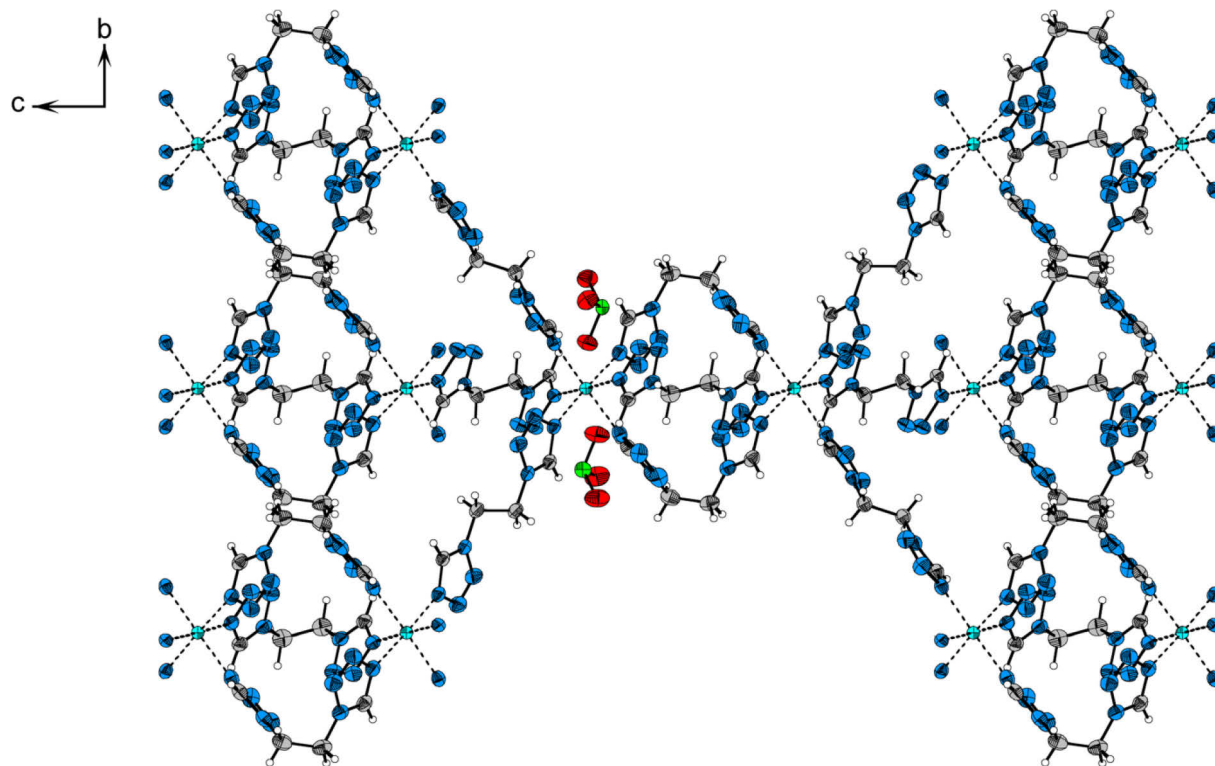


Figure S5. Cutout of the three-dimensional structure of **14** with view along the *a*-axis.

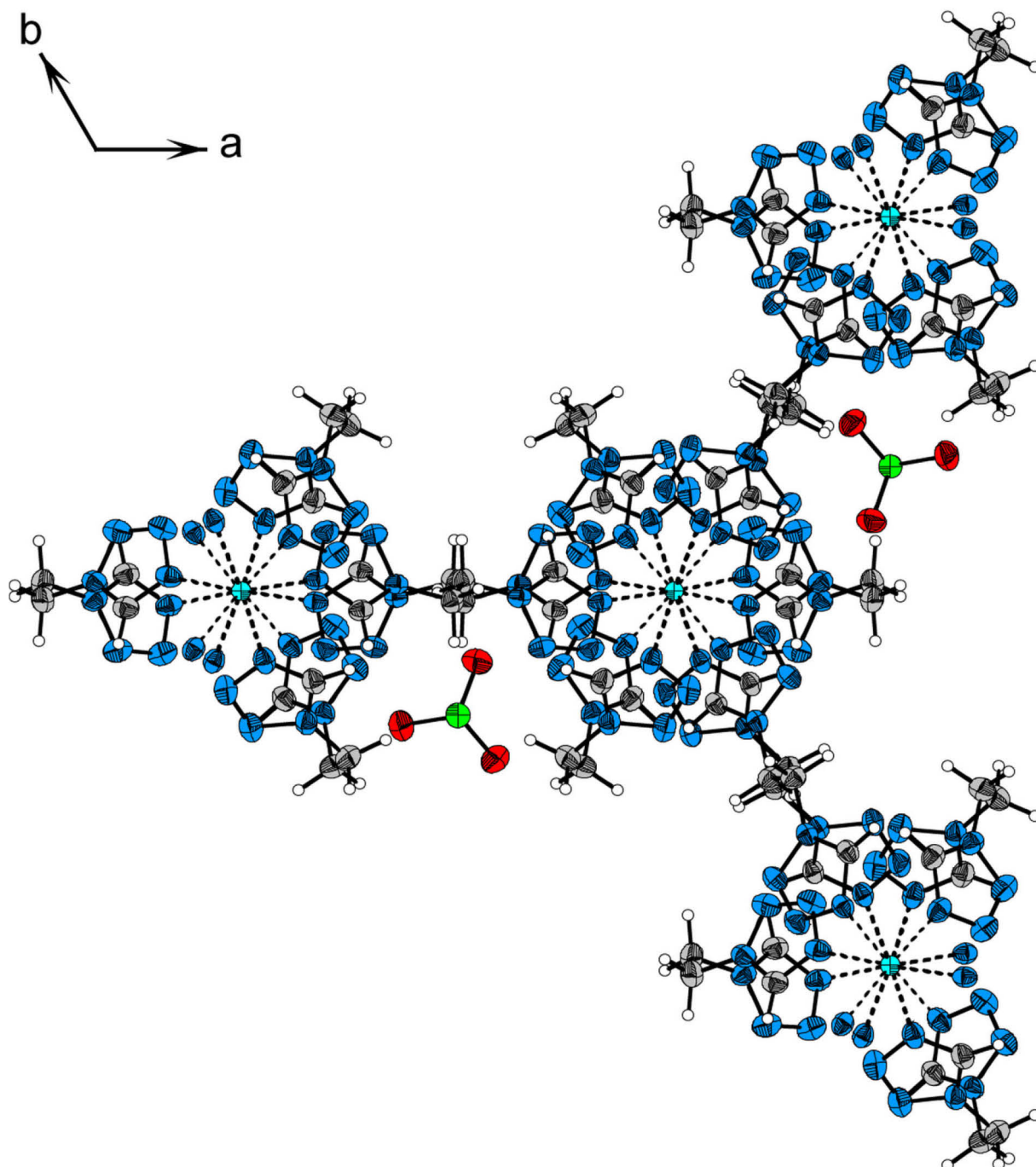


Figure S6. Cutout of the three-dimensional structure of **14** with view along the c -axis.

An exemplary illustration of a one-dimensional coordination polymer structure with anti-oriented dte units is given for compound **15** in Figure S7.

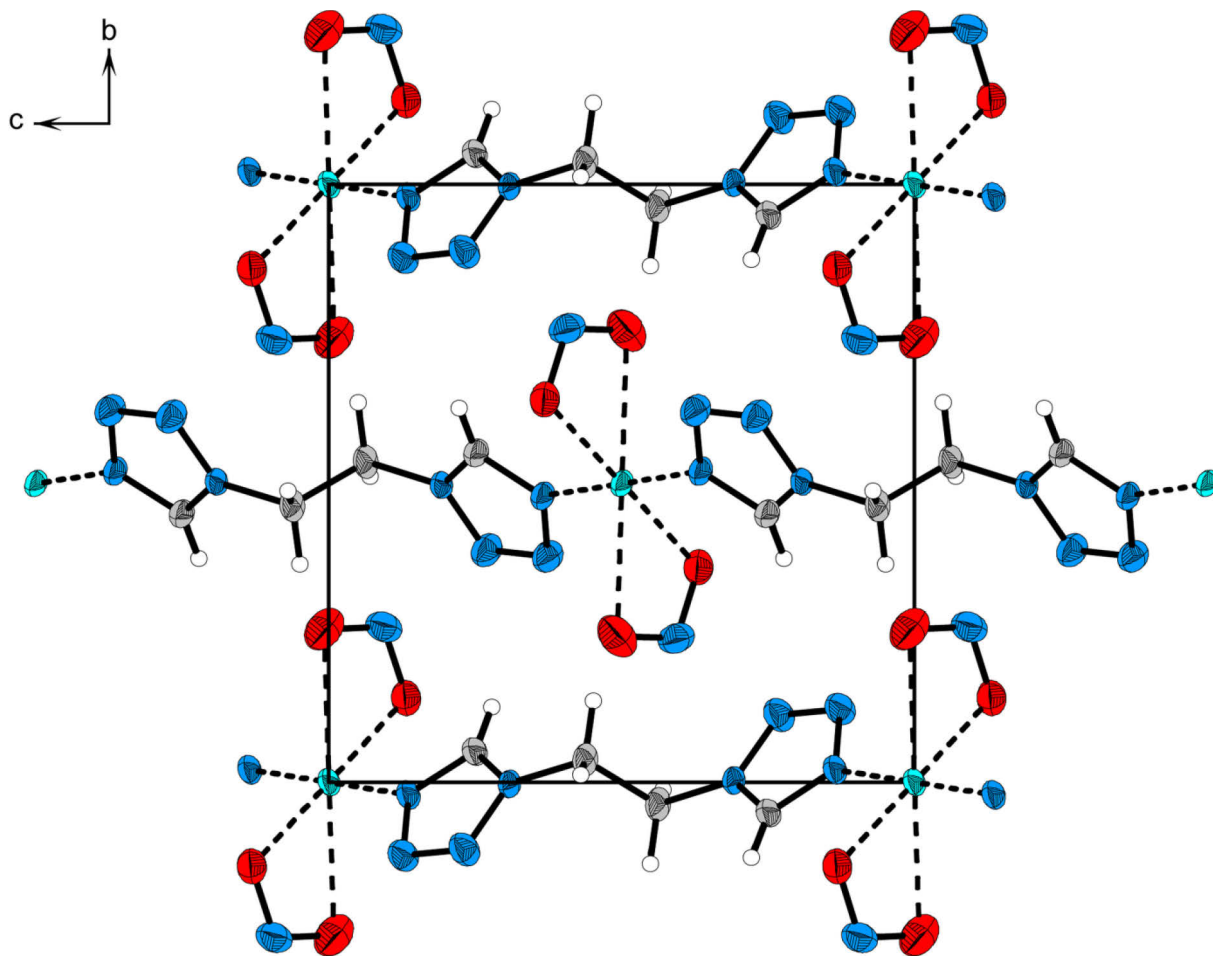


Figure S7. Unit cell of the one-dimensional coordination polymer **15** with view along the a -axis.

An exemplary illustration of a two-dimensional coordination polymer structure with *gauche*- and *anti*-oriented dte units is given for compound **16** in Figure S8.

An exemplary illustration of a one-dimensional coordination polymer structure with *gauche*-oriented dte units is given for compound **17** in Figure S9.

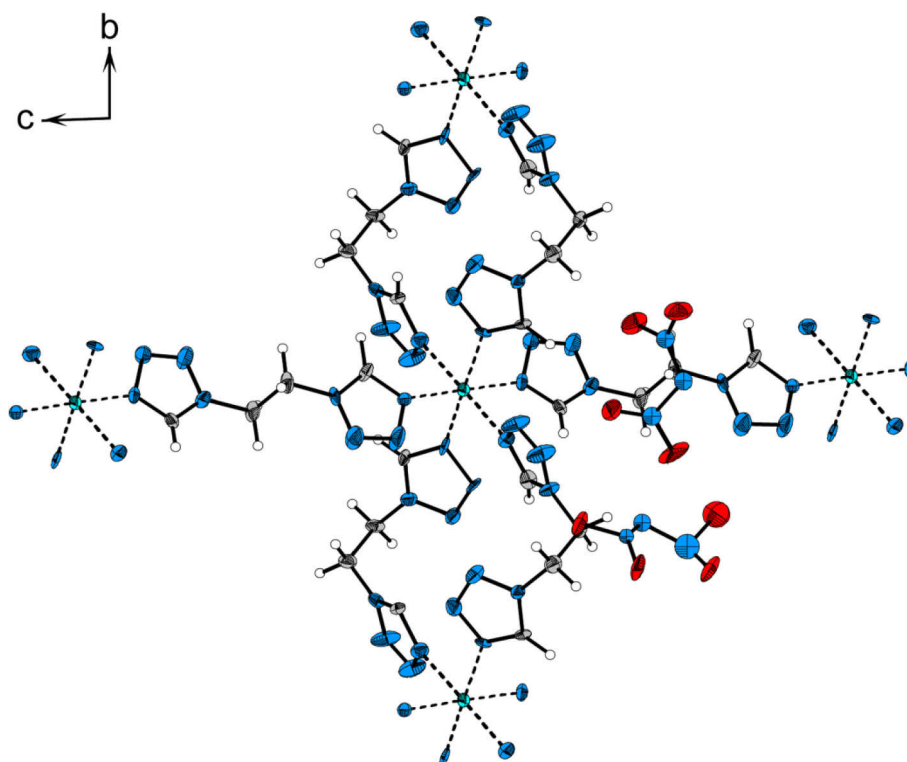


Figure S8. Unit cell of the two-dimensional coordination polymer **16** with view along the *a*-axis.

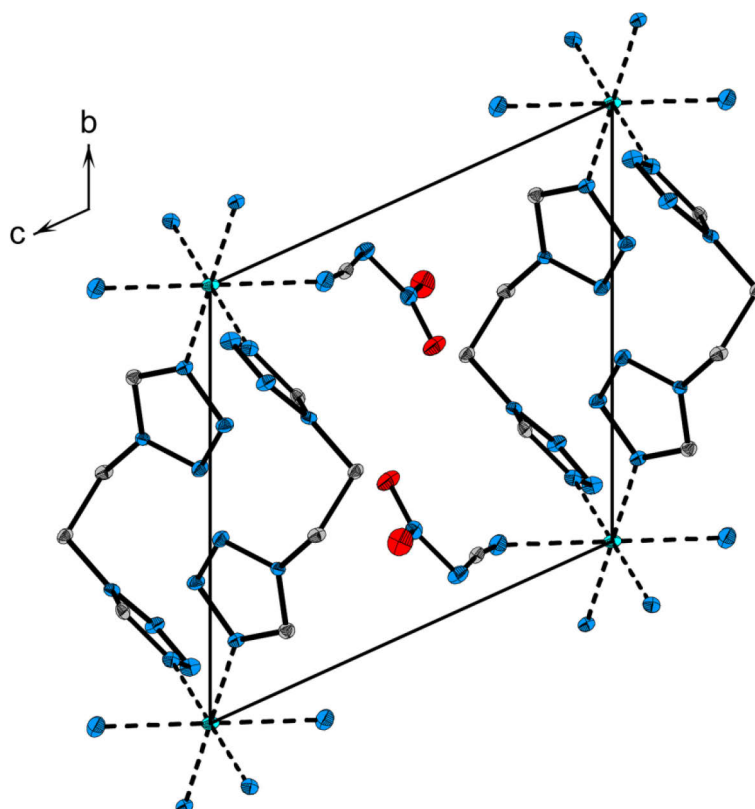


Figure S9. Unit cell of the one-dimensional coordination polymer **17** with view along the *a*-axis. Hydrogen atoms are omitted.

A4. Supporting Information Chapter 10

Laser Initiation of Tris(carbohydrazide)metal(II) Perchlorates and Bis(carbohydrazide)diperchloratocopper(II)

Table of Content

1. Experimental

Experimental

[Mg(CHZ)₃](ClO₄)₂ (1). Yield: 0.74 g (1.5 mmol, 75 %). DTA (5 °C min⁻¹) onset: 239 °C; IR (ATR): $\tilde{\nu}$ = 3405 (vw), 3392 (vw), 3353 (w), 3317 (w), 3307 (w), 3232 (w), 1645 (s), 1604 (w), 1546 (m), 1544 (m), 1446 (w), 1426 (w), 1326 (vw), 1306 (vw), 1208 (w), 1192 (w), 1150 (w), 1066 (vs), 1009 (m), 962 (m), 935 (m), 908 (m), 761 (m), 695 (w) cm⁻¹; elemental analysis for C₃H₁₈Cl₂MgN₁₂O₁₁ (493.46 g mol⁻¹): calcd. C 7.30, H 3.68, N 34.06 %; found C 7.64, H 3.65, N 33.62 %; BAM impact: 2.5 J; BAM friction: 60 N; ESD: 0.200 J (at grain size < 100 μm).

[Mn(CHZ)₃](ClO₄)₂ (2). Yield: 0.63 g (1.2 mmol, 60 %). DTA (5 °C min⁻¹) onset: 263 °C; IR (ATR): $\tilde{\nu}$ = 3391 (vw), 3348 (w), 3324 (w), 3308 (w), 3235 (w), 1645 (s), 1596 (m), 1576 (w), 1541 (m), 1538 (m), 1445 (w), 1425 (w), 1328 (vw), 1303 (vw), 1207 (w), 1190 (w), 1146 (m), 1062 (vs), 1012 (m), 992 (m), 960 (m), 933 (w), 907 (w), 758 (m), 692 (w) cm⁻¹; elemental analysis for C₃H₁₈Cl₂MnN₁₂O₁₁ (524.09 g mol⁻¹): calcd. C 6.88, H 3.46, N 32.07 %; found C 7.19, H 3.37, N 30.58 %; BAM impact: 2 J; BAM friction: 24 N; ESD: 0.500 J (at grain size < 100 μm).

[Co(CHZ)₃](ClO₄)₂ (3). Yield: 0.79 g (1.5 mmol, 75 %). DTA (5 °C min⁻¹) onset: 243 °C; IR (ATR): $\tilde{\nu}$ = 3389 (vw), 3350 (w), 3327 (w), 3299 (w), 3228 (w), 1645 (s), 1595 (w), 1541 (m), 1444 (w), 1423 (w), 1210 (w), 1191 (w), 1149 (w), 1066 (vs), 963 (m), 934 (w), 909 (w), 757 (m), 695 (w), 668 (w) cm⁻¹; elemental analysis for C₃H₁₈Cl₂CoN₁₂O₁₁ (528.09 g mol⁻¹): calcd. C 6.82, H 3.44, N 31.83 %; found C 6.65, H 3.72, N 31.64 %; BAM impact: 1 J; BAM friction: ≤ 5 N; ESD: 0.035 J (at grain size < 100 μm).

[Ni(CHZ)₃](ClO₄)₂ (4). Yield: 0.82 g (1.6 mmol, 78 %). DTA (5 °C min⁻¹) onset: 273 °C; IR (ATR): $\tilde{\nu}$ = 3405 (vw), 3389 (w), 3366 (w), 3344 (w), 3328 (w), 3308 (m), 3232 (w), 1645 (s), 1600 (m), 1544 (m), 1444 (w), 1425 (w), 1211 (w), 1195 (w), 1151 (w), 1065 (vs), 1021 (m), 963 (w), 934 (w), 909 (w), 756 (m), 700 (vw) cm⁻¹; elemental analysis for C₃H₁₈Cl₂NiN₁₂O₁₁ (527.85 g mol⁻¹): calcd. C 6.83, H 3.44, N 31.84 %; found C 7.08, H 3.34, N 31.43 %; BAM impact: 1 J; BAM friction: ≤ 5 N; ESD: 0.300 J (at grain size < 100 μm).

[Zn(CHZ)₃](ClO₄)₂ (5). Yield: 0.80 g (1.5 mmol, 75 %). DTA (5 °C min⁻¹) onset: 268 °C; IR (ATR): $\tilde{\nu}$ = 3389 (vw), 3350 (w), 3329 (w), 3304 (w), 3225 (w), 1645 (s), 1602 (w), 1541

(m), 1538 (m), 1447 (w), 1426 (w), 1210 (w), 1192 (w), 1147 (w), 1067 (vs), 963 (w), 934 (w), 915 (w), 759 (m), 697 (vw) cm^{-1} ; elemental analysis for $\text{C}_3\text{H}_{18}\text{Cl}_2\text{N}_{12}\text{O}_{11}\text{Zn}$ ($534.53 \text{ g mol}^{-1}$): calcd. C 6.74, H 3.39, N 31.44 %; found C 6.66, H 3.50, N 31.57 %; BAM impact: 1.5 J; BAM friction: 20 N; ESD: 0.700 J (at grain size $< 100 \mu\text{m}$).

[Cu(ClO₄)₂(CHZ)₂] (6). Yield: 0.55 g (1.2 mmol, 62 %). DTA ($5 \text{ }^\circ\text{C min}^{-1}$) onset: $186 \text{ }^\circ\text{C}$; IR (ATR): $\tilde{\nu} = 3368$ (w), 3303 (w), 3263 (w), 3187 (w), 1671 (w), 1635 (m), 1616 (m), 1573 (w), 1503 (m), 1447 (vw), 1402 (vw), 1367 (w), 1249 (w), 1185 (w), 1075 (vs), 1061 (vs), 932 (w), 749 (w) cm^{-1} ; elemental analysis for $\text{C}_2\text{H}_{12}\text{Cl}_2\text{CuN}_8\text{O}_{10}$ ($442.62 \text{ g mol}^{-1}$): calcd. C 5.43, H 2.73, N 25.32 %; found C 5.80, H 2.27, N 23.19 %; BAM impact: 3 J; BAM friction: $< 5 \text{ N}$; ESD: 0.020 J (at grain size $< 100 \mu\text{m}$).

A5. Supporting Information Chapter 11

Cocrystallization of Photosensitive Energetic Copper(II) Perchlorate Complexes with the Nitrogen-rich Ligand 1,2-Di(1H-tetrazol-5-yl)ethane

Table of Content

1. X-ray Diffraction
2. Powder Diffraction
3. Infrared Spectroscopy

X-ray Diffraction

	2	3	4	6
Formula	C ₃₂ H ₅₆ Cl ₈ Cu ₄ N ₆₄ O ₃₆	C ₈ H ₁₆ Cl ₂ CuN ₁₆ O ₁₂	C ₈ H ₁₂ CuN ₁₈ O ₆	C ₁₂ H ₂₄ Cl ₂ CuN ₁₆ O ₁₀
$M_r / \text{g mol}^{-1}$	2451.17	666.84	519.90	686.91
Color	intense blue	violet	blue	blue
Habit	needle	block	block	block
Crystal size / mm	0.28 × 0.20 × 0.14	0.30 × 0.28 × 0.28	0.47 × 0.28 × 0.14	0.39 × 0.32 × 0.19
Crystal system	triclinic	orthorhombic	triclinic	monoclinic
Space group	$P\bar{1}$	$Pbc2_1$	$P\bar{1}$	$P2_1/c$
$a / \text{Å}$	8.2764(4)	6.7273(1)	7.5458(6)	7.6396(3)
$b / \text{Å}$	13.5187(8)	21.9914(4)	7.8676(9)	15.2017(5)
$c / \text{Å}$	19.4324(11)	15.9205(3)	8.7089(9)	11.2882(5)
$\alpha / ^\circ$	81.570(5)	90	65.66(1)	90
$\beta / ^\circ$	83.197(4)	90	73.373(8)	103.540(4)
$\gamma / ^\circ$	86.156(4)	90	73.506(9)	90
$V / \text{Å}^3$	2132.9(2)	2355.32(7)	443.14(8)	1274.52(9)
Z	1	4	1	2
$\rho_{\text{calc.}} / \text{g cm}^{-3}$	1.908	1.881	1.948	1.790
T / K	173	173	100	100
$\lambda (\text{Mo-K}\alpha) / \text{Å}$	0.71073	0.71073	0.71073	0.71073
$F(000)$	1236	1356	263	702
μ / mm^{-1}	1.36	1.25	1.32	1.15
θ range / °	4.2–26.4	4.3–26.4	4.2–27.9	4.3–27.5
Dataset ($h; k; l$)	$-10 \leq h \leq 8$ $-15 \leq k \leq 16$ $-23 \leq l \leq 24$	$-8 \leq h \leq 8$ $-27 \leq k \leq 27$ $-19 \leq l \leq 19$	$-9 \leq h \leq 9$ $-10 \leq k \leq 10$ $-11 \leq l \leq 11$	$-9 \leq h \leq 9$ $-14 \leq k \leq 19$ $-14 \leq l \leq 12$
Measured reflections	11499	33668	7417	10966
Independent reflections	8625	4785	2102	2910
Observed reflections	6895	4627	1858	2591
R_{int}	0.026	0.032	0.043	0.028
Parameters	696	382	175	281
Restraints	0	11	0	0
R_1 (obs.)	0.050	0.046	0.029	0.027
wR_2 (all data)	0.124	0.117	0.067	0.070
S	1.05	1.08	1.07	1.05
Resd. dens. / e Å ⁻³	-0.83, 0.92	-0.41; 3.80	-0.45; 0.35	-0.39; 0.40
Solution	SIR2004	SIR97	SIR2004	SIR97
Refinement	SHELXL-97	SHELXL-97	SHELXL-97	SHELXL-97
Absorption correction	multi-scan	multi-scan	multi-scan	multi-scan
CCDC	1005245	1012873	1005244	1005246

Powder Diffraction

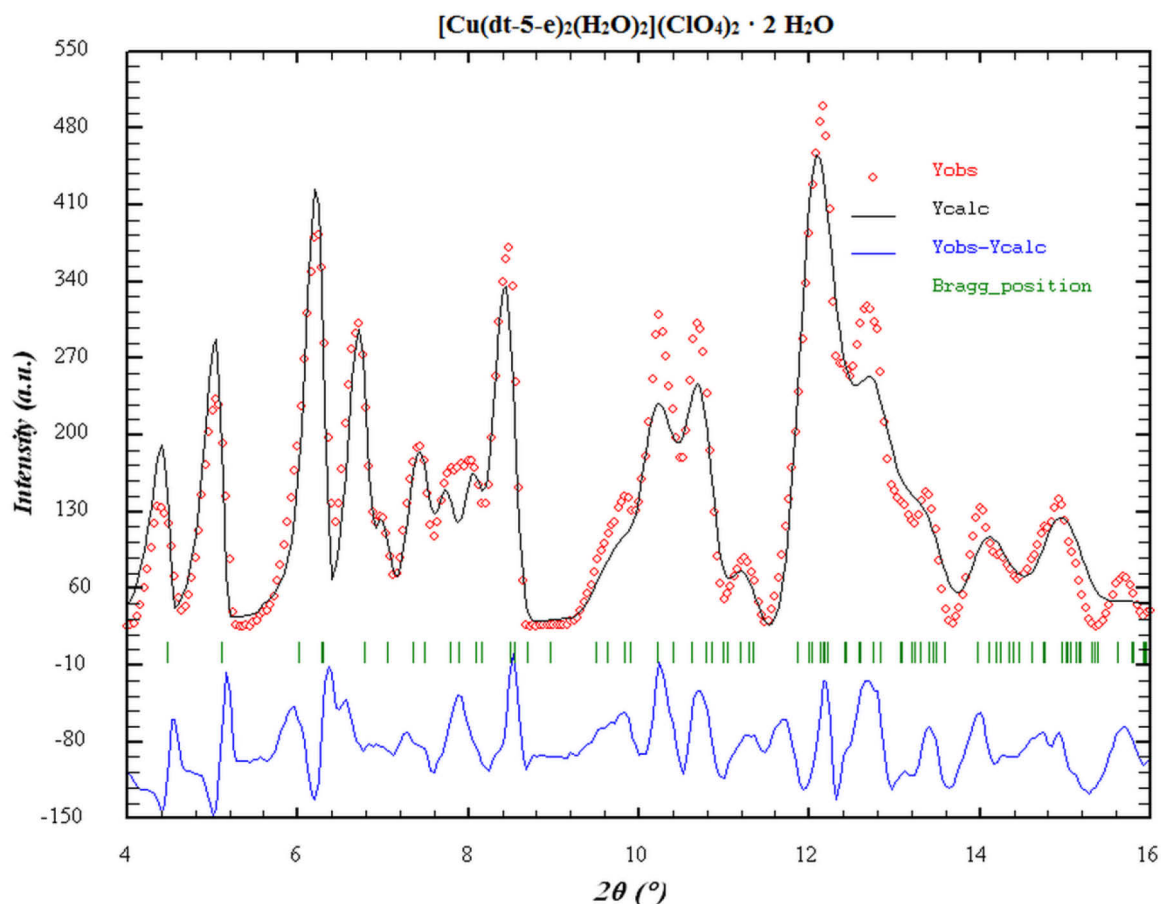


Figure S1. Rietveld plot of complex **3** ($R = 0.15$, $R_{wp} = 0.20$) obtained with MoK_{α1} radiation at room temperature (space group $Pbc2_1$, 59 crystallographic independent atoms). Powder diffraction was performed with a sample of the same batch from which a single crystal for X-ray diffraction was taken. For the Rietveld analysis, the lattice and the positional parameters of the single crystal of **3** were used. Both diffractograms show similar diffraction patterns. Compound **3** is stable under heating up to 50 °C for 2 h.

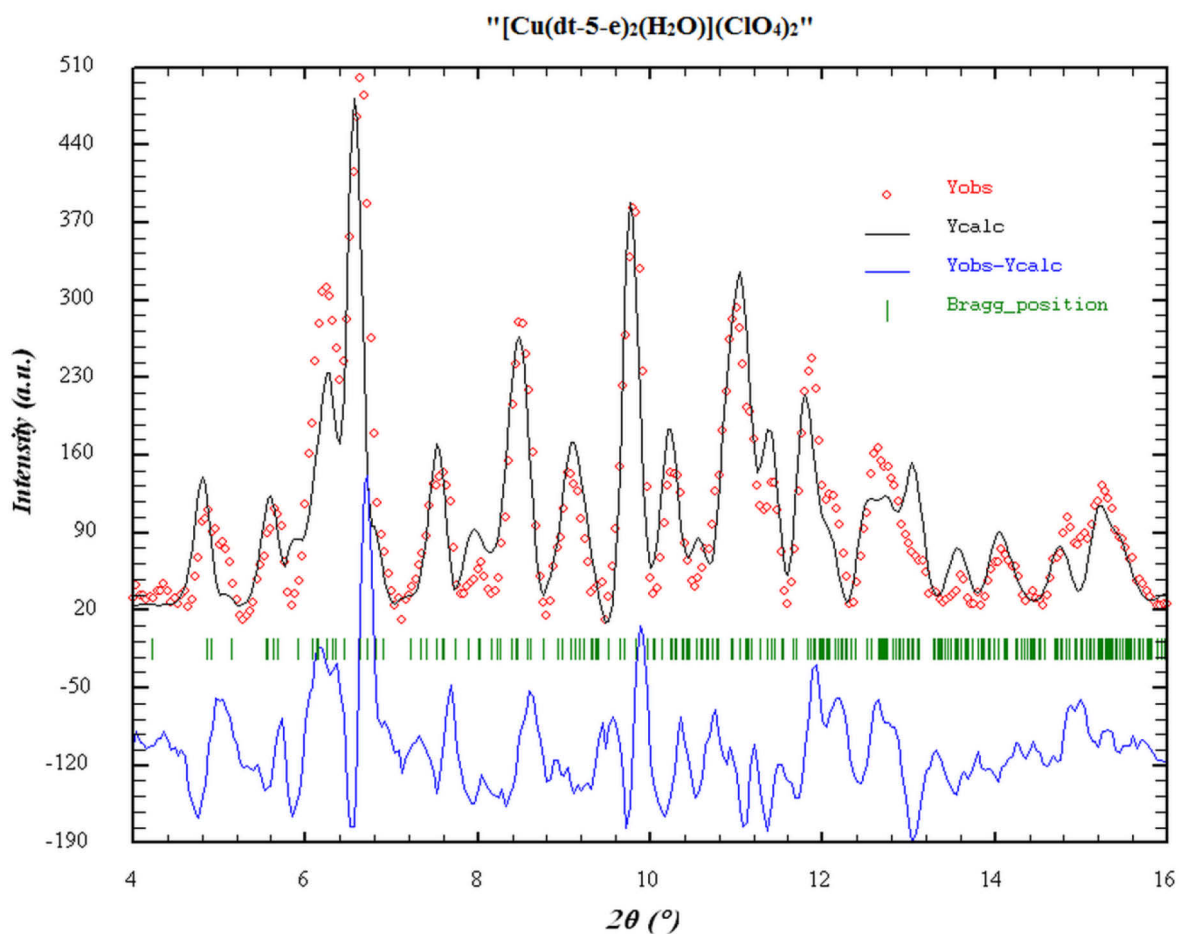


Figure S2. Rietveld plot of complex **2** ($R = 0.28$, $R_{wp} = 0.36$) with MoK_{α1} radiation at room temperature (space group $P\bar{1}$, 106 crystallographic independent atoms). Compound **2** was obtained by drying **3** at 70 °C for two hours and was used for the powder diffraction. For the Rietveld analysis the lattice and the positional parameters of the single crystal of **2**, which was obtained from the mother liquor, were used. Both diffractograms show similar diffraction patterns. The complete transition of compound **3** to **2** is obtained by heating to 70 °C for 2 h.

Infrared Spectroscopy

Infrared spectra were recorded for all samples. The IR spectra of compounds **1**, **4** and **5** are shown in Figure S3 and compounds **2**, **3** and **6** in Figure S4.

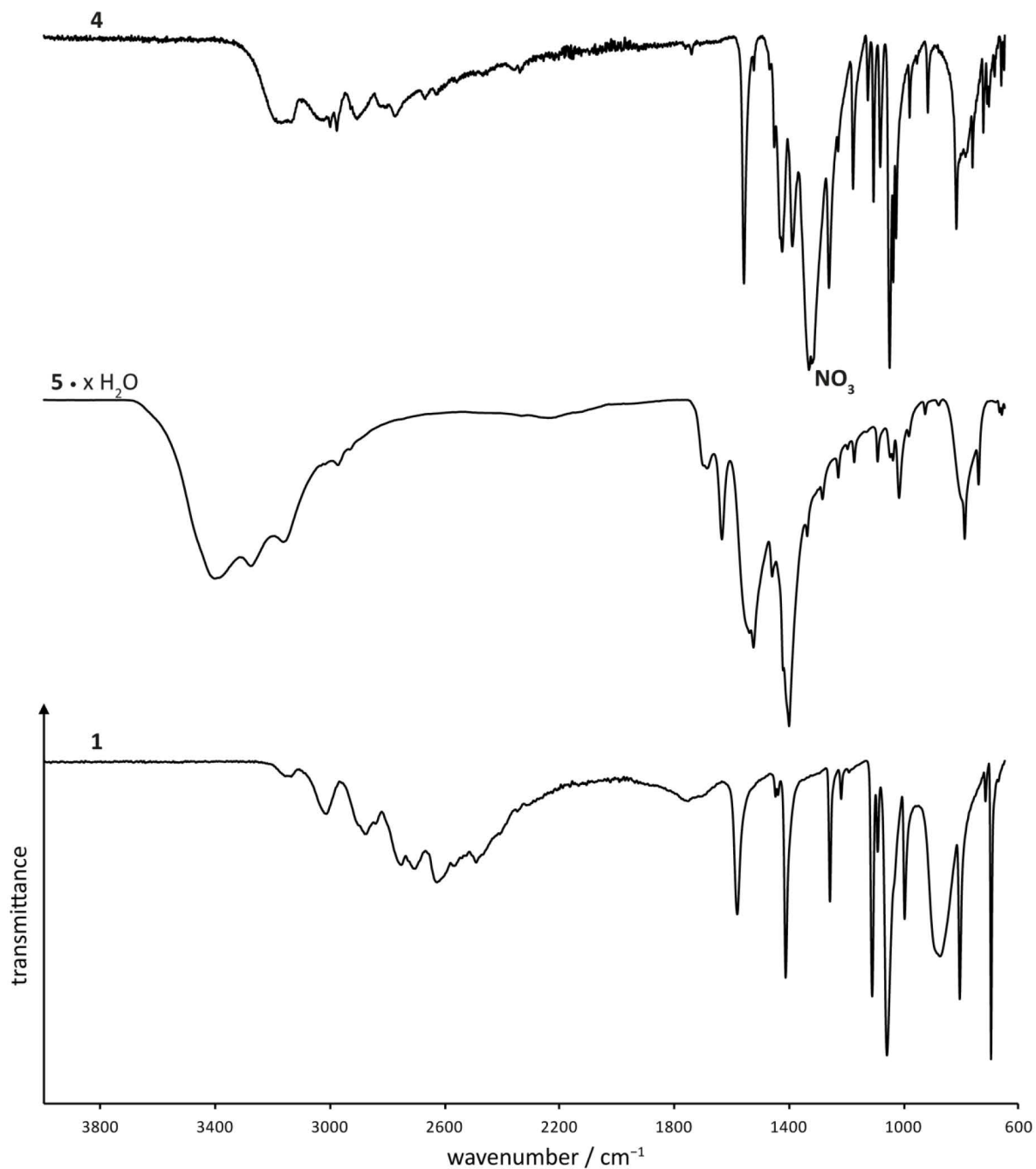


Figure S3. IR spectra of **1**, **4** and **5**.

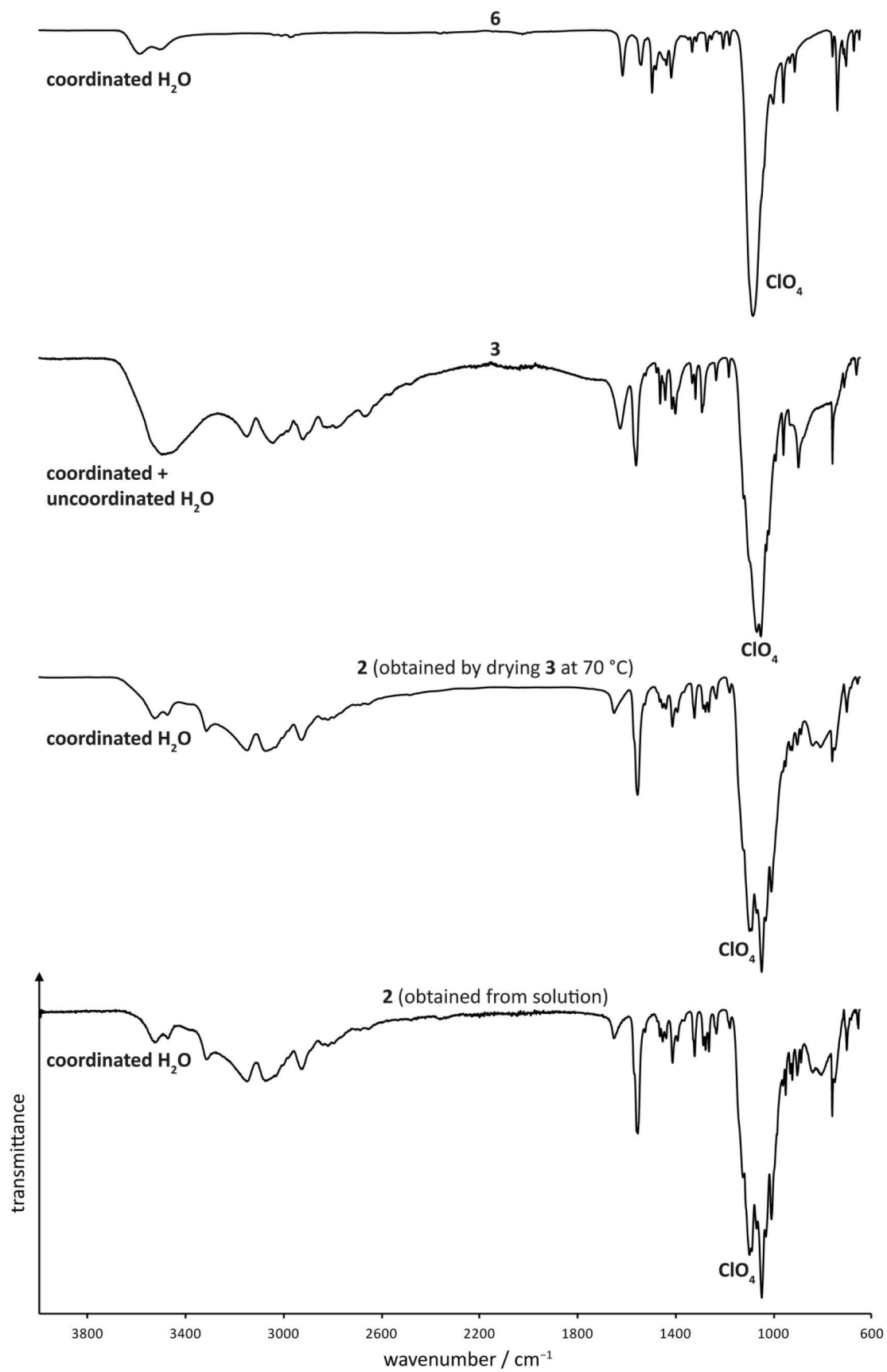


Figure S4. IR spectra of 2, 3 and 6.

A6. Experimental Data of Unpublished Compounds

Experimental

General Methods. To a hot solution of the alkyl-bridged ditetrazole (**dtp**: 0.72 g, 4.00 mmol; **dtb**: 0.78 g, 4.00 mmol) in ethanol (25 mL) was added a concentrated aqueous solution the corresponding metal(II) perchlorate (2.2 mmol, Fe(ClO₄)₂ · x H₂O: 0.56; Co(ClO₄)₂ · 6 H₂O: 0.81; Ni(ClO₄)₂ · 6 H₂O: 0.80 g; Zn(ClO₄)₂ · 6 H₂O: 0.82) under stirring. In case of Fe(ClO₄)₂ · x H₂O, ascorbic acid (0.18 g, 1.00 mmol) was added. The solution was slowly cooled down to room temperature under stirring. The products precipitated within an hour as fine powders which were filtered off, washed with a small amount ethanol and dried under ambient conditions.

{[Fe(dtp)₃](ClO₄)₂]_n}: Yield: 0.76 g (0.96 mmol, 72 %). Color: slightly yellow. DTA (5 °C min⁻¹) onset: 233 °C (decomp.); IR (ATR): $\tilde{\nu}$ = 3131 (vw), 3004 (vw), 1492 (w), 1455 (w), 1449 (w), 1434 (w), 1394 (vw), 1366 (vw), 1350 (vw), 1314 (vw), 1308 (vw), 1274 (vw), 1184 (w), 1091 (vs), 1079 (vs), 1030 (w), 1018 (w), 989 (m), 931 (w), 920 (w), 885 (w), 752 (vw), 717 (vw), 677 (m), 659 cm⁻¹ (m); elemental analysis calcd. (%) for C₁₅H₂₄Cl₂FeN₂₄O₈ (795.26 g mol⁻¹): C 22.65, H 3.04, N 42.27; found: C 22.92, H 2.98, N 41.45; BAM impact: 1 J; BAM friction 40 N (at grain size < 100 μm).

{[Co(dtp)₃](ClO₄)₂]_n}: Yield: 0.91 g (1.14 mmol, 85 %). Color: orange. DTA (5 °C min⁻¹) onset: 284 °C (decomp.); IR (ATR): $\tilde{\nu}$ = 3131 (vw), 3010 (vw), 2986 (vw), 2972 (vw), 1496 (w), 1455 (w), 1437 (vw), 1396 (vw), 1367 (vw), 1348 (vw), 1313 (vw), 1276 (vw), 1185 (w), 1091 (vs), 1081 (vs), 1034 (w), 993 (w), 922 (w), 887 (w), 753 (vw), 718 (vw), 677 (w), 661 cm⁻¹ (w); elemental analysis calcd. (%) for C₁₅H₂₄Cl₂CoN₂₄O₈ (798.35 g mol⁻¹): C 22.57, H 3.03, N 42.11; found: C 22.93, H 3.09, N 42.17; BAM impact: 1 J; BAM friction 18 N; ESD: 0.30 J (at grain size < 100 μm).

{[Ni(dtp)₃](ClO₄)₂]_n}: Yield: 0.96 g (1.20 mmol, 90 %). Color: violet. DTA (5 °C min⁻¹) onset: 283 °C (decomp.); IR (ATR): $\tilde{\nu}$ = 3133 (vw), 3016 (vw), 3005 (vw), 2976 (vw), 1498 (w), 1451 (w), 1437 (vw), 1397 (vw), 1368 (vw), 1347 (vw), 1314 (vw), 1276 (vw), 1186 (w), 1092 (vs), 1082 (vs), 996 (w), 929 (w), 921 (w), 886 (w), 753 (vw), 719 (vw), 678 (w), 661 cm⁻¹ (w); elemental analysis calcd. (%) for C₁₅H₂₄Cl₂N₂₄NiO₈ (798.11 g mol⁻¹): C 22.57, H 3.03, N 42.12; found: C 22.99, H 3.11, N 42.33; BAM impact: 1 J; BAM friction 40 N; ESD: 0.30 J (at grain size < 100 μm).

{[Zn(dtp)₃](ClO₄)₂]_n}: Yield: 0.96 g (1.19 mmol, 89 %). Color: colorless. DTA (5 °C min⁻¹) onset: 256 °C (decomp.); IR (ATR): $\tilde{\nu}$ = 3129 (vw), 3007 (vw), 1784 (vw), 1494 (w), 1455 (w), 1449 (w), 1436 (w), 1395 (vw), 1374 (vw), 1366 (vw), 1353 (vw), 1312 (vw), 1275 (vw), 1185 (w), 1091 (vs), 1080 (vs), 1031 (w), 992 (m), 931 (w), 921 (w), 889 (w), 751 (vw), 717

(vw), 677 (m), 660 cm^{-1} (m); elemental analysis calcd. (%) for $\text{C}_{15}\text{H}_{24}\text{Cl}_2\text{N}_{24}\text{O}_8\text{Zn}$ ($804.79 \text{ g mol}^{-1}$): C 22.39, H 3.01, N 41.77; found: C 22.54, H 2.98, N 41.64; BAM impact: 7 J; BAM friction 80 N; ESD: 0.70 J (at grain size $< 100 \mu\text{m}$).

$\{\{\text{Fe}(\text{dtb})_3\}(\text{ClO}_4)_2\}_n$: Yield: 0.78 g (0.93 mmol, 70 %). Color: slightly yellow. DTA ($5 \text{ }^\circ\text{C min}^{-1}$) onset: $216 \text{ }^\circ\text{C}$ (decomp.); IR (ATR): $\tilde{\nu} = 3134$ (w), 2975 (vw), 2955 (vw), 2940 (vw), 2874 (vw), 1505 (w), 1468 (w), 1451 (w), 1439 (w), 1381 (vw), 1367 (vw), 1323 (vw), 1299 (vw), 1268 (vw), 1237 (vw), 1206 (vw), 1181 (w), 1134 (w), 1089 (vs), 1022 (w), 1013 (w), 995 (m), 913 (vw), 892 (w), 790 (w), 752 (w), 740 (vw), 718 (w), 676 (w), 662 cm^{-1} (w); elemental analysis calcd. (%) for $\text{C}_{18}\text{H}_{30}\text{Cl}_2\text{FeN}_{24}\text{O}_8$ ($837.34 \text{ g mol}^{-1}$): C 25.82, H 3.61, N 40.15; found: C 26.09, H 3.68, N 39.23; BAM impact: 1 J; BAM friction 80 N (at grain size $< 100 \mu\text{m}$).

$\{\{\text{Co}(\text{dtb})_3\}(\text{ClO}_4)_2\}_n$: Yield: 0.91 g (1.08 mmol, 81 %). Color: orange. DTA ($5 \text{ }^\circ\text{C min}^{-1}$) onset: $261 \text{ }^\circ\text{C}$ (decomp.); IR (ATR): $\tilde{\nu} = 3137$ (w), 2957 (vw), 2931 (vw), 2873 (vw), 1505 (w), 1468 (w), 1445 (w), 1381 (vw), 1367 (vw), 1326 (vw), 1300 (vw), 1267 (vw), 1244 (vw), 1208 (vw), 1181 (w), 1134 (w), 1087 (vs), 1024 (w), 998 (w), 935 (vw), 913 (vw), 894 (w), 892 (w), 791 (w), 773 (vw), 753 (w), 741 (vw), 739 (vw), 718 (w), 676 (w), 663 cm^{-1} (w); elemental analysis calcd. (%) for $\text{C}_{18}\text{H}_{30}\text{Cl}_2\text{CoN}_{24}\text{O}_8$ ($840.43 \text{ g mol}^{-1}$): C 25.72, H 3.60, N 40.00; found: C 26.12, H 3.77, N 38.85; BAM impact: 4 J; BAM friction 128 N (at grain size $< 100 \mu\text{m}$).

$\{\{\text{Ni}(\text{dtb})_3\}(\text{ClO}_4)_2\}_n$: Yield: 1.00 g (1.19 mmol, 89 %). Color: violet. DTA ($5 \text{ }^\circ\text{C min}^{-1}$) onset: $283 \text{ }^\circ\text{C}$ (decomp.); IR (ATR): $\tilde{\nu} = 3140$ (w), 2957 (vw), 2946 (vw), 2876 (vw), 1507 (w), 1467 (w), 1444 (w), 1381 (vw), 1367 (vw), 1324 (vw), 1300 (vw), 1268 (vw), 1245 (vw), 1206 (vw), 1182 (w), 1135 (w), 1086 (vs), 1003 (w), 934 (vw), 914 (vw), 890 (w), 791 (w), 777 (vw), 753 (w), 740 (vw), 719 (w), 676 (vw), 664 cm^{-1} (w); elemental analysis calcd. (%) for $\text{C}_{18}\text{H}_{30}\text{Cl}_2\text{N}_{24}\text{NiO}_8$ ($840.19 \text{ g mol}^{-1}$): C 25.73, H 3.60, N 40.01; found: C 25.85, H 3.71, N 38.82; BAM impact: 8 J; BAM friction 120 N (at grain size $< 100 \mu\text{m}$).

$\{\{\text{Zn}(\text{dtb})_3\}(\text{ClO}_4)_2\}_n$: Yield: 0.86 g (1.01 mmol, 76 %). Color: colorless. DTA ($5 \text{ }^\circ\text{C min}^{-1}$) onset: $228 \text{ }^\circ\text{C}$ (decomp.); IR (ATR): $\tilde{\nu} = 3136$ (w), 2973 (vw), 2955 (vw), 2941 (vw), 2876 (vw), 1506 (w), 1468 (w), 1441 (w), 1382 (vw), 1368 (vw), 1327 (vw), 1299 (vw), 1268 (vw), 1236 (vw), 1206 (vw), 1181 (w), 1135 (w), 1088 (vs), 1014 (w), 998 (m), 914 (vw), 893 (w), 790 (w), 752 (w), 740 (vw), 718 (w), 676 (vw), 662 cm^{-1} (w); elemental analysis calcd. (%) for $\text{C}_{18}\text{H}_{30}\text{Cl}_2\text{N}_{24}\text{O}_8\text{Zn}$ ($846.87 \text{ g mol}^{-1}$): C 25.53, H 3.57, N 39.69; found: C 25.98, H 3.63, N 39.60; BAM impact: 5 J; BAM friction 288 N (at grain size $< 100 \mu\text{m}$).

A7. Unpublished Results of Laser Initiation Experiments

Laser Initiation

Table S1. Laser initiation of the $\{[M(\text{dte})_3](\text{ClO}_4)_2\}_n$ complexes with 2.5 % PTFE as binder.

Metal cation	Fe ²⁺	Co ²⁺	Ni ²⁺	Cu ²⁺	Zn ²⁺
T_{decomp} (onset) [°C]	240	288	298	256	280
IS [J]	2	1	1	1.5	2
FS [N]	14	6	6	10	42
Laser initiation ^[a]	1	1	1	1	4

[a] Parameters of the laser beam: $\lambda = 940$ nm, $\tau = 600$ μs , $\sigma = 105$ μm , $\Phi_e = 12.5$ W. Results of irradiation with diode laser light: 1: detonation; 2: deflagration; 3: combustion or fragmentary decomposition; 4: no ignition.

Table S2. Laser initiation of the $\{[M(\text{dtp})_3](\text{ClO}_4)_2\}_n$ complexes with 2.5 % PTFE as binder.

Metal cation	Fe ²⁺	Co ²⁺	Ni ²⁺	Cu ²⁺	Zn ²⁺
T_{decomp} (onset) [°C]	233	284	283	235	256
IS [J]	1	1	1	4	2
FS [N]	40	18	40	10	72
Laser initiation ^[a]	1	1	1	1	4

[a] Parameters of the laser beam: $\lambda = 940$ nm, $\tau = 600$ μs , $\sigma = 105$ μm , $\Phi_e = 12.5$ W. Results of irradiation with diode laser light: 1: detonation; 2: deflagration; 3: combustion or fragmentary decomposition; 4: no ignition.

Table S3. Laser initiation of the $\{[M(\text{dtb})_3](\text{ClO}_4)_2\}_n$ complexes with 2.5 % PTFE as binder.

Metal cation	Fe ²⁺	Co ²⁺	Ni ²⁺	Cu ²⁺	Zn ²⁺
T_{decomp} (onset) [°C]	216	261	283	230	228
IS [J]	1	4	8	12.5	5
FS [N]	80	128	120	120	288
Laser initiation ^[a]	2	4	4	3	4

[a] Parameters of the laser beam: $\lambda = 940$ nm, $\tau = 600$ μs , $\sigma = 105$ μm , $\Phi_e = 12.5$ W. Results of irradiation with diode laser light: 1: detonation; 2: deflagration; 3: combustion or fragmentary decomposition; 4: no ignition.

Table S4. Laser initiation of the $[M(\text{chz})_3](\text{ClO}_4)_2$ and $[M(\text{chz})_3](\text{NO}_3)_2$ complexes with 2.5 % PTFE as binder.

Cation / Anion	Co ²⁺ / ClO ₄ ⁻	Ni ²⁺ / ClO ₄ ⁻	Zn ²⁺ / ClO ₄ ⁻	Co ²⁺ / NO ₃ ⁻	Ni ²⁺ / NO ₃ ⁻
T_{decomp} (onset) [°C]	243	273	268	219	238
IS [J]	1	1	1.5	7.5	7.5
FS [N]	≤ 5	≤ 5	20	192	192
Laser initiation ^[a]	4	1	4	4	4

[a] Parameters of the laser beam: $\lambda = 940$ nm, $\tau = 100$ μs , $\sigma = 105$ μm , $\Phi_e = 12$ W. Results of irradiation with diode laser light: 1: detonation; 2: deflagration; 3: combustion or fragmentary decomposition; 4: no ignition.

A8. Unpublished Results of Detonator Capability Testing

Electric Match Type Blasting Cap Test

The setup of electric match type blasting caps (see Chapter 1 – Introduction, Figure 5) was used. Copper blasting caps were filled with a defined amount of explosive material. The explosives were hand-tight pressed into the tube. To check the capability of the primary explosives (1. charge) to initiate a secondary explosive (2. charge), two initiation tests (one only with primary explosive and another one with primary and secondary explosive; Figure S1) were performed in each case. An electric match (Schaffler Type A) was used for ignition of the primary explosive. The results are presented in Table 1.

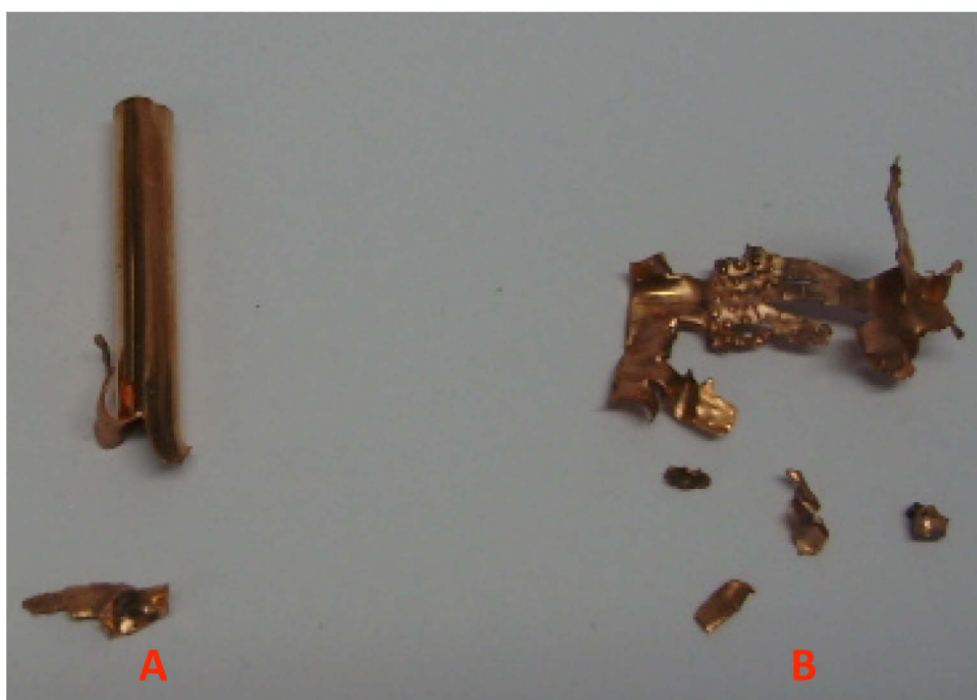


Figure S1. Copper tubes after successful ignition of $\{[\text{Cu}(\text{dte})_3](\text{ClO}_4)_2\}_n$ (A) and $\{[\text{Cu}(\text{dte})_3](\text{ClO}_4)_2\}_n + \text{RDX}$ (B) by an electric match.

Table S1. Results of copper blasting cap test.

1. Charge: primary explosive	<i>m</i> / g	Result	2. Charge: secondary explosive	<i>m</i> / g	Result
{[Cu(dte) ₃](ClO ₄) ₂ } _n	0.10	Detonation	RDX	0.40	Detonation
{[Zn(dte) ₃](ClO ₄) ₂ } _n	0.09	Deflagration	RDX	0.40	No initiation
{[Ni(dte) ₃](ClO ₄) ₂ } _n	0.10	Detonation	RDX	0.40	Detonation
{[Ni(dte) ₃](ClO ₄) ₃ } _n	0.10	Detonation	PETN	0.10	Detonation
{[Ni(dte) ₃](ClO ₄) ₂ } _n	0.10	Detonation	HNS	0.10	No initiation
{[Ni(dte) ₃](ClO ₄) ₂ } _n	0.05	Detonation	HNS	0.30	No initiation
{[Cu(dte) ₃](NO ₃) ₂ } _n	0.10	Deflagration	RDX	0.40	No initiation
{[Cu(dte) ₃](NO ₃) ₂ } _n	0.15	Deflagration	PETN	0.10	No initiation
{[Cu(dte) ₃](N(NO ₂) ₂) ₂ } _n	0.10	Deflagration	PETN	0.15	No initiation
[Cu ₂ (N ₃) ₄ (dte)] _n	0.02	Detonation	PETN	0.20	Detonation
[Cu(NO ₃) ₂ (hmht)] ₂	0.10	Deflagration	PETN	0.10	No initiation
[Cu(ClO ₄)(μ- mht)(hmht)] ₂	0.02	Detonation	RDX	0.40	Detonation

A9. List of Abbreviations

Abbreviation	Meaning
ADN	ammonium dinitramide
anq	3-amino-1-nitroguanidine
AP	ammonium perchlorate
BAM	Bundesanstalt für Materialforschung und -prüfung
bmhte	1,2-bis[5-(1-methylhydrazinyl)tetrazol-1-yl]ethane
bmte	1,2-bis(1-methyltetrazol-5-yl)ethane
BNCP	tetraammine- <i>cis</i> -bis(5-nitro-2 <i>H</i> -tetrazolato- <i>N</i> ²)cobalt(III) perchlorate
chz	carbohydrazide
CL-20	2,4,6,8,10,12-hexanitrohexaazaisowurtzitane
CP	pentaammine(5-cyano-2 <i>H</i> -tetrazolate)cobalt(III) perchlorate
DBX-1	copper(I) 5-nitrotetrazolate
DDNP	diazodinitrophenol
DDT	detonation-to-deflagration transition
DN	dinitramide
DSC	differential scanning calorimetry
DTA	differential thermal analysis
dtb	1,4-di(1 <i>H</i> -tetrazol-1-yl)butane
dte	1,2-di(1 <i>H</i> -tetrazol-1-yl)ethane
dt-5-e	1,2-di(1 <i>H</i> -tetrazol-5-yl)ethane
dtp	1,2-di(1 <i>H</i> -tetrazol-1-yl)propane
EBW	exploding-bridgewire
ECC	energetic coordination compound
EFI	exploding-foil initiator
EM	energetic material
ESD	electrostatic discharge
FS	friction sensitivity
FOX-7	1,1-diamino-2,2-dinitroethene
HATr	3-hydrazino-4-amino-1,2,4-triazole
HMHT	5-(1-methylhydrazinyl)-1 <i>H</i> -tetrazole
HMX	High-Molecular weight rdX, octogen
HNS	hexanitrostilbene
HTPB	hydroxyl-terminated polybutadiene
IF	infrared spectroscopy
IS	impact sensitivity
KDNP	4,6-dinitro-7-hydroxybenzofuroxan potassium salt
LA	lead azide
LDI	laser diode initiator
LS	lead styphnate
m	medium
MF	mercury(II) fulminate
MIC	metastable intermolecular composite
MMH	monomethylhydrazine
NATO AOP	North Atlantic Treaty Organization Allied Ordnance Publication
NC	nitrocellulose
NF	nitroformate
NG	nitroglycerin
NIR	near infrared

APPENDIX

Abbreviation	Meaning
NMR	nuclear magnetic resonance
NPED	non-primary explosive detonator
NQ	nitroguanidine
NTO	nitrogen tetroxide
ONC	octanitrocubane
PA	picric acid
PETN	pentaerythritol tetranitrate; nitropenta
RDX	Research Department Explosive; hexogen
s	strong
SII	simple initiating impulse
TATB	1,3,5-triamine-2,4,6-trinitrobenzene
TATP	triacetone triperoxide
TNT	2,4,6-trinitrotoluene
UV	ultra-violet
Vis	visible
vs	very strong
vw	very weak
w	weak

A10. List of Publications

Articles and Conference Proceedings

- [1] M. Joas, T. M. Klapötke, J. Stierstorfer, Preparation and crystal structure of diaqua(μ -5,5'-bistetrazolato- $\kappa^4 N^1, N^2, N^5, N^6$)copper(II), *Crystals* **2012**, 2, 958–966.
- [2] S. Böcklein, S. Günther, R. Reichelt, R. Wyrwich, M. Joas, C. Hettstedt, M. Ehrensperger, J. Sicklinger, J. Wintterlin, Detection and quantification of steady-state ethylene oxide formation over an Ag(1 1 1) single crystal, *Journal of Catalysis* **2013**, 299, 129–136.
- [3] N. Fischer, M. Joas, T. M. Klapötke, J. Stierstorfer, Transition Metal Complexes of 3-Amino-1-nitroguanidine as Laser Ignitable Primary Explosives: Structures and Properties, *Inorganic Chemistry* **2013**, 52, 13791–13802.
- [4] M. Joas, T. M. Klapötke, J. Stierstorfer, N. Szimhardt, Synthesis and Characterization of Various Photosensitive Copper(II) Complexes with 5-(1-Methylhydrazinyl)-1*H*-tetrazole as Ligand and Perchlorate, Nitrate, Dinitramide, and Chloride as Anions, *Chemistry – A European Journal* **2013**, 19, 9995–10003.
- [5] M. Joas, T. M. Klapötke, N. Szimhardt, Synthesis and characterization of energetic 5-(1-methylhydrazinyl)-1*H*-tetrazole copper(II) complexes as laser ignitable explosives, *16th Seminar of New Trends in Research of Energetic Materials* **2013**, Pardubice, Czech Republic, 708–721.
- [6] M. Joas, T. M. Klapötke, N. Szimhardt, Photosensitive Metal(II) Perchlorates with 1,2-Bis[5-(1-methylhydrazinyl)tetrazol-1-yl]ethane as Ligand: Synthesis, Characterization and Laser Ignition, *European Journal of Inorganic Chemistry* **2014**, 2014, 493–498.
- [7] M. Joas, T. M. Klapötke, Polynuclear Chlorido Metal(II) Complexes with 1,2-Di(1*H*-tetrazol-1-yl)ethane as Ligand Forming One- and Two-dimensional Structures, *Zeitschrift für anorganische und allgemeine Chemie* **2014**, 640, 1886–1891.
- [8] M. Joas, T. M. Klapötke, Laser Initiation of Tris(carbohydrazide)metal(II) perchlorates and Bis(carbohydrazide)diperchloratocopper(II), *Propellants, Explosives, Pyrotechnics* **2014**, DOI: 10.1002/prop.201400142.
- [9] J. Evers, I. Gospodinov, M. Joas, T. M. Klapötke, J. Stierstorfer, Cocrystallization of Photosensitive Energetic Copper(II) Perchlorate Complexes with the Nitrogen-rich Ligand 1,2-Di(1*H*-tetrazol-5-yl)ethane, *Inorganic Chemistry* **2014**, 53, 11749–11756.
- [10] M. Joas, S. Kießling, T. M. Klapötke, P. C. Schmid, J. Stierstorfer, Energetic Complexes of 5-(4-Amino-1,2,4-triazol-3-on-5-yl)tetrazole and Ionic Derivatives of its 2*N*-Oxide, *Zeitschrift für anorganische und allgemeine Chemie* **2014**, 640, 2759–2765.